2016

LOW TEMPERATURE SPLIT INJECTION SPRAY COMBUSTION: IGNITION, FLAME STABILIZATION AND SOOT FORMATION CHARACTERISTICS IN DIESEL ENGINE CONDITIONS

Ahmed Abdul Moiz
Michigan Technological University, amoiz@mtu.edu

LOW TEMPERATURE SPLIT INJECTION SPRAY COMBUSTION: IGNITION, FLAME STABILIZATION AND SOOT FORMATION CHARACTERISTICS IN DIESEL ENGINE CONDITIONS

By

Ahmed Abdul Moiz

A DISSERTATION

Submitted in partial fulfillment of the requirements for the degree of

DOCTOR OF PHILOSOPHY

In Mechanical Engineering - Engineering Mechanics

MICHIGAN TECHNOLOGICAL UNIVERSITY

2016

This dissertation has been approved in partial fulfillment of the requirements for the Degree of DOCTOR OF PHILOSOPHY in Mechanical Engineering - Engineering Mechanics.

Department of Mechanical Engineering - Engineering Mechanics

Dissertation Advisor:	*Dr. Seong-Young Lee*
Committee Member:	*Dr. Jeffrey D. Naber*
Committee Member:	*Dr. Sibendu Som*
Committee Member:	*Dr. Chol-Bum Kweon*
Department Chair:	*Dr. William W. Predebon*

Table of Contents

LIST OF FIGURES

LIST OF TABLES

PREFACE

The materials in chapters 9, 10, 11, 12, 13 and 14 are from separate publications. The author order on the publications along with their status at the time of writing this dissertation is tabulated below. I was the second author for the publication in chapter 9 where I performed numerical work, wrote the numerical chapter and some part of conceptual diagram comments. For chapter 9, my co-authors at both MTU and participating institutions have performed experimental rate of injection testing and combustion vessel tests while sharing the responsibility of describing the experiments and their results. For the publications of chapters 10, 11, 12, 13 and 14, I performed experiments (Rate of injection, Mie, Schlieren, OH* chemiluminescence and Planar laser induced fluorescence), experimental data analysis (using MATLAB and Fiji software), CFD simulation work (using CONVERGE CFD code), CFD data analysis (using MATLAB and EnSight software), made plots and wrote the manuscript. My advisor has helped in setting up the complicated laser setups and overseeing the experiments (also from a safety point of view) when the testing is initiated. My co-authors (including my advisor) in publications of Chapters 10, 11, 12, 13 and 14 helped in setting up the experiments, proof-read the manuscripts and provided their valuable suggestions.

Chapter	Author order	Publication status	Publication
9	2	Published	Proceeding of the Combustion Institute
10	1	Published	Society of Automotive Engineers (Technical Paper)
11	1	Published	National Combustion Meeting
12	1	Accepted	Journal of Energy Resources and Technology
13	1	In Review	International Journal of Engine Research
14	1	Published	Combustion and Flame

ACKNOWLEDGEMENTS

As I start writing this acknowledgement with a feel of anxiety of completing the dissertation, I cannot say enough how my PhD days have transformed me in so many ways. I had a longing for the field of combustion since my undergraduate and to perform some quality research in this area. In the very first few days when I was in discussions with my advisor Dr. Lee about the PhD program, I knew I was in for a tough ride. I would like to thank Dr. Lee from the bottom of my heart for making this experience an enjoyable one. Dr. Lee leads a student by showing how it's done with all the hard work, determination and wit.

There were many times when I wanted to quit, but something just kept me waiting for the next day just curious to see how things would turn up; graduate life has been no less than an eye-opening adventure. Thanks for my committee members Dr. Jeff Naber, Dr. Mike Kweon and Dr. Sibendu Som for guiding me in my research with their friendly aura. Thanks for my then roommates and friends Krishna, Shahid, Qadeer, Aditya and Bharani for getting me into 'real life' after I get home and making me survive through the initial take-off of PhD. I am thankful to my fellow colleagues Khanh and Anqi who made me understand the workings of the complex CV lab (multiple times) with patience (lots of it!). Thanks to Meghraj for teaching me the CFD code handling. Thanks to Emma for being a very good friend and thanks to Sheldon, Tejas and Sathya for being really cool officemates to discuss just about anything. Thanks to Meng, Kyle and Henry for making CV lab a place not just for work but for friendly chatter. I would like to thank Sibendu for helping me learn CFD by giving chances for multiple internships at ANL along with a future post-doc position.

Thanks to my Ammi (mom) and Pappa (dad) who gave me the freedom to pursue what I liked. I know you had done so many sacrifices for me, most of them I am not even aware of. Thanks for being there by my side every single time; helping me in a multi-year foreign PhD is truly a big gift. I hope to make you, Dr. Lee and MTU proud with ever better work in the future. My gratitude to all those who taught me that the name of the game is perseverance.

NOMENCLATURE

IC	internal combustion
AHRR	apparent heat release rate
ASOI	after start of injection
ROI	rate of injection
ASMI	after start of main injection
PLIF	planar laser induced fluorescence
PLII	planar laser induced incandescence
FWHM	full-width at half maximum
LII	laser induced incandescence
CFD	computational fluid dynamics
CV	combustion vessel
RANS	reynolds averaged numerical simulation
TKE	turbulent kinetic energy
Z-T	mixture fraction - temperature
PAH	Poly-aromatic hydrocarbons
IXT	intensity-axial-time
CI	compression ignition
ICCD	intensified charge-couple device
NTC	negative temperature coefficient
PCCI	premixed charge compression ignition
LES	large eddy simulation
NOx	nitric oxides

ABSTRACT

The aim of the PhD work is to investigate the fundamental differences in combustion behavior when split injections are used in low temperature combustion regime. In this thesis, the first injection is also called as pilot injection and second injection is also called as main injection. The broad aspects which are studied encompassing the investigation is to study the ignition delay, lift-off and soot formation of such a double split spray combustion. The mechanisms of ignition, lift-off and soot production are to be studied since the main ignition and lift-off were found to differ from the pilot which effect net soot production. The planned studies in the present work are divided into 1) experimental and 2) numerical approaches. Experimental approach involves high-speed schlieren and luminosity imaging to visualize the spray/flame progress and qualitative soot formation respectively. This is often coupled in a simultaneous way to the laser-based planar laser induced fluorescence (PLIF) technique to visualize ignition behavior in terms of formaldehyde presence and soot precursor visualization of poly-cyclic aromatic hydrocarbons (PAH). As part of CFD simulations, thorough validations of the fuel liquid length, vapor (mixture) presence, temporal and spatial species (formaldehyde, soot) presence, ignition delay, lift-off length, and heat release rate are performed. The main objective of the proposal work would be to perform experimental research with split injection strategies, simulate them using CFD and then understand the underlying mechanisms of important processes of ignition, lift off mechanisms in subsequent injections and the associated soot production mechanisms.

CHAPTER 1

INTRODUCTION

Combustion is one of the major driving forces behind the progress of the modern society. Combustion has significantly benefitted many sectors such as power generation, transportation, metallurgy, to name a few. One of the major takers of combustion science is the Internal Combustion (IC) engine, a remarkable invention and one of the biggest ones since the inception of modern world. Combustion is also made use of in external combustion machines like gas turbines, which make air travel and power generation possible. Population explosion is compelling the humanity on increasing dependence on combustion related machines, and the resulting combustion of fuels is in turn depleting the environment. Over the past 20 years, nearly three-fourths of human-caused emissions came from the burning of fossil fuels . Since, fuel used in major combustion engines is not a renewable source, and is a fossil fuel; extra care has to be taken in its usage. Petroleum is the foremost contender in the fossil fuel section, with automobiles and power generation sector being the primary users of it. With increasing demand in automobile and power, there is an increasing risk of petroleum reserves drying up and leaving us with a highly emission filled environment.

1.1 Motivation

Efficient and cleaner power generation is strictly needed to curb the issue dealing with depletion of fossil fuel and degradation of the environment. According to a report by the environmental protection agency , on-road automobiles contrinute to 38.7% of NOx and 40.5% of CO which are the primary emissions effecting human health. 28% of greenhouse gas (GHG) emission comes from transportation in US in 2012 . With increasing dependence on fossil fuel run autmobile, one of the major ways to prevent pollution and rapid fossil fuel depletion is to work on efficient combustion technologies. There are various technologies in use for efficient combustion viz. partially premixed compression ignition (PPCI), spark assisted compression ignition (SACI), homogenous charge compression ignition (HCC), gasoline compression ignition (GCI), and low-temperature combustion (LTC) concepts. Multiple inection strategies have been used since decades to tackle the various problems of emission reduction, fuel efficiency along with other issues of combustion noise reduction

and heat release phasing [(Chen 2000, Dürnholz, Endres, and Frisse 1994, Imaoka et al. 2015, Martin et al. 2010, Mendez and Thirouard 2009, O'Connor and Musculus 2013a, b, O'Connor and Musculus 2014, Tow, Pierpont, and Reitz 1994)]. A split injection is a general form of multiple-injection schedule where during a fuel injection event, the net quantity of fuel injection is split into separate portions. Split-injection strategy, used primarily in diesel engines, is one of the primarily used technologies to realize some of the above mentioned technologies like PPCI and is also assosciated with other engine combustuion concepts in regular usage. LTC concept is gaining popularity due to its capability of handling emissions without the need of any costly after-treatment devices. As such using mutliple injections is one of the ways in which LTC can be efficiently used to curb some of the deficiencies it has in terms of combustion noise and hydrocarbon emissions.

Diesel engines are the major sources of the NOx and soot (particulate matter) which casue human health problems and one of the ways to tackle this problem is simply by dividing the fuel injetion into multiple shots into the combustion region. Variety can be exercised by doing so viz., varying the mass of each injection, injection duration, time duration between each injection and number of injections and more importantly the timing of each injetion with respect to piston location in an ICE. Various studies in this area have been performed previosuly by researchers, but most of them are in the form of outputs from an IC engine cylinder. It is logical to check with the engine outputs, since these are the end products of the fuel combustion process, but it is noteworthy at the same time, that control studies of fluid dynamic link-up with the emission cannot be easily performed in an engine enviroment. For this sake, emphasis has been focussed in controlled and easily accesible environments like a constant volume combustion chamber, which simulates the same conditions as in an IC engine, but now with providing a better optical access allowing for extensive non-intrusive optical diagnostics. Experimental studies in such well controlled and well aware conditions reveal wealth of fundamental data. At the same time, modeling these phenomena is critical for predicting the outcomes without performing experiments in the future. Thus usage of Computational Fluid Dynamics (CFD) has been an integral tool always in diesel spray combustion study and so is in this present work.

1.2 Objectives

The primary goal of this study is to investigate the fundamental differences in combustion behavior in using split injections in low temperature combustion regime. Various double split injection strategies are utilized. In this thesis, the first injection is called as pilot injection and second injection is called as main injection. The broad aspects which are studied encompassing the investigation is to study the ignition delay, lift-off and soot formation of double split spray combustion. The mechanisms of ignition, lift-off and soot production are to be studied since the main ignition and lift-off were found to differ from the pilot which has a complementary effect on net soot production. The planned studies in the present work are divided into 1) experimental and 2) numerical approaches. Experimental approach involves high-speed schlieren and luminosity imaging to visualize the spray/flame progress and qualitative soot formation respectively. This is often coupled in a simultaneous way to the laser-based planar laser induced fluorescence (PLIF) technique to visualize ignition behavior in terms of formaldehyde presence and soot precursor visualization of poly-cyclic aromatic hydrocarbons (PAH). For CFD simulations, Converge CFD code is used. As part of running a CFD simulation, thorough validations of the fuel liquid length, vapor (mixture) presence, temporal and spatial species (formaldehyde, soot) presence, ignition delay, lift-off length, and heat release rate are performed. The main objective of the proposal work would be to perform experimental research with split injection strategies and replicate them, as close as possible, using CFD and then understand the underlying mechanisms of important processes of ignition, lift off mechanisms in subsequent injections and the associated soot production mechanisms.

1.3 Thesis organization

The thesis begins with giving a brief introduction about (conventional) single injection diesel sprays along with introducing the state-of-the-art concepts of diesel spray combustion. This is followed by differentiating this conventional diesel spray combustion concept with that of a low temperature combustion. Split injection diesel spray combustion area is then introduced as a literature review.

Background about CFD simulations and their accuracy in simulating a split injection spray combustion event is discussed followed by a chapter introducing the experimental techniques used in the thesis. Ways of analyzing the CFD an experimental results are discussed in the following chapter.

The next six chapter come from six publications, they followed a through process as part of this investigation and hence have been laid out in that order. Giving a brief overview of the chronological order in which research was done, experimental study on split injection began with conventional diesel spray combustion split injection tests and attempting to simulate those scenarios. Later, during the ECN 4 experimental campaign, LTC combustion regimes were experimented with. The learning obtained during the CFD effort in the conventional diesel spray tests were used to further carry out CFD work. Here is a line-up of publications which will be explained from chapter 9 onwards.

1. Spray-Combustion Interaction Mechanism of Multiple-Injection under Diesel Engine Conditions
    - Performed split injection spray combustion tests by changing the dwell time between the pilot and main injections in three levels and their mass distribution in two levels under the conditions of 23 kg/m^3 ambient density with 0% O_2 (non-combusting) and 15% O_2 (combusting) ambient conditions, at injection pressure of 120 MPa. Natural Luminosity experiments were performed combined with CFD. A conceptual split injection spray combustion model was proposed.
    - CFD study starts with assessments from this work
2. Lagrangian Spray and Combustion Model Assessments for Split Injection Diesel Spray Combustion Study in a Constant-Volume Combustion Vessel
    - An in-depth assessment of Lagrangian and combustion model selection to properly simulate double split injection sprays was performed
3. Premixed Combustion Efficiencies of Split Injection Diesel Flames
    - Used the same ambient conditions as the above publication for further analysis of premixed combustion efficiencies in the main flames. This is because higher premix peaks were seen in the main combustion heat release rates.

4. Simultaneous Schlieren-PLIF Studies for Ignition and Soot Luminosity Visualization with Close-Coupled High Pressure Split injections of n-Dodecane
    - Aim to investigate further in LTC combustion regime for ignition and soot formation behaviors for the main injection in particular. Simultaneous schlieren and PLIF split injection spray combustion tests performed by changing the mass distribution between the pilot and main injections in two levels and for three ambient temperatures. Also changed the dwell time in three levels for one of the temperature condition.

5. Ignition, Lift-off, and Soot Formation Studies in n-dodecane Split Injection Spray-Flames
    - CFD RANS simulations were run with the learning from previous Lagrangian and combustion model assessment study. Simulations were thoroughly validated. Ignition and flame stabilization mechanisms are argued along and a reasoning is sought for soot production in double split injections using CFD.

6. Study of Soot Production for Split injections of n-Dodecane in CI Engine-like Conditions
    - An LES approach is adopted to understand the split injection combustion process with high-fidelity. Extensive validation was performed as in the previous paper and LES approach was setup to simulate split injection combustion scenarios. With LES, a dwell time variation of 0.65 ms was performed to reveal the sensitivity of soot production to minor variations in the dwell time.

The thesis concludes with conclusions and future work chapter.

CHAPTER 2

SINGLE INJECTION DIESEL SPRAYS

A background of single injection diesel sprays is provided further for ease in understanding of some of the spray and spray-combustion concepts. Going towards split injections there would be added complexity layered over that of single injections concepts. In some instances, the second injection has different behaviors than the first injection. Discussion about coming further with the single injections will help understanding the differences.

Fuel injection with spray technology is widely used in industrial and research sectors. It is one of the pivotal technology and prominent working process in internal combustion (IC) engines. Spray injection has a big influence on the vaporization of injected fuel, which impacts the thermochemical interaction with the surrounding oxidizer, and eventually affects the combustion processes. Proper spray injection results in improved fuel vaporization and air-fuel mixing, leading to efficient combustion, combustion stability and emissions reduction.

Some prominent characteristics of fuel injection as part of single injection are discussed in following sections.

2.1.1 Non-reacting sprays

Knowledge of non-reacting sprays is necessary to investigate the near nozzle flows (which are mostly not reacting) and also the mixture formation until the ignition event. Apart from these, modeling efforts of a non-reacting spray simplify the process of establishing a path forward to the reacting (combusting) spray aspect.

Fuel delivery from the injector is effected by a variety of factors with discrepancies starting from within an injector. Fuel delivery is effected by the nozzle hesitation mainly caused by a delay in beginning transverse motion of the needle. The final position of the needle renders the spray penetration to stay at a constant value during the injection duration. Undesirable and unaccountable fuel delivery after the end of the injection duration is a commonly seen phenomenon in spray studies and is mainly attributed to the spring compression force at end of injection timings. Rate of injection profile correlations together

with the input current waveform and high speed image visuals are a valuable aid to reach at conclusions relating to such undesirable behaviors of the injection phenomenon, which are expected to occur more for split injection strategies as will be discussed later.

The other factor affecting spray characteristics is the injector type and more specifically the injector geometry. A series of experiments were ran by Schugger [Schugger and Renz 2003] to study the effect of hole geometry on the spray features by employing different hole structures in two set of injectors. The nozzle with a round inlet hole led to a smaller plume angle and longer penetration, which is why round holes are conventionally used in modern injectors. With relation to the injector technologies in diesel engines, piezo and solenoid-type if injectors, are in conventional use. In most of the modern engines, piezo injector is used due to its quicker response. The faster the injector response the better the control over the mass flow rate profile [Desantes et al. 2010]. Although, injection delay is dependent upon other factors like the injection pressure [Abdelghaffar et al. 2007] for some injectors. It is notable that such dependency is not the case with every injector, different injectors (with varying nozzles types, internal geometries etc.) have different dependency levels [Karimi 2007]. The nozzle types are classified into three types of categories, the mini sac, micro sac and valve covered orifice (VCO) with the sac volume reducing from mini to micro sac and becoming negligible in VCO type. The sac feature in a nozzle leads to the UHC at end of injection times and has been studied in the past for its effectiveness. Farrar et al. [Farrar-Khan et al. 1992] performed an effectiveness check of sac volume by varying it's volume and concluded that the nozzles without a sac exhibit spray quality degradation due to a throttling effect [Zhao 2009]. Another factor closely related to the injector geometry is the cavitation. That said, cavitation occurs by a different mechanism in non-sac and sac type injector nozzles; with the former observing a 'conventional' cavitation and the latter a 'vortex'-type cavitation [Afzal et al. 1999, Bae and Kang 2006].

In addition, there are effects from the fuel pressure, fuel temperature, fuel properties, ambient pressure and density, ambient temperature which greatly have an effect on the spray progression.

→ With higher injection pressures, smaller droplets are created, liquid momentum is increased and this enables the liquid droplets to have an intense interaction with the ambient air. This interaction occurs throughout the lateral and front periphery of the spray plume which increases the air entrainment. With an increase in injection pressure as well as the chamber pressures a reduction of breakup time and breakup length is observed [Karimi 2007]. Fig. 1 shows how an increase in injection pressure decreases the soot (luminosity) which corresponds to soot emissions. Reducing the nozzle diameter also has a similar effect, since it results in smaller droplets too.

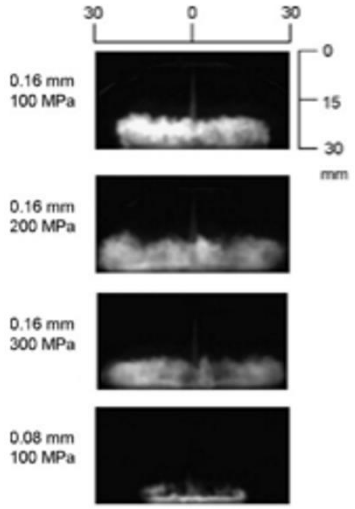

Figure 1: Raw images of flame luminosity at end of injection with different injection pressure and nozzle sizes. [Wang et al. 2011]

→ Fuel temperature effects the spray break-up behavior by dominantly causing cavitation [Zeng et al. 2012]. Apart from increasing fuel temperatures causing more cavitation which helps in spray break-up and faster liquid atomization and increased air-entrainment; it also can lead to a phenomenon termed as 'hydraulic flip' under extreme condition which degrades the atomization characteristics [Allen et al. 2003].

→ The primary influential fuel properties found in the literature are *viscosity, surface tension and volatility*. With more energy required to counter-act the viscous force,

the break-up of droplets is effected and the spray plume are more or less 'stabilized' in nature [Mojtabi 2011]. With reduction in viscosity, more droplet break-up occurs, which results in less spray penetration and higher spreading angles [Shimizu et al. 1984, Chen and Lefebvre 1994, Chang and Farrell 1997]. Surface tension in terms of atomization relates to the amount of energy expended to cause an increase in the drop (or bubble) size [Aleiferis et al. 2010]. Apart from that the property of volatility effects the vaporization characteristics. A high volatile liquid vaporizes at a faster rate causing smaller drops occurring at faster rates which decreases the liquid length of the liquid jet significantly.

→ The effect of ambient pressure (/density) and temperatures are correlated and often oppose each other. With an increase in ambient density, an increase on plume angle and reduction in liquid length are observed [Zeng et al. 2012, Hiroyasu and Arai 1990, Zhu et al. 2013]. On other hand, observations from Hiroyasu & Arai [Hiroyasu and Arai 1990] claim that hot ambient air can cause higher fuel vaporization at the spray peripheries which results in lower spray angles. Sibiers [Siebers 1999] studied the dependence of liquid length on the ambient conditions using injectors with orifice sizes from 100-500 µm and with various fuels.

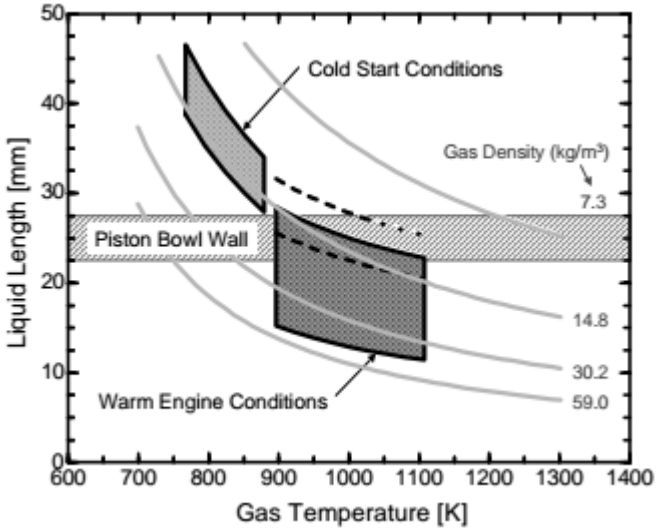

Figure 2: Liquid lengths expected in the heavy-duty diesel engine. Figure from Ref. [Siebers 1999]

Fig. 2 shows the impact of the ambient temperature and density on the liquid length parameter which effects piston wall wetting. The lower gray region represents the range of liquid lengths expected for warm running engine conditions. The upper gray region represents the range of liquid lengths expected for cold start engine conditions. The cross-hatched horizontal band across the middle of the Fig. 2 represents typical maximum distances from the injector to the piston bowl wall. The light gray curves are liquid lengths for lines of constant density which are included in reference [Siebers 1999].

2.1.2 Reacting sprays

To explain the reacting sprays, Fig. 3 shows a typical heat release rare curve which signifies the pattern of heat release per unit time when the injected spray burns.

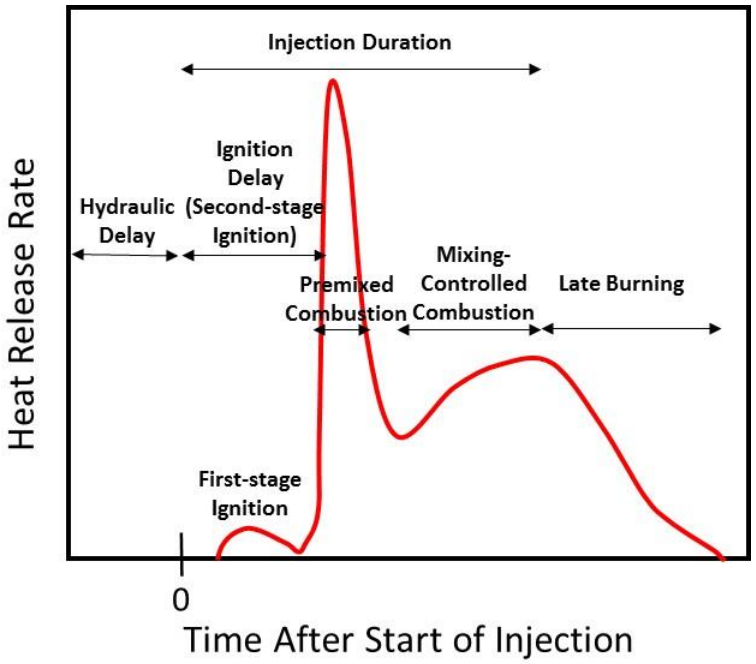

Figure 3: Different phases of heat release during a typical diesel spray combustion event

From start of command (SOC) to start of injection (SOI) is a 'hydraulic delay' which is the time duration between electrical command from the injector driver to the pressurized fuel issuance from the nozzle orifice. The hydraulic delay changes (slightly) with electrical

excitation voltage, ambient conditions, injection pressure and fuel temperature. After the fuel gets injected, it starts vaporizing in the hot ambient. After a duration of an 'ignition time delay', auto-ignition of the vaporized fuel takes place. Auto-ignition is the reason why diesel engines are called compression ignition engines, meaning the increased density of the piston compression ignites the fuel volumetrically in the chamber. Depending on the ambient conditions, this ignition might be two staged: first event is a low-temperature heat release event (cool flame) called first stage ignition and the second event is the high-temperature heat release event called second stage ignition. During the high temperature ignition event, there is a premixed combustion peak where bulk combustion of the vaporized fuel-air mixture takes place. The late the ignition event, the more the time for the fuel vapor to mix with the ambient oxidizer which results in a higher premix combustion peak. After the premix combustion phase, as the fuel gets injected, there is mixing or injection-rate controlled combustion phase. This phase has a positive slope as long as the fuel injection is active. This phase is strictly controlled by (spray) mixing which is induced by the injection event. As soon as the injection ends, fuel stops entering the chamber and the heat release drops rapidly while it continues burning the rest of the fuel in the chamber. This phase is termed as 'late burning'.

Diesel spray combustion was experimentally investigated in quasi-steady stabilization state by Dec [Dec 1997] as drawn in Fig. 4. Some of the concepts in the schematic of Fig. 4 have been re-visited by researchers and so this is not state-of-the-art diesel spray combustion scenario. A recent conventional diesel spray combustion schematic is introduced later in Fig. 6.

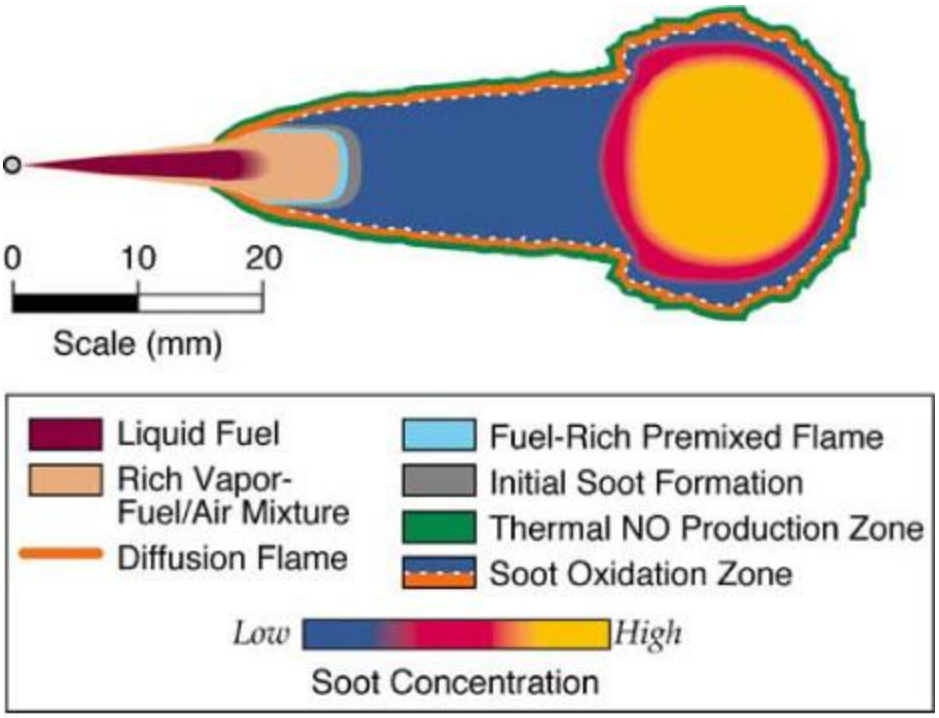

Figure 4: Quasi-steady diesel spray combustion visualization. Figure from Ref. [Dec 1997]. Reprinted with Permission from SAE International

Liquid injection from the nozzle orifice has a characteristic length which is called as liquid length. This is because after the axial extent of the liquid length location, the liquid fuel vaporizes. As the vaporized fuel travels downstream, it starts to oxidize with low temperature reaction chemistry happening closer to the liquid extent locations. This is a rich fuel-air mixing zone. As these reactive species travel further downstream they lean-out and undergo a thermal runaway event. This leads to a volumetric (auto) ignition and the resultant mixture is termed as an 'ignition kernel'. This high temperature reaction chemistry further causes more ignition reactions to occur nearby and a diffusion-type flame is established, generally slightly upstream of the ignition location of the first kernel formation. As the injection continues, the diffusion flame continues to stabilize at this location. Since there are minor variation in the axial extent of this stabilization, this stabilization behavior is termed as a 'quasi-stable lift-off'. Ambient oxidizer continuously gets entrained into the flame from beneath the lift-off location. Fig. 4 is a conceptual snapshot of this stabilized instant. As can be seen from the Fig. 4, the rich fuel-air mixing zone is located downstream

of the liquid length and later converts to a rich premixed flame front. The higher the richness of the fuel-air mixture (higher equivalence ratio), the higher the soot production downstream. The oxygen entrained from beneath the lift-off location causes leaning of this fuel-air-radical mixture and the flame front continues as a leaner combustion zone. Due to availability of entrained oxidizer, oxidation of the produced soot in a 'soot oxidation zone' is observed which does not totally zero-out the net soot but rather reduces it. Further downstream, due to oxygen getting used up upstream further soot oxidation is reduced causing high concentration of soot in the downstream locations. While this happening, there is also production of other emissions like NOx (primary component being NO), which forms in the high temperature regions of the flame following mostly the thermal route of NOx production predicted by a Zeldovich mechanism [Heywood 1988]. After the injection ends, the flame travels further downstream and late-burning of fuel takes place.

CHAPTER 3

CONVENTIONAL VS. LOW TEMPERATURE COMBUSTION

Most of the above concepts are related to conventional combustion of single injected diesel spray. There are a few deviations when the spray combustion occurs in a low temperature combustion environment. Fig. 5 shows the combustion event in an equivalence ratio and temperature space, outlining the differences in a conventional event and other technologies like LTC, PPCI and HCCI.

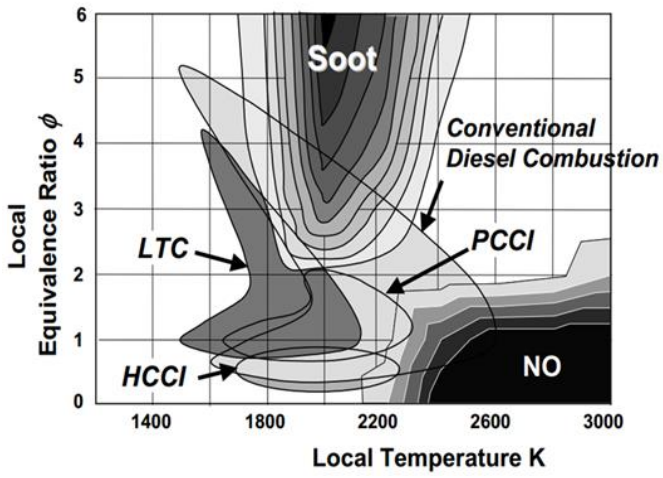

Figure 5: New strategies for diesel engine emission control. Figure from [Neely et al. 2005].
Reprinted with Permission from SAE International

In the equivalence ratio - temperature plot of Fig. 5, soot and NOx are plotted. There is little room for a combustion regime to place itself in a spot which is free from both soot and NOx. In reality, some of the space in the plot cannot be actually inhabited by any spray combustion event for eg. the top right portion containing both the high temperature and high equivalence ratio do not occur simultaneously. By increasing the injection pressure a lowering of the local equivalence ratio is observed which reduces the soot output from spray combustion. But in the case of rich combustion of the formed fuel-air mixture (due to the ambient conditions) there is little room to escape from the soot peninsula in conventional diesel combustion. This is not the case with low temperature combustion where the

ambient in which the combustion occurs is different than conventional combustion. It can be seen form Fig. 5 that the combustion zone has similar shape as in conventional diesel combustion but moves down towards fuel lean mixtures and moves left towards lower temperatures.

The conventional diesel spray combustion model shown previously in Fig. 4 has been modified in Fig. 6 by Musculus et al. [Musculus et al. 2013] to account for the cool flame and accommodate low temperature combustion concept. The original conceptual model was only for the quasi-steady spray combustion period, and so did not describe the combustion process after end of injection.

The diesel spray takes similar characteristics in the initial few time instants for both the conventional and LTC conditions. Since LTC conditions involve lower ambient pressure and temperature, the liquid length is usually ~10 mm longer for LTC than conventional diesel case. However, this may not be not be true for late-injection LTC where fuel injection takes place near TDC in an engine. Soon after vaporization of the liquid fuel takes place, first stage ignition happens in the conventional diesel case. Due to the nature of faster ignition near the liquid zone, there is high amount of soot and soot precursors forming during the ignition times and continue to form in the quasi-steady spray combustion periods. The degree of air

entrained from beneath the lift-off is critical in conventional diesel spray combustion.

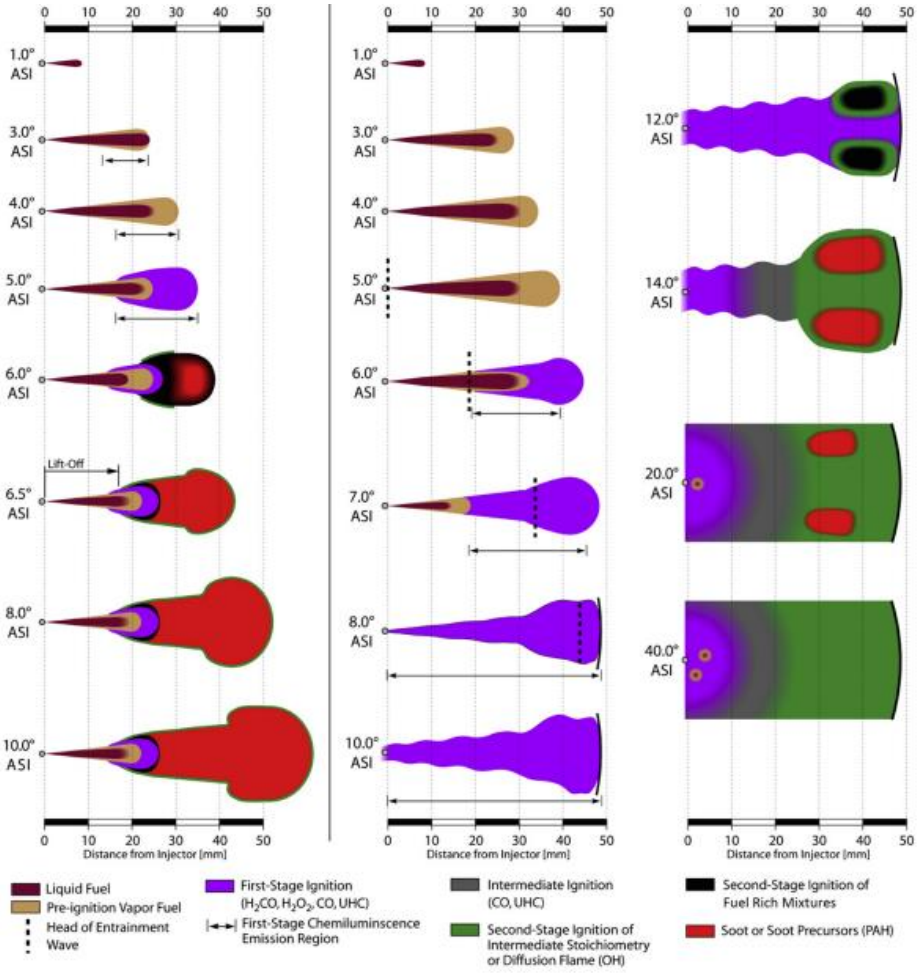

Figure 6: Conceptual model for conventional diesel combustion (left) and partially premixed low temperature diesel combustion (right) [Musculus et al. 2013]

This causes enough premixing to cause the fuel-air mixture to burn lean downstream. Unlike conventional diesel combustion, in low temperature combustion, high temperature ignition happens after a very long time due to the nature of the ambient conditions employed in LTC. The first stage ignition starts late in LTC case and prevails for time until after injection. The temperature arising from the low temperature heat release reduces the liquid length of the LTC spray which was ~10 mm longer the conventional until the ignition event. A gradual blending of the air-fuel mixing field is observed with wave like patterns. Second stage ignition occurs later in the combustion cycle and causes low amount of soot and soot

precursors further downstream (in some fuel rich pockets) which get oxidized later by mixing with the ambient. Later in the combustion cycles, there might be dribble of liquid droplets from the nozzles or sac volumes. This causes locally fuel rich spots and result in UHC and CO emissions.

With this brief introduction of conventional single injection diesel spray combustion and the differences observed when moved to a low temperature combustion regime, the writing further discusses details of split injection diesel sprays.

CHAPTER 4

SPLIT INJECTION DIESEL SPRAYS

2.2 Considerations for injecting multiple shots

Split injections differ from single injections in varying degrees beginning from their injection events. Rate of injection (ROI) profile has been an important criteria to quantify an injection event which effects the spray velocity distributions and spray-vapor formation. The control and measurement of the ROI is pivotal to any spray study. Baniasad [Baniasad 1994] conducted a study which showed that the ROI profiles also determine the unburnt hydrocarbons, particulate matter and NOx emissions. Aiming at uniform delivery of fuel with accurate mass output is a conventional task done by the injector manufacturers, but shaping of the ROI curve for an entire injection duration is a complicated task [Bosch 1966].

When considering split injection events, interactions due to the pressure waves generated within the injector due to a former injection event cause changes in the injected volume of the subsequent injections [Ladommatos et al. 2000, Kastner et al. 2009, Desantes et al.]. This was found to be due to a 'water hammering' or 'fluid hammering' effect [Baratta et al. 2008, Catania et al. 2008] where a pressure surge is created when a fluid in motion is forced to change its direction or come to a complete stop causing a sudden momentum change. The oscillations generated in such a manner effect the injected volumes when the dwell time is varied and worsens the precision of small injection volumes which are injected after very short dwell times, like in a main-post or main-after injection event [Catania et al. 2009].

The pressure waves have known to have a compression-rarefaction or peak-valley pattern. Depending on the type of waves generated in the common rail in a split injection event, if the second injection starts in sync with the compression or peak wave in the nozzle, the fuel injected as part of the second injection increases. Likewise, if the second injection begins in synch (or in-phase) with the presence of a rarefaction or valley, then the injected quantity from the second injection decreases. This is true for the electrically-hydraulically actuated solenoid injectors and the indirect acting piezo-electric injectors. If the needle is not ballistic, this change in the injected volumes disappear which is the case with the direct-acting piezo-electric injectors [Ferrari and Mittica 2012]. Avoiding these disturbances with respect to

reducing the needle end-strokes to low values have been found beneficial to reduce fuel consumption and emissions [Baratta et al. 2008].

These disturbances and the consequences caused can be used to shape injection rate profile for solenoid injectors. For very short dwell times, an injection fusion occurs, which is more evident and has a wide range in main-post or main-after schemes. Injection fusion causes the injection rates of the two injections to unite. Thus a boot-type injection rate can be designed which is similar to the one used with the direct-acting piezo-electric injectors [Ferrari and Mittica 2016].

Fig. 7 conceptualizes some events which can occur when the dwell time is varied. In the Fig. 7, 'period' refers to an event when the volume injected and the pressure waves created are in synch or phase.

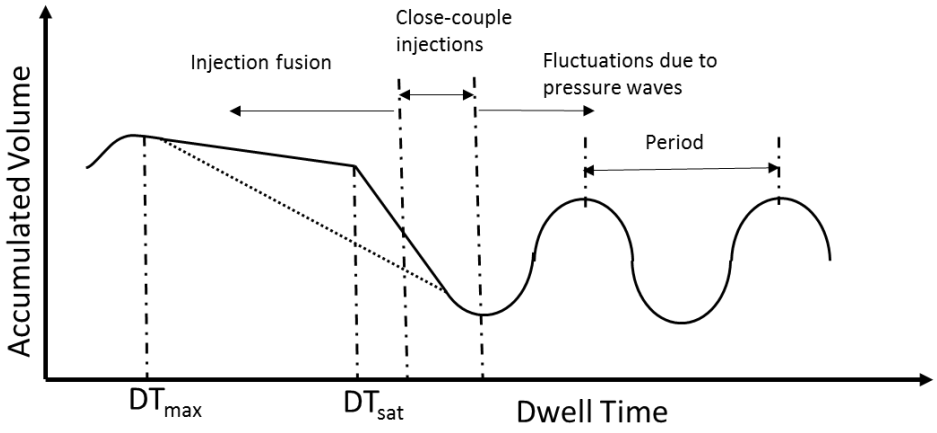

Figure 7: Different events occurring during split injection as dwell time varies. Figure re-drawn from Ref. [Ferrari and Mittica 2016]

Badami et al. [Badami et al. 2003] performed pilot-pilot-main injection tests with same amount of commanded injection durations for the two pilot injections. They observed that the second injection had a slightly different injection rate than the first which changes the heat release behavior slightly. They concluded that this phenomenon highly relies on the pressure waves generated in the common rail, which follow each injection. If a peak (compression) or a valley (rarefaction) in the pressure waves generated by the first injection in synch with the peak (compression) or a valley (rarefaction) of the next injection, a

considerable variation of the injection pressures and hence the injection rate can be observed.

A set of mass flow rate profiles were obtained by a Bosch method [Bosch 1966] by Wang et al. [Wang et al. 2015] who utilized a piezo injector for performing single and split injection experiments. Part of their study focused on finding a cross-over point in injection time when no such interaction exists in the rail of the injection system as was also done by Badami et al. [Badami et al. 2003].

A comparison between a single injection comparison with a set of split injection experiments (where dwell time) is varied was made by Wang et al. [Wang et al. 2015]. A good correspondence of the first injection from both the split and two single cases was observed. The second injection from the split injection case was lower than the second injection of the two single injection case, but this was not the case for the higher dwell time case where both of them have same heights. Dwell time thus determines the interaction of splits injection even before they come out of the injector in the form a reduced mass flow when the dwell time is low. This dependency or interaction is reduced with higher dwell times. Thus, to obtain an equally split injection strategy, a longer TTL time for the second injection has to be commanded.

2.3 Split Injection specifics

There are many parameters to be kept in mind while designing a split injection strategy, viz., masses of individual injections, injection pressure, injection durations, dwell times and number of injections. Their effects on the overall spray combustion characteristics are summarized below from literature.

2.3.1 Mass of injection

The effect of mass of each injection on the overall combustion behavior is prominent for the fact that fuel mass is the source of all energy release and interacting fuel/combusting masses effect the heat release and emission behavior. Recent work done by Desantes and coworkers [Molina et al. 2010, Desantes et al. 2007] discussed a “split-flame” concept, where there is no interaction among the injections and fuel from each injection burns

separately. Fig. 8 shows the concept of split flame where the flame from the main and post injections are experimentally seen to burn separately. It was concluded from the study that any soot reduction observed should be due to lack of soot formed when the injections are split. Later on, there have been many studies both from other literature sources [Hasse 2004, Hessel et al. 2014, O'Connor and Musculus 2013a, b, O'Connor and Musculus 2014, O'Connor and Musculus 2013b, a] and also as will be discussed further as part of this PhD work where contrasting views from the split-flame idea are discussed.

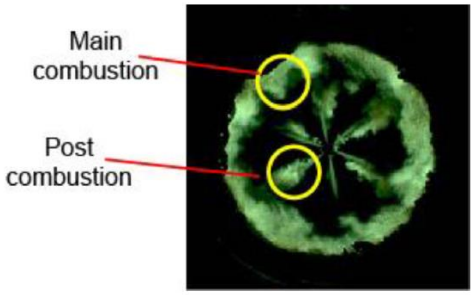

Figure 8: "Split flame" image from [Desantes et al. 2007]

Nehmer and Reitz [Nehmer and Reitz 1994] conducted tests for triple injection and indicated that the same amount of soot reduction was achieved either by 19% of the total fuel mass during the last injection as well as using 49% of the total fuel mass during the last injection, although different NOx emissions were recorded. Also, they concluded that in-cylinder rise in pressure and engine emissions are very much affected by the quantity of the pilot injection. The authors established that, more the fuel in the pilot injection, more is the NOx and less are the particulate emissions.

2.3.2 Injection duration

There are numerous studies stressing on the fact that the injection duration, especially of the subsequent injections, has an effect on the emission characteristics [Arrègle et al. 2008, Beatrice et al. 2002, Desantes et al. 2007, Molina et al. 2010]. This is a general idea of 'jet replenishment' which was investigated by Han et al. [Han et al. 1996] who have done CFD simulations to study how the active injection actually feeds the spray head where most of the soot is produced due to the presence of the fuel-rich mixtures [Dec 1997]. Any splitting of the fuel taking place, changes the mixture formation in the jet head and a reduction in

soot formation is seen. A similar mechanism can be employed to investigate the reduction in NOx due to reduction in flame temperatures and reduction in UHC due to more complete burning of the left-over fuel by the on-coming flame. Brands et al. [Brands et al. 2013] performed split Injection studies in constant volume combustion vessel for an 800 K 50 bar ambient condition. By performing PLIF, OH*, PLII, NL experiments they found that the pilot injection forms very little soot due to the short time for which the fuel injection actually overlaps with high temperature combustion. This interaction would be higher if the injection durations are longer. For the main ignition a 5-fold decrease in ignition delay (over pilot) was observed. This increased the temporal overlap of the active injection with the high temperature combustion which results in higher amount of soot from the main injection. Thus, injection duration is a key factor in deciding emissions especially originating from subsequent injections.

2.3.3 Dwell time

Apart from the in-injector physics related to pressure fluctuations affecting the needle movements and thus the injected fuel masses and the injection fusion occurring when the dwell times are too small (cf. chapter 2.2.2), the effect of a previous flame (for e.g., pilot) on the subsequent flame (for e.g. main) is expected to differ with dwell time [Cung et al. 2015]. This is because combustion of the pilot has a significant effect on the main combustion, in terms of temperature and the composition of the ambient it leaves behind.

For the case of a short dwell time, the short separation time of pilot and main would leave a relatively hot region behind for the main injection, which will likely yield a shorter ignition delay compared to longer dwell time cases. However, the lack of oxidizer in the region that the pilot leaves behind under short dwell time would give the frontal area of the main injection less of a chance to combust compared to the outer boundary area of its spray. This will likely leave the main flame to have a flame on the boundary, instead of being hot in the spray core.

In the case of a medium dwell time, the pilot flame is well formed. Main injection is pushed into a hot flame and the result is that the main flame has a large heat transferring region,

which causes the front region of the main flame to burn aggressively along with the nearby spray boundary.

In long dwell time cases, pilot combustion is complete, and the remaining cooled products gradually warm the frontal region of the main injection. This results in a well-shaped confining main flame in which temperatures are, to some extent, evenly distributed along the spray. The pilot may have a different shape and temperature mode with varying dwells, due to the increased availability of oxidizer owing to the late occurrence of the main flame on increased dwells. Different dwell times were also found to yield different tail shapes for the main combustion [Cung et al. 2015].

Apart from this, at high-temperature ambients, the influence of events like combustion recession [Knox and Genzale 2015a] of the first flame on the oncoming fuel jet also depends on proper dwell time (to avoid the combustion recession event). A combustion recession might further accelerate the ignition of oncoming fuel jet which leads to early and rich ignition leading to development of higher PAHs and soot later on [Skeen et al. 2015b] .

2.3.4 Number of injections

Having number of injection which comprise of an injection train for one engine cycle is the idea behind split injections. Choosing the right number of injections is dependent on the aim for which the split injection technology is put to use. Having different number of injection would depend on what the application they are geared for, for e.g., for tackling engine noise, soot-NOx trade-off and after treatment device functioning a minimum of 3 injections are usually used in the industry [Mohan et al. 2013], one pre-,one main and one post-injection. Of course, the mass of each injection, injection pressure and dwell time for each of these injections is also critical apart from the number of injections. New generation of solenoid-based injectors are used in common rail injection systems to produce up to 8 injections per engine-cycle especially after modifications of pressure balanced valves which allow them to be used for short dwell times with fast actuation. Not only solenoid-based injectors, but also direct-acting and indirect-acting piezo-electric injectors allow for shorter dwell times and quick actuations [d'Ambrosio and Ferrari 2015, Desantes et al.]. Early research done in a number of studies on split injections have chosen a few number of injections, optimizing the

injection scheme and reporting if the role of the extra injections was beneficial in what aspect of in-cylinder engine combustion enhancement. Sometimes opposite results might be found in the literature for the same aspect enquired, for e.g., Nehmer and Reitz [Nehmer and Reitz 1994] concluded that a short injection is needed as a third injection in a triple split injection strategy to reduce the soot formation rate while Ehleskog et al. [Ehleskog et al. 2007] divided the number of main injections to three or four (with pilot being the first injection) but it only increased the PM, CO and HC with a reduction in NOx. Choosing the number of injections has to deal with when the injection is actually being activated especially in an engine study. Fig. 9 shows a schematic about how the main injection targeting (bowl in top versus the squish in bottom) affects soot reduction when a post injection is used.

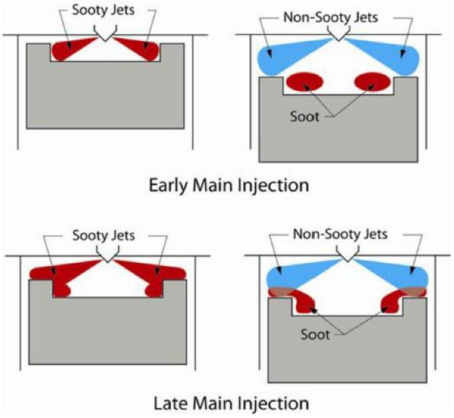

Figure 9: Spray directionality in decided emissions formation with split injections. Figure from Ref. [Bobba et al. 2010]

Thus targeting of the post jet becomes crucial and should complement the main injection with actually having an interaction with them. In the case of Fig. 9, the late main injection (bottom figure set) is helpful in reducing the net soot. While considering the soot reduction is important for an engine study, so is the consideration of other detrimental results of combustion like combustion noise and other emissions (like NOx, UHC) using split injection schemes.

Fig. 10 shows one of the usual injection strategies employed to tackle the major problems from IC engine usage coming from combustion noise, soot and NOx emission and treatment of regenerative devices in exhaust systems.

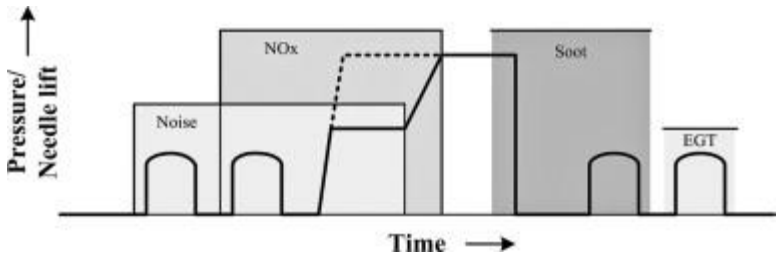

Figure 10: Contributions of noise, NOx and soot production directly effecting from split injection scheduling. Figure from [Mohan et al. 2013]

Fig. 10 proposed two pilot injections to be used for noise and NOx treatment, main to be used for NOx treatment by efficiently couple it with pilot, a post injection to be used for soot reduction and an after injection to be used to efficiently operate exhaust regenerative devices.

2.3.5 Injection pressure

Nowadays, high pressure common rail fuel injection systems allow a very high degree of flexibility in the timing and quantity control of split injections, which can be used to obtain significant reductions in engine noise and emissions without compromising its performance and fuel consumption. Modern fuel injection systems have the capability to control not only the timing and quantity of each injection but also the pressure of each injection within a split injection sequence [Mahr 2004]. Pressure modulation is one of the keys in which efficient combustion noise reduction, fuel efficiency and emission benefits are realized. Usually, in a split injection train, one or two pilot injections are injected at low pressures to deal with engine noise and NO*x* emissions. Then a main injection will support the NOx reduction when done in association with a close-coupled pilot injection. Then a close-coupled post injection is done at high injection pressures to tackle with the soot problem. This might be followed by an after- or late-post injection done at moderate injection pressure to generate sufficient exhaust gas temperature for efficient regeneration of diesel particulate filter and at the same time to provide hydrocarbons for NO*x* adsorber catalyst [Mohan et al. 2013, Mahr 2004].

Injection pressure effect can be also looked from a fundamental point of view. There are many researchers who argue that the combustion of the second injection occurs in a

fundamentally different way than the first injection. Researchers [Felsch et al. 2009, Gong et al. 2015, Lim et al. 2010] find the second injection to be premix flame propagation stabilized. This is also discussed in the present work as will be elaborately explained in chapter 13. Injection pressure becomes important with a 'propagation' type concept rather than an auto-ignition type concept. This is because, the transport of the bulk vaporized mass (which is the reactive mixture) happens in the form of propagation of species until the lift off position. The lift-off position is where the high temperature flame dynamics get started. With a higher injection pressure, a faster motion of the second injection reactive species towards this combustion zone occurs. Fig. 11 shows that as the injection pressure is increased the second ignition delay is lowered, but no change in ignition delay is observed while the injection pressure is kept the same and the ambient temperature increased.

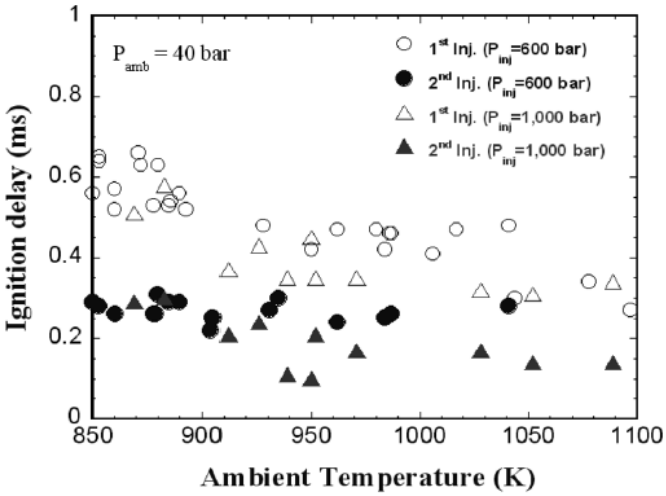

Figure 11: Injection pressure effect the ignition of the second injection, accelerating it faster than the first injection's ignition delay. Figure from Ref. [Lim et al. 2010]

For the first injection this might not be a dominant factor since the first injection (in most low-to-medium temperature ambient cases) is auto-ignition stabilized. This means a volumetric thermal run-away event defined combustion dynamics for the first injections in multi-injection trains.

All or some of these parameters are considered in a design of experiment or genetic algorithm approach, either using experiments or CFD, for a particular engine to arrive at the right amount of the target quantity to be used for the engine operation based on target costs [d'Ambrosio and Ferrari 2015, Hiroyasu et al. 2003a, Hiroyasu et al. 2003b, Shrivastava et al. 2002].

2.4 Past split injection efforts

Before going into details of the work performed as part of this PhD, this chapter details some of the prior work done to characterize non-reacting and reacting sprays coming from a split injection event in both ICE and constant volume environments and mostly from a conventional combustion regime. Some of the fundamental differences between conventional single injection and conventional split injections are laid out. Split injections in an LTC regime will be discussed as part of the PhD work and contrasting trends from this chapter and the present work can then be easily interpreted.

2.4.1 Non-reacting sprays

Understanding spay growth with technical aids has been a challenge, due to short injection durations and the need for high spatial and temporal resolution of images to visualize the spray characteristics like liquid and vapor region with clarity. In the section below, a brief background of these efforts has been covered.

With the introduction of modern photographic equipment and other optical aids, spray visualization has taken an interesting turn with more accurate understanding of the underlying physics happening in the spray growth. With the implementation of split injection strategies in diesel engines, these techniques needs to be elevated to a higher precision due to the complex fluid dynamic interaction of the multiple sprays.

Pulsed Doppler anemometry is used to check with the velocities, spatial drop distribution and drop sizes of the pilot and main spray plume heads by Yoshizu and Nakasyama [33]. They employed a relatively low injection pressure of 25 MPa for a 250 um single nozzle hole. The authors found that the pilot injection exhibited a "stratified size distribution", which means that the drops increased in size from the spray axis to some radial location, and from

there-on they decreased to the spray edge. This was thought due to the spray-spray interaction on a volumetric scale. Arai and Amagai [34] did studies related to the spray velocities. They found that the second spray had a higher spray tip velocity than the first for their split injection experiment of 25 MPa injection from a 270 un nozzle in 3 MPa ambient. This velocity increase was more as the dwell time decreased. This behavior was anticipated due to the flow field of the pilot spray, again signaling that spray-spray interaction is one of the primary reasons for velocity variations and drop size reductions, making it more important to study.

The interactions between the individual injections effects many areas of spray-flame characteristics. Bruneaux and Maligne found that for short dwell times the interaction of the velocity fields induced by the individual injections led to an increased mixing rate at the second injection front.[Bruneaux and Maligne 2009] Under non-reacting conditions, faster vapor penetration of a second injection relative to the first may be observed due to a 'split-stream' effect.[Skeen et al. 2015b] Simply stated, the second injection enters an ambient environment already possessing a downstream velocity induced by the first injection.

Pierpont et al. [7] had another interesting study, in which he pointed out that the optimum split injection strategy also depends upon the spray separation/inclination angles. Tests were conducted for two diesel injector nozzles having different separation angles under the effect of exhaust gas recirculation (EGR). Nozzle with lesser separation angle was found to yield low NOx.

Tonini et al. [Tonini et al. 2010] conducted a CFD study to understand the effect of pilot injection, dwell-time, and number of injections on diesel spray propagation. It was found that if the pilot quantity is small then the liquid and vapor penetration are unaffected; the vapor penetration would be the same as that of a similar single injection case with the dwell time subtracted from the split injection case. However, some researchers do not agree with this claim in experiments. Skeen et al. [Skeen et al. 2015a] report a 'slip-stream' effect which renders the second injection to travel faster in the stream of the first jet with no spray-head shock as the first injection would undergo (slowing the first injection). Tonini et al. [Tonini et al. 2010] also found that eventual spread of the fuel, when studied in terms of the fuel

vapor mas fraction contours, does not significantly different form the single injection case either. But this fuel spread is affected if the main injection is divided as a main-post strategy or if it is simply divided into two portions. They comment that during the third pulse, a more than 5 per cent change in vapor fractions can be seen depending on the mass in this pulse. Borz et al. [Borz et al. 2016] performed some experiments on gas jets in constant volume chambers for split injection strategies and found that in the near-nozzle region, slip-stream effect is mainly felt downstream and not near the nozzle where the momentum is dominated by the injection pressure. They also found a maximum of around 4 degrees difference in the jet spreading angle among the first and second injections, which may indicate changes in their entrainment behaviors and mixing. Bruneaux and Maligne [Bruneaux and Maligne 2009] investigated the effect of injection timing and dwell time on mixing using laser-induced exiplex fluorescence (LIEF) technique for single injections and main-plus-post-type injections. They have visualized low fuel concentrations near the jet-tails which resulted from the entrainment wave after the end of injection. Also, the head of the jet experienced high fuel concentrations due to limited mixing. When the dwell time was shortened, a lower level of fuel concentration gradient was observed which implies more mixing at the jet head.

Moving focus to combustion, the information available on the dwell time, individual injection masses, number of injections and their effect on various factors in a non-engine environment is still in development. This is needed to study the spray-flame and flame-flame interaction behaviors and their effect on various combustion aspects. This interaction is one of the keys to a successful injection and ignition strategy, as it administers the temporal and spatial fuel distribution which governs various flame characteristics, the most important being emissions. Also, performing accurate computational modelling of these sprays and their combustion is very important at the later stages, leading to less dependency on the experiments and at the same time staying confident about the numerical model outputs.

2.4.2 Combusting sprays

Split injection in combusting sprays is mainly used for reducing the soot and NOx formation; reducing combustion noise is also one of its advantages. Large number of studies have been

done focusing on the concept of split injections which include pliot-main injections [35, 36], pilot-main-post injections [37] and double pilot injections [38, 39].

A short discussion is provided below showing some of the prominent literature in chronological for IC engine related split injection work in the past.

Tow et al. [Tow et al. 1994]

- For a split injection case particulate reduction by a factor of three, with no increase in NOx and only 2.5% increase in BSFC compared to single injection, were found at a 75% load.
- For a triple injection case particulate reduction by a factor of two with no increase in NOx and only a 1.5% increase in BSFC was found at a 75% load.

Han et al. [Han et al. 1996]

- Using CFD concluded that there is replenishment of the spray tip caused by the introduction of the subsequent injection, leading to leaner combustion and thus avoiding the soot-producing rich regions
- A single injection made later in the cycle (retarded injection) has a similar reduction in the NOx

Nishimura et al.[Nishimura et al. 1998]

- Pilot injection cause better ignition and this ignition can be controlled. This leads to a smoother rate of heat release
- Pilot injection is a good technique for reducing NOx and combustion noise
- An increase in smoke is observed due to poor (richer) creation of mixture after pilot combustion

Badami et al. [Badami et al. 2003]

- For reducing the combustion noise and not sacrificing fuel usage efficiency a pilot-pilot-main injection strategy is more effective but results increase in emissions

- Pilot-main-after can be used to reduce soot with careful selection of the timing at which the after injection is introduced. (After injections are different from post injection. After injections are solely for emission reduction in after-treatment devices and are introduced late in the combustion cycle and do not lead to power production)
- The introduction of closely couple injection causes pressure disturbances in the common rail

Hotta et al. [Hotta et al. 2005]

- Combustion noise benefits observed at medium load conditions by dividing early injection into a series of smaller injections, which also reduces wall wetting
- An increase in HC emission and decrease in smoke observed in light load and low speed conditions
- An after injection cause reduction in HC, smoke and fuel consumptions

Hardy and Reitz [Hardy and Reitz 2006]

- Reduction in HC and NOx with increase in PM, CO and BSFC observed with a pilot injection
- The BSFC decreases with no significant variation in PM, NOx, CO and HC emissions as the pilot is injected for longer durations
- Decrease in CO, PM and BSFC and increase in HC and NOx observed with advancing the main injection
- Pilot-main-after injection strategy is better suited for emission reduction than the pilot-main strategy

Ehleskog et al. [Ehleskog et al. 2007]

- A decrease in CO, PM emissions and increase in NOx and fuel efficiency observed when the main injection is further injected as two injections

- No change in combustion duration was seen but a mere division of heat release from the original peak shape to the a gradual division of peak in later stage of heat release was observed
- Dividing number of main injections to three or four only increased the PM, CO and HC with a reduction in NOx

Thurnheer et al. [Thurnheer et al. 2011]

- With advancing the pilot injection a decrease in fuel conversion efficiency is observed
- Reducing the pilot fuel mass reduces PM
- Centre of combustion and the peak heat release rate are not affected by the post injection mass as well as timing

O'Connor and Musculus [O'Connor and Musculus 2013a]

- With low EGR conditions i.e by having higher oxygen intake (18% and 21%), post injections reduce soot
- With high EGR conditions i.e by having lower oxygen intake (12.6% and 15%), post injection also reduce soot
- One of the core mechanisms of soot reduction is fluid mechanic in nature.

O'Connor and Musculus [O'Connor and Musculus 2013b]

- After reviewing in detail the post injection efficacy in causing soot reduction, O'Connor and Musculus [O'Connor and Musculus 2013b] found some interesting trends as in Fig. 12.

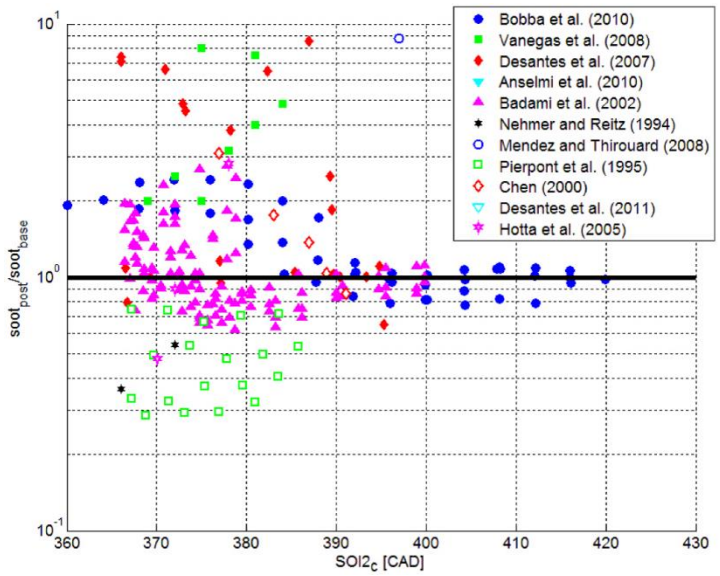

Figure 12: Post injection efficacy in soot reduction has not been established from engine experiments given the large variations in the soot reduction scatter. Figure from [O'Connor and Musculus 2013b]

- This basically means a detailed understanding of how the post injection reduces soot is necessary, since there are almost equal chances for the post injection to increase the soot production too.

Split injection strategies also function as promoters of partially premixed combustion regimes [Kim et al. 2007, Tanov et al. 2014, Zhang et al. 2015], where the first injection creates the necessary mixture stratification for the next injection to combust. Taking advantage of the stratification created by the pilot combustion[Tanov et al. 2014], a cleaner partially premixed combustion can be achieved [Kalghatgi et al. 2010, Manente et al. 2011, Manente et al. 2010]. Fig. 13 shows a conventional diesel combustion in a Lambda-Temperature (λ-T) and a λ-T diagram for the premixed combustion with early injection. Substantial reductions in soot along with some reductions in NOx can be realized from this conceptual chart.

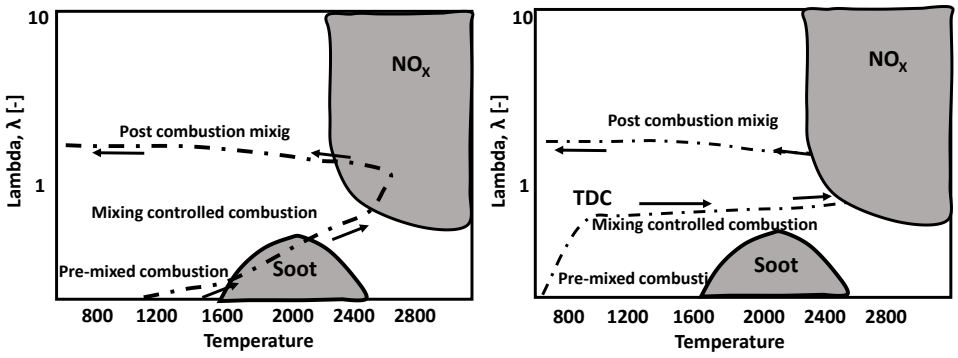

Figure 13: Conventional diesel combustion (left), premixed combustion with early injection (right). Figure adapted from [Thygesen 2012]

An effective strategy for combusting sprays has been focused on engine-out emissions in the wealth of the literature and little focus has been on emissions from flame studies under quiescent state in engine like conditions. Such a study would give more understanding of the interaction phenomenon and conclusive results for planning a better course of action with respect to the split injection strategy implementation in IC engines.

CHAPTER 5

CFD SIMULATIONS DETAILS

As part of this PhD work, split injection sprays were investigated both numerically and experimentally. This chapter deals with the different aspects of CFD simulations viz., spray modeling, turbulence modeling, combustion modeling (TCI and non-TCI discussion), emissions modeling, chemical mechanism selection, typical simulation setups and best practices which were utilized in running spit injection CFD simulations. Converge CFD code has been utilized to perform CFD simulations [Richards et al. 2012].

2.5 Spray modeling

Liquid injection can be modelled as various distributions (as injected from nozzle exit) along with different discharge coefficients and rate shapes. The most important sub-model in the spray model, however, is the break-up model; modified Kelvin-Helmholtz- Rayleigh Taylor (KH-RT) with no break-up length model being the one used in spray calculations of this work. Interaction of the droplets with the walls and other droplets in the field is also modelled along with droplet vaporization. The No Time Counter (NTC) collision method of Schmidt and Rutland [48] is used as collision model in the simulations. The NTC model has a computational cost that is linear with the number of spray parcels, while traditional models have a cost that increases with the square of the number of parcels. This paves the way for the usage of the NTC model for a better representation of a spray due to more parcels being used to represent a given amount of injected fuel. At the time of collision, the outcome is predicted to be bouncing, stretching separation, reflexive separation, or coalescence based on the conditions at impact [49]. A multi-component vaporization model can be incorporated in Converge calculations. The basis of the multi-component model is the Frossling correlation which calculates the time rate of change of drop radius based on the laminar mass diffusivity of the fuel vapor, a mass transfer number, and a Sherwood number. All these come within the realm of Lagrangian spray modelling, which is used in the present work. Eulerian spray modelling is another approach of spray modeling and has recently come in the interest of various researchers in accurate modelling and coupling of internal nozzle flow with near nozzle flows.

Table 1 shows the important spray sub-models chosen for throughout the present work.

Table 1: Spray sub-models used

Spray sub-model	**Chosen model**
Injection distribution	Blob model (No distribution) [Reitz and Diwakar 1987]
Spray Breakup	Modified KH-RT [Patterson et al. 1994]
Discharge coefficient model	Dynamic calculation of Cv
Drop drag	Dynamic drop drag [Liu et al. 1993]
Collision model	No-time counter [Schmidt and Rutland 2000]
Collision outcomes model	Post [Post and Abraham 2002]
Drop turbulent dispersion	O'Rourke [Amsden et al. 1989]
Drop/wall interaction	Rebound/slide model [Gonzalez D et al. 1992]
Evaporation model	Frossling model [Amsden et al. 1989]

2.6 Turbulence modeling

The prediction of turbulent diffusivity and therefore the vapor phase diffusion has a direct impact on the flame propagation and combustion characteristics. It is due to the fact that, in simulations involving spray injection in high temperature-pressure ambient conditions, the thermal field is highly coupled with flow dynamics. Thus, turbulence modeling also plays an important role in emission predictions, especially to predict thermally sensitive species such as NOx and so is worth discussing briefly further.

The main turbulence models can be classified as RANS and LES. In a RANS modeling concept decomposition of the field into ensemble mean and fluctuating component takes place and is temporally averaged whereas in an LES concept decomposition into a resolved field and a sub-grid field takes place with spatial filtering.

In the context of RANS simulations, in the engine community, two equation k-ε models are widely used for modeling vapor phase turbulent diffusion and its combustion [Amini and

Khaleghi 2011, Han and Reitz 1995, Rutland et al. 1995, Senecal et al. 2014, Som et al. 2012]. The two equation k- ε models are easy to solve, converge pretty fast, are robust and stable numerically, with the ability to obtain solution for large domains involving high Reynolds numbers, and at the same time do not cost much in computational expense. All the above said features of a model are key to its usage in industrial CFD applications. Among the family of k-ε models, the RNG k-ε model of [Yakhot et al. 1992] has been a considerable improvement over the prevalent standard k-ε models of the mid-1990's. But, the original RNG k-ε model by [Yakhot et al. 1992] was introduced for incompressible flows. Later on, Han et. al [Han and Reitz 1995] improved the Re-Normalization Group (RNG) methodology of from the original RNG k- ε model [Yakhot et al. 1992] accounting for the variable-density engine flows, calling it a modified RNG k-ε model. The modified RNG k-ε model takes into account the compressibility effects. Successful implementation of the RNG model was performed by Han et. al [Han and Reitz 1995] and Rutland et. al [Rutland et al. 1995] for diesel spray combustion modeling. The success of the application of the modified RNG k-ε model to diesel spray modeling in engine conditions lends itself to the fact that the ratio of the turbulent to mean-strain time scales is considerable due to spray-generated mean flow gradients, and the model now includes a term to account for these effects. Applications of these models in other modern engine CFD simulation tools have been performed recently by Som et. al [Som et al. 2012] and comparison with results from corresponding large-eddy simulations (LES) revealed success in their usage. In non-engine communities, two equation k-ω based models especially the SST k-omega have become famous. k-ω based models take into account the principal turbulent shear stress in the transport equation for the k term whereas blending functions and a cross diffusion term are considered to model the dissipation rate in far field and near wall respectively, which go in the omega (ω) calculation. The SST k-ω model is mostly effectively for high accuracy boundary layer simulations but has not been extensively used and validated for diesel spray combustion simulations. Due to the promising results shown by the engine community in using the modified RNG k- ε models, the present work chose the modified RNG k- ε model.

In the context of Large Eddy Simulations (LES), usually a resolved and sub-grid field is discussed. When considering a velocity field, the resolved part of velocity would represent

the large-scale eddies whereas the sub-grid part of the velocity field would represent small scale eddies. The effect of the small scale eddies on the large scale eddies is considered by sub-grid scale modeling. LES models can be broadly divided into two classes: zero-equation and one-equation. The one-equation solves for the transport equation but the zero-equation does not. The sub-models in the zero equation models class (available in converge) are: upwind LES, Smagorinsky model, dynamic Smagorinsky model; and the one equation models are: one equation viscosity model, dynamic structure model, consistent dynamic structure model. In some portion of the present PhD work, one equation dynamic structure sub-grid LES turbulence model is used.

2.7 Combustion modeling

To validate a CFD model, it is necessary to consider accurate predictability of important target outcomes like ignition time of fuel-air mixture, flame stabilization location, heat release from the combustion event, target species level and spread across the spray-flame domain. Nevertheless, the strength or weakness of a model (and associated sub-models) needs to be kept in mind before making conclusions. This is further more important, since the present work identifies the occurrence of a different ignition and flame stabilization behavior for the first injection and the subsequent injections, which calls for an in-depth understanding of the fundamental model assumptions.

Spray simulations in engine scenarios are of high Reynolds numbers. Particular emphasis is put on reactive spray simulations here. These simulations are solved using RANS or LES methods where the turbulence equations are solved for average or filtered quantities respectively. In some of the spray combustion scenarios, it so happens that the timescales of the fluid flow overlap with the timescales of the chemical rate of reactions [Peters 2000]. Thus, when solving a spray combustion problem, chemistry and flow (turbulence) cannot be separated, since they actually occur simultaneously in similar time scales. This is the idea behind considering a turbulence-chemistry interaction in reacting flow simulations. In the context of numerics, a closure for the chemical source term needs to be considered. This closure has been one of the major challenges due to the non-linearity of chemistry (obeying Arrhenius-type exponential expression). Not only that it is a challenge, but also the concept of applying a TCI for diesel spray combustion problem has been debated in literature. With

a well-defined target conditions, Engine Combustion Network [Pickett et al. 2014b] has been a major player in investigating diesel reacting sprays in the context of experiments and help the modelers build physically accurate predictive CFD tools. From ECN2 to ECN4 workshops there has been a tremendous improvement in the CFD modeling side. Overall, a TCI closure necessity has not been established yet but utilization of non-TCI models have given inferior results in context of RANS. Using high-fidelity LES models have been found to bridge the gap since the sub-grid fluctuations have been well treated in LES models [Pei, Som, Kundu, et al. 2015, Pei, Som, Pomraning, et al. 2015].

In a non-TCI model the mean chemical source term is calculated using the mean temperature and composition with no consideration of turbulent fluctuations. This approach is come across by many names in the literature as well-mixed (or perfectly stirred) reactor, CHEMKIN models (detailed chemistry) and direct integration. In spite of the physically inadequate assumption in a non-TCI model, various studies have successfully applied them for diesel engine conditions [Han et al. 1996, Moiz et al. 2015, Senecal et al. 2014, Singh et al. 2006, Som et al. 2012, Vishwanathan and Reitz 2010, Wang et al. 2013]. A role of flame propagation, turbulent mixing, and volumetric heat release in diesel spray combustion has been discussed in Ref. [Kokjohn and Reitz 2011]. Sound arguments of diesel combustion being volumetric heat release governed were made which pushed the TCI treatment as a secondary consideration.

In contrast to a simplistic non-TCI model, the TCI family of combustion models have been applied to diesel engine conditions from the early 90's, especially after the introduction of flamelet based models. Some of the TCI models in present use include flamelet models [Pitsch et al. 1996], transported probability density function model[Pope 1985], conditional moment closure model [Klimenko and Bilger 1999], progress variable model[Pierce and Moin 2004], flamelet generated manifold model [Oijen and Goey 2000] , flame surface density based models (including ECFM3Z) [Tap and Veynante 2005] [Colin et al. 2003] and partially stirred reactor model [Golovitchev et al. 2000]. Two of the popular and fairly successful TCI models, flamelet model and transported PDF model, have been briefly explained further.

The most used TCI model was the one of RANS based laminar flamelet model developed by Peters [Peters 1984] as steady laminar flamelet model. This was extended to use a LES turbulence modeling approach [Pitsch and Steiner 2000]. In spite of this, the inherent deficiency in the flamelet models has been that, the cross scalar dissipation rate does not have an accurate closure with the simplified expressions being employed.

The transported PDF method [Pope 1985] has been proved to be a pretty accurate solution methodology. A good review of this has been presented in Refs [Haworth 2010, Pope 2001]. This approach solves the transport equation for the one-time one-point joint PDF of velocity and composition (in some cases composition only). In this approach, no closure problems arise. This is due to non-linear terms resulting from averaging of one-point quantities pertaining to chemistry. But this is also the reason why application of this method is very time consuming. Nonetheless, this model has been successfully applied for diesel spray combustion cases [Pei, Hawkes, et al. 2015, Pei et al. 2013a, b, Bhattacharjee and Haworth 2013].

In purview of CFD of split injection spray combustion, prior work has been done in both the TCI and non-TCI communities. In the TCI community, a flamelet model has been well studied, developed and applied [Doran et al. 2012, Felsch et al. 2009, Hasse and Peters 2005, Moiz et al. 2015]. For split injection, a conditional moment closure model consisting of a sequential two-feed system (not a conventional three-feed system) was also developed [Bolla et al. 2014]. Usage of a non-TCI modeling approach based on well-mixed type models have also been prevalent and yielding satisfactory prediction. Prior works using these models come from the Engine Research Center of University of Wisconsin-Madison (ERC). As discussed in these references [Han et al. 1996, Hessel et al. 2014], split injections replicated the in-cylinder heat release with very good accuracies. Various assessment studies for performance or applicability of various combustion models for single injection spray combustion have been done in the past [D'Errico et al. 2014, Pei et al. 2013a, Singh et al. 2006]. The conclusions of such studies stress on the consideration of TCI based models which fared better in a few aspects such as low temperature combustion (~800 K) and species spread, although no drastic difference in simulation outcomes was reported with a non-TCI based modeling approach. An assessment study pertaining to split injection spray

combustion was performed in this PhD work [Moiz et al. 2015] involving various popular combustion models to gauge their applicability, which will be presented in the discussions further.

2.8 Soot modeling

Since studying the soot formation is one of the main aspect of the dissertation, the two step soot model utilized is discussed further. The present work uses a Hiroyasu model [Hiroyasu and Kadota 1976] to simulate soot formation and Nagel Strickland-Constable (NSC) model [Nagle and Strickland-Constable 1962] to simulate soot oxidation. The net soot formation is a competition between soot formation and soot oxidation. The Hiroyasu model is a single step model given by Equation 1 as

$$\dot{M}_{sf} = A_{sf} P^{0.5} \exp(-\frac{E_{sf}}{R_u T}) M_{form} \quad (1)$$

Where $\dot{M}_{sf}$ is the soot formation rate in grams/sec, M_{form} is the mass of soot formation species (C_2H_2) in grams, P is the cell pressure in bar, R_u is the universal gas constant in cal/(Kgmol), T is the cell temperature in K, E_{sf} is the activation energy in cal/gmol, and A_{sf} is the Arrhenius pre-exponential factor with units of 1/(s $bar^{0.5}$). Thus, as soon as C_2H_2 starts forming, there will be some presence of soot detected in the computational cell.

The NSC soot oxidation model is a single step model given by Equation 2 as

$$\dot{M}_{so} = A_{so} \frac{6 M_s}{\rho_s D_s} R_{total} M w_c \quad (2)$$

$\dot{M}_{so}$ is the rate of oxidation of soot species, Mw_c (g/mol) is the molecular weight of carbon, A_{so} is a scaling factor, M_s is the total soot particle mass in grams, ρ_s is the soot density in gram/cm^3, D_s is the nominal soot particle diameter, R_{total} is the net reaction rate (which is a

function of partial pressure of O_2 and Temperature) and Mw_c is the molecular weight of carbon in g/mol.

Although, RANS model along with Hiroyasu-NSC model was not found to correlate well with quantitative soot data (from laser extinction imaging) [Skeen et al. 2016], it is used here to qualitatively understand the mechanism of soot production.

2.9 Chemical kinetic mechanism

Simulation work of the dissertation used single surrogate chemical kinetics of diesel. In some of the works (chapter 9, 10) n-Heptane was used as a (chemical surrogate) representation of diesel fuel where the reacting spray simulations employed a reduced n-heptane mechanism consisting of 42 species and 168 reactions from Chalmers University [Nordin 1998]. This mechanism is validated in the past [Som et al. 2012] for a range of constant volume spray-combustion condition as shown in Fig. 14.

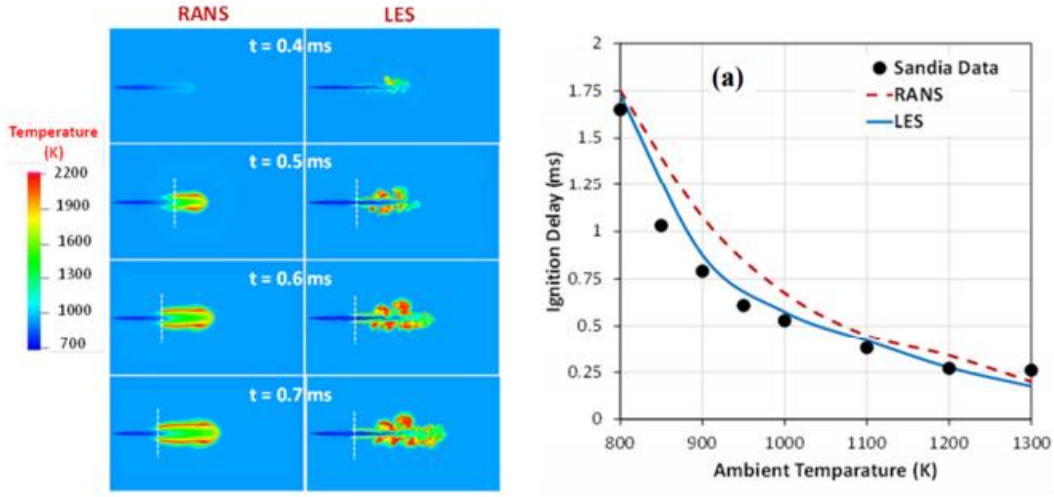

Figure 14: Using the 42 species n-heptane mechanism (Left) comparison of lift-off length with experiments and (right) validation of ignition delay [Som et al. 2012]

In some other works (chapter 13,14), n-Dodecane was used consisting of 54-species, 269-reactions [Yao et al. 2015]. The 54 species mechanism is developed to predict the pyrolysis and oxidation of diesel (chemically represented by n-dodecane) at both high and low temperature conditions. It is a skeletal mechanism derived from JetSurF mechanism (USC)

and was also tuned to simulate 3-D spray combustion in constant volume combustion conditions to validate against experimental data from the Engine Combustion Network (ECN) community as shown in Fig. 15.

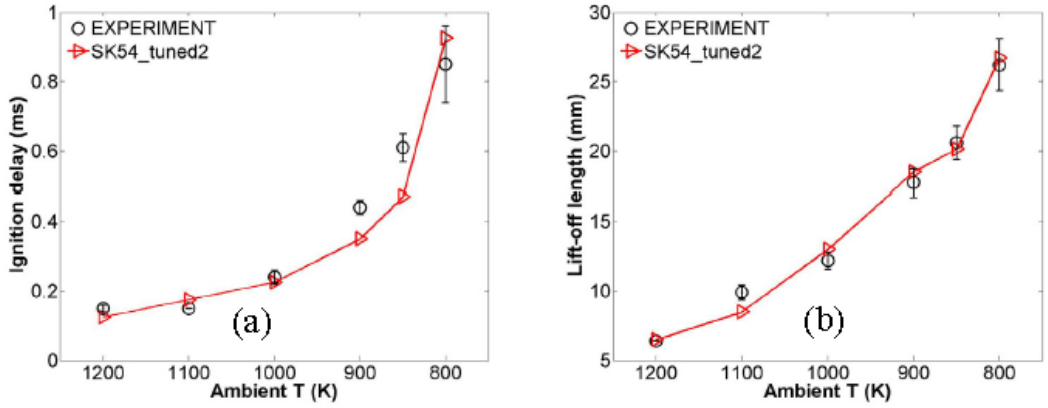

Figure 15: Ignition delay and LOL vs. ambient temperature predicted by the 54 species mechanism and validated against experiments. Figure from Ref. [Yao et al. 2015]

Both these chemical mechanisms resulted in good predictions for the combustion of the first injection and also the second injection's combustion

2.10 Best practices and typical simulation setup

Setting up of a properly validated non-reacting spray is pivotal for establishing the right mixture presence before ignition and eventual combustion in a reacting spray. Also, as part of the best practices for running any numerical simulation, grid convergence should be established. A series of logical steps were charted out, as discussed in length in chapter 10, so that the numerical spray can be finely tuned to the experimental spray especially with respect to non-reacting spray parameters of liquid and vapor penetration length. The importance of selecting the particular parameters for tuning the sprays is emphasized in Refs. [Bravo et al. 2014] and [Senecal et al. 2014] and in the global sensitivity analysis carried out in Ref. [Pei et al. 2014]. A typical simulation setup employed as employed in this work is shown in Table 2.

Table 2: Typical simulation setup used in this work

	RANS Modeling	**LES Modeling**
Modeling Tool	CONVERGE v2.3	CONVERGE v2.1
Dimensionality and grid	3D, Adaptive Mesh Refinement	3D, Adaptive Mesh Refinement
Smallest and largest characteristic grid sizes	Base grid size: 2 mm Finest grid size: 125 µm Gradient based AMR on velocity and temperature fields Fixed embedding in the near nozzle region: 125 µm	Base grid size: 1 mm Finest grid size: 62.5 micron Gradient based AMR on velocity and temperature fields Fixed embedding in the near nozzle region: 62.5 micron
Turbulence	RNG k-ε model	Dynamic structure LES model
Spray sub-models	Injection: Blob Breakup: KH-RT Collision: No Time Counter Drag-law: Dynamic model Evap.: Frossling correlation	Injection: Blob Breakup: KH-RT Collision: No Time Counter Drag-law: Dynamic model Evaporation: Frossling correlation
Spray model constants	B_0 = 0.8, B_1 = 11.67, C_1 = 0.188, C_t = 1, C_{RT} = 0.1	B_0 = 0.61, B_1 = 4.0, C_1 = 0.188, C_t = 1, C_{RT} = 0.1
Turbulence model constants	$C_{\varepsilon 1}$ = 1.42, $C_{\varepsilon 2}$ = 1.68, β = 0.012, η_0 = 4.38	C_{tke_les} = 2, $C_{tke\_visc\_les}$ = 1, C_{eps_les} = 1
Soot model	Hiroyasu (C_2H_2 - soot precursor)	Hiroyasu (C_2H_2 - soot precursor)
NOx model	Extended Zeldovich	Extended Zeldovich

CHAPTER 6

EXPERIMENTAL TECHNIQUES

This chapter introduces some experimental details before moving forward to the results and discussions section where various findings are presented. The main aspects covered are about the injection system, rate of injection testing, combustion vessel introduction, explanation of various optical diagnostics and the image processing technique.

2.11 Injection system overview

The fuel injection system comprises of a high-pressure (>3500 psi) liquid pump, two accumulators and an injector. The fuel injector used in this study is an electronically controlled solenoid activated singe-hole injector designed by Bosch. It is placed in one of the windows of the constant volume combustion vessel with its single hole oriented in the center of the chamber. The salient features of the injector are the control needle, the solenoid, the main needle, and the fuel supply and return lines. Fig. 16 shows a schematic of the injector with the various passages.

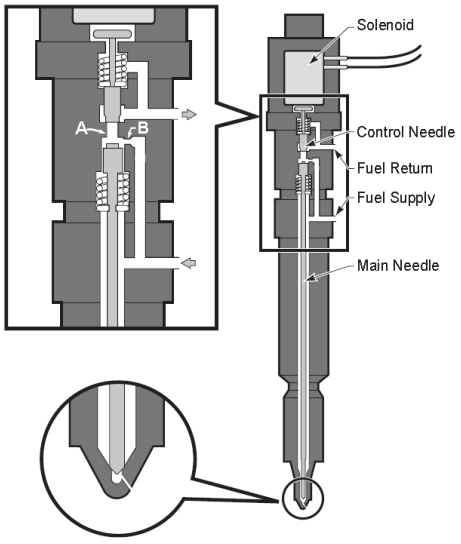

Figure 16: Schematics of the common-rail fuel injector [Naber and Siebers 1996]. Reprinted with Permission from SAE International

As the solenoid is electronically activated the control needle is lifted from its seat. This opens the orifice above the main needle. This causes the fuel to flow from the supply lines into an orifice connecting to a small chamber above the main needle. Any excess fuel cause it to overflow from above the main needle into a return line. Since this orifice is larger than the orifice through the nozzle hole, it has much less line pressure. This causes an imbalance of the force on the main needle, causing it to lift from it seat and result in fuel injection. On electronic deactivation of the solenoid, the control needle is reseated, no pressure difference in line exists now (with the fuel pressure above control needle at supply pressure) and the injection is ceased.

Fig. 17 shows a photograph of the diesel fuel injection system used in the tests. Two accumulators present upstream of the injector supply the fuel. The accumulators are placed in series. The accumulators have 100 mg fuel in them to limit the pressure loss during the injection event. The pressure loss with the accumulators is estimated to be less than 1%. The injection pressure was measured using a Kistler model 607L piezoelectric pressure transducer combined with a Kistler model 5010B charge amplifier and a 60 kHz low pass filter.

Figure 17: Diesel injection system in CV lab

2.12 Rate of injection testing

Rate of injection testing was performed using a momentum flux measurement device as shown in Fig. 18.

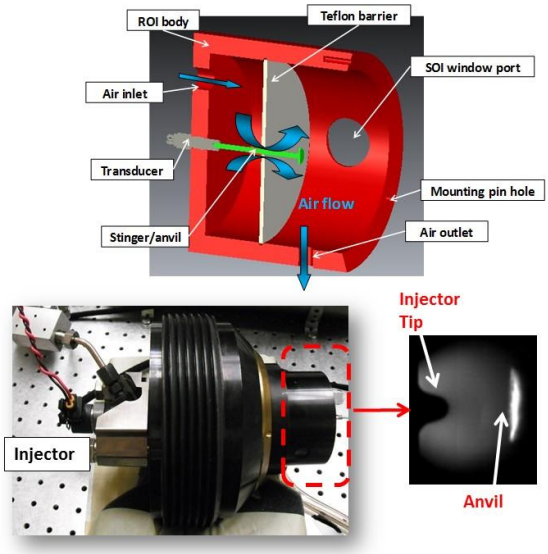

Figure 18: Rate of injection measurement device. Close of injector tip and anvil

Injection was performed in a small enclosed cubic chamber at atmospheric pressure with the injected spray impinging on an aluminum anvil attached to the force sensor. A Kistler 9215 force sensor, which is capable of precise force measurements from the injected impacting spray (2 N to 200N), was used for momentum flux measurements. A Kistler 5010B charge amplifier amplifies the signal output from the force sensor and the resultant signal is recorded in an oscilloscope. Using momentum relationships, the mass flow rate of injection is back calculated.

Force measurements were repeated 100 times for each injection schedule and the data were later averaged and filtered as shown as a sample in Fig. 19.

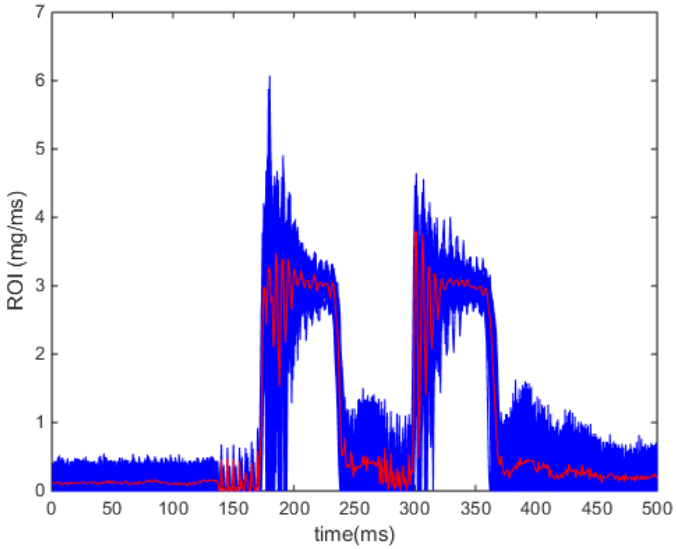

Figure 19: A 0.5.0.5/0.5 ms injection strategy. Blue lines are the 100 raw ROI profiles. Red line is the average of the 100 raw ROI profiles

The steps taken to obtain the mean ROI are presented below.

- Sampling rate is kept 500 kHz
- 100 injections are considered for each injection strategy
- Take 100 ROI voltage profiles coming from the DAQ
- Offset each ROI voltage profiles with the initial mean voltage value until the start of injection signal
- Take average of these offset voltage profiles
- Using a 'moving average filter on 15 points' make a filtered voltage signal
- Convert the filtered voltage signal to ROI (mg/ms) profiles using force transducer sensitivity and charge amp setting

Slight signal fluctuations, due to the sudden impact of the injecting liquid on the anvil, are observed as the spray first hits the anvil orthogonally. After approximately 0.15 ms, the force from the spray is relatively steady and outputs as a proportional charge from the force sensor. As the injection ends, the anvil tends to settle down with back and forth fluctuating movements due to its inertia and so minor fluctuations in the output signal are seen during the dwell time and after the main injection.

A single-hole solenoid injector (Injector# 375020) from the ECN community[Pickett et al. 2014b] was used to create split injections using a MOSFET driver. To generate split injections, electronic commands from another ECN injector (#210370) were chosen as a baseline. Split injection tests were performed for the injector #210370 by Skeen et al.[Skeen et al. 2015b] in the past. The commands for the MOSFET driver were adjusted to match the corresponding current profiles of injector #210370. This exercise would facilitate future data comparisons and would be helpful to the modelers and the ECN community.

Fig. 20 shows a sample ROI where the injection duration and dwells were matched with Sandia data. The height of the ROI is not the same since Sandia has used a different injector with a slightly larger nozzle diameter. The bumps seen during the dwell time in the MTU data may be anvil reflexes after the spray hits and shuts down. The bumps are also observed to some extent in Sandia data.

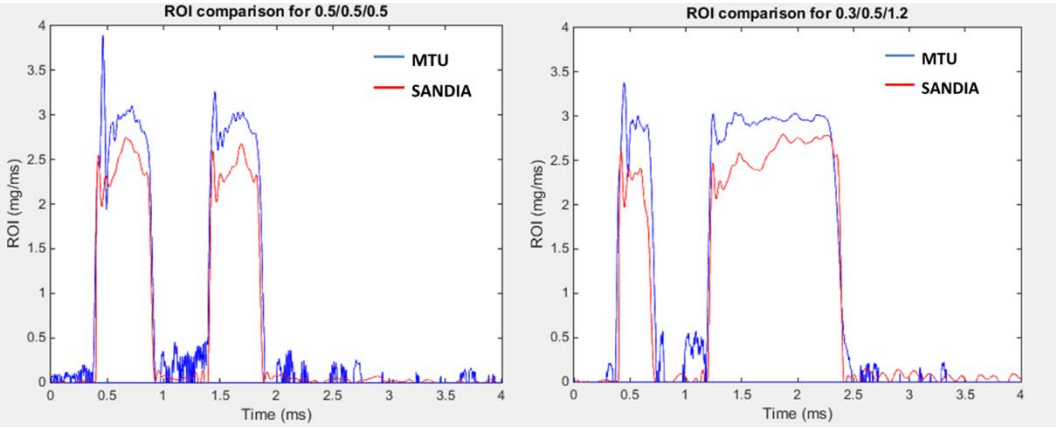

Figure 20: ROI comparison with Sandia and MTU data to obtain similar injection duration and dwell times

Injector commands have smaller durations than the hydraulic fuel delivery in solenoid injectors. For split injection events, extra care is to be taken to set the commanded duration of the subsequent injection due to rail pressure oscillations. For e.g. an injector command of 378-652-382-µs was used to generate an ROI for a 0.5/0.5/0.5-ms injection sequence of n-Dodecane injections at room temperature conditions with an injection pressure of 1200 bar. The difference in the pilot and main TTL durations in the command sequence of 378-

652-382 is due to the interactions among the individual splits during the injection event within an injector. These interactions increase for close-coupled injection strategy and are alleviated as the dwell times increases [Wang et al. 2015]. It was found by Wang et al.[Wang et al. 2015] that the main injection tends to be shorter while maintaining similar level of rate of injection if equal TTL signal commands were given. This was also observed in the present work. Thus, to maintain similar injected masses between the pilot and main, the TTL signal duration for the main injection was set to be slightly higher (382 μs) when compared to the pilot injection (378 μs).

While there is some uncertainty in making this type of visual assessment of the injection duration, it appeared that the durations visualized from high speed images in actual testing are longer than those measured during the ROI experiments by about 0.15 ms and 0.2 ms for the first and second injections, respectively. The dwell time is also proportionally reduced by approximately 0.15 ms. The reason for this discrepancy is unclear yet, but a change in solenoid behavior is anticipated. The rate of injection testing has been done with fuel at atmospheric temperatures. Whereas the experimental testing has been done with the fuel temperature at 90^{o}C. In addition to potential impacts from viscosity of fuel at higher temperatures, the solenoid can also behave very differently at higher temperatures. This is the most plausible explanation for the mismatch of injection durations. It is to be noted, however, that the start of second (or main) injection occurs at the prescribed timing of 1 ms after start of the first (or pilot) injection. Thus, for performing the CFD work, an ROI profile for the visualized injection durations was obtained from the CMT ROI generator as shown in Fig. 21 for a 0.5-ms injection of pilot spray, a 0.5-ms dwell time, and a 0.5-ms main 1200 bar spray injection.

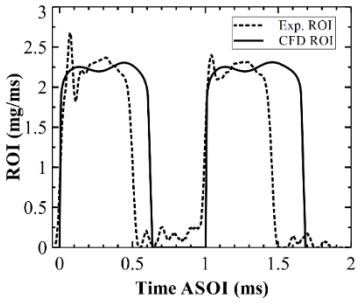

Figure 21: Experimental and CFD Rate of injection profile for 1200 bar injection for the 0.5/0.5/0.5-ms injection sequence

2.13 Combustion vessel overview

The constant volume combustion vessel at Michigan Tech has been built on a similar design as the one from Sandia National Laboratory [Naber and Siebers 1996]. MTUs combustion vessel is shown in Fig. 22. This combustion vessel is a 1.1 L constant volume combustion chamber and the chamber is cubical with an interior of 100 mm per side.

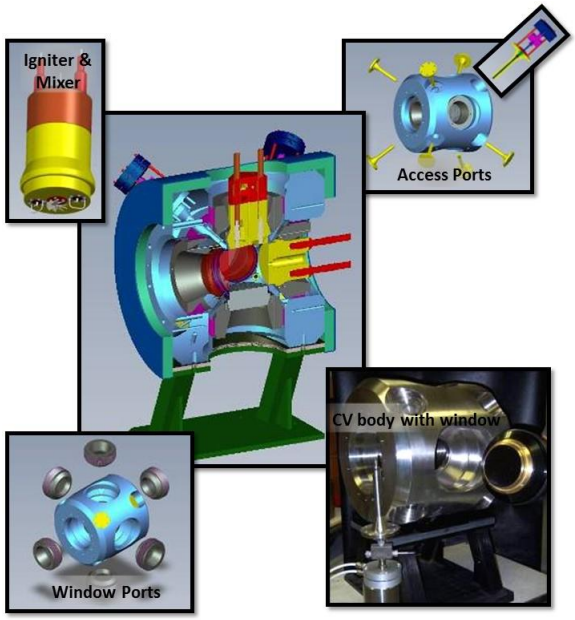

Figure 22: The constant volume combustion vessel with blown up views of access ports, windows and igniter

On each of the six faces of the cube are ports. In three of these ports windows are installed providing unobstructed orthogonal optical access to the combustion chamber. Optical windows provide access for high-speed imaging to study spray development. The top face port houses the spark plug assembly and two fans in order to create turbulence inside the vessel. A face port houses the injector assembly. On the eight vertices of the combustion chamber there are instruments located with actuator access ports. In four of these ports are an intake and two exhaust ports and a dynamic pressure transducer. The various prime components of the combustion vessel and the combustion vessel itself are shown in Fig. 22. The constant volume combustion vessel is the core of experimentation involving testing of injectors, visualizing spray and combustion phenomenon and spark-ignition characteristics. There are various techniques to visualize the spray structure to diagnose the various physical phenomena at a fundamental level using combustion vessels both qualitatively and quantitatively. They include using schlieren imaging [Naber and Siebers 1996], performing mixing measurement using planar laser induced exciplex fluorescence [Melton 1983] , predicting the ignition delay of a reacting spray using pressure measurements [Higgins et al. 2000], visualizing the reacting flame sheet using OH* chemiluminescence [Siebers and Higgins 2001], cool flame visualization by planar laser induced fluorescence (PLIF) [Skeen et al. 2015a], measuring the soot (PM) emissions using laser induced incandescence [Musculus and Pickett 2005] and obtaining ambient flow field information using particle image velocimetry [Ge et al. 2014]. The basis of a constant volume combustion vessel to create high temperature and pressure conditions present during the injection event in an internal combustion engine cylinder is by using a pre-burn event. A high-pressure and high-temperature ambient environment, replicating the thermodynamic conditions of a diesel engine, is obtained by burning a controlled premixed (reactant) gas mixture. This mixture is introduced at a predetermined pressure and then ignited by a spark while the combustion products are continuously mixed by means of a rotating fan inside the combustion chamber. By changing the initial reactant composition and pressure, the resulting combustion products can be controlled to simulate the ambient species that would be otherwise present in a range of diesel engine operating conditions. This combustion causes the chamber temperature and pressure to rise until the desired target thermodynamic condition is

reached, at which point the fuel is injected. Constant volume pre-burn type vessels such as the one used in this work have been well characterized as part of the ECN effort [Meijer et al. 2012]. Changes in ignition delay resulting from minor species remaining from the pre-burn event are small relative to those from major species of CO_2, H_2O, and O_2. A detailed description of the combustion chamber and other details about negligible effect of the resultant post pre-burn combustion gases on diesel spray ignition can be found in Ref.[Nesbitt et al. 2011].

Fig. 23 (left) shows the chemical composition of the reactants needed to be in the combustion chamber which when ignited create the necessary species in the products.

Products (composition at diesel injection time)					Reactants (prior to spark ignition)			
O_2	N_2	CO_2	H_2O	MW	rC_2H_2	rH_2	rO_2	rN_2
21	69.33	6.11	3.56	29.47	3	0.5	28.38	68.12
20	70.3	6.13	3.57	29.43	3.01	0.5	27.42	69.07
19	71.27	6.15	3.58	29.4	3.02	0.5	26.46	70.02
18	72.24	6.17	3.59	29.36	3.03	0.5	25.5	70.97
17	73.21	6.19	3.6	29.32	3.04	0.5	24.54	71.92
16	74.18	6.21	3.61	29.28	3.05	0.5	23.59	72.87
15	75.15	6.23	3.62	29.24	3.06	0.5	22.63	73.82
14	76.12	6.24	3.63	29.21	3.07	0.5	21.67	74.77
13	77.09	6.26	3.64	29.17	3.08	0.5	20.71	75.72
12	78.06	6.28	3.65	29.13	3.09	0.5	19.75	76.67
11	79.04	6.3	3.66	29.09	3.1	0.5	18.79	77.61
10	80.01	6.32	3.67	29.06	3.1	0.5	17.83	78.56
9	80.98	6.34	3.68	29.02	3.11	0.5	16.87	79.51
8	81.95	6.36	3.69	28.98	3.12	0.5	15.91	80.46
7	82.92	6.38	3.7	28.94	3.13	0.5	14.96	81.41
6	83.89	6.4	3.71	28.91	3.14	0.5	14	82.36
5	84.86	6.42	3.72	28.87	3.15	0.5	13.04	83.31
4	85.83	6.44	3.73	28.83	3.16	0.5	12.08	84.26
3	86.8	6.46	3.74	28.79	3.17	0.5	11.12	85.21
2	87.77	6.48	3.75	28.75	3.18	0.5	10.17	86.15
1	88.74	6.5	3.76	28.72	3.19	0.5	9.21	87.1
0	89.71	6.52	3.77	28.68	3.2	0.5	8.25	88.05

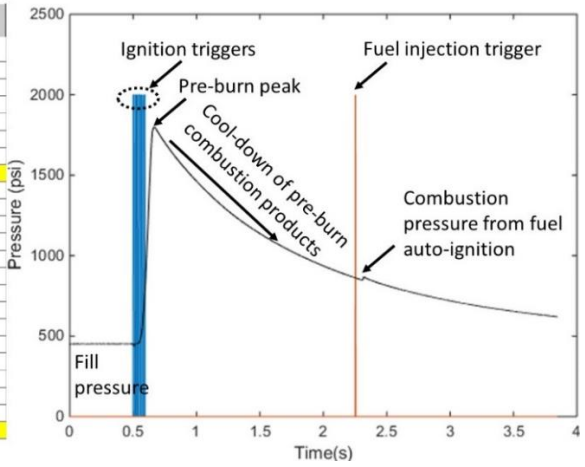

Figure 23: The matrix used to prepare a pre-burn mixture (left). The ignition- preburn and injection-spray-combustion events (right)

To achieve a proper temperature and pressure of the ambient species in the chamber, the chamber has to be filled with a set pressure labelled as 'Fill pressure in the Fig. 23(right) the pre-burn event which is necessary to create the high temperature pressure condition at the time of injection. Spark ignition events, typically 5, are used to trigger and ignite the combustible pre-burn mixture. As the peak is reached and the pressure in the chamber is reduced and the products cooled down, a fuel injection event is triggered at the right moment when the targeted pressure is reached. Usually a positive positive offset of 30 psi (called enable pressure) is given to make the pressure transducer ready to trigger the

injector. As the fuel injector is triggered, it takes some time for the injector (varies with solenoid, piezo, HEUI-type) to actually raise the needle and allow the fuel flow in chamber. This time is in addition to the reactivity time the fuel needs to get ignited. The net sum of these time create a time delay between fuel injection trigger and actual auto-ignition event of the fuel, after which there is another small peak origination from the combustion pressure rise from just the fuel burning in the ambient of the pre-burnt combustion products. In the Fig. 23 (left), two sample cases, one with 0% oxygen in the ambient and one with 15% oxygen in the ambient are highlighted. A 0% oxygen in the ambient is chosen to study just the vaporizing characteristics of the fuel. So no second combustion peak is created from the auto-ignition of fuel since there is no oxygen in the chamber to cause a combustion event. A 15% oxygen ambient is used to replicate an exhaust gas recirculation, since going from 21% oxygen in natural ambient to a 6% less value of 15% oxygen, implies exhaust gas presence in the chamber.

2.14 Optical diagnostics

There are various optical diagnostics used in the lab depending on the problem at hand. The commonly studied spray characteristics on a non-reactive spray are Mie scatter for liquid detection and Schlieren for spray-flame progress (boundaries). Mie scatter and schlieren are also used in a reacting spray test. Additionally, in a reacting spray, natural luminosity is used to qualitatively investigate soot presence, OH* chemiluninescence is used to measure the stabilization location of a spray flame called the lift-off length (LOL), planar laser induced fluorescence (PLIF) and planar laser induced incandescence (PLII) techniques are used to detect the presence of formaldehye and soot presence respectively. PLII combined with laser extinction imaging can reveal quantitative soot data. These methods are briefly explained below.

2.14.1 Schlieren and natural luminosity

A Schlieren/natural luminosity schematic is shown in Fig. 24. A Photron Fastcam SA1.1 high-speed camera operating at 37500 fps with a 26.67-us exposure time captures schlieren and luminosity images. During schlieren experiments, an LED (white 5500-K) (model number: HPLS-36AD3500) provides broadband collimated back-illumination by passing the source

through a converging lens and a pin-hole aperture before it is reflected from a 750-mm focal length, 152-mm diameter parabolic mirror.

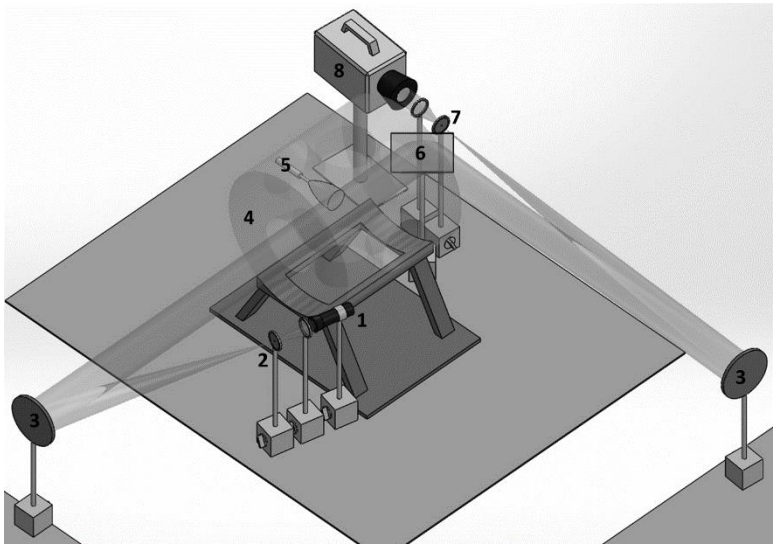

Figure 24: 1. LED light source 2. Pin-hole aperture 3. Parabolic reflector 4. Combustion vessel 5. Injector 6. Reflecting mirror 7. Schlieren stop 8. High-speed camera

After passing through the spray chamber, the schlieren light is reflected by a flat folding mirror toward a second parabolic mirror. The converging/diverging beam then passes through a partial schlieren stop, placed at the focal length of the parabolic mirror, before entering a negative bi-convex lens (F.L. 200 mm) and then the 85-mm f/2.8 Nikkor camera lens. The negative bi-convex lens acts as a focusing lens. An optimal schlieren stop of 10-mm diameter was determined by trial and error. The high speed camera is equipped with a 600-nm short pass filter to capture only the highest intensity flame and (hotter) soot emission. The image acquired had a projected pixel size of 0.156 mm/pixel. This constitutes the setup for the modified Z-type schlieren setup which is also used to collect light emission from the flame luminosity (majorly soot emission) through a spectral filter. If there is no flame i.e. if the experiment consists of a vaporizing (non-reacting) spray, then the 600 nm filter is taken away and this enables visualization of the entire visible spectrum to efficiently detect the schlieren boundaries. Detection of schlieren boundaries is key to define key target parameters of vapor penetration and jet spread angle. A sample of the raw schlieren

image is shown in Fig. 25. The image processing technique for boundary detection is explained in chapter 6.5.

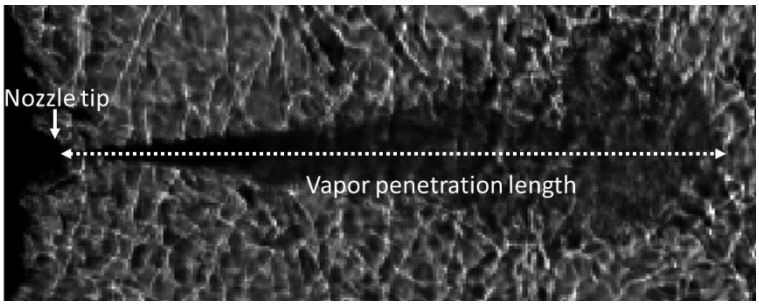

Figure 25: Sample schlieren image with nozzle tip and vapor penetration length marked

2.14.2 Mie scattering of liquid

Mie scattering is a technique originally proposed by Mie [Mie 1908] based on scattering of light when it passes through a transparent substance. In theory, the wavelength of the light should be smaller than the droplet diameter for Mie scattering to take effect. In present testing two pulsed light emitting diodes (LEDs), HPLS-36AD3500, are used to shine the liquid region of the injected spray, as shown in the Mie scattering schematic in Fig. 26. Uniformity in light spread throughout the liquid region is obtained by trial-and-error.

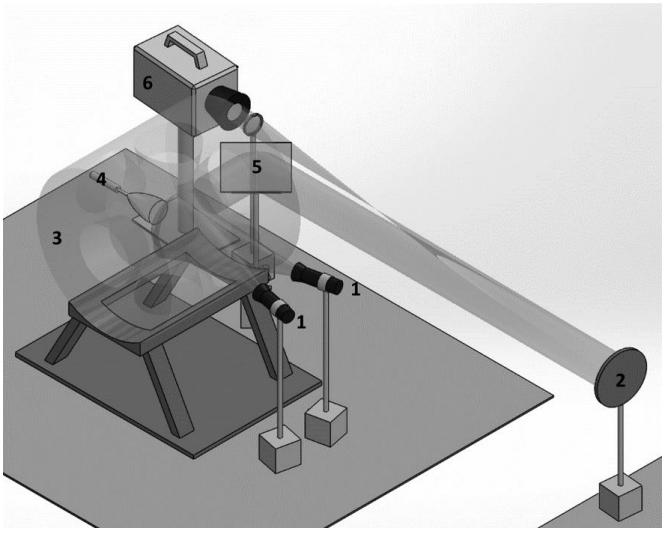

Figure 26: 1. LED light sources 2. Parabolic reflector 3. Combustion vessel 4. Injector 5. Reflecting mirror 6. High-speed camera

The pulsed LEDs are set to digital mode where they are operated as per a particular duty cycle, which means they are kept ON for a certain duration of the total pulse period. This results in higher intensity of emitted light. An analogue mode is also available to operate the LEDs, which renders it to stay ON all the time, which causes lesser intensity light when compared to the digital mode. The scattered light from the liquid droplets is reflected off the reflecting mirror and is directed into the high-speed camera after a reflection from the parabolic mirror. A concave lens in the front of the camera acts as a focusing lens. After the collection of the series of images from the injection sequence (which is a liquid jet), the images as post-processed in MATLAB to obtain useful information of liquid length measurement. Fig. 27 shows a sample of the visualized liquid jet from a single-hole nozzle.

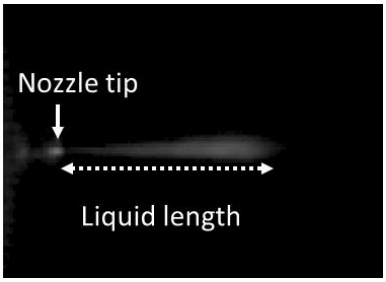

Figure 27: Sample Mie scatter image of liquid injection with nozzle tip and liquid length marked

Both Mie scattering and Schlieren can be used in tandem, which has been called as the 'Hybrid' imaging technique. Using a hybrid imaging technique reduces the number for recorded frames for each kind of image by 2. To avoid that, the targeted frame size can be reduced, but usually even after doing this, the temporal resolution is still quite low. With reduced temporal resolution in the image sequences, the liquid length or vapor penetration trends look 'patchy' and key information especially in the inception of the spray (when the spray travels faster) is lost. A good temporal resolution is far more important when the experimental measurements of liquid length and vapor penetration are to be used to validate a CFD model. The hybrid imaging technique is not used for majority of the present work.

2.14.3 PLIF/PLII

PLIF imaging setup used in this work is shown in Fig. 28. It also shows a modified Z-type schlieren setup which is often used together with PLIF imaging for a simultaneous acquisition. Fluorescence from formaldehyde (CH_2O) and polycyclic aromatic hydrocarbons (PAH) along the central plane of the spray axis is induced by a 54-mm wide, 0.4-mm thick sheet of 10-Hz (10-ns pulse) 355-nm light. The 355-nm pulses are generated from the third harmonic of an Nd:YAG laser with an average pulse energy of 95 mJ or a fluence of 0.44 J/cm^2 (whereas for PLII a 266-nm from the fourth harmonic is used). Previous work has shown that this energy fluence is sufficient to achieve saturation of the formaldehyde fluorescence [Juli 2002].

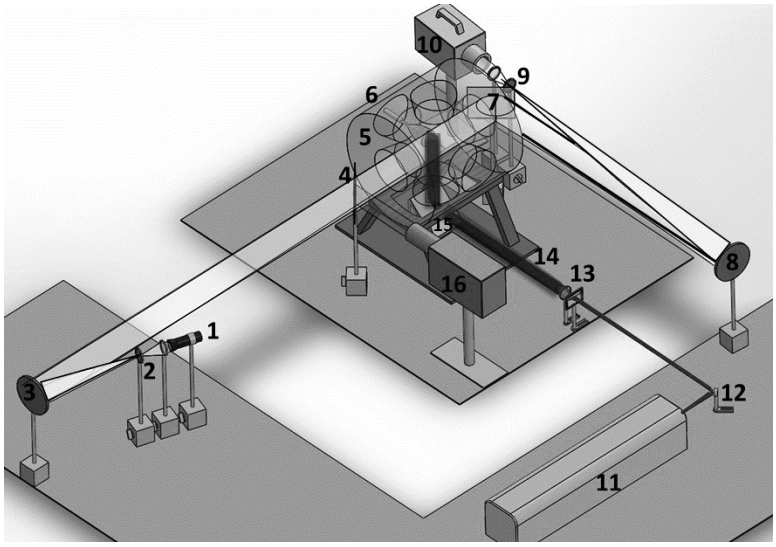

Figure 28: 1. Optical setup for simultaneous imaging of schlieren and PLIF diagnostics. Labels are as follows: 1.LED light source 2.Pin-hole aperture 3,8. Parabolic reflector 4. 50/50 beam splitter 5. Combustion vessel 6. Injector 7. Reflecting mirror 9. Schlieren stop 10. High-speed camera 11. Nd:YAG laser 12. Dichroic mirror 13. Spherical and cylindrical lens 14. Laser sheet 15. Laser power mirror 16.I-CCD camera

A gradually diverging (in width) laser sheet is formed by a set of spherical and cylindrical lenses. Before the laser sheet becomes too wide, the laser is reflected through the bottom vessel window by a 355-nm mirror. Fluorescence emitted from the spray flame is reflected

by the aforementioned 50/50 beam-splitter onto an I-CCD camera. The ICCD camera is equipped with a 400-nm (20 nm FWHM) bandpass interference filter to capture the fluorescence signal from the formaldehyde and PAH species. One of the advantages of the PLIF technique for formaldehyde detection consists of the fact that it can also detect PAH formation, since signal detection wavelengths for both species are close to one another.[Lachaux and Musculus 2007, Bruneaux 2008] Usually, PAH is formed at a different spatial location than formaldehyde which makes the PLIF technique useful to detect the formaldehyde presence and to differentiate it from the PAH signal.[O'Connor and Musculus 2013a] Also, PAH appears in a 'saturated' fashion. This is because, the formaldehyde signal is a lower magnitude signal and stops rising in intensity at a certain threshold, unlike PAH/soot signal, which can rise until higher magnitudes thus appearing saturated in a 355-nm PLIF image.

The laser timing diagram along with the double shutter openings of the ICCD camera is shown in Fig. 29.

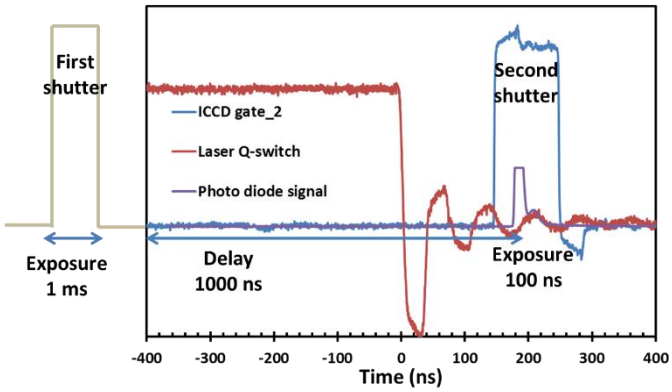

Figure 29: Laser timing diagram along with the ICCD camera shutter time

It is to be noted that, a 1 ms long exposed (chemiluminescence) image was also stored in the camera from the first shutter event. This image does not represent any fluorescence signal since there was no laser excitation of the spray combustion event at this shutter. The target shutter was the second shutter with a 100 ns exposure time and the laser was shot during the first half of the shutter duration. This was set on a trial and error basis to allow for maximum fluorescence signal, since fluorescence species take some time to absorb the

laser energy, rise to an exited state and then emit fluorescence light (PLIF signal) as they return to ground state. The laser shot was detected using a photo-diode with a 50 ohm resistor for higher sensitivity.

Fig. 30 shows the PLIF images taken along with a simultaneous schlieren image. Since PLIF was from a single shot ICCD camera and Schlieren was from high speed. A separate injection and pre-burn event was need to obtain each ICCD image to realize 3 repeats for the same test condition. But while one ICCD image was being taken, a high speed Schlieren movie was recorded for the whole injection-spray-combustion event. Fig. 30 also shows good repeatability of the PLIF images.

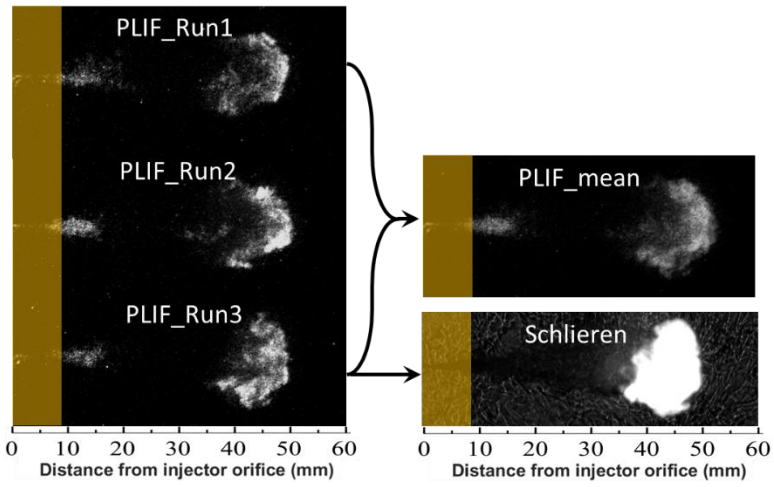

Figure 30: Sample raw image from formaldehyde PLIF with 3 runs (PLIF_Run1-3), their mean image (PLIF_mean) and Schlieren image corresponding to one of the PLIF runs (here PLIF_Run3). A shaded mask is shown covering the liquid length zone

2.14.4 OH^* Chemiluminescence

The emission from excited OH radical constitutes a chemiluminescence signal. It is captured by an Intensified CCD camera (DiCam Pro). A picture of the camera placement is shown in Fig. 28 as part of the PLIF/PLII optical setup.

The DiCam Pro camera has resolution of (horizontal x vertical) 1280x1024. It has a 12 bit A/D dynamic range. A Coastal optics UV lense (UV-MICRO-APO) of 105 mm focal length and f number of 2.8-4.5 is usually used to capture the chemiluminescence signal. The lens mounts

on the DiCam pro camera using a C-type mount unlike traditional F-mount for the high-speed camera. A conventional way of using the DiCam Pro is by using it in a simultaneous fashion with Schieren imaging. This way the light from the spray combustion event passes through the beam-splitter and is captured by the I-CCD chip in the camera. This arrangement is similar to the one shown in Fig. 28, except that the laser will not be active for an OH* chemiluminescence capture. The beamsplitters of 75/25 and 50/0 reflection/transmission ratios are available to use. In this study, a 50/50 beamsplitter is used. A band-pass filter (310 nm centered, 10nm FWHW) was used to obtain the OH* chemiluminescence. OH* chemiluminescence arises from the energy release from the reaction CH + O2 ->OH* + CO. The spectral peak of light emission from the energy release is near 308 nm. The reaction gives valuable information about high-temperature ignition processes and flame structure and can be considered as a marker of flame commencement slightly upstream from the stabilization zone [Kojima et al. 2000, Pickett and Siebers 2004]. The capturing of OH* chemiluminescence is done with a longer exposure time of close to 1.0 ms in the second shutter of the ICCD camera (cf. Fig. 29) during the quasi-steady portion of the flame. A 0.08-0.09 mm/pixel spatial resolution was obtained for various optical arrangement of the ICCD camera. An example of OH* chemiluminescence images is shown in Fig. 31. These long exposure times are reasonable to obtain an overall structure of the spray over its active periods which improves the statistics when determining stabilization location (LOL). Not many OH* chemiluminescence tests were performed for this thesis. Due to the low injection durations of the participating injections, there was not enough luminescence captured for the low exposure times the ICCD camera had to be set for.

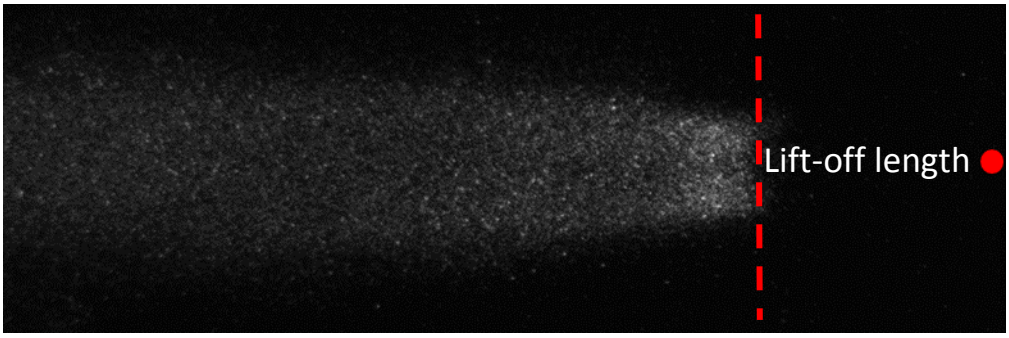

Figure 31: OH* chemiluminescence signal with the red dot as nozzle orifice location

2.14.5 Other

2.14.5.1 Pressure-trace based analysis

The pressure trace of the combustion event was recorded at a data acquisition frequency of 150 kHz using a pressure transducer. The signal from the pressure transducer is later amplified using a Kistler 5010B charge amp. Usually, the pressure signal recorded has some noise which arises when there are signal interferences through elecro-magnetic interaction between the electrical devices. This is generally termed as signal cross-talk which has to be further processed to get rid of noise.

In the Fig. 32, typical pressure curve processing steps are shown when there is signal cross-talk from other electronic and electrical circuits nearby. In Fig. 32, an interference of flash lamp and injector driver are cleaned.

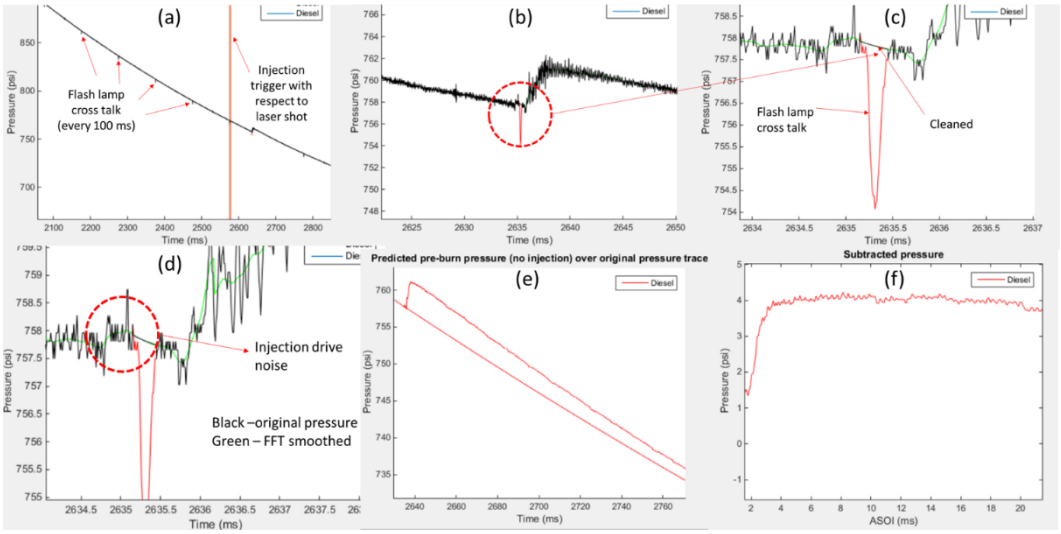

Figure 32: Process of cleaning the pressure trace to obtain heat release rate

Typically, the spark event, the injection trigger event and the flash-lamp from the laser operation are found to have cross-talk with the signal going from the pressure transducer into the charge-amp. The cross-talk can be easily avoided by shielding with an appropriate electro-magnetic signal shield which can be as simple as an aluminum foil. Some tests in the presented work had a clean pressure trace. But for some tests, when laser was being used, interferences from flash lamp and injection driver were observed, so cleaning had to be

done as shown in Fig. 32. A polynomial fit across the cross-talk region was employed. Since the flash lamp repeated its operation every 100 ms, one can know when the cross-talk actually happens. A Matlab code was made to catch this transient, place polynomial fit with 15 points before and after the center of this cross-talk dip and then replace the actual pressure curve with these points. For the injection trigger, sometimes a manual adjustment was made to replace the noise signal with a polyfit. Fig. 32 (e) is the pressure curve obtained after all this process. It is then subtracted by the fit on the slope of the pressure curve before any injection event happens. Fig. 32 (f) is the subtracted pressure curve which will be later used in calculations to arrive at heat release rate.

The pressure signal which is cleaned of any signal cross talk is used to convert to an apparent heat release rate (AHRR).A a mutli-step Fourier filter was employed to smooth the pressure trace. This smoothing was not done at one filter level throughout the signal. This is because, employing the same filtering parameters at high-temperature ignition (a high rate of pressure rise event) would over-smooth the pressure just prior to ignition time. Just prior to ignition, for low temperature cases as in this work, there is a first-stage ignition event where small-magnitude pressure rise or heat release from cool-flame reactions occur. Therefore, just prior to the high temperature ignition event, a lower-order filter is used. A manually chosen noise threshold of 0.24 bar, on the smoothed pressure rise defines the second-stage ignition delay time. The relationship used in the AHRR calculation is provided by Equation 3 as

$$\frac{dQ}{dt} = \frac{\gamma}{\gamma-1} P \frac{dV}{dt} + \frac{1}{\gamma-1} V \frac{dP}{dt} = \frac{1}{\gamma-1} V \frac{dP}{dt} \qquad (3)$$

where P is chamber pressure, V is the combustion vessel volume (1.1L), and γ is specific heat ratio (1.359 for 750 K, 1.354 for 800 K and 1.344 for 900 K mixtures)[Heywood 1988]. In reality, there is heat loss from the combustion chamber as the combustion event happens. This heat loss is unaccounted for in the Equation 3. When accounting for the heat loss, Equation 3 would take the form as Equation 4. Neglecting the heat transfer co-efficient does result in some error in heat release estimation, which is considered negligible and would be in same scale as the pressure curve filtering process itself.

$$\frac{dQ_{net}}{dt} = \frac{1}{\gamma - 1} V \frac{dP}{dt} + hA(T(t) - T_0) \quad (4)$$

where Q_{net} is the net heat release, and h is the averaged/equivalent convective heat transfer coefficient and A is the inner surface area of combustion vessel, T is the temperature estimates at different times as T(t) at any time instant t after the start of the heat release and T_0 is the Temperature at zero time (start of any combustion). T is calculated based on ideal gas laws which give a Temperature ∝ Pressure relation.

2.15 Image processing

Visualization of raw schlieren and luminosity obtained images provides wealth of information if they are interpreted in the correct way through proper image processing. Schlieren effect is mainly caused by the variation of the refractive indices of the ambient gas as temperature gradients are formed in the ambient gas. The MTU vessel being a pre-bun type combustion vessel, the background refractive index variation (background noise) gets denser as the fuel gets injected at higher temperatures. Determination of vapor penetration and spray angles is dependent on proper identification of the boundaries by avoiding the capturing of these background disturbances, since most of these disturbances might have similar gray scale values, as that of the vaporized spray. Background subtraction of the schlieren image is exercised using a software code to obtain a processed boundary with minimal error. An in-house MATLAB script is used for identification of boundaries of vapor phase and luminosity containing regions from the vaporized spray and flame images, respectively.

Successive subtraction of images is performed from the immediate preceding image following an I_n-I_{n-1} methodology (as shown in Appendix as Figure 106). The success of such successive intensity subtraction comes from the fact that the inter-frame time duration for image acquisition is low, in this case it is 26.67 µs. This enables a low variation of the refractive index in the background of the successive two images. Also, a grayscale intensity offset is used between an image and the preceding image involved in the subtraction, such that the resulting image intensity is enhanced and the non-moving elements of the spray are visualized as solid dark grey regions. This enhances the visibility of the vapor spray and

any bright luminosity, thus enabling efficient boundary tracking. In practice, any image which is easy to visibly track by the human eye is easy to track by a computer code.

Fig. 33 shows a sample schlieren image processing to visualize the bleak vapor region of the spray.

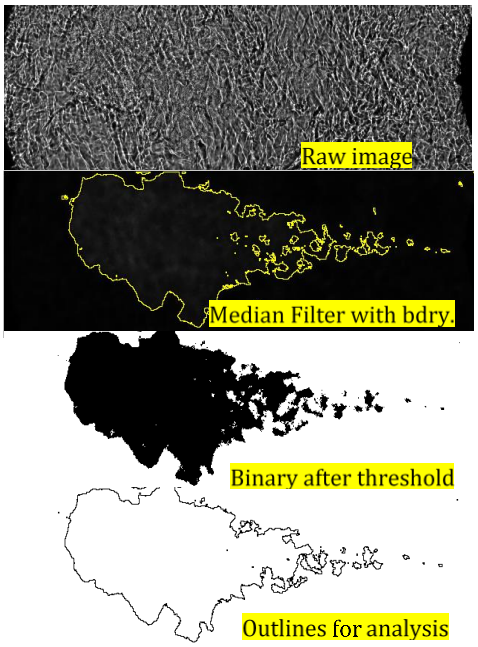

Figure 33: Sample image-set showing boundary detection procedure starting from a schlieren image

CHAPTER 7

ANALYSIS TOOLS

Some of the results presented further in the discussions heavily use the analysis techniques of integrates plots (hereby called IXT plots) and mixture fraction-temperature (Z-T) plotting. These are introduced in the following sub-sections.

2.16 IXT plot

Temporal and spatial features of the flame are studied by integrating information at each axial location for a 2D matrix containing either experimental or CFD information. This is named as an IXT (Intensity-aXial-Time) plot defined mathematically as in Equation 5.

$$IXT(x,t) = \int_{-R}^{R} I(x,r,t)dr \tag{5}$$

where x is the axial direction, r is the radial direction, and R is intensity boundary width. Although, IXT plot was previously used [Cung et al. 2015] on experimental imagery to investigate aspects such as lift-off length (soot lift-off), flame height, and some aspects of internal flame structure, it can also be employed on quantitative CFD data in a similar manner. For 3D CFD simulation output, first the target quantity along the line-of-sight has been integrated and projected on a plane which was later considered for transverse integration operations along the axial length for the various time steps (in a similar way as in experiments). IXT plots are depicted in Fig. 34 as explained above.

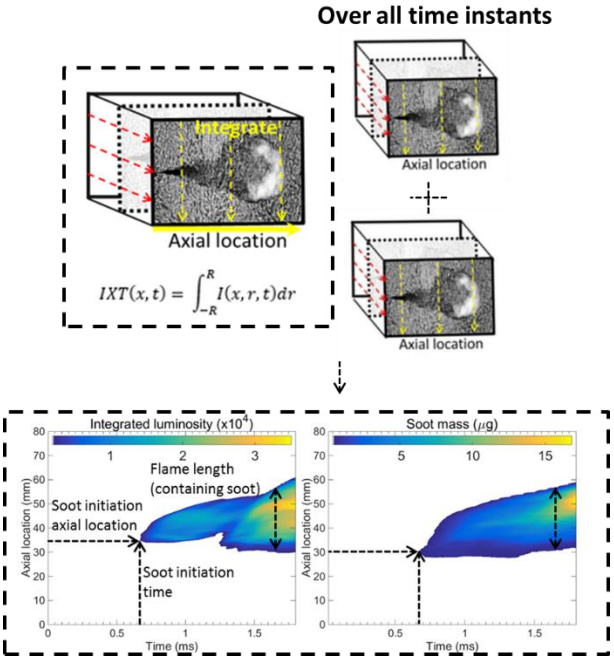

Figure 34: Integration of both experimental (sample procedure shown in top) and CFD data (bottom) to obtain IXT plots. Bottom left: experimental flame luminosity bottom right: soot information from CFD.

2.17 Z-T plot

A traditional Z-T plot is used to study the richness/leanness of mixture. The current usage of Z-T plot is by implementing binning of the computational domain into mixture fraction bins (each bin is of 0.005) and temperature bins (each bin is of 40 K). Each bin is then filled with the information of the target of interest. Similar plotting technique was used by Janardhan et. al [Kodavasal et al. 2015] to study the reaction space just before ignition in a spark ignited engine. It is possible to actually correlate a Z-T plot to actual location in a flame. An illustrative diagram has been provided in Fig. 35, with Z-T plot in the bottom and actual locations of the flame in the top. It can be seen that this plot has a delta-like (Δ) shape. The right-most vertex of the delta (Δ) is the central zone of the high temperature region of the flame. The section constituting the bottom region bins is the far downstream region containing the outer end of the flame tip which has relatively lower temperature than the flame tip itself. The bottom portion of the right-side edge region is the high temperature

flame core region which extends upstream. The top portion of the right-side binned region is the medium temperature flame core region. The left-side binned region is the low temperature region which is located near the lift off. The region encompassed by all the edges is the region just downstream of the lift off length having slightly medium temperature extending until the medium temperature region is reached.

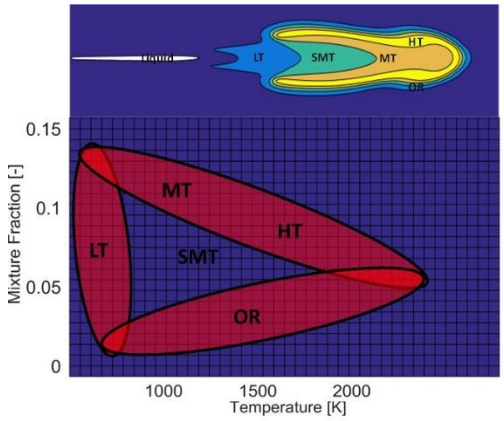

Figure 35: A Z-T plot with legends given as follows - LT: Low temperature (700-1000K) ; SMT: Slightly medium temperature (1000-1400), MT: Medium Temperature (1400-1800), HT: High Temperature (1800-2200), OR: Outer Region (Zone outside the upstream of HT region, but at lower temperatures)

CHAPTER 8

TEST CONDITIONS

During the course of the PhD, many tests were performed and some of them were simulated using CFD. Table 3 provides details of the experimental test conditions tested along with the CFD simulation performed (bold-italicized). The experimental tests include a variety of optical diagnostics like Mie scattering, Schlieren, Natural luminosity, OH* chemiluminescence and PLIF.

Table 3: Summary of test conditions with CFD simulations bold-italicized

Parameter	Test Set #1	Test Set #2
Fuel	n-heptane	n-Dodecane
Nozzle dia. (µm)	100	93.8
Inj. press. (MPa)	120	***120, 150***
Split injection time	0.26/0.74 ***0.26/0.95***	***0.5/0.5*** ***0.3/1.2***
Dwell (ms)	***0.17, 0.77, 1.37***	0.3, ***0.5***, 0.6, 0.9
Gas density (Kg/m^3)	23	22.8
Oxygen level (%)	***0, 15***	***0, 15***
Chamber temp. (K)	453	453
Bulk T at injection (K)	***950***	750, ***800, 900***

CHAPTER 9

SPRAY-COMBUSTION INTERACTION MECHANISM[1]

3.1 Background

In this work, a pilot injection study is carried out numerically and experimentally to investigate the different phases of spray combustion and their interaction with mixture fields in a multiple-injection event. The importance of dwell time is understood by analyzing the experimental results including hybrid shadowgraph, Mie scattering, and flame luminosity imaging for combustion cases. Numerical simulation results provide an understanding of the spray penetration profile and mixing of non-combusting cases, with temperature and velocity vectors characterized in combusting cases.

A simultaneous shadowgraph and Mie scattering imaging technique was used to measure liquid/vapor fuel spray, and flame luminosity with a neutral density filter as a pseudo-simultaneous measurements of shadowgraph and Mie scattering images [Zhang et al. 2014]. The oxygen concentration within the combustion chamber was 0%, while flame luminosity images were taken for an oxygen concentration of 15%. A single-hole solenoid injector (details in Table 1) was used to generate multiple-injection. An example of two consecutive injections (15%/85% mass-base) is shown in Fig. 36, including raw rate of injection (ROI) data, filtered ROI, and input ROI for CFD modeling, overlapped with the driver current profile.

[1] The material contained in this chapter was previously published in *Proceedings of the Combustion Institute.*
Cung, Khanh, Abdul Moiz, Jaclyn Johnson, Seong-Young Lee, Chol-Bum Kweon, and Alessandro Montanaro. 2015. "Spray–combustion interaction mechanism of multiple-injection under diesel engine conditions." Proceedings of the Combustion Institute 35 (3):3061-3068.

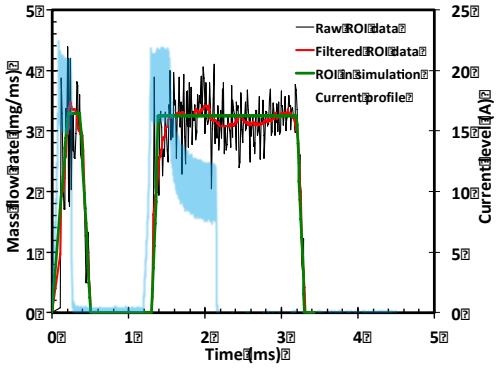

Figure 36: Profiles of rate of injection and injector current command (0.26ms/0.95ms with DT=0.77ms)

The pilot-main injection event was set to keep the same injection pulse width. The ROI was measured using a Bosch type accumulator. The injector had a few test shots before every run to confirm the distinguishable pilot and main injections in time. The pressure variation in the injector high-pressure line is negligible during the injection event as the high-pressure fuel system includes two 100 mL accumulators to store the pressurized fuel for the injection event. The chamber pressure was recorded to calculate the heat release rate. Mass ratio of pilot to main injection quantities were selected at 15%/85% and 20%/80%. Dwell time (DT), which is the time between the end of the pilot and the start of the main, was set at 0.17, 0.77, and 1.37 ms. The experimental test conditions are summarized in Table 3 (column with n-Heptane as fuel).

The measured ROI profile had significant noise, which needed to be filtered. Filtered ROI signal looked close to a trapezoidal shape as shown in Fig. 36. In the simulation, the injection pressure is closely coupled to the ROI (mass in general), so a noisy ROI will lead to noisy pressure output. Therefore, a trapezoid profile generated from the filtered ROI was utilized to have a stable numerical injection pressure output.

The simulations were conducted using the commercial CFD software package CONVERGE^{TM} [Richards et al. 2012]. The base grid size was limited to 4 mm for all the cases, and a total of 77,293 orthogonal hex volume mesh elements were generated during the simulation. Local mesh embedding used in the region of spray was completed with an

embedded shape of a frustum of a cylinder with a minimum radius of 0.1 mm, maximum radius of 10 mm, and cylinder length of 0.1 m. The embedding scale was set to an order of 2, thus a minimum element size of 1 mm after mesh refinement (both AMR and local embedding) was generated in the region of fuel spread for all the cases. For the CONVERGE simulation, the spray angle was kept at 20°, and the unsteady RNG k-ε turbulence model [Han and Reitz 1995] was used for turbulence simulation. The spray parcel count was set as 50,000 per injection, which is sufficient based on the previous study [Johnson et al. 2013]. An ambient gas composition of O_2 (0.0%), N_2 (89.7%), CO_2 (6.5%), and H_2O (3.8%) was chosen to simulate experimental condition of vaporization case. For combustion simulations, the characteristic time combustion (CTC) model [Abraham et al. 1985] was used for achieving less computational time by simulating the rate of change of the density of species. CTC combustion model does not take into account any detailed combustion chemistry, but it has calculations based on characteristic time to achieve equilibrium [Kong et al. 1995].

3.2 Results and discussion

3.2.1 Vapor penetration

In-house image processing using Matlab® from experimental shadowgraph images provided measurements of vapor penetration shown in Fig. 37 along with simulation results for the mass ratio of 15%/85%.

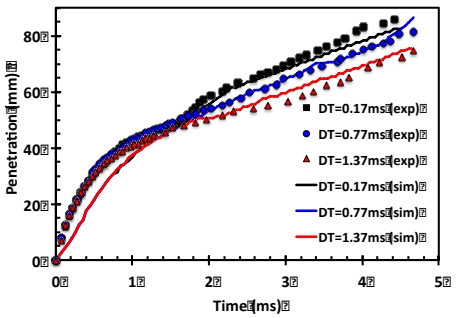

Figure 37: Vapor penetration length for 15%/85% case

Shorter DT resulted in a faster penetration rate, as main injection provides momentum for the pilot injection to penetrate into the surroundings. Both experimental and numerical results showed similar pilot penetration followed by main injection after corresponding DT. The difference between numerical simulations and experimental data could be due to the test-to-test experimental variability. Vapor penetration in the simulation was determined from the leading spray boundary by setting the threshold to be the location where 0.1% of the fuel mass fraction remains. Additionally, cell size plays an important role in matching numerical results with actual measurements. With reduction in cell size, the vapor penetration decreases slightly and becomes closer to the actual experimental penetration and so is the case with the liquid penetration [Senecal et al. 2014].

3.2.2 Flame luminosity

Fig. 38 shows the time-dependent flame luminosity images after the start of the main injection (AMI) for the 15%/85% mass ratio case. Images are false color depictions and can be tracked for flame growth and decay, approximately, by following the ROI profile (injection duration and dwell).

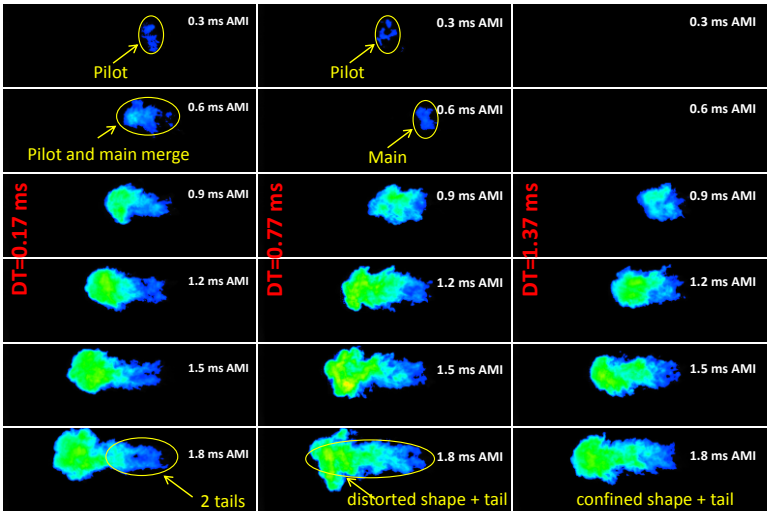

Figure 38: Pilot and main flame luminosities (false color) after main injection (AMI) for DT = 0.17 ms (left), DT = 0.77 ms (middle), and DT = 1.37 ms (right) for 15%/85% case

For a short DT (i.e., 0.17 ms), main combustion started while the pilot combustion was still active (AMI = 0.6 ms). As the DT became longer, main combustion started when the pilot combustion was diminished or extinguished, as in the cases of DT = 0.77 ms and DT = 1.37 ms, respectively. Thus, it is clear that the spray-combustion interaction of two injections is more aggressive as the DT becomes shorter, which results in higher luminosity; that is, soot generation due to a higher local equivalence ratio which results from insufficient mixing time. For the case of DT = 0.17 ms, the main flame appears to be less distorted in its shape when compared to the other cases. The tail structures of each DT are also different, with two tails in the boundary for DT = 0.17 ms, a single, moderately thin tail for DT = 0.77 ms, and a bold, more confined tail shape in DT = 1.37 ms. Further description of the emerging phenomena between pilot and main flame is described in the CFD simulation section later.

Temporal and spatial flame luminosity was calculated by integrating flame luminosity at each axial location of each frame for the 15%/85% mass ratio as shown in Fig. 39 (a-c). This is called *IXT* (Intensity-aXial-Time) plot defined as $IXT\ (x,t) = \int_{-R}^{R} I(x,r,t)dr$, where x is the intensity axial direction, r is the radial direction, and *R* is intensity boundary width.

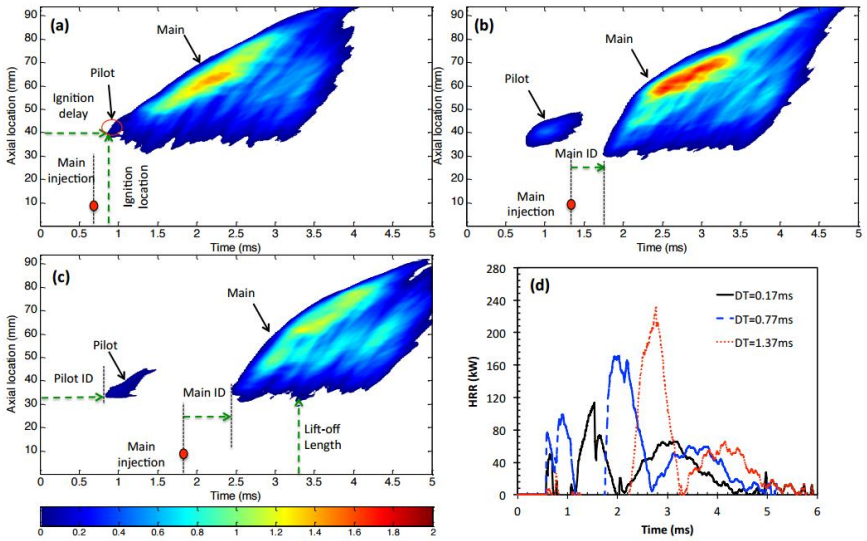

Figure 39: Instantaneous axial integration of flame luminosity for (a) DT = 0.17 ms, (b) DT = 0.77 ms, (c) DT = 1.37 ms, and (d) corresponding relative heat release rates for 15%/85% case

IXT contour provides rich information of spray combustion progress including the ignition delay, lift-off length, flame height, and some aspects of internal flame structure. The two islands on the *IXT* contour represent pilot (small) and main (larger) events and the *IXT* contour clearly shows the time and location of the pilot and main combustions. The main injection shapes on the contour are similar for three dwells with differences in start of ignition and the high intensity of the combustion region. The exact mechanism of non-monotonicity of peak luminosity values with dwells on the contour is unclear at the moment. However, the peak luminosity values were repeatable. Three repeats have been performed for each test run and a visual check has been performed to ensure good repeatability. Because of very limited test runs and expensive testing, it is difficult to extract the uncertainty in the present study.

The CV pressure trace is used to determine the heat release rate (HRR) from the combustion event. Before defining the HRR, the pressure data was pre-processed to isolate the region of interest, and then was filtered to remove noise. The pressure differential (change in pressure) for each time step (10 μs) was determined over the entire filtered

pressure region of interest during the combustion event (both pilot and main) and used in the HRR relationship provided by the equation: $\frac{dQ}{dt} = \frac{\gamma}{\gamma-1} P \frac{dV}{dt} + \frac{1}{\gamma-1} V \frac{dP}{dt} = \frac{1}{\gamma-1} V \frac{dP}{dt}$, where *P* is chamber pressure, *V* is the combustion vessel volume, and γ is specific heat ratio. This equation was simplified, since the combustion vessel is constant volume (1.1L), so the volume – time derivative can be neglected. The pressure – time derivative was calculated and γ is a constant representing the ratio of specific heats of the charge-gas environment, approximated as 1.35 for these tests. The cumulative heat release and the total heat released can be determined using this HRR trace. Note that there is some uncertainty in these results from pressure due to noise in the data from signal cross talk, however, this should provide a good indication of the heat release processes under the different dwell conditions.

In Fig. 39 (d) there exist two main heat release rate contributions by pilot and main injections, which are separated in time. For the main injection HRR, there exist distinct combustion modes after the main injection ignition delay, the premixed period followed by the mixing controlled period. The peak HRR and total heat released (integrated HRR) during the premixed period show a significant increase with longer dwell while the total heat release during the mixing controlled period changes little. This plot demonstrates the significant influence of the dwell on the main HRR in the premixed period. It should be pointed out that there is some uncertainty to estimate the pilot HRR using the pressure trace, since the magnitude of pressure induced by pilot combustion is low for the analysis, due to the relatively large vessel volume.

The *IXT* contour plot also shows other important parameters including lift-off length (LOL), ignition delay (ID), and the locations of pilot and main injection. Fig. 40 shows that multiple-injection lift-off length varied with dwell time for the case of 15%/85% and 20%/80% mass ratios.

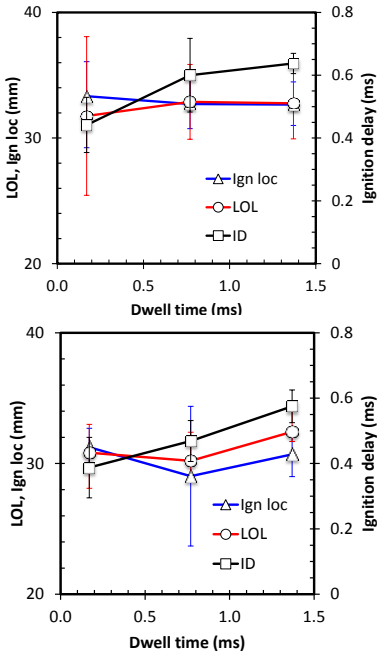

Figure 40: Ignition location, ignition delay, and average lift-off length of main flame (top) 15%/85% and (bottom) 20%/80% cases

This temporal shift of lift-off length was due to the influence of the pilot combustion. Longer lift-off length was observed for shorter DT, which can be explained by the combined momentum of the pilot and main injection pushing the ignition location downstream. However, as the DT becomes longer, the lift-off lengths are stabilized. This is a result of the momentum of the pilot injection decaying as main injection occurs. As explained earlier, in trials with shorter DT, fuel from the main injection started burning as it was injected, resulting in shorter ignition delay. Ignition delay reached an asymptote as DT increased.

The ignition delays of all DT cases were shorter than single injection, where ignition delay was observed to be approximately 0.75 ms. Note that the ignition delay was the elapsed time from the start of the main injection. Therefore, a time (pilot injection duration + dwell time) was subtracted from the start of pilot injection time until the occurrence of luminosity value of the main injection to arrive at the main ignition delay. Such short ignition delay for multiple-injection would reduce the premixed combustion phase and enhance the main injection combustion process, which was observed in Fig. 39 (d) for the reduction in

the premixed controlled combustion for the shorter DT case. Additionally, the results indicate that longer ignition delay may increase time for fuel-air mixing, which in turns possibly increases the rate of heat release. The trend of the locations of main ignition was not clear and additional tests are required for a definite conclusion. While main ignition location is longest for a medium DT in cases of 15%/85% mass ratio, it is shortest for the case of 20%/80% mass ratio. However, in both mass ratio cases, shorter lift-off length and longer ignition delay were observed as DT was increased.

3.2.3 Simulation

Contour plots of temperature and velocity fields at the AMI = 1 ms are shown in Fig. 41 to explore spray-combustion interaction with air entrainment for the 15%/85% mass ratio with different dwells.

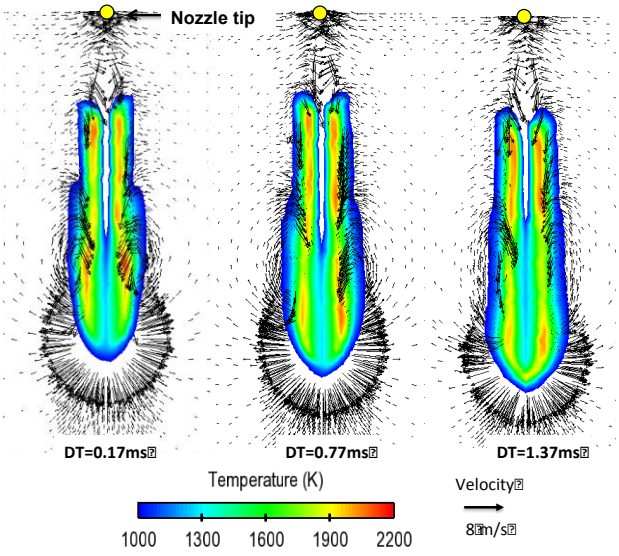

Figure 41: Simulated temperature and velocity vector at AMI = 1 ms for 15%/85% case

The main liquid injection is seen in the middle of the temperature fields, and this liquid length varies with different dwells. The behavior of the flame at the contact of pilot with main is seen as an outward bulge, which becomes lesser and lesser with increasing dwells. Another observation is the position of the vortex core exhibited by the velocity vectors, which depict the contact region of the pilot with main flame.

The temperature contours reveal an important character of the pilot flame propagation. At DT = 0.17 ms, the flame has high temperature regions in the middle section of the flame, due to the location of the freshly burned pilot which is by-passed by the high-momentum less-combusted (air-deficit) main flame. The bulge in the DT = 0.17 ms case represents the pilot flame deformation. In longer dwells, the main has more entrained air for its combustion and the pilot products cool down. Thus, pilot leads the flame structure with lesser deformation in the interaction boundary region, since there is reduced effect of the main on the pilot due to increased dwells. Air entrainment in split injection sprays is studied in the diesel engine study of Ref. [Dec 1997], where there is increased entrainment of main spray under increased dwell time conditions.

At DT = 1.37 ms, when the pilot flame extinguishes and products cool down, the main injection will be warmed up gradually by the hot products of pilot flame while simultaneously entrained in air. This results in a confined shape of the main flame similar to the flame image seen in Fig. 38. The agreement between the CFD simulation and experimental images provides a solid foundation to obtain a good fundamental understanding of spray-combustion interaction within a multiple-injection event.

3.3 Spray-combustion interaction model

Fig. 42 shows the visualization of the spray-combustion interaction model for single injection (a) and multiple-injection with different DTs (b-d) conceptually. This concept was conjectured from the liquid/vapor penetration lengths and flame luminosity images through experiments and the CFD model.

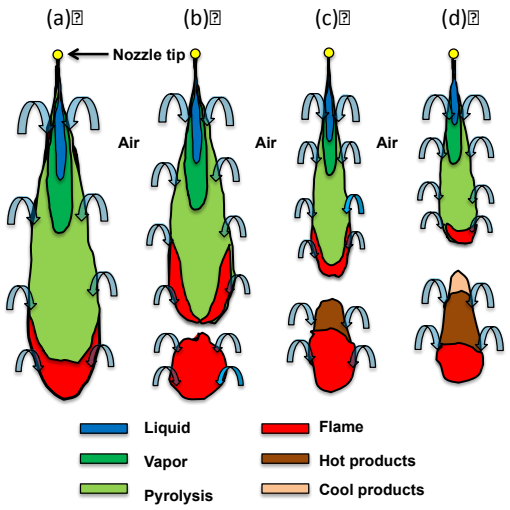

Figure 42: Spray combustion interaction model for single and multiple-injection by varying dwell time; (a) single injection: (b) short DT: (c) medium DT: and (d) long DT

For shorter DT, vapor penetration lengths became longer and mixing time of pilot and main injections with surrounding air was insufficient. Thus, ignition delay and main ignition location became longer. The result, based on the flame image, provides evidence for agglomerated intense combustion. As the DT became longer, the vapor penetration length, ignition delay, and main ignition location became shorter. Fig. 41 shows that a longer DT increases mixing time, which is presented as more evenly distributed temperature regions.

In a single injection event seen in Fig. 42(a), fuel is injected into ambient and air entrainment follows from the spray boundary to spray core. Fuel is vaporized by hot gas and the fuel rich region is formed. Fuel and air are subsequently well-mixed to an ignitable mixture. The fuel oxidation process takes place in the fuel-rich mixture region near the downstream of liquid penetration and is continued to the boundary of the diffusion flame[Dec 1997, Han et al. 1996]. The conceptual model of multiple-injection is introduced by selecting three different DTs, i.e., short, medium and long dwell times, where the effect of pilot on the main flame is expected to differ for each individual DT. This is because combustion of the pilot has a significant effect on the main combustion, in terms of temperature and the composition of the region it leaves behind. Note that the reference time is when the pilot is injected. For the case of a short DT, the short separation time of

pilot and main would leave a relatively hot region behind for the main injection, which will likely yield a shorter ignition delay compared to longer DT cases. However, the lack of oxidizer in the region that the pilot leaves behind under short DT would give the frontal area of the main injection less of a chance to combust compared to the outer boundary area of its spray. In this case, the main injection is moving toward a “circle of flame” left by the pilot. This will likely leave the main flame to have a flame on the boundary, instead of being hot in the spray core.

In the case of a medium DT, the pilot flame is well formed. Main injection is pushed into a hot “ball of flame,” and the result is that the main flame has a large heat transferring region, which causes the front region of the main flame to burn aggressively along with the nearby spray boundary. In long DTs, pilot combustion is complete, and the remaining cooled products gradually warm the frontal region of the main injection. This results in a well-shaped confining main flame in which temperatures are, to some extent, evenly distributed along the spray. Note that the pilot has a different shape and temperature mode with varying dwells, due to the increased availability of oxidizer owing to the late occurrence of the main flame on increased dwells. These three different DTs are likely yielding different tail shapes for the main combustion as described earlier.

Soot formation can also be reduced by optimizing the split injection scheme. This is evident from the studies of Ref [Jafarmadar and Zehni 2009] investigating various effects related to split injection in diesel engines including the effect of mass ratio on the NOx and soot. It shows reduction of NOx and soot as the mass of the pilot is reduced and the main increased, however this reduction occurs in small amounts. In their study the increased NOx from a single injection to a split injection scenario is observed while showing a reduction in the soot amounts.

3.4 Concluding remarks

Interaction of spray and flame were investigated through experimental and numerical work. For non-reacting cases, vapor penetration was accelerated with a shorter dwell time, as main injection provides higher momentum to the pilot injection compared to longer dwell

cases in both experimental and numerical results. Flame luminosity imaging of main combustion enabled characterization of the ignition processes and flame structure for each case of dwell time. It is possible to conceptually categorize the shape of the main flame depending on when it is injected. As dwell time increases, ignition delay of main flame increases, but the trends of LOL and ignition location are not well defined. Agreement in CFD simulation with experimental result provides a useful tool to further investigate the interaction of spray-to-flame or flame-to-flame in a multiple-injection scheme, especially to fully understand the characteristic of main flame. Future work will focus on detailed CFD models, such as large eddy simulation (LES) to characterize flame boundary interaction with air entrainment, extracting soot formation from experimental data, and identifying optimal schematics including duration of pilot injection, dwell, and main injection.

CHAPTER 10

LAGRANGIAN, GRID AND COMBUSTION MODEL ASSESSMENTS[2]

3.5 Background

Spray and combustion numerical modelling is a key aid in developmental studies of many areas viz., turbines, internal combustion engines etc. It is usually found that the accuracy of a numerical simulation when compared to the experiments varies, as the spray and combustions models are varied. Also, the computational grid plays a crucial role in model correctness. Of primary importance in this work are the combustion model solutions obtained after a grid-converged Lagrangian spray modeling exercise. As part of this exercise, a structured methodology is followed to obtain an experimentally validated solution of a Lagrangian spray considering the effects of key Computational Fluid Dynamics (CFD) parameters viz., grid size, injected parcels and spray break-up time constant. Four combustion models namely the SAGE (a well-mixed reactor with detailed chemical kinetics), the Multiple Representative Interactive Flamelet model (mRIF), the 3-Zone Extended Coherent Flamelet (ECFM3Z), and SHELL+ Characteristic Time Combustion (Shell + CTC) models were examined using the grid-converged CFD settings. Ignition delay, lift-off length along with spatial and temporal CFD-to-experiment comparisons have been adopted keeping in mind the unique interaction region between the pilot and the main sprays (or flames). Deficiencies in model predictions for a split injection combustion problem are pointed out along with proposed improvements. The comparisons concluded that for non-detailed chemistry CFD modeling, ECFM3Z model shows acceptable run-time/accuracy trade-off whereas for detailed chemistry applications the non-multizone enabled SAGE solver has an upper hand.

[2] The material contained in this chapter was previously published as a technical paper in *Society of Automotive Engineers*

Moiz, Ahmed Abdul, Sibendu Som, Luis Bravo, and Seong-Young Lee. 2015. Experimental and Numerical Studies on Combustion Model Selection for Split Injection Spray Combustion. *SAE Technical Paper*.

Recently, there have been new findings with respect to divergence of the spray-flame related phenomenon of split injections from the conventionally used single injected sprays. Non-reacting split injection studies have shown that the vapor phase velocity of the second injection is greater than that of the first injection, due to a 'split-stream' effect [Skeen et al. 2015b]. These phenomena are explained by faster propagation of the main stream in an ambient provided by the vaporized pilot stream without the formation of a stagnation plane. It was also found that with using split injections, ignition delay of the second injection can be reduced to almost half the delay time of the first injection [Cung et al. 2015, Skeen et al. 2015b], but this leads to the formation of soot in the second injection. This soot can then can be encountered by introducing an additional third injection called 'post' injection [O'Connor and Musculus 2013a, O'Connor and Musculus 2014]. A study of split injections in controlled environment such as a constant volume combustion chamber allows for a more detailed characterization of the spay combustion phenomenon and also greatly helps the modelers to build durable multi-physics models. Using experiments together with CFD provides deeper insights of the fluid-dynamic linkup of the constituting injections which results in gauging associated benefits/losses in their applications.

As in any CFD modeling setting up exercise, there are many factors which should be taken into account to avoid numerical inaccuracies and thus bad predictions. Especially, in the popularly used lagrangian spray setup to simulate fuel injection, there is high amount of uncertainty which arises from choosing the right amount of lagrangian parcels to be injected, associated break-up constants with respect to the fuel employed and of course obtaining a grid convergent result while doing so. Senecal et al. [Senecal et al. 2014] have demonstrated a methodology for obtaining grid convergent CFD solutions for a single injection non-reacting spray. It is briefly explained in the previous section that a split injection is a unique case with special characteristics in both the non-reacting and reacting spray scenarios. Thus, in this work, a detailed analysis of the non-reacting sprays is performed to confirm proper setting up of the mixture distribution for a split injection case. This proper setting will be later be employed to explore the differences observed between usages of various combustion models. Any significant deviations in prediction of a combustion model will then arise due to its formulation and application to this problem and

not due to spray-grid related numerical artifacts. Combustion modeling has been performed by the various researchers [Campbell et al. 2009, Cung et al. 2015, Felsch et al. 2009, Hasse and Peters 2005, Hessel et al. 2014, Lim et al. 2010] for split injection spray combustion previously. The results of their work show promising results in terms of gaining additional insights in split injection combustion progression and emissions formation. Hasse and Peters [Hasse and Peters 2005] used a two mixture fraction flamelet model for split injection in diesel engine conditions. In their work, the 3D mixture field in the computational domain is analyzed using a multi-dimensional PDF function, and an interaction coefficient describes the degree of merging of the mixture fields. Depending on this interaction coefficient, different phases of combustion and interaction (due to the different injections) between the mixture fields are obtained. Felsch et al. [Felsch et al. 2009] used a Representative Interactive Flamelet (RIF) model which was previously limited to two consecutive injection, but later got extended to any number of split injections. They concluded that the ignition of the second injection occurs in a premixed combustion mode whereas that of the first injection occurs in an auto-ignition mode. Thus, it might not be a given fact that these ignition regimes can be captured by all the models used in the present day commercial solvers. Lim et al. [Lim et al. 2010] modified the flamelet combustion model applying it only near the stoichiometric region to reduce the computational time. The results obtained by Lim et al. [Lim et al. 2010] were consistent with the flamelet combustion models available in the literature. The above mentioned combustion models mostly looked into global validations relating to ignition delay and heat release, whereas validated spatial and temporal progression of combustion related phenomenon was largely not done. Comparisons of spatial and temporal progression between experiments and simulations is a much needed step for coherence of experiment and simulation. Such works were however attempted by Singh et a. [Singh et al. 2006] (in KIVA-3V code) and more recently by G.D'Errico et al. [D'Errico et al. 2014] (in openFOAM code) for single injection diesel sprays under a variety of conditions and also using various combustion models. Singh et al. [Singh et al. 2006] had one test point of split injection for which a detailed chemistry well-mixed model was found to be better suited than the characteristic time combustion and multiple representative interactive flamelet models. Han et al. [Han et al. 1996] and Hessel et al.

[Hessel et al. 2014] have used a Characteristic Time Combustion (CTC) model to investigate split injections, but mostly focused on global validations of heat release. They concluded good validations of heat release rate and NOx emissions. Cung et al. [Cung et al. 2015] used a CTC model, but showed weak spatial correlation experimental data. Campbell et al. [Campbell et al. 2009] used an extended coherent flame model with 3 zones (ECFM3Z) and demonstrated the prediction of combustion aspects relating to prediction of premixed flame, diffusion flame and auto-ignition with spatial and temporal validations from experimental data wherever possible. The afore-mentioned modern combustion models have led to better ways for CFD combustion calculations which will be explored in this work, but might need another look for applications to split injection spray combustion. Additionally, it is expected that, with identifying the deficiencies in the combustion models, the modelers come one step closer in developing those aspects in near future. As part of the present study, a structured grid convergent procedure for a lagrangian spray is laid out which is later followed by reacting simulations involving comparison between four combustion models. The prospective utilization of each of these combustion models is characterized based on some deciding factors as a conclusion of this study. Table 3 shows the test conditions for the experimental work out of which only the 0.26ms/0.95ms condition was considered with the dwell time of 1.37 ms in this work. The procedure of the experimental setup and the results of the experiment with split injecting vaporizing and combusting sprays used in this paper, are previously published by Cung and coworkers [Cung et al. 2015].

3.6 Simulation details

In the present work, CONVERGE CFD [Richards et al. 2012] solver has been used for CFD computations. For the sake of maintaining common computational power to gauge the core-hour usage of each combustion model, simulation for each combustion case have been performed on 32 cores on a Dual Xeon 3.4 GhZ CPU workstation with 64 GB RAM. The other simulation details except the combustion model details have been covered in chapter 5 and so will not be discussed here for brevity.

3.6.1 Combustion modeling

Combustion model selection is an important area of the present work. The theory of the four (4) combustion models used in this study is briefly presented in the following sections.

3.6.1.1 3 Zone Extended Coherent Flame Model (ECFM3Z)

The 3 Zone Extended Coherent Flame Model (ECFM3Z) present in the CONVERGE CFD solver originates from the Extended Coherent Flame Model [Colin et al. 2003]. This model is modified to model combustion in perfectly or partially mixed mixtures and also considers for unmixed combustion. The idea of the ECFM model is based on the surface density of the flame front which is affected (wrinkled) by the turbulent eddies. The ECFM3Z model is for a diesel like application unlike the gasoline application of the ECFM model. This calls for an inclusion of a 'mixing state' for diesel like combustion to account for the unmixed combustion. Thus, the ECFM model is applied to 3 zones, a pure fuel zone (injected fuel), a pure air plus possible residual gases zone (burnt fuel and re-circulating air or EGR) and a mixed zone. The mixed zone is calculated based on a mixing model accounting for incoming unmixed fuel with the surrounding air fuel. Using the ECFM3Z model for diesel combustion scenario requires the predictability of auto-ignition together with premixed and diffusion flame construction. In this paper, auto-ignition is modeled using the Chemical Equilibrium Solver (CEQ) [Pope 2004] while the premixed turbulent flame modeling is possible through ECFM model. It is to be noted that ECFM3Z is not a detailed chemistry solver. But successful implementation of this model on qualitative grounds was performed for a single injection diesel spray flame by [Campbell et al. 2009] where the basic combustion physics relating to the mode of combustion occurrence was demonstrated.

3.6.1.2 SAGE

SAGE [Richards et al. 2012] is one of the detailed chemistry solvers for CONVERGE, which calculates the reaction rates for each elementary reaction based on Arrhenius type correlation, while the CFD code solves the species transport equations. It belongs to the well-mixed category of combustion models, where each computational cell is treated as homogenous reactor. SAGE neglects the effect of turbulence-chemistry interaction (TCI). This might result in errors under some simulations conditions due to nonlinearity of the

chemical source term. The chemical source term is exponentially dependent on the temperature and thus on the turbulence fluctuation. However, it is seen that with an accurate reaction mechanism, SAGE can be applied for modeling any combustion regime viz., ignition, premixed and mixing-controlled in gasoline and diesel combustion scenarios in both RANS and LES cases [Pei, Som, Pomraning, et al. 2015, Senecal et al. 2014, Som et al. 2012]. It is to be noted that the SAGE is commonly used with a multi-zone solver, which solves the cells with similar thermodynamic conditions in groups and saves run-time. The multi-zone solver is not used in the present work to allow for minor thermal, fluidic field changes to have an effect on the simulation outputs.

3.6.1.3 SHELL and Characteristic Time Combustion (CTC) models

SHELL and CTC models are two separate models now used in conjugation. SHELL model [Lafossas et al. 2002] was originally developed to predict knock in gasoline engines. It is used to predict the auto-ignition in diesel engines based on a set of 8 reactions. CTC model [Halstead et al. 1977] on the other hand is a simplified combustion model, and assumes that seven species are involved in the combustion process: fuel (C_nH_{2m}), O_2, N_2, CO_2, H_2O, CO, and H_2. The species are solved by a set of atom balances, equilibrium constant equations and water-gas shift reaction using a Newton-Raphson solver technique. It bases its calculations on the characteristic time to achieve the equilibrium. Thus, by using the Shell and CTC models concurrently, the Shell model solves for the computational cells which are in the ignition phase and the CTC model solves the cells which are in the combustion phase. This model is mostly used for faster simulations to predict emission outcomes using empirical soot models (passive soot) and thermal NOx (passive NOx) which does not require detail chemistry solutions.

3.6.1.4 Multiple Representative Interactive Flamelet (mRIF) model

The mRIF model is based on the laminar flamelet concept by Peters [Peters 1984]. Pitsch et al. [Pitsch et al. 1998] later developed this model which calculates the species mass fraction based on a stable term of the Favre-averaged mixture fraction and a varying term of mixture fraction variance. The species conservation is used to derive the flamelet equations after applying a coordinate transformation to the mixture fraction space [Peters

1984]. During the solution process, mass fraction of the species is found as a function of mixture fraction. A β-PDF distribution of the mixture fraction is assumed to calculate back the mass fraction in each cell. One of the inadequacies of the RIF model is that a domain-averaged value of the stoichiometric scalar dissipation rate is used. The scalar dissipation generally has large spatial variations and a single value of stoichiometric scalar dissipation rate does not accurately represent the whole domain. But having multiple flamelets, each accounting for a certain amount of fuel injected, counters this deficiency and is the idea behind the multiple RIF (mRIF) model. It is to be noted that, detailed chemistry can be handled by the mRIF model (succinctly called the RIF model from henceforth). An assessment of RIF model application for single injection diesel spray combustion simulations was performed recently by Kundu et al. [Kundu et al. 2014] and some of their conclusions are used in this study for split injection combustion model setup.

In the next section(s), description of the grid convergence methodology based on non-reacting spray RANS modeling is discussed followed by the application of the afore-mentioned combustion models to simulate spray combustion.

3.7 Grid convergence

Setting up of a properly validated non-reacting spray is pivotal for establishing the right mixture presence before ignition and eventual combustion happens in a reacting spray. Also, as part of the best practices for running any numerical simulation, grid convergence should be established. A series of logical steps were charted out, as shown in Fig. 43, so that the numerical spray can be finely tuned to the experimental spray especially with respect to non-reacting spray parameters of liquid and vapor penetration length. The importance of selecting the particular parameters (cf. Fig. 43) for tuning the sprays is emphasized by [Bravo et al. 2014] and [Senecal et al. 2014] and in the global sensitivity analysis carried out by [Pei et al. 2014].

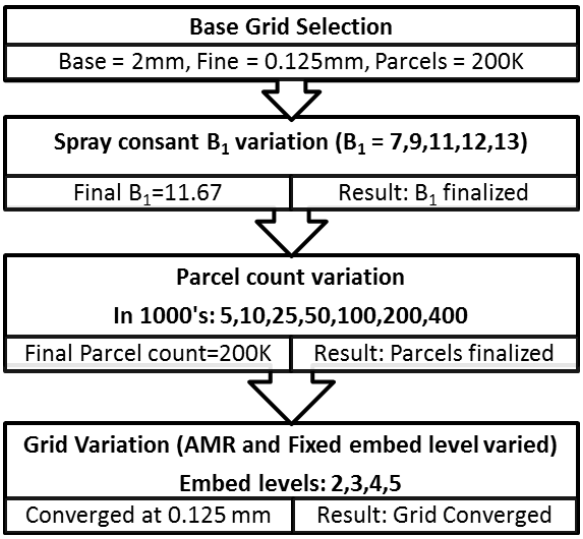

Figure 43: Flow chart of methodology followed for parametric variation and grid-convergence

In the present work, Adaptive Mesh Refinement (AMR) strategy is employed to efficiently increase the resolution of regions having high local sub-grid velocity gradients (critical sub-grid velocity is pre-set) during run-time. Also, temperature is also used as an AMR cell creation criteria. Fixed embedding is employed which freezes the refined grid throughout the simulation without dynamically re-positioning it unlike AMR. The level of refinement of both the fixed embedding and AMR embedding is controlled by defining levels of refinement called as embed levels. The levels of refinement are meshed additionally upon a base mesh size. Base mesh size is the grid at start of the simulation. Fine grid is obtained from the base grid as in Equation 6.

$$Fine\ grid = \frac{(base\ grid)}{(2^{(embed\_level)})} \tag{6}$$

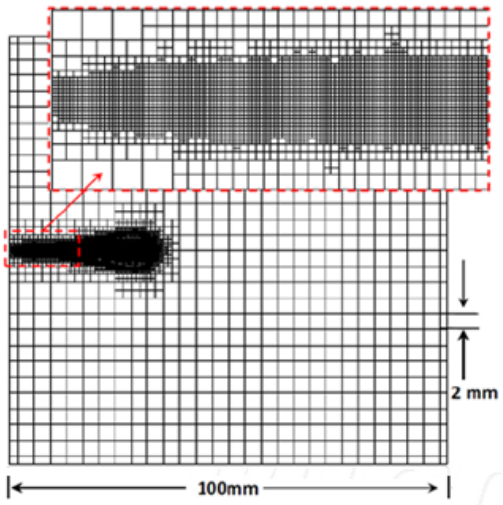

Figure 44: Computational grid showing the base grid (2mm), fixed grid and the dynamically varying AMR grid (in zoomed view)

Fixed embedding was employed in a cylindrical shape of 200 µm starting across the nozzle exit and extending until 15 mm upstream. This is to cover the probable spatial extent of the liquid presence. Following Fig. 43, a medium configuration of base grid, embed level and parcels per injection is selected to start with the grid convergence process involving lagrangian non-reacting spray. A parametric study is then carried out with the breakup time spray constant, B_1, where the magnitude of the liquid penetration length is evaluated against measurements. After that, a parametric variation of the number of parcel is done. Following this, the embed levels are varied for the grid refinement (and grid convergence) procedure. It is noteworthy to mention that during the grid convergence process, as the embed level is stepped up one unit, the parcel count is multiplied by a factor of four and vice versa. This is because, if the grid is refined with no increment in parcel number performed, there will be a condition when the mass contained in a cell will be lesser than the mass of a parcel. At this point, the liquid momentum makes the velocity of the cell reach the liquid velocity. This results in minimal or no drag on the parcels located in the spray plume boundaries leading to higher penetration. Note that the liquid length was chosen as a parameter of validation since it attains a (pseudo) steady value during the latter stages of injection and hence facilitates the comparison. The final values of the physically optimized

spray break-up time constant (B_1), parcel number and the grid size will be used in the combusting spray simulations.

Fig. 45 shows the rate of injection (ROI) profile from the experiment and the simulation. One of the principal objectives in this study is to determine a grid converged numerical configuration that would guide our future computational work having different dwell times, rate of injection (ROI) profiles and injection pressures but using the same fuel (n-heptane). This is the reason to simplify the experimental ROI profiles as a 'top-hat' shape (cf. Fig. 45), but at the same time, keeping the mass of injection (area under the ROI curve) the same.

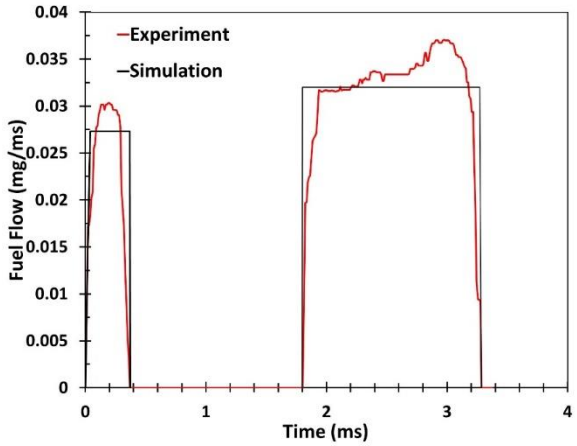

Figure 45: Filtered experimental Rate of Injection (ROI) profile and simplified rectangular ROI profile used for CFD work

The results of other rectangular-type shaped ROIs should not differ much since injection pressure and minor fluctuations in an ROI do not affect the liquid length adversely [Siebers 1998]. However, later in the combustion simulations, a filtered version of the raw experimental ROI was applied, yielding encouraging results.

Fig. 46 shows the experimental liquid and vapor lengths which are used to validate their CFD counter-parts at every stage of comparative computational work.

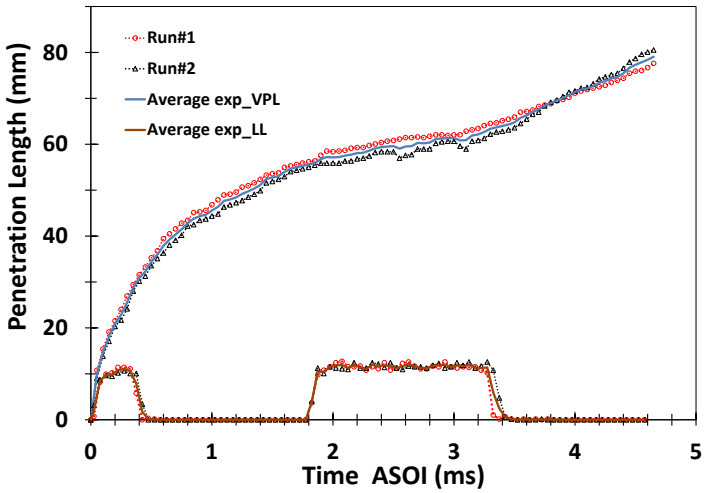

Figure 46: Experimental vapor penetration and liquid lengths. The individual shots and averaged values are shown

The conditions for the above test data (0% ambient oxygen) are shown in Table 3. The test data demonstrated good reproducibility and so just two runs were performed at each test condition considering the cost involved for each run of experiment. One interesting feature of Fig. 46 is that of the main injection vapor penetration after 1.80 ms after start of injection (ASOI). A higher slope of the main vapor penetration is observed than the pilot in those time instants. This happens due to the main injection constituents traveling in the slip-stream of the vaporized pilot, resulting in their faster downstream propagation.

The numerical liquid and vapor penetration lengths are defined as in Table 4

Table 4: Liquid length and Vapor penetration length definitions used in CFD

Parameter	Definition
Liquid length	Axial distance encompassing 97% of the injected liquid fuel mass.
Vapor penetration length	Maximum axial distance from the injector orifice where the fuel mass fraction Yf=0.01%.

The results of parametric variation of spray break-up time constant, parcel counts (number of parcels injected) along with the grid-convergent study are presented further in this section. A configuration of base grid = 2mm, embed level = 4 (Fine grid = 0.125 mm) and 200,000 parcels per injection is chosen to start with.

The break-up time constant (B_1) is an important parameter related to the Kelvin-Helmholtz break-up theory. It has a profound effect on the spray characteristics and is related to the initial disturbance level in the spray jet. Equation 7 shows the relation between the KH break-up time and the time constant B_1. The lesser the KH break-up time, the faster the spray break-up process.

$$\tau_{KH} = \frac{3.726 B_1 r_0}{\Lambda_{KH} \Omega_{KH}} \tag{7}$$

Fig. 47 shows the B_1 value variation which is the first step in the parametric variation according to Fig. 43. A value of 11.67 was obtained (cf. Fig. 47) corresponding to the average measured liquid length.

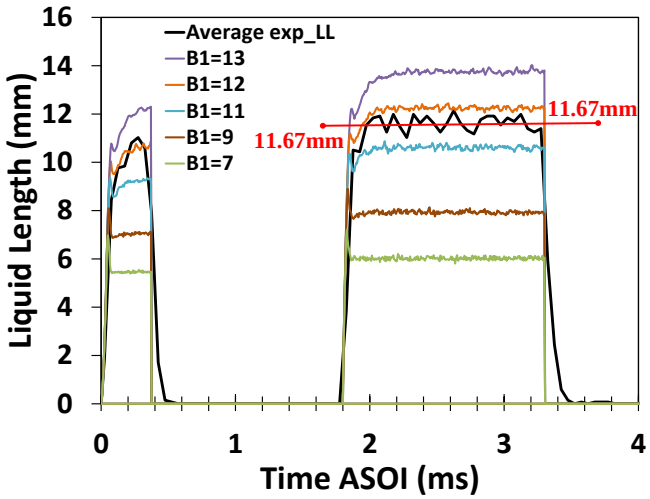

Figure 47: Influence of spray break-up time constant (B_1) variation on liquid penetration and liquid length

Fig. 48 shows a quasi-linear behavior of the liquid length variations with the spray constant value. Similar findings were obtained by [Pei et al. 2014] as part of their global sensitivity

studies. Note that previous investigations [Bravo et al. 2014] have demonstrated the spray constant parameter to be fuel dependent. As such fuel correlations like these, would be very helpful in choosing the spray constant value accurately without performing a parametric sweep every time.

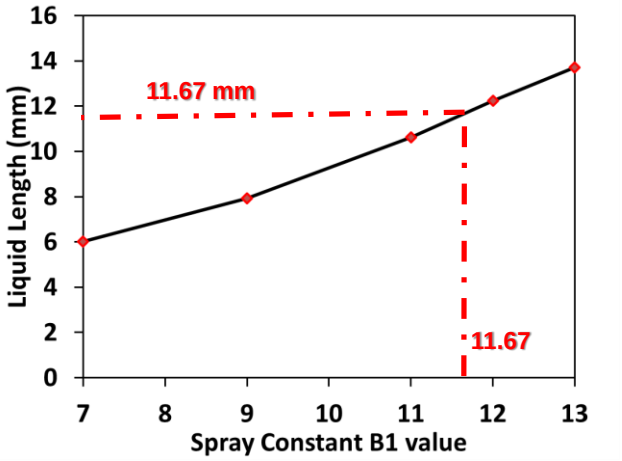

Figure 48: Spray break-up time constant B1 correlation with the liquid length. Liquid length (11.67 mm) correlates with B_1=11.67

Since the spray break-up tine constant (B_1) was the only spray constant varied, its final value along with the rest of the modified KH-RT model constants used in this work are tabulated in Table 5.

Table 5: Spray constant used in this study

B_0	B_1	C_1	C_t	C_{RT}
0.8	11.67	0.188	1	0.1

After the spray constant value determination, the parcel number was widely varied as shown in Fig. 49. A parcel count value whose standard deviation of liquid length is ~< 1 mm was chosen; it came around 200,000 parcels as shown in the Fig. 50. Parcels are the Lagrangian particles (massless and shapeless markers of liquid) injected into the computational domain to represent the liquid fuel. The number of these parcels used to represent the total mass of liquid is critical in spray calculations. There is a point at which

the number of parcels used would not have any impact on the results anymore, which results in statistical convergence with number of injected parcels. Using more than the required number of parcels might not adversely affect the numerical solution, but will result in an increased computational overhead. Providing insufficient number of parcels leads to over-prediction in liquid lengths due to artificial hydrodynamic drag effects. The adopted approach resolves this issue.

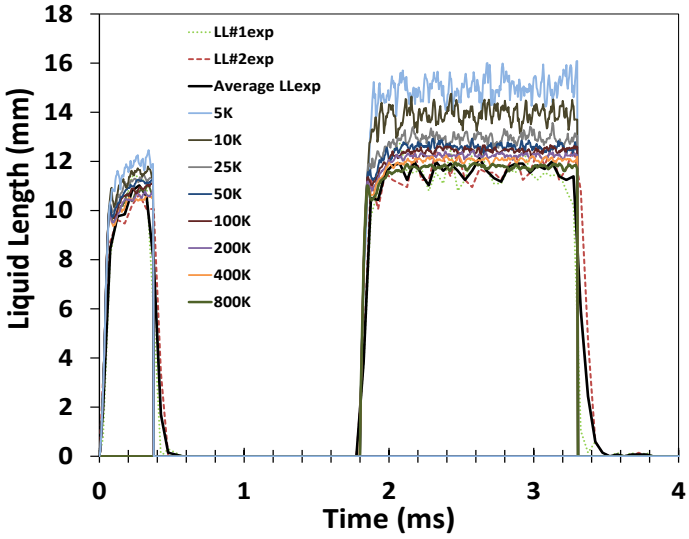

Figure 49: Effect of the number of parcels injected per injection on liquid penetration and liquid length

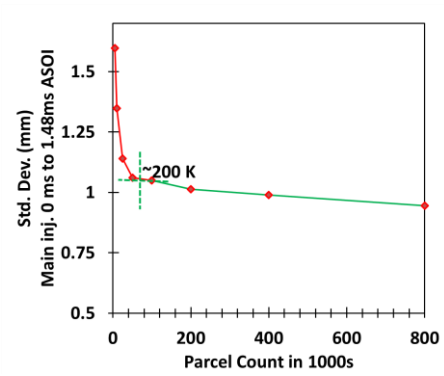

Figure 50: Estimating the number of parcels needed for acceptable deviation (~ 1 mm) of liquid length

Fig. 51 shows the final result of the grid convergence procedure obtained as the embed levels were varied from 2 to 5.As mentioned previously, as the embed level was increased (grid refined), the number of parcels injected were quadrupled and vice versa. Performing this procedure, the grid convergent results were obtained at embed level of 4 with a base mesh size of 2 mm (fine mesh size of 0.125 mm), and a parcel count of 200,000 parcels per injection.

In the present study, modeling the main injection vaporization and eventual combustion is the primary focus. For the pilot injection, it is seen in the Figures 49 and 51 that the statistical convergences of number of parcels and grid size respectively take place at relatively lower values. But, since the later part of this study is focused on the main injection rather than the pilot injection, emphasis was on setting up proper numerical parameters for the main injection and this needed finer grid size and higher number of parcels to be considered as part of the parametric variation and grid convergent process. Having higher levels of such criteria will not affect the pilot numerics, but will ensure that any possible numerical artifacts in simulating the main injection are avoided.

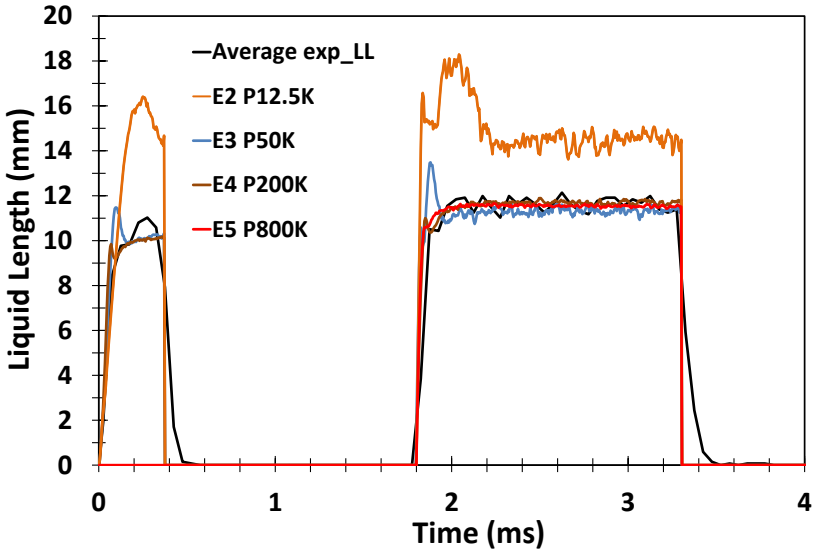

Figure 51: Grid convergence study plotting the liquid penetration and liquid length vs. time. The plot is labeled in the format of Ex Py (x=embed level, y=parcels injected)

It is to be noted that for the blob model employed in this investigation, it is best practice to use a fine grid value whose d_n/dx value (no. of grids in the nozzle diameter) is greater than 1; but due to anticipation of heavy computational load for the future repetitive simulations (since the grid would be too fine a size), a d_n/dx of 0.8 was settled for. This value of 0.8 is still acceptable as grid-convergent studies using lesser d_n/dx values have been performed previously yielding physically correct results [Senecal et al. 2014]. Also note that, the grid convergence plot of Fig. 51 does shows better convergence between embed scale 4 and 5, where d_n/dx crosses a value of 1. Table 6 shows details of minimum cell size, d_n/dx and parcel count, related to for this grid convergence study.

Table 6: Details of the grid size and the corresponding parcel count value with a base mesh size of 2 mm

Embed Scale	Minimum Cell Size, dx (mm)	d_n/dx	Parcel Count
2	0.5	0.2	12,500
3	0.25	0.4	50,000
4	0.125	0.8	200,000
5	0.0625	1.6	800,000

It was found that the vapor penetration length (VPL) profiles are also grid converged with the present setting as seen in Fig. 52. But they do not match the experimental case. Previous work done by [Senecal et al. 2014] had similar results of under-predicted vapor penetration lengths. Although grid convergence behavior was observed in their case, the numerical VPL profiles were still distinctly low. They attributed the low values of numerical vapor lengths to uncertainty in experimental measurements. In actual experiments (also in the present work), vapor boundary lies around the bulk of vapor mass which extends a little further away from the jet head, sometimes in the form of disjoint eddy protruding outwards. It is to be noted that, such unsymmetric structures might not lead to large discrepancies of VPL as

seen in the present work. Nevertheless, these unsymmetrical structures cannot be captured by a true RANS model which calculates the jet head in a round shape. Although, having a coarser grid may help the numerical VPL match the experimental VPL due to coarser grids entailing higher numerical error (cf. Fig. 52), it is not a correct approach due to no grid convergence established. There should be more emphasis in the modeling community on investigating the low VPL values at later time instants using an RNG k-ε model, since this discrepancy has also been encountered by of various other researchers [Campbell et al. 2009, Magi 2001, Senecal et al. 2014, Cung 2015]. Better results with respect to VPL predictions were observed by [Xue et al. 2013] with an LES dynamic structure modeling approach. They also showed that the predictions of vapor penetration profiles by LES modeling are more effective than a RANS approach. Future studies will explore the potential of using LES models for spray and combustion simulations.

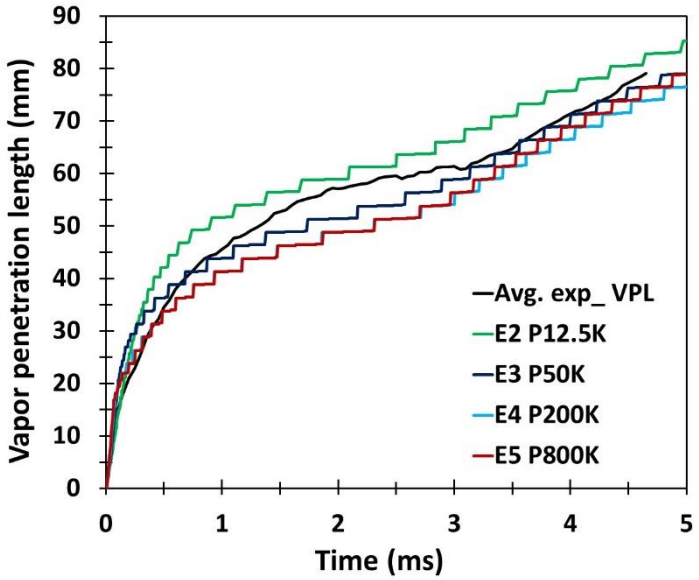

Figure 52: Vapor penetration length obtained through grid convergence study along with experimental profile, labeled in the format of ExPy (x=embed level, y=parcels injected)

Although a proper match of numerical VPL was not observed in this work, accuracy in the combustion simulations can still be obtained. This is assumed since until the time of the ignition (ignition delay, cf. Fig. 15), the vapor penetration profile of the grid converged case

of E4 P200K case (cf. Fig. 52) is still well-matched to the experimental profile. After the ignition delay, as the combustion is initiated, the reacting spray-flame predictions take little effect from the weak predictions of non-reacting penetrations. Perhaps for the same reason, well-validated combustion simulations were also observed by researchers [Campbell et al. 2009, Cung 2015, Senecal et al. 2014] who observed under-predicted VPL's in non-reacting spray simulations.

Before getting into details of the combustion modeling results, it would be beneficial to look into the experimental results. Fig. 53 shows the experimental average liquid and vapor penetration lengths from non-reacting (inert) spray experiments together with the flame penetration profile from flame luminosity experiments.

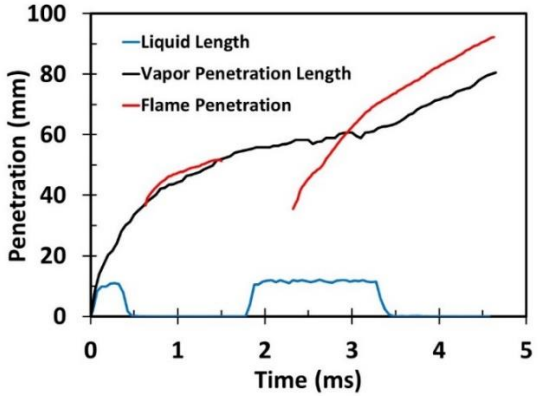

Figure 53: Experimental vapor penetration length, liquid length and flame penetration length

In Fig. 53, the points from where the flame starts shows the ignition time (X-axis) and Ignition location (Y-axis). It is seen from Fig. 53 that the ignition delay of main injection (with respect to start of its injection time) is shorter than the pilot ignition delay. Also, the location of the main ignition is farther upstream than the pilot ignition location. The location of the main flame front initiation is assumed to be a variable dependent upon pilot mass injected, dwell time between successive injections, main fuel mass injected and surrounding thermodynamic conditions. But it occurs upstream of the pilot ignition location due to the presence pilot induced higher thermal and reactivity conditions in the ambient of the main injection (Skeen et al., 2015).

3.8 Combustion simulations

Reacting spray simulations employed a reduced n-heptane mechanism consisting of 42 species and 168 reactions from Chalmers University [Nordin 1998]. This mechanism has been validated in the past [Som et al. 2012] for a range of constant volume spray-combustion conditions. Fig. 54 shows the predictions for the CFD ignition delay (top) based on the time instant after start of respective injections and when temperature crosses 2000 K. Also shown is the lift-off length data in Fig. 54 (bottom). Contour of Hiroy-soot, obtained by an empirical soot modeling approach [Hiroyasu and Kadota 1976, Nagle and Strickland-Constable 1962], is utilized for the CFD lift-off estimation whereas flame luminosity imaging is utilized for experimental lift-off length estimation. This flame lift-off comparison assumes that the experimental measurement of flame luminosity is majorly derived from soot radiation, which is modeled using the empirical Hiroyasu soot model in the simulations. From Fig. 54, some CFD data points of ignition delay (ID) and lift-off length (LOL) might not lie in the standard deviations of the experimental data which is provided as a shaded box. But for discussion sake, they are still considered to be in 'reasonable agreement' here, if they lie close to the locations of the shaded box for eg. SAGE model predictions of ID and LOL for the pilot and main. Recognizing the defects of the various combustion model, suggestions for their improvements will be made wherever possible.

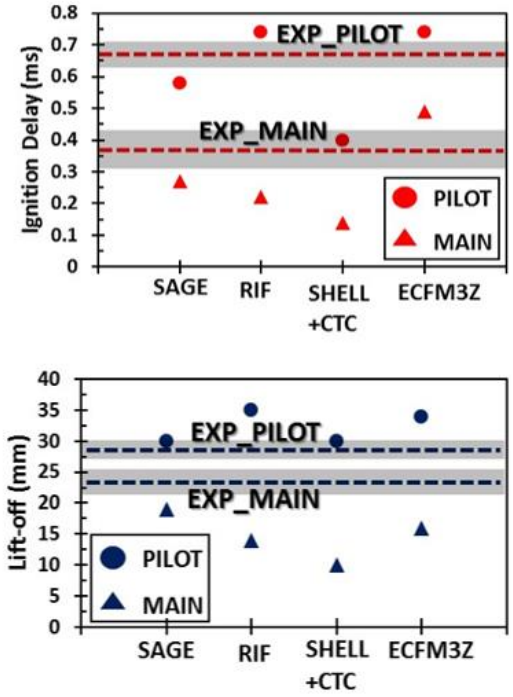

Figure 54: Ignition delay and Lift-off predictions of the pilot and main sprays with different combustion models

From Fig. 54, it can be observed that the main flame has an advantage of lower ignition delay and flame lift-off than the pilot in both experiments and simulations. Similar observations were made by other researchers as mentioned previously [Cung et al. 2015, Pickett, Kook, et al. 2009b, Skeen et al. 2015b]. It can be seen from Fig. 54 (top) that for SAGE and ECFM3Z models, if their pilot IDs are higher/lower than the experimental pilot ID, then their respective main IDs are also almost equally higher/lower than the experimental main ID. This trend is not observed for the SAGE model lift-off and worsens for the ECFM3Z lift-off correlation (cf. Fig. 54 bottom). This kind of correlation seems to be indicative of the fact that perhaps the initial conditions set by the pilot combustion are actually taken into consideration for the main ignition in both these models. SAGE being a detailed chemistry solver has shown good agreements with experiments for ID and LOL in prior works for single injection spray flames [Senecal et al. 2014]. Thus, treatment of a well-mixed model with a good chemistry mechanism can be one of the good approaches to simulate split injection flames. More details about spatial and temporal performance will be laid out in further

discussions before arriving at any conclusions. The weak, but better (than SHELL+CTC and RIF) predictions for ID and LOL with ECFM3Z model arise from its general idea of considering a combination of sub-models for auto-ignition, premixed propagating flame and diffusion flame simultaneously. [Felsch et al. 2009] and Gong et al., (2015) had concluded that in fact main flames get ignited and stabilized in a premixed flame propagation way. Thus, for predictions with a non-detailed chemistry model such as ECFM3Z, it can said that, while the pilot ID and LOL predictions were reasonable due to the consideration of auto-ignition sub-model, the reasonably good ID and LOL agreements of the main injection relates to the idea of considering a premixed flame propagation sub-model. To improve the predictions of the ID and LOL for the ECFM3Z model, improvement in the sub-grid mixing model and flame surface density model usage can be considered. In the present formulation of ECFM3Z model, the flame surface density is modeled with a transport equation which may not account for the high strain rates near the upstream near-nozzle locations. These locations are subjected to premixed combustion due to local mixing of fuel and air. Local quenching of flame can occur due to the high strain rates prevalent in these zones. An under-estimation of the flame surface density might lead to inconsideration of these aspects and thus a longer ignition delay (cf. Fig. 54 top). Also to simulate the sub-grid mixing, a 3-point dirac delta sub-grid mixing model is employed. A better prediction of the fuel-air mixing near the lift-off location (and the diffusion flame zone) will yield better accuracy of lift-off predictions. A suggestion to improve the LOL predictions can thus be to consider a more complete PDF modeling approach. But increase in run-times will be imminent. The bad main ignition and lift-off predictions of an (non-detailed chemistry based) auto-ignition based Shell+CTC model strengthens the idea of premixed flame propagation based ignition of the main injection. Thus, it is seen that the ID of the SHELL+CTC is much under-predicted but LOL is within good agreements. Shell+CTC model was also not observed to capture a proper ignition delay by [Som et al. 2013] and resulted in lower IDs than a detailed chemistry SAGE solver. Considering the turbulent-chemistry enabled RIF model, the pilot ID and LOL can be said to be within reasonable agreement but are still on the over-predictive side. The main ID and LOL from the RIF model does not follow an over-prediction trend and are lower than the experimental values with a bigger difference than the pilot predictions. The reason for

this lies in the formulation of the RIF models which requires multiple flamelets, with the number of required flamelets depending on the ambient temperature conditions [Kundu et al. 2014]. For an ambient of 900 K, reasonably well predictions pertaining to the pilot ID and LOL for RIF model have been found by simulating 20 flamelets in this work following [Kundu et al. 2014]. For the high local temperature conditions (~1500) experienced by the main injection, 60 flamelets were to be initialized, but it was not done in the present work due to the associated increased computational overhead. More details about RIF models implementation and bad predictions for main flame are discussed in further sections.

On the whole, predictions of SAGE, RIF and ECFM3Z can be considered acceptable for pilot IDs. For the main IDs however, SAGE and ECFM3Z perform reasonably well. All the combustion models did a pretty decent job in predicting LOL for the pilot injection. SAGE and for some extent ECFM3Z model can be considered acceptable for main LOL predictions. Fig. 55 shows a snapshot of flame contours from experiment and CFD for an instant of time of 3 ms ASOI. 3 ms ASOI would be a time when the main injection is still active and the main flame has a stabilized lift-off in all the cases.

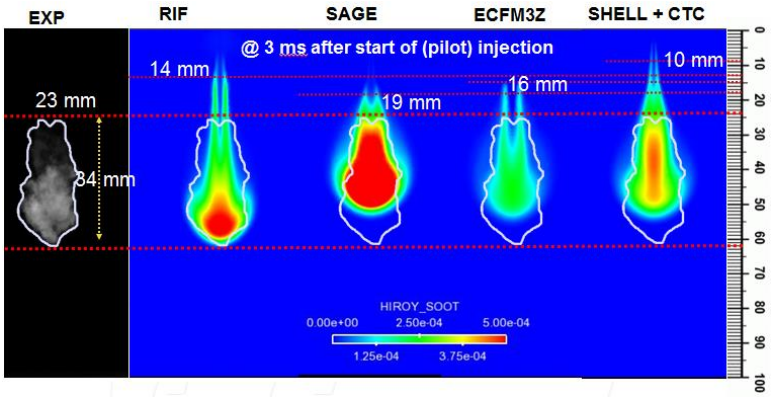

Figure 55: Comparison of flame lift-off, global flame structure, and flame length for the different combustion models from CFD against experiment

The (main) lift-off predictions following the Fig. 55 follow the same reasoning as in the previous section. However, more emphasis is put here on the flame length and the overall flame structure. Comparisons made in Fig. 55 may not be conclusive, since the ignition delay for the CFD cases are different within themselves and with the experimental case too. An

earlier ignition may result in faster penetration of the mixture in the form a diffusion flame head. In the case of a slower ignition, the mixture travels slowly in the form of a vaporizing mixture until the time instants of ignition. Comparing the various model results from Fig. 55, RIF has captured the flame penetration properly, but failed to give a good correlation of the (main) lift-off length. As mentioned previously, the simulation for RIF was done following the good practices from [Kundu et al. 2014]. 40 flamelets were initialized for the simulation; 20 flamelets for the pilot and 20 for main. The pilot shows a good correlation of the ignition delay and the flame lift-off, but the main failed to do so. One of the reasons for this is due to the main spray entering a much hotter local environment (~1500 K) created by the pilot combustion when compared to the ambient temperature condition experienced by the pilot (900 K). Following [Kundu et al. 2014], an environment of ~1500 K, would need around 60 flamelets for the main. The low number of flamelets used for main in this work (20), causes inefficiency on the part of the RIF model to capture the mixture fracture variations in the main-pilot interaction region and hence the incorrect lift off length (and ID). Since, the flame penetration is majorly pilot flame driven, it is captured well due to the sufficiency of the flamelets for the pilot injection. Better results are expected for main injection if more flamelets are considered, but this is not in the realm of the present study due to increase in run-times considerably [Kundu et al. 2014]. One suggestion about probable usage of the RIF model for split-injection spray combustion application is to enable the usage of multiple flamelets (few hundreds), to ensure that no dependency on the number of flamelets would cause numerical inconsistencies. To avoid the high run-times associated with usage of high number of flamelets, a look-up table approach might be employed where the solutions of the flamelets (for various thermal and species compositions) are pre-computed using standard one-dimensional flamelet codes and stored in the form of a flamelet library. From the Fig. 55, on the non-detailed chemistry model side, ECFM3Z model has good correlations of the lift-off length and flame tip penetrations when compared to the SHELL + CTC model due to the considerations of the various physical regimes of combustion in its model formulation. SAGE model is overall better performing amongst all the combustion models as per Fig. 55, also considering the fact that the flame length modeled using SAGE is closer to the experimental value. Similar results may be expected by analyzing more instants of

time. Since, lift-off is a quasi-steady condition, the flame penetration data was considered and further examined from start of main ignition times to gauge the progression of the flame and thus the performance of the combustion models.

Fig. 56 shows the flame penetration length for the experiment and the CFD cases shortly after the ignition of main.

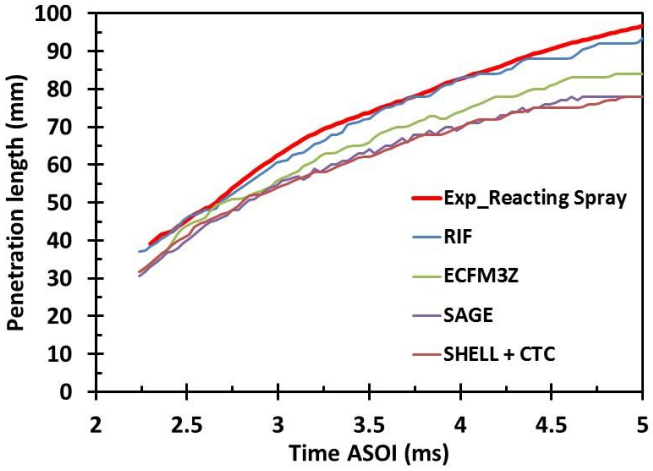

Figure 56: Flame penetration lengths by different combustion models from CFD calculations compared against the experimental data

From Fig. 56, RIF flame tip penetration is close to the experimental values throughout the simulation times. This is followed by ECFM3Z results, which are slightly lower than RIF results but higher than the SAGE and SHELL+CTC results at any instant of time. For the SAGE and SHELL+CTC models, the flame tip penetration have similar magnitudes and result in least penetration among all the models. As mentioned before, the close predictions of RIF model for the flame penetration can be attributed to the good prediction of pilot flame (due to sufficiency of flamelet number), since the pilot flame actually resides in the outer region of the combined pilot-main flame structure. SAGE resulted in lower predictions of the flame penetration. Similar lower predictions of flame penetration for a single injection case with SAGE model employing same turbulence model as used in this work were observed by [Pei, Som, Kundu, et al. 2015] using n-Dodecane as fuel. The inconsistency in capturing the flame head by SAGE model cannot yet be explained. However, [Pei, Som, Kundu, et al. 2015] did

observe better predictions employing a higher fidelity large-eddy simulation turbulence modeling approach along with using SAGE model. Apart from observing very good predictions of jet penetration they also obtained good quantitative soot mass predictions although employing an empirical soot modeling approach as used in this work. Their results suggest that perhaps using a better turbulence modeling approach might be the right direction to better capture combustion physics along with using a detailed chemistry solver (like SAGE) to solve for the chemistry. Among the non-detailed chemistry models of Fig. 56, ECFM3Z performs better than SHELL+CTC in capturing the flame head. Reasonably well predictions (although slightly under-predictive) of ECFM3Z model were also observed by [Campbell et al. 2009] using n-Heptane as a fuel for a single injection case. They concluded that inclusion of a mixing treatment and a partially premixed combustion sub-model may be plausible reasons for the good predictions and better predictions may be obtained by improving these aspects. By considering results from other researchers relating to SHELL+CTC model usage, similarity between SAGE and SHELL+CTC predictions for flame penetration were also observed by [Som et al. 2013].

To investigate further with the fluid dynamic effects with the combustion model usage, Fig. 57 shows a depiction of velocity vectors with contour plot of the predicted soot using the Hiroyasu model. Vortex or ‘lobes’ are found to be created when the main flame interacts with the pilot. These lobes are a good indication of mixing and interaction between the pilot and the main flame and are useful to gauge the fluid dynamics related performance of the simulations involving the various combustion models.

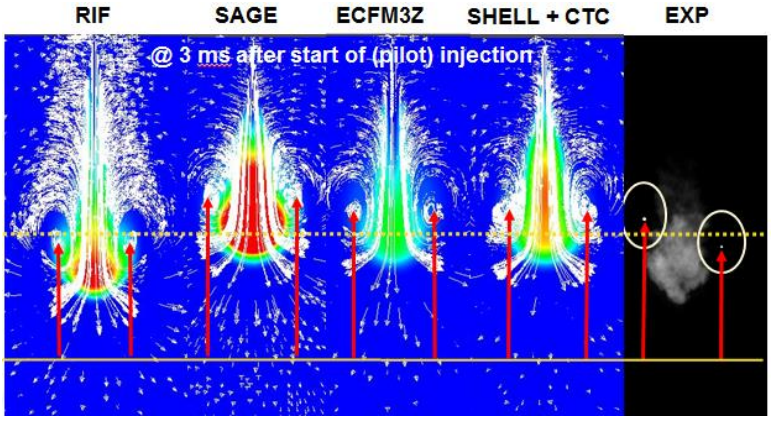

Figure 57: Velocity vectors plotted over soot contours depicting vortex ('lobe') formation at 3 ms ASOI

On the extreme right of the Fig. 57, the experimental flame is seen with the average lobe position line marked. From the Fig. 57, RIF, SHELL + CTC and ECFM3Z models correlate reasonably well with the lobe position; the RIF model slightly over-predicting the lobe position and the latter two models under-predicting it. RIF is superior in predicting the lobe position due to accurate pilot flame prediction (cf. Figures 54, 55 and 56), but due to the main flame not accurately modelled, it might lead to over prediction of the lobe position. Although, ECFM3Z does not have detailed chemistry, it can fairly well capture the lobe position, not to mention the reasonable predictions of lift-off length, ignition delay and flame penetration length as demonstrated from the previous discussions (cf. Figures 54, 55 and 56). Weak prediction of the SAGE model were observed. Since SAGE does not involve turbulence chemistry interaction, stepping up on turbulence modeling towards an LES modeling approach would help covering this defect [Pei, Som, Pomraning, et al. 2015]. Considering SHELL+CTC model, better predictions with regards to the position of the lobe might arise due to its very early ignition. An early ignition causes higher penetration of the head in the form of a faster traveling diffusion flame front. Thus, conclusions regarding the SHELL+CTC model should be made with caution. Improvement in the SHELL+CTC model can be made to tailor its usage for split-injection spray combustion modeling. Considering proper ignition modeling, in SHELL+CTC model, there are a total of 26 model constant related to SHELL reactions, and only one of the model constant related to the rate-limiting step is usually tuned to match the ignition time. However, tuning of this constant is not

effective at all times. Since, there is also an impact of local gas temperature cut-off and a delay factor. Below a specific cut-off temperature and delay factor value SHELL model reactions takes place to simulate ignition whereas above those values CTC reactions occurs to simulate combustion. Even if all the tuning operations are performed to match the pilot combustion, it might not guarantee good predictions for the main ignition and combustion. Since, the ambient of the main injection has higher temperature and relatively higher level of mixing (higher strain rates) [Felsch et al. 2009]. In CTC model, there is one constant each for turbulent and chemical time-scales associated with mixing. Thus, it is imperative, not just to have one set of these tunable terms in the SHELL+CTC model; but employ multiple sets of them on a per-injection basis. Such considerations were not performed in the present work. Although it would be very cumbersome to tune, it is one of the ways to improve the weak predictions of SHELL+CTC model.

3.9 Run-time trade-off

Table 7 shows the run-time (in core hours) and peak cell count.

Table 7: Run time and peak cell counts for the different combustion models run on a common computation power of 32 cores

Model	Core hours	Peak cell count	Comment
SAGE	3200	601,370	High run-time. Good predictions of pilot and main flame
RIF	1720	407,113	Main flame modeling yet to be improved by considering high no. of flamelets
ECFM3Z	356	125,252	Good balance of run-time and prediction accuracy with non-detailed chemistry
SHELL + CTC	384	138,433	Unimpressive predictions for pilot and main. Tuning of model constants is cumbersome

Fig. 58 proposes a flame development schematic for the split injection combustion scenario. This schematic is hypothesized based on experimental and CFD flame development/propagation visualization from the present work.

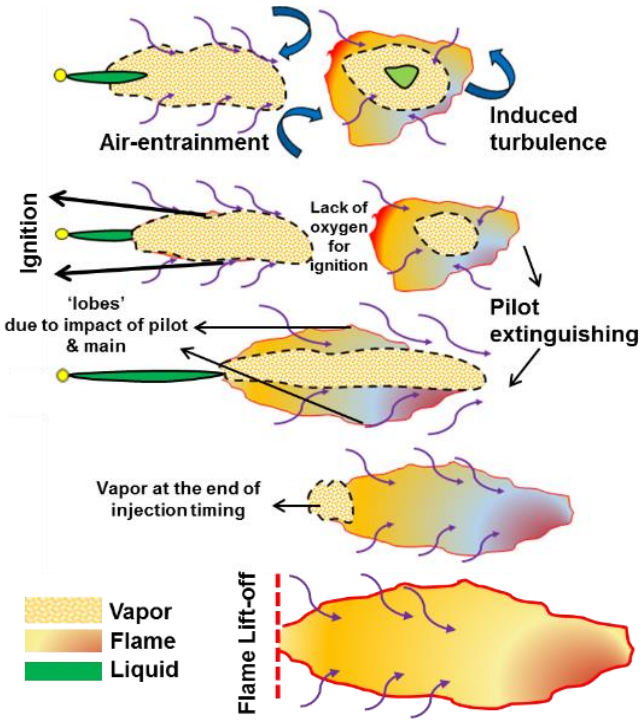

Figure 58: Schematic of flame propagation for split injection scheme

From Fig. 58, it can be hypothesized that, as the pilot flame burns and uses the local oxygen, the main flame has lesser oxygen to use and combust in its leading edge, thus ignition occurs in the surrounding boundaries. The ignition points for the main spray can be developed at any point on the main spray's vapor boundary where the conditions are apt. At the same time, air entrainment continuously replenishes the boundary of the main spray with oxidizer, causing ignition and combustion in the boundary locations. Ignition can also occur at varying times after start of main injection depending on the pilot/main mass ratio and the dwell time [Cung et al. 2015]. As the flame proceeds, ignition and combustion proceed towards the head portion of the main spray from the boundary locations. After the main injection ends, the air-entrainment causes the tail portion of the main spray (which is now

vaporized) to burn utilizing the freshly entrained air, causing the flame to move little backwards and approach a stable lift-off later on.

3.10 Concluding remarks

Model usage recommendations based on the above study are put together in Table 8.

Table 8: The criteria (both global and structural) along with the model that performed most reasonably to mimic the experimental trend for main flame simulation

Criteria	Decision
Global	
Ignition delay	SAGE, ECFM3Z
Lift-off	SAGE, ECFM3Z
Core hours used	ECFM3Z (non-detail), RIF (detail)
Structural	
Flame Penetration	RIF
Flame Length	SAGE, ECFM3Z
Lobe position	RIF, ECFM3Z, SHELL + CTC

This work is aimed at providing a direction to the commercial CFD user to make decisions on setting up a grid convergent solution for lagrangian sprays and at the same time selecting a suitable combustion model for their applications based on run-time and accuracy trade-off. It involved a split-injection spray and combustion problem. To summarize, four of the modern combustion models are utilized for the simulation of a split injection scheme after performing grid convergent studies. The relevant parameters to be considered for performing a grid convergent study for a Lagrangian spray model considered were number of lagrangian parcels injected, spray break-up time constant and grid size. After ensuring

that the spray model is grid converged solution and validated with liquid and vapor penetration lengths, a combustion model assessment was performed. Any large deviations in predictions of the combustion models will thus arise from their formulation. Deficiencies and areas of improvement for using the combustion models especially for a split-injection combustion case are provided. The Hiroyasu soot empirical model prediction was considered for comparisons with the experimental flame luminosity test data. Ignition delay, flame lift-off length, flame penetration length, flame length, and global flame structures generated by the four combustion models were compared with the experimental results. SAGE model showed better predictions over its detailed chemistry modeling counter-part, RIF. The comparisons also showed overall good predictions for ECFM3Z model which is a non-detailed chemistry model, when compared to SHELL + CTC model. RIF model was found to be a good approach towards detailed chemistry modeling, and would be more suitable if higher number of flamelets are employed for proper main flame modeling. Run-time trade-off was also arrived at for a 32 core computation load for each of the combustion simulations. SAGE model showed large run-times, but on the other hand, had good comparisons with the experimental test results. SAGE with multi-zone solver could reduce the run-time, but may decrease the accuracy A detailed analysis using these combustion models across various test conditions will yield more useful insights about the accuracy of these models in their predictions. Finally, a combustion schematic for split injection flames was proposed based on the visualizations from the experiments and the CFD.

CHAPTER 11

PREMIXED COMBUSTION EFFICIENCIES[3]

3.11 Background

In the present work, a split injection scenario main flame combustion efficiency is investigated. The premixed and diffusion phases of the main flame are detected by two peaks in its heat release rate curve. Using such heat release data, the theoretical calculations of burnt gas volumes are computed and compared with experimental luminosity imagery (for the premixed combustion phase only). Such calculations give an indication of combustion efficiencies. Finally, the combustion enhancements are compared between three dwell time cases of split injection schemes tested.

The experimental results for split combusting sprays are previously published in Ref.[Cung et al. 2015] and are the same as in chapter 11.

A single-hole solenoid injector was used to generate multiple-injection. An example of two consecutive injections (15%/85% mass-based) is shown in Fig. 36, including raw rate of injection (ROI) data and filtered ROI overlapped with the driver current profile. The pilot-main split injection event was set to keep the same injection pulse width. The ROI was measured using a Bosch type accumulator. The injector had a few test shots before every run to confirm distinguishable pilot and main injections. The pressure variation in the injector high-pressure line is negligible during the injection event as the high-pressure fuel system includes two 100 mL accumulators to store the pressurized fuel for the injection event. Dwell time (DT), which is the time between the end of the pilot and the start of the main, was set at 0.17 ms, 0.77 ms, and 1.37 ms.

[3] The material contained in this chapter was previously published in *National Combustion Meeting* Moiz, Ahmed Abdul, and Seong-Young Lee. 2015. Coupled Luminosity-Heat Release Rate Analysis for Split Injection Diesel Flames, *9th U. S. National Combustion Meeting, Central States Section of the Combustion Institute, May 17-20 2015, Cincinnati, Ohio*

3.12 Discussion

Calculations of theoretical burnt volumes and flame volumes were performed following Ref. [Balles and Heywood 1989] with slight modifications as explained here. A combination of pressure data from combustion experiments, high-speed luminosity imagery and burnt-gas temperature data from CFD culminated in a combustion efficiency term of the main premixed combustion. The pressure trace of the combustion vessel is used to determine the heat release rate (HRR) from the combustion event of the fuel. The recorded combustion pressure data was processed to isolate the region of interest, and then was filtered to remove noise. The pressure differential (change in pressure) for each time step (10 μs) was determined over the entire filtered pressure region of interest during the combustion event (both pilot and main) and used in the heat release rate relationship provided by the Equation 8

$$\frac{dQ}{dt} = \frac{\gamma}{\gamma - 1} P \frac{dV}{dt} + \frac{1}{\gamma - 1} V \frac{dP}{dt} = \frac{1}{\gamma - 1} V \frac{dP}{dt} \tag{8}$$

here P is chamber pressure, V is the combustion vessel volume, and γ is specific heat ratio. This equation was simplified, since the combustion vessel is constant volume (1.1L), so the volume – time derivative can be neglected. The pressure – time derivative was calculated and γ is a constant representing the ratio of specific heats of the charge-gas environment, approximated as 1.35 for these tests. A cumulative heat release can be determined using this heat release rate trace.

The cumulative heat release trace ($Q(t)$) is divided over the lower heating value of the fuel (Q_{HV}) to obtain the burnt mass of the fuel (m_{bf}) as in Equation 9.

$$m_{bf} = \frac{Q(t)}{Q_{HV}} \tag{9}$$

Later the burnt mass of the fuel is multiplied with the stoichiometric air-fuel ratio for n-heptane fuel $(\frac{A}{F})_s$, 15.4, to get the mass of air burnt (m_{ba}) as in Equation 10.

$$m_{ba} = m_{bf}\left(\frac{A}{F}\right)_s \quad (10)$$

Adding the mass of the fuel (m_{bf}) and mass of air (m_{ba}) burnt will give the total mass burnt (m_b) which is later applied in the ideal gas law with the inclusion of the burnt gas temperature (T_b) and the pressure trace from the vessel (p) to obtain the burnt gas volume (V_b) as shown in Equation 11.

$$V_b = \frac{m_b R T_b}{p} \quad (11)$$

The burnt gas temperature was computed from the CFD simulations of previous work of [Cung et al. 2015] which gave very close predictions of ignition delay and flame lift-off.

A flame volume (geometric) term is also needed to be calculated to compare with the burnt gas volume from Equation 11. For calculation of the flame volume, starting from the flame area, the image from the high-speed camera is processed in the MATLAB image processing toolbox to trace the boundaries of the flame geometry. The process of arriving at a proper flame boundary is started by subtracting the raw image with the background image (image before fuel injection), then applying a medium filter to the subtracted image and later adjusting the threshold for the filtered image. The obtained image is converted to gray-scale with the applied threshold. Later, the maximum area of the flame is found along with area opening operation which enables the removal of all connected components having fewer than specified amount of pixels, producing another binary image. Finally, image segmentation is done by using a morphological operator (dilation with diamond structural element) to output a uniform boundary. This analysis is performed for the flame imagery obtained for the three dwell time cases. The experimental flame volume is calculated by considering an axisymmetric assumption of the 2D flame boundary, by assuming a circular flame geometry in the plane perpendicular to the flame propagation. This results in the luminous flame volume V_f. Fig. 59 summarizes the equations and assumptions utilized to calculate theoretical burnt volume which is compared with luminous flame volume from the experiments.

The analysis is carried just for the main injection and not for the pilot injection, since the pressure trace from the pilot injection was very small due to the small amount of pilot mass involved in the combustion process. This hindered the pressure transducer to catch the small transients in pressure. This also gave a very small magnitude of heat release, which is not trustable. However for the main injection, the pressure rise (and thus heat release) involve higher amount of the mass in combustion, rendering the pressure transducer to better catch the transients, resulting in better pressure trace (and heat release) output. However, results from Ref.[Balles and Heywood 1989] can be considered to be applicable to a pilot (or single) injection scenario, due to their operating conditions being very close with that of the present work. A pilot combustion efficiency of 0.5 can thus be approximated.

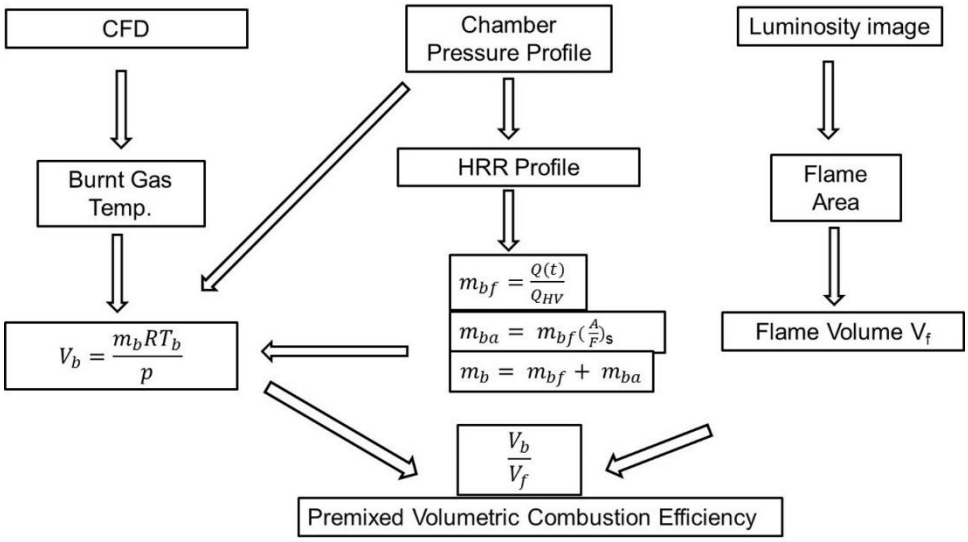

Figure 59: Procedure for calculation of Vb/Vf ratio

As mentioned before, the premixed zone of the main flame is estimated from the clear first peak of the heat release rate curve as shown in Fig. 60 where the premixed durations from the main flames of respective main flames have been highlighted on the time axis. The heat release obtained as in Fig. 60 is used to carry out the series of steps leading to burnt-mass calculation as illustrated in Fig. 59.

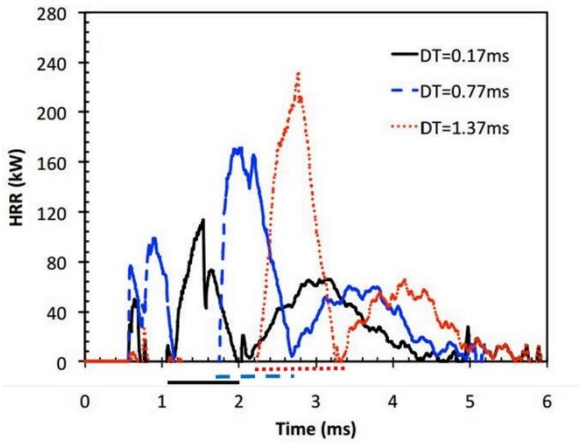

Figure 60: Mean heat release rates of the 3 different dwell time cases. Premixed combustion phases of the respective main flame are highlighted on time axis

Fig. 61 shows the flame areas for the three dwell time cases considered. As seen from Fig. 61, the three dwell time cases are interesting to study because the flame areas of the pilot and main injections for lowest dwell time case (0.17 ms) are overlapped, for the intermediate dwell time case (0.77 ms) the flame areas just touch each other whereas for the high dwell time case (1.37 ms) the flame areas are separated in space and time. The flame areas as seen in Fig. 61 are used to calculate the flame volume as illustrated in Fig. 59.

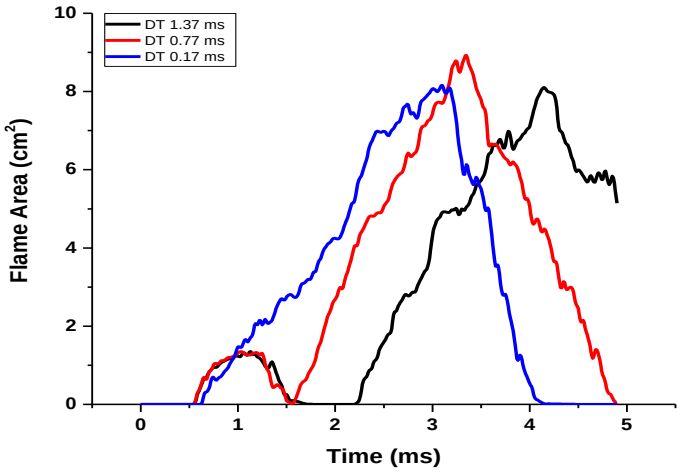

Figure 61: Flame area for three cases of split injections

The ratio of $\left(\frac{V_b}{V_f}\right)$ was found to be around 0.5 by Balles and Heywood [Balles and Heywood 1989]. Their analysis was in the premixed zone of the diesel flame combustion with experimental conditions being similar as in the present case. By following the calculation procedure as shown in Fig. 59, it is found in the present work that the ratio of $\left(\frac{V_b}{V_f}\right)$ returns different values for the main flame with different dwell times. Figures 62, 63, and 64 show the behavior of the term $\left(\frac{V_b}{V_f}\right)$ for the three different dwell time cases analyzed. One of the compromises in the comparison of calculated burnt volumes and visualized experimental flame volumes is the extent of dependence (or linearity) which is observed in the premixed zone of combustion, whereas turbulence effects start to act in the mixing controlled combustion phase rendering the comparison not useful in the latter phase (cf. Figures 62, 63, and 64).

Figures 62, 63, and 64 (left) span from the start of main ignition until when the flame hits the wall of the constant volume chamber. A linear correlation of burnt mass volume (V_b) and enflame volume (V_f) is found from the start of ignition until the end of premix combustion for all the dwell time (DT) cases analysed. It is to be noted for the DT 0.17 ms (cf. Fig. 62) case that, since the dwell time is very small (0.17 ms) the split injection scenario is close to a continuous single injection. The value of $\left(\frac{V_b}{V_f}\right)$ for the main flame of DT 0.7 ms case is 0.65 (on average). The value of $\left(\frac{V_b}{V_f}\right)$ signifies combustion efficiency and is related to the amount of fuel (volumetric basis) which is still left unburnt in the flame. Fig. 63 shows the same characteristics with a 0.77 ms dwell time split injection. Here the ratio $\left(\frac{V_b}{V_f}\right)$ is found to be 0.94 on average. This shows the enhancement effect of the pilot injection on the main injection given a proper dwell time between them.

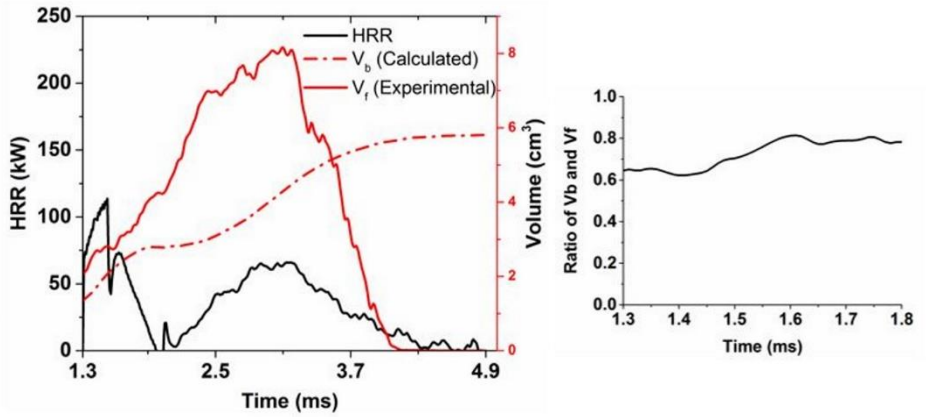

Figure 62: Vb, Vf, HRR behavior (left) and Vb/Vf curve (right) for DT 0.17 ms case

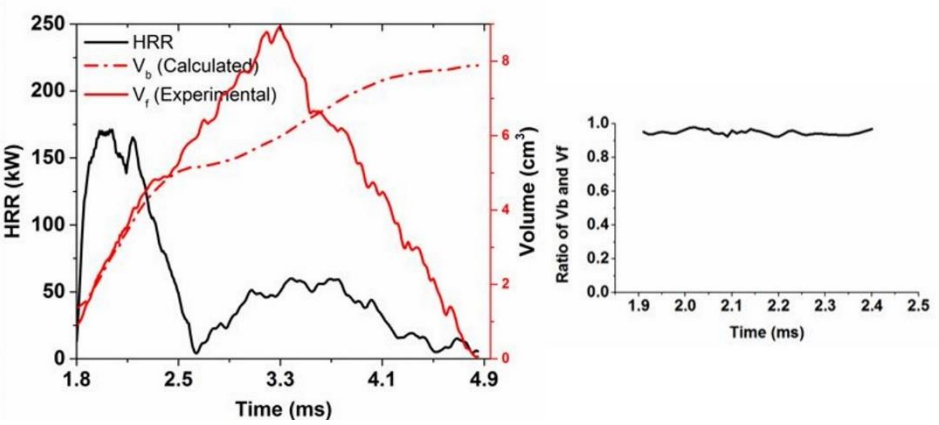

Figure 63: Vb, Vf, HRR behavior (left) and Vb/Vf curve (right) for DT 0.77 ms case

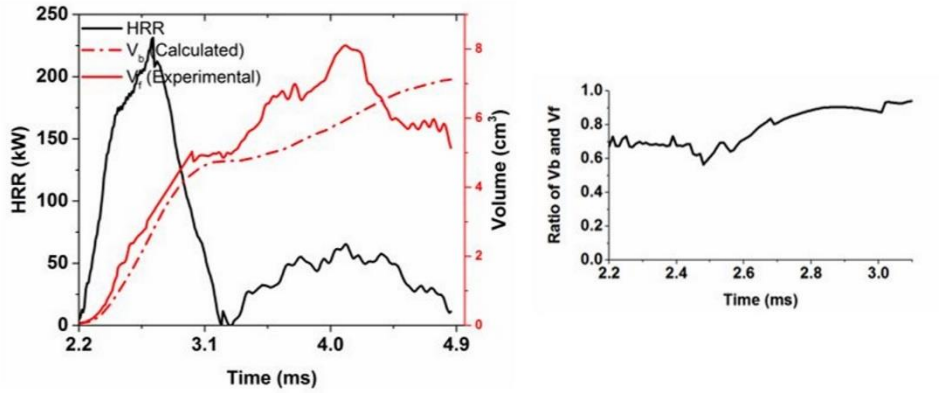

Figure 64: Vb, Vf, HRR behavior (left) and Vb/Vf curve (right) for DT 1.37 ms case

It is pointed out in various studies [Bruneaux and Maligne 2009, Cung et al. 2015, Han et al. 1996], that the dwell time between the injections needs to be optimized so that the gas temperature observed by the main injection remains high enough to accelerate the combustion. This might be the reason for the better performance of the medium dwell time flame. A brief investigation pertaining to reasoning of combustion enhancement is present in a further section. Fig. 64 depicts a lower ratio of $\left(\frac{V_b}{V_f}\right)$, 0.75 on average, for the higher dwell time (DT 1.36 ms) case. This lower $\left(\frac{V_b}{V_f}\right)$ value is perhaps because the dwell time is quite high and flame has missed the thermodynamic sweet-spot for experiencing enhanced combustion. A point to be noted in the higher dwell time (1.37 ms) case is that as the main starts igniting, it starts with a $\left(\frac{V_b}{V_f}\right)$ ratio of similar to the DT 0.17 ms case, this is because the pilot flame has moved further downstream due to the high wait time the main had before its injection. When the main injection vaporized and ignited, it does not experienced a higher temperature environment in its immediate vicinity due to the surrounding cooler oxidizer entrainment happening continuously. This can be considered as a single injected flame in its initial stages of injection with no interaction effect from the pilot. But as the higher momentum main flame develops and approaches closer behind the lower momentum pilot flame, it comes in the interaction region of the pilot flame; thus the $\left(\frac{V_b}{V_f}\right)$ numbers rise from then on and approach the numbers closer to the 0.77 ms DT case. The present analysis also brings us to a qualitative conclusion such that 0.77 ms dwell time is a ball-park estimate of the optimized dwell time for these injection conditions.

The volumetric ratio of $\left(\frac{V_b}{V_f}\right)$ is a measure of the combustion efficiency. This ratio can be converted to a mass ratio of unburnt mixture to the total enflamed mass (m_{ub}/m_f), by assuming a density ratio of 4 between unburnt and burnt mass. The m_{ub}/m_f ratio correlations for the three dwell time cases are shown in the Fig. 65.

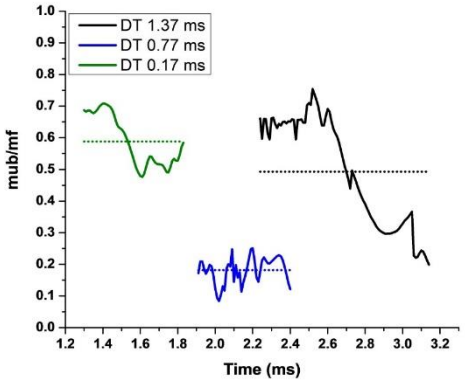

Figure 65: Ratio of unburnt mass to enflamed mass for the premixed portion of main flames

From Fig. 65, it can be seen that the short dwell time case of 0.17 ms has an average unburnt mass to enflamed mass ratio (m_{ub}/m_f) of 0.58, indicating that 58% of the main flame is composed on unburnt mixture in the premixed region of the main flame. As the dwell time increases to 0.77 ms, this ratio decreases considerably to 20%, meaning, on an average, only 20% of the fuel-air mixture is yet to be burnt in the premixed phase of the main flame. As the dwell time is further increased to 1.37 ms, this ratio goes higher initially, approaching the (m_{ub}/m_f) values of 0.17 ms DT case, but as the main injection proceeds further downstream, m_{ub}/m_f ratio drops down significantly to approach the (m_{ub}/m_f) values of 0.77 ms DT case.

As mentioned before, the mixing controlled combustion phase is difficult to analyze using the approach followed here. This is because, as the flame transforms to a diffusion type, other parameters relating to mixing and turbulence are responsible for combustion progress. This renders the simple theoretical equations for the burnt gas volume estimation not to relate well with the enflamed volumes due to inherent non-linearity in the various other physical processes. Thus a near-constant number is not obtained for the mixing controlled flame combustion event as obtained from a premixed controlled combustion event. Perhaps, deriving an empirical relationship accounting for the complex physical processes encountered with diffusion type flames can aid in better ratio calculation in diffusion flame zone as well.

3.12.1 Combustion enhancement

Ignition and combustion progression of the main flame has a strong influence from the dwell time between pilot and main. Hasse and Peters [Hasse and Peters 2005] have used CFD modeling to conclude that the transfer of heat and mass between the pilot-main mixture fields results in ignition of the main injection mixture and the timing between pilot and main effects how these two fields interact. The high mixture fraction gradients in the pilot mixture results in an increase of main flame premixed flame propagation speed, leading to reduction in the main ignition delay. Optimization of split injection strategies, with dwell time as one of the vital criterion, was shown as a key to realize combustion efficiency and emissions benefits in ICEs [Bakenhus and Reitz 1999, Chen 2000, Hotta et al. 2005, Shayler et al. 2005]. One of the prominent theories resulting in better combustion in split injection flames is realized by interruption of the fuel flow itself which enhances replenishment of the sprays heads. Avoidance of a continuous fuel enrichment of the downstream spray by interrupting the fuel injection results in a near-stoichiometric combustion[Bakenhus and Reitz 1999]. Additionally due to this interruption, there is better oxygen availability in the constituting injections which leads to higher soot oxidation rates. That said, optimum dwell times consideration is also important to make sure that the main injection happens in a lean and hot environment so that the newly entering main injected fuel burns rapidly and efficiently. It can be said that, with lesser dwell time there might not be enough oxygen in the tail of the pilot combustion making the local main environment rich and hot. This is not an ideal environment for the main to burn efficiently. With higher dwell time, the tail of the pilot combustion might be lean due to oxygen entrainment happening but might not be as hot as the lower dwell time case. An optimum dwell time ensures hot and lean environment for the main to burn efficiently. To support this discussion, Fig. 65 shows the temporal evolution of flame observed in the present work through false-colored flame luminosity images with the areas of the flame displayed in white text boxes. Flames are shown with respect to their start of injection times, with the total main injection duration being 1.37 ms for all the cases. From the Fig. 66, 0.9 ms after start of main injection (ASMI) is a time when the main flames are ignited (within close contacts of pilot flame) and the main flame kernel growth is seen.

The 0.9 ms time instant shows slightly higher disturbed main flame head for the low dwell time case, but the intermediate dwell time has higher areas among other cases. This can be considered due to a higher (temporary) impact of the main fuel jet which slips through the nearby hotter pilot field creating more disturbance throughout. The ambient experiences by the main injection is less hot as the dwell time is increased. This is due to pilot flame traveling further away with increased dwell time along with the effect of the entrainment of the cooler ambient in the upstream of pilot. As the ASMI times are investigated further, one can observe the disturbed flame head is seen in the medium dwell time case, with it yielding highest flame areas for all the ASMI times. The flames of low and high DT appear more similar with each other than the medium DT case, the flame areas are similar too.

A higher radial flame spread (disturbed flame) implies more mixing from the ambient oxygen. For an already combusting spray-flame, this leads to efficient combustion. Since, the flame areas of the medium dwell time cases are consistently higher than the other two cases, the main flame of the medium DT case is considered to better mixed with the ambient. This may be due to the presence of right thermodynamic conditions in the ambient of the main injection, viz. hot and lean, which leads to it well-mixed flame propagation. This is thought to be the reason for higher premixed combustion efficiency obtained from the analysis outlined in the previous section.

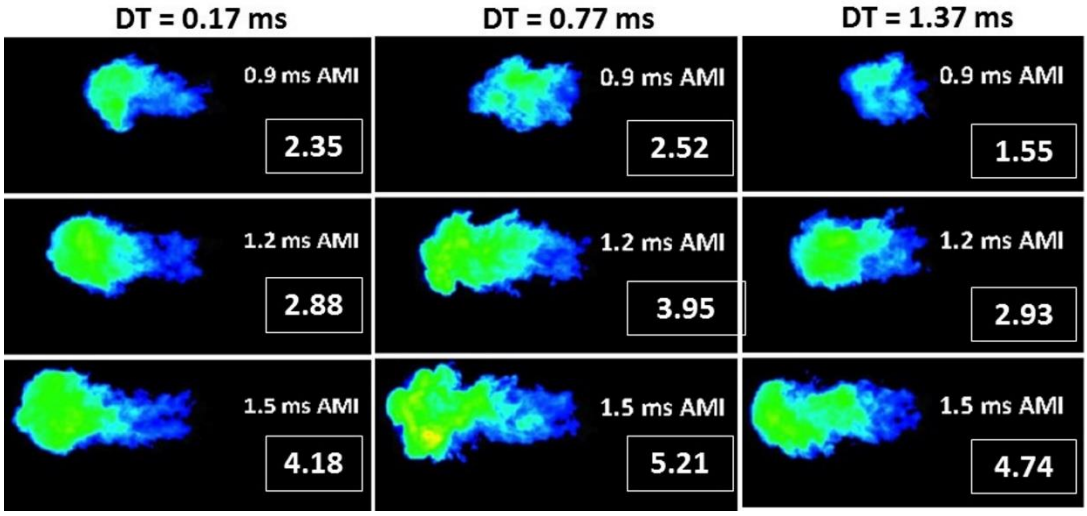

Figure 66: False color luminosity images showing main flame progression relative to after start of main injection (ASMI) times for the various dwell time cases experimented. White text boxes signify flame areas in cm^2

3.13 Concluding remarks

This work brings forward a unique and simple way to look at the combustion efficiency of the main flame in its premixed combustion phase for a split injection scenario. It utilizes experimental pressure (also heat release rate) data, experimental imagery of the flame and simulated burnt gas temperature data. The combustion efficiency for the main flame in the split injection scenario was found to be higher than the combustion efficiency of a single injection diesel flame. This signifies a combustion enhancement due to the effect of pilot flame on the main flame in the interaction region (premixed combustion zone). The combustion efficiencies were estimated by the ratio of the calculated burnt gas volume and the experimentally visualized enflamed volume (V_b/V_f). By assuming a density ratio of 4 between unburnt and burnt mass, the unburnt mass to enflamed mass ratio (m_{ub}/m_f) was calculated. The ratio m_{ub}/m_f indicates how much unburnt mass is present in the flame. The m_{ub}/m_f ratio for 0.17 ms, 0.77 ms and 1.37 ms dwell time cases resulted as 0.58, 0.2 and 0.5 respectively. Thus, a thermodynamic sweet-spot for higher combustion efficiency was found at an intermediate dwell-time of around 0.77 ms between the pilot and the main. Also, the

behavior of the main flame for the longer dwell time (1.37 ms) is interesting, as in the premixed combustion duration, it exhibits the behaviors of a shorter dwell time case (0.17 ms) initially and later exhibits the characteristics of intermediate dwell time case (0.77 ms DT), which is evident from the (V_b/V_f) (or (m_{ub}/m_f)) over time curves. Main injection causes increased mixing in the pilot-main flames which results in eventual ignition and combustion in a hot and lean environment for the medium dwell time case. This is expected be the cause for higher combustion efficiency in the medium dwell time case.

CHAPTER 12

EXPERIMENTATION IN LOW TEMPERATURE COMBUSTION REGIME[4]

3.14 Background

Experimental techniques like PLIF combined with high-speed schlieren imaging have been successfully implemented in the past [Skeen et al. 2015b, Skeen et al. 2015a] to visualize the ignition process in high pressure diesel flames. Similar studies have been performed in this work for split injection n-Dodecane (diesel surrogate) sprays to gauge the combustion characteristics of the subsequent injection. The aim of the present work is to understand the ignition, heat release characteristics, PAH and soot formation of high-pressure n-Dodecane injections under different ambient temperature conditions. Of interest to this work is to experiment at the lower end of low temperature combustion (LTC) regime (750K) and analyze the impact of injection pressures on ignition behavior. Furthermore, the effect of dwell time on ignition and heat release from a split injection combustion event for a slightly higher LTC (800K) condition was explored. A 1200 bar n-Dodecane injection with various injection strategies and ambient temperatures as shown in Table 3 is considered in this work. Fig. 28 shows the experimental setup for the simultaneous acquisition of 355-nm PLIF and high-speed schlieren/luminosity imaging.

3.15 Results and discussion

This section is divided into five subsections. Firstly, the rate of injection (ROI) measurement method is briefly discussed. This is required to define the nomenclature of the split injection sequences. Following this, there is a discussion of effects of ambient temperature on a split injection event; three repeats were performed per condition for these tests. The ambient temperatures of 900 K, 800 K, and 750 K reported here are the core-temperatures and not the bulk temperatures. Investigation of ambient temperature effects leads to the

[4] The material contained in this chapter has been accepted for publication in *Journal of Energy Resources and Technology*
Moiz, Ahmed Abdul, Cung, Khanh, and Seong-Young Lee. 2015. Simultaneous Schlieren-PLIF Studies for Ignition and Soot Luminosity Visualization with Close-Coupled High Pressure Double Injections of n-Dodecane. Accepted at *Journal of Energy Resources and Technology*

identification of an interesting phenomenon at low temperature (750 K) at a higher injection pressure of 1500 bar, which is discussed in the next section. Efforts were made to capture the dwell time effect at an ambient temperature of 800 K. The ambient temperature of 800 K was pointed out as an interesting test point by researchers earlier since the ignition and heat release of the pilot flame occurs during the dwell time in the 0.5/0.5/0.5 ms injection scheme [19]. Following this section, there is a short discussion on ignition enhancement in 750 K ambient temperature case due to various split injection strategies.

3.15.1 Rate of injection profile

Fig. 67 shows the rate of injection profile with a 0.5 ms injection of pilot spray, a 0.5 ms dwell time, and a 0.5 ms main spray injection. From this time forward, such injection schedule will be referred as 0.5/0.5/0.5 ms.

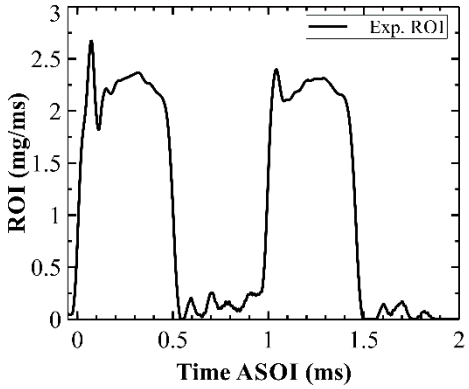

Figure 67: Rate of injection profile for 1200 bar injection for the 0.5/0.5/0.5 ms injection sequence

A Kistler 9215 force sensor, which is capable of precise force measurements from the injected impacting spray (2 N to 200N), was used for momentum flux measurements. Injection was performed in a small enclosed cubic chamber at atmospheric pressure with the injected spray impinging on an aluminum anvil attached to the force sensor. A Kistler 5010B charge amplifier amplifies the signal output from the force sensor and the resultant signal is recorded in an oscilloscope at a sampling rate of 500 kHz. Using momentum relationships, the mass flow rate of injection is back calculated.

Force measurements were repeated 100 times for each injection schedule and the data were later averaged and filtered. Slight signal fluctuations, due to the sudden impact of the injecting liquid on the anvil, are observed as the spray first hits the anvil orthogonally. After approximately 0.15 ms, the force from the spray is relatively steady and outputs as a proportional charge from the force sensor. As the injection ends, the anvil tends to settle down with back and forth fluctuating movements due to its inertia and so minor fluctuations in the output signal are seen during the dwell time and after the main injection. While there is some uncertainty in making this type of visual assessment of the injection duration, it does appear that the durations visualized from high-speed images in actual testing are longer than those measured during the ROI experiments by about 0.15 ms and 0.2 ms for the first and second injections, respectively. The dwell time is also proportionally reduced by approximately 0.15 ms. The reason for this discrepancy is unclear yet, but a change in solenoid behavior is anticipated. The rate of injection testing has been done with fuel at atmospheric temperatures. Whereas the experimental testing has been done with the fuel temperature at 90^{o}C. In addition to potential impacts from viscosity of fuel at higher temperatures, the solenoid can also behave very differently at higher temperatures. This is the most plausible explanation for the mismatch of injection durations. It is to be noted, however, that the start of second (or main) injection occurs at the prescribed timing of 1 ms after start of the first (or pilot) injection.

3.15.2 Effect of ambient temperature

A 0.5/0.5/0.5 ms split injection event (ROI based nomenclature) is used as a basis, since detailed analysis of this study was performed previously [Skeen et al. 2015b] as part of ECN efforts.

Fig. 68 shows the mean heat release rate (HRR) of the combustion events for the three ambient conditions tested over 3 repeats with the actual injection durations highlighted in the time axis.

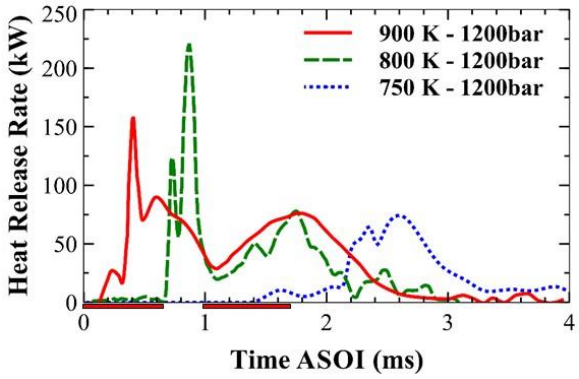

Figure 68: Heat release rate profiles for the different ambient temperature cases for the 0.5/0.5/0.5 ms injection sequence at 1200 bar injection pressure. The actual injection durations highlighted in the time axis

The HRRs in Fig. 68 show that higher ambient temperatures lead to earlier ignition of the pilot and main sprays. For the 900 K and 800 K, heat release rates due to ignition and combustion of the main injection can be clearly differentiated from that associated with the pilot. For the 800 K ambient, since there is more mass of combustible mixture which undergoes a second stage ignition, the peak of heat release rate for the 800 K is higher than the 900 K case. It can also be seen that, for both 900 K and 800 K ambient, the pilot flames show a combination of premixed combustion phase and a mixing-controlled combustion phase characteristics; whereas the main flames show a mixing-controlled combustion phase only. In a premixed combustion phase, the conversion of the premixed fuel (fuel+oxidizer) into some product species takes place. The mixing controlled combustion phase is dependent on the level of oxidizer available to the fuel as a result of air-entrainment induced by the injection event. Thus, the mixing controlled combustion phase has a positive slope (or zero slope for long injection case) of HRR in the active main injection periods as observed in Fig. 68. This also acts as a proof that the effective injection duration in the experiments was indeed longer than measured using ROI experiments as mentioned in the ROI section. For the 750 K case, a bulk (pilot-main combined) ignition and combustion processes were observed. This is a consequence of an ignition delay occurring after the end of the main injection, which gives ample time for fuel vaporization and fuel-oxidizer mixing prior to ignition.

On comparison with the raw images from the high speed camera in Fig. 69, it can be observed that 'schlieren softening' and premixed combustion (visualized by the occurrence of dim light at the leading edge) occur at similar times as evident from the initial heat release rate rises in Fig. 68.

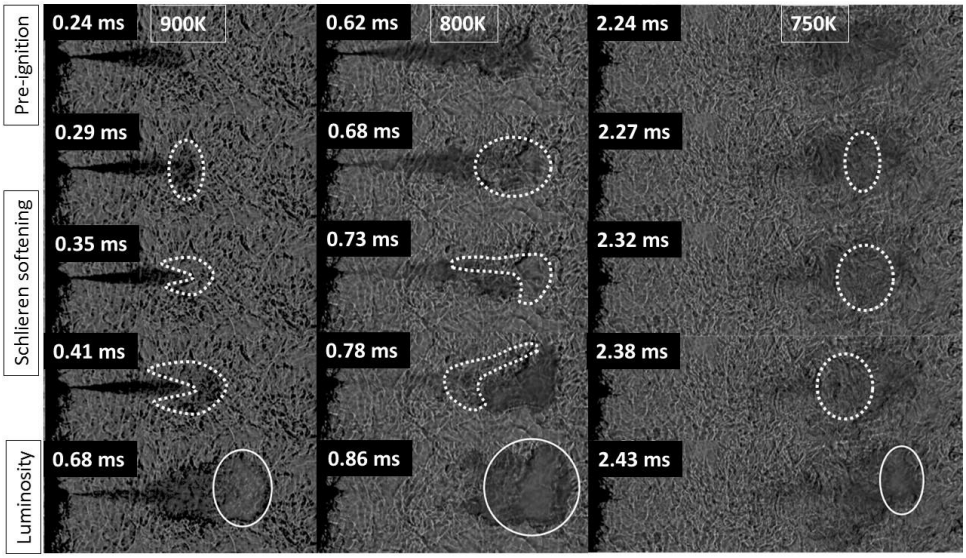

Figure 69: Raw schlieren images for the 0.5/0.5/0.5 ms injection event at 900 K (left), 800 K (middle), 750 K (right). White dashed structures indicate schlieren softening and sold white lines indicate luminosity events

Schlieren softening denotes the large scale organization of fuel mass with similar equivalence ratio mixture accumulation, ready to undergo the first stage ignition [Skeen et al. 2015b]. In Fig. 69, white dashed and solid line structures are labeled according to schlieren softening and (early) luminosity events, respectively. It can be said that, for the 900 K ambient, ignition of the pilot starts as it is injected, for the 800 K condition ignition of the pilot injection occurs at its end of injection times and for the 750 K a combined pilot-main ignition and combustion takes place after end of the pilot and main injection events.

For the 900 K ambient schlieren softening is a more or less symmetric and homogenous where as for the 800 K case, there is an inhomogeneous distribution of ignitable mixtures in the leading edge of spray. For the 900 K and 800 K, a 'bump' in the early HRR times indicates first stage ignition whereas for a later peak indicates second stage ignition (cf. Fig. 68). These

correspond to the schlieren softening events and luminosity events from the schlieren images (cf. Fig. 69). For the 750 K ambient, due to ignition delay being very long, the vaporization and eventual increase in temperature of the vapor fuel mass makes the schlieren brighter for the fuel spread regions. On close observation, there are few mild schlieren softening events taking place from ~ 2.27 ms to 2.37 ms and luminosity is seen at ~2.43 ms.

Image sets acquired using a simultaneous schlieren/luminosity and 355-nm PLIF technique are presented further. Specifically, each test involved either the simultaneous schlieren/PLIF or luminosity/PLIF. Thus the mutual overlap of PLIF, schlieren boundary and luminosity boundary is not an imaging of a single event of the spray from the three techniques at one time and required choosing one of the images from either the schlieren or natural luminosity to overlap with the other simultaneous set. It is also noted that, while natural luminosity is a line-of-sight technique (signal integrated in the line-of-sight) for visualization of luminosity coming from high temperature regions, a PLIF image corresponds to intensity regions captured on a thin sheet and thus is a 2D technique. A one-to-one correspondence of imaging from both these technique might not always give similar results if the variable of interest has an unsymmetrical existence.

Fig. 70 (left) shows the set of images for the 900 K ambient injection case. From the images, it can be seen that there are early traces of formaldehyde at 380 μs, which shows the evidence of first-stage ignition or cool flame formation.

The high-speed images from Fig. 69 show schlieren softening (a first stage ignition event) at similar time instants for the 900 K case. At 954 μs, which is roughly at the start of main injection, the upstream schlieren is seen to be deformed due to the oncoming of the main liquid jet. An observation that can be made here is that the injection of the main is occurring in an environment of high temperature gases which have receded upstream (combustion recession) [Knox and Genzale 2015a] as evident from the schlieren boundaries from the time stamps originating at 954 μs. This type of injection of main in high temperature products from the pilot combustion is one of the reasons for its lower (almost half the value) ignition delay when compared to the pilot ignition delay. This also causes richer ignition of the main

spray, leading to more soot from the main spray. As the main injection enters the combustion chamber at ~ 954 μs, there is evidence of PAH formation downstream of the flame. The high-speed images from Fig. 69 show schlieren softening (a first stage ignition event) at similar time instants for the 900 K case. At 954 μs, which is roughly at the start of main injection, the upstream schlieren is seen to be deformed due to the oncoming of the main liquid jet. An observation that can be made here is that the injection of the main is occurring in an environment of high temperature gases which have receded upstream (combustion recession) [Knox and Genzale 2015a] as evident from the schlieren boundaries from the time stamps originating at 954 μs. This type of injection of main in high temperature products from the pilot combustion is one of the reasons for its lower (almost half the value) ignition delay when compared to the pilot ignition delay. This also causes richer ignition of the main spray, leading to more soot from the main spray. As the main injection enters the combustion chamber at ~ 954 μs, there is evidence of PAH formation downstream of the flame.

One of the advantages of the PLIF technique for formaldehyde detection consists of the fact that it can also be used to visualize PAH formation, since signal detection wavelengths for both species are close to one another [Bruneaux 2008, Lachaux and Musculus 2007]. A fraction of the broadband soot incandescence can also be observed in a PLIF image in this range. Usually, PAH is formed at a different spatial location than formaldehyde which makes the PLIF technique useful to detect the formaldehyde presence and to differentiate it from the PAH signal [O'Connor and Musculus 2013a]. Also, PAH appears in a 'saturated' fashion, in this case, colored as dark red. This is because, the formaldehyde signal is a lower magnitude signal and stops rising in intensity at a certain threshold, unlike PAH/soot, which can rise until higher magnitudes thus appearing saturated in the PLIF images.

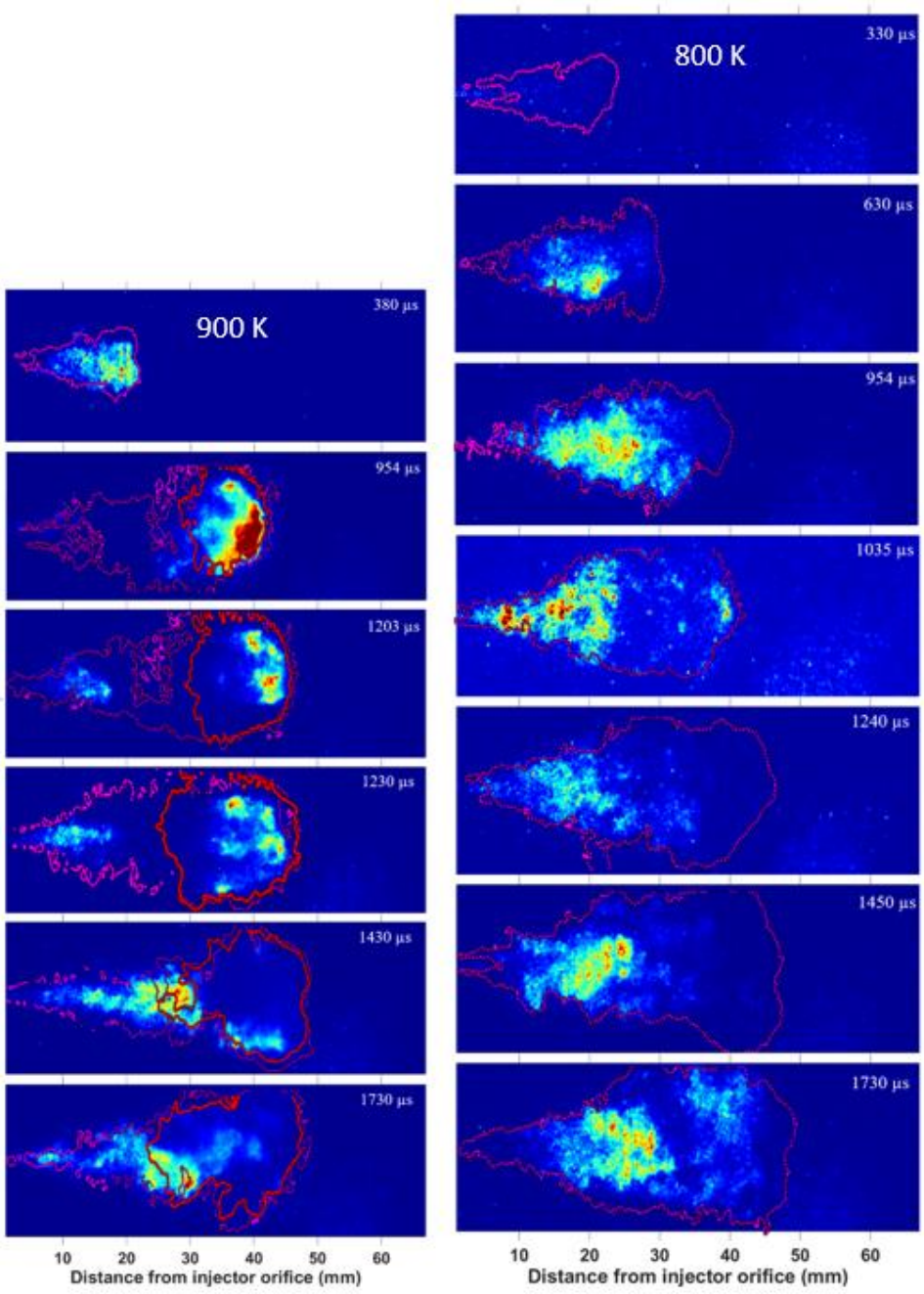

Figure 70: Simultaneous PLIF imaging of the 0.5/0.5/0.5 ms spray combustion event at 1200 bar for the 900 K (left) and 800 K (right) ambient case; dotted pink contour line denote schlieren boundaries, red contour line denotes soot luminosity, background Red-Blue-Green

image is a PLIF image for formaldehyde measurement. Red indicates high intensity and blue indicates low intensity in the RGB color scheme

Continuing with Fig. 70, the pilot flame PAH signal weakens as pilot soot matures in the next time stamp of 1203 μs. At the same time, formaldehyde from the main injection starts forming in the downstream of the main injection, which continues to form until the mid-way of injection duration at 1230 μs. Close to the end of main injection times of 1430 μs, dark red regions in the flame tip of main injection denote the start of PAH species from the main injection. This is confirmed by the spread of the red boundary from the natural luminosity imaging. At 1730 μs, it can be observed that combustion recession of the main injection has occurred as visualized by the schlieren boundaries near the injector tip.

Fig. 70 (right) shows the 800 K ambient condition tests. For this condition, cool flame starts forming at around 630 μs which is roughly the time at which heat release rate starts to rise in the 800 K case shown in Fig. 68. In Fig. 70 (right), the schlieren structure begins to deform at the leading edge at around 630 μs due to the low temperature species presence (signified by formaldehyde). At 954 μs, the formaldehyde travels downstream. The schlieren boundary, which denotes the vapor/flame boundary, extends further downstream. Between 630 μs and 954 μs, there was dim soot luminosity visualized from the high-speed camera images, as shown by the time stamps of 0.810 μs and 0.890 μs in the right column of Fig. 71.

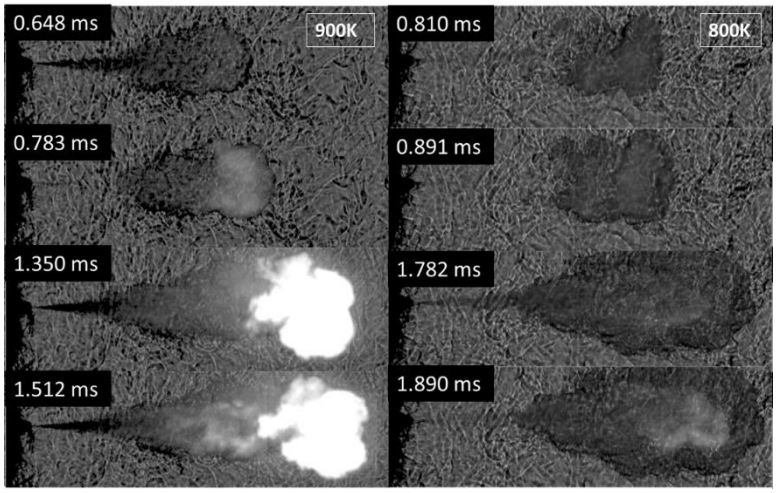

Figure 71: Soot luminosity images of 0.5/0.5/0.5 ms injection sequence for the 900 K ambient (left) and 800 K ambient (right) at 1200 bar injection pressure

At 1035 µs, complete consumption of formaldehyde after the premixed combustion occurs and can be confirmed from the premixed peak in HRR profile in Fig. 68. The main injection starts roughly around these times, and starts to form formaldehyde at a lower time after its onset of injection when compared to the time delay of formaldehyde formation for the pilot injection. At 1730 µs, further downstream of the image, there is slight occurrence of light blue region, which actually denotes the onset of PAH in the flame. As can be confirmed by the high-speed images from Fig. 71, soot from the main flame has started to be seen at very later times of ~ 1.9 ms for the 800 K case, when compared to the main flame luminosity initiation times for the 900 K case at ~ 1.5 ms. Similar trends of soot formation for the pilot flames were recorded to be ~ 0.9 ms ASOI for the 800 K case and ~ 0.77 ms ASOI for the 900 K case. For the 750 K case, there was no bright (soot) luminosity observed for all the repeats. Recall that soot luminosity here means detection of flame luminosity with a 600-nm short pass filter mounted on the high-speed camera lens.

Comparing between the soot luminosities of the pilot and main injections for the 800 K case, increased soot for the main injection is due to its injection into an environment of low temperature reactive intermediates as evident from the image at 1035 µs in Fig. 70 (right), where there is appearance of formaldehyde near the nozzle. Although formaldehyde is not

a reactive intermediate, its presence is an indicator that reactive species such as hydrogen peroxide (H2O2) are present. Thus, not only the low temperature intermediates, originating from the pilot spray play a key role in its earlier ignition as in the case of 800 K ambient injections, but also the recessed high temperature products of the pilot combustion causes earlier (and richer) main ignition leading to more soot as in the case of a 900 K ambient injection.

3.15.3 Effect of injection pressure

Fig. 72 shows the set of simultaneous images for the 750 K ambient injection case.

For the 1200 bar injection pressure (Fig. 72 - left), no cool flame is observed in the PLIF images until approximately 1.8 ms ASOI. At the last image in the sequence, there is significant formaldehyde formation as well as flame propagation, as denoted by the schlieren boundaries at further downstream locations. Ignition has long occurred at 2690 μs (from the heat release in Fig. 68) and the fuel injected is left mostly unreacted upstream which will result in the presence of unburned hydrocarbons and hence low combustion efficiencies. For the same condition of 750 K ambient, at a higher injection pressure of 1500 bar, formaldehyde signal was observed at a relatively lesser ASOI time as evident from Fig. 72 (right). At 1790 μs, there is a strong formaldehyde signal, which was not observed in the case with 1200 bar pressure (Fig. 72 - left) at the same thermodynamic ambient conditions. Also, a high intensity emission was observed at around ~2090 μs for the 1500 bar injection

case, whereas in the 1200 bar injection case, it was not observed all throughout the combustion process.

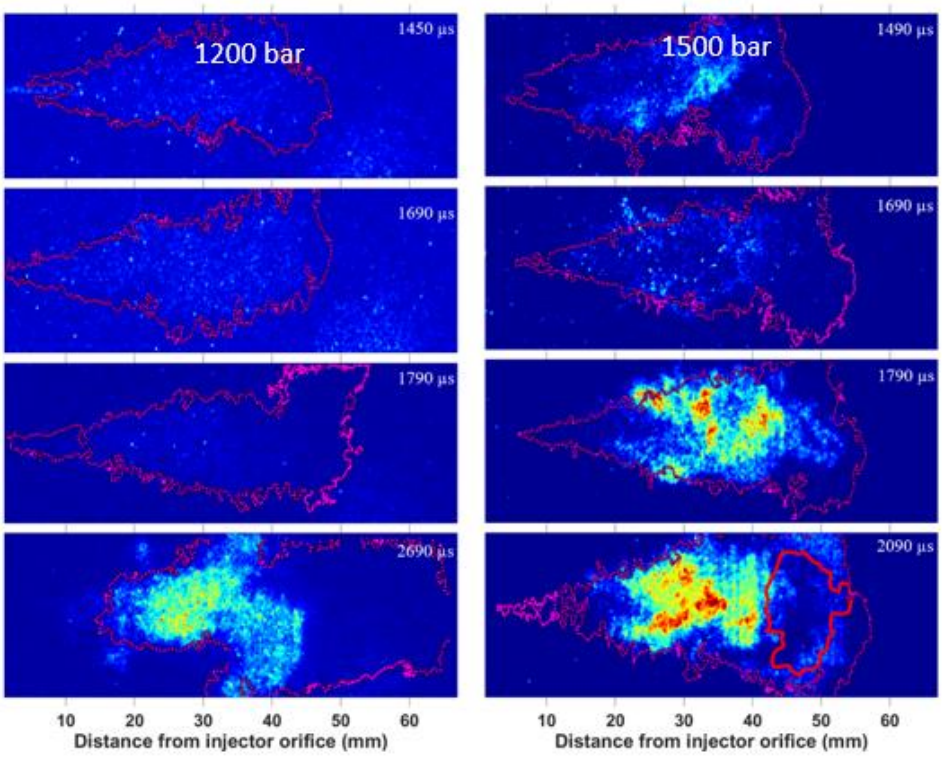

Figure 72: Simultaneous PLIF imaging of the 0.5/0.5/0.5 ms injection spray combustion event at 1200 bar (left) and 1500 bar (right) injection pressure for a 750 K ambient

The high intensity emission (red boundary at 2090 µs in Fig. 72 - right) is the one observed from the natural luminosity high-speed images where the high-speed camera is capped with a 600-nm short pass filter enabling visualization of the high temperature flame. This might not directly correlate with the soot species emission and might as well mean strong chemiluminescence from the CH* species when it is seen around ignition times [Nesbitt et al. 2010]. In the present case, the high intensity emission at 2090 µs is presumed to be a CH* chemiluminescence signal for the 1500 bar case.

A comparison of the mean heat release rate profiles of the 0.5/0.5/0.5 ms injection sequence at 1200 and 1500 bar injection pressures reveal interesting trends about the characteristics of combustion and its dependence upon mixing-chemistry relations at

relatively low temperature condition of 750 K. It can be seen in Fig. 73, that for the 750 K case, the ignition delay is ~ 0.8 ms later in the case of 1200 bar than the 1500 bar injection case. There is a delayed rapid rise in heat release for the 1200 bar case and an early gradually increasing rise in heat release for the 1500 bar case. Similar heat release rate profile was observed for the 1500 bar case by Skeen at. al [Skeen et al. 2015b]. Thus, there is a significant increase in ignition delay (~ 0.8 ms) in the 750 K case with a decrease in the injection pressure by 300 bar (from 1500 bar to 1200 bar). This can be attributed to enhanced spray-gas mixing due to high injection pressure, which aids in ignition of the main spray. Since 750 K is on the lower end of a low temperature combustion (LTC) regime, the extra turbulence induced by a higher injection pressure might be critical to affect the relatively slow chemistry involved in low temperature reactions. Reasoning for the early ignition of main injection can be obtained from studies of Felsch et al.[Felsch et al. 2009], where the authors concluded that the main ignition occurs by a premixed flame controlled mechanism. Unlike pilot ignition, the ignition of main is influenced by the higher mixing due to its premixed flame controlled nature. Additionally, an increase in mixing, by increasing the injection pressure, will further reduce the ignition times following this theory.

For a qualitative comparison of the performance of sprays at different injection pressures, a combustion efficiency term based on normalizing the cumulative heat release (integration of Equation 8) with the product of mass injection and lower heating value of the fuel was calculated. This calculation also assumes no heat loss from the combustion event to the chamber walls. For the 1200 bar and 1500 bar injection 750 K ambient cases, the normalized combustion efficiency came to 59% and 68% respectively. This indicates better combustion with usage of higher injection pressure for the lowest (750 K) case. Thus, the energy content of the pilot injected fuel, which is sufficiently heated until low temperature reaction intermediates form, affects the ignition and combustion of the main spray. As seen in the PLIF images of Fig. 72 (left), there is no formaldehyde signal until late ~ 1.8 ms, indicating no low temperature chemistry in effect until then for the 1200 bar injection case. Whereas in Fig. 72 (right), formaldehyde signal appears at earlier times of ~1.5 ms giving indication of early low temperature chemistry initiation and hence more chances of early ignition for the 1500 bar injection case. These trends are consistent with the initial rise in heat release times

for the 750 K case in Fig. 73.

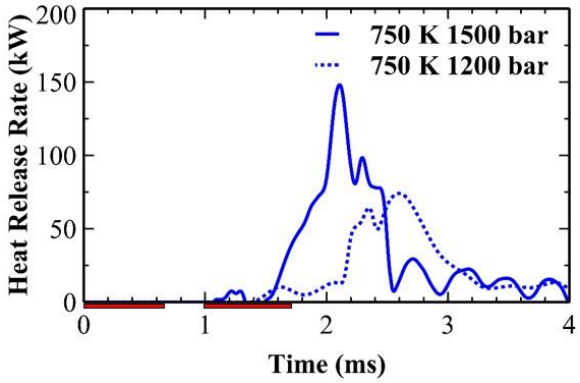

Figure 73: Heat release rate comparison of the 1200 bar and 1500 bar injection pressure cases of the 0.5/0.5/0.5 ms injection event at the 750 K ambient temperature case. The actual injection durations highlighted in the time axis

3.15.4 Effect of dwell time

For the 800 K ambient case, the HRR plots shown in Fig. 68 indicated that the ignition of the pilot injected fuel occurs during the dwell. Also, from the simultaneous PLIF images of Fig. 70 (right) and from the natural luminosity images of Fig. 71, it was evident that the soot formation takes place in the main flame and not in the pilot flame. This soot formation was due to rich ignition of the main spray. There is also a possibility of injecting the main in a more reactive environment of pilot generated low temperature reactive intermediates if the dwell time between successive injections is reduced. Conversely, increasing the dwell time would cause the injection of main into a region occupied by a lower concentration of low temperature intermediates which may or may not change the ignition and soot formation characteristics. This exercise of dwell time variation was performed at 800 K. As shown in Fig. 74, the pilot and main injection durations were kept constant at 0.5 ms, but the dwell time between them was varied as 0.3 ms, 0.6 ms and 0.9 ms.

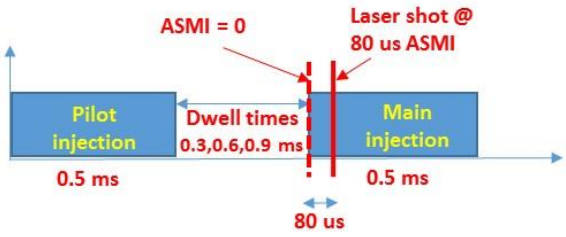

Figure 74: Schematic of PLIF shot timing in the dwell time variation tests

There was a PLIF shot at 80 µs after the start of main injection (ASMI). This time of 80 µs ASMI was selected based on the visualization from high-speed imaging when the main injection's liquid boundary was just touching the boundary of the pilot structure (in a 0.5/0.5/0.5 ms injection event). Ideally, as the liquid comes out from the nozzle, it lends itself to the chemical reactions; but it can be assumed that at an early time of 80 µs ASMI, the main injection's vapor phase did not start to chemically interact with the pilot structure.

Each dwell time test is a separate injection event with laser shot at same time (80 µs ASMI); with three repeats in the testing. A mean of three repeats is presented further. Fig. 75 shows the heat release rate profiles of the injection sequences attempted with varying dwell times. A 'star' symbol on each curve indicates the timing of the PLIF shot acquisition. One observation from these results is that the premix peak of the pilot spray combustion occurs at similar times for all the dwell time cases.

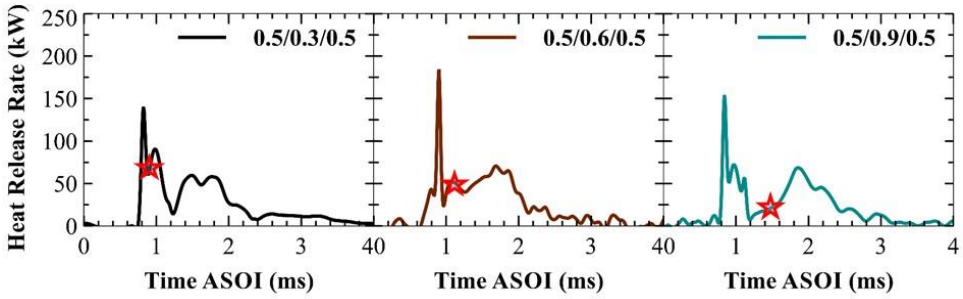

Figure 75: Heat release rate profiles of the injection sequences with varying dwell times at 800 K. A 'star' symbol on each curve indicates the timing of the PLIF shot acquisition

There is a gradual delaying of the start of increase of heat release rate for the main injection but the main heat release rate for the three dwell time peak at similar levels. Combustion efficiency by normalizing net heat release with a product of lower heating value and mass of fuel injection comes around ~ 95% for the three dwell time cases. The PLIF images overlapped with the schlieren boundaries and natural luminosity contours in the continuing section involve the schlieren boundaries just from the pilot structure.

Fig. 76 is a simultaneous PLIF shot for the 0.3 ms dwell time at ~ 80 µs after main injection.

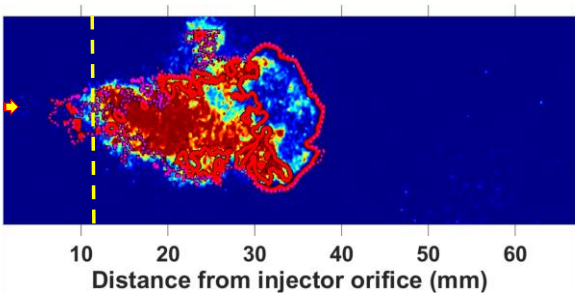

Figure 76: Simultaneous PLIF imaging for a 0.5/0.3/0.5 ms injection sequence. Image is acquired at ~880 µs ASOI

The corresponding heat release rate plot can be found in Fig. 75 along with the other two dwell times tested. The dashed yellow line in Fig. 76 (and 77, 78) represents the extent of the main injection liquid from the nozzle hole. The nozzle location is marked by the yellow arrow. It can said that the contours and structures after the yellow line ideally represent the activity arising from the pilot spray dynamics. From the PLIF image of Fig. 76, one can observe that there is a rich presence of formaldehyde in the pilot structure. Very dim luminosity was also captured from the natural luminosity images (red boundary). This luminosity is expected to be largely from CH* radical, since it is mostly seen during the ignition stages and lies around the 400-nm wavelength range [Nesbitt et al. 2010]. Also, red structures are seen along the periphery of the pilot structure, implying that there are ignition reactions occurring along the boundary which emits CH* radical emissions.

As the pilot is given more time to react in the chamber during the longer dwell times, without the influence of the main injection, there is development of weak PAH/soot which

is also confirmed from the overlapped red boundaries from the natural luminosity imaging in Fig. 77 for the 0.5/0.6/0.5 ms case.

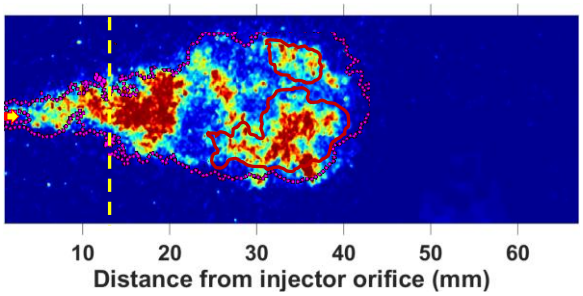

Figure 77: Simultaneous PLIF imaging for a 0.5/0.6/0.5 ms injection sequence. Image is acquired at ~1180 µs ASOI

The PAH/soot signal from Fig. 78 for the 0.5/0.6/0.5 ms injection is then extinguished completely in Fig. 78 for the 0.5/0.9/0.5 ms case. As the dwell time is increased there is enough time for the formaldehyde to get consumed in the downstream spray as in Fig. 78. This leaves the upstream low temperature intermediate species (signified by formaldehyde presence) to react with the oncoming main injection.

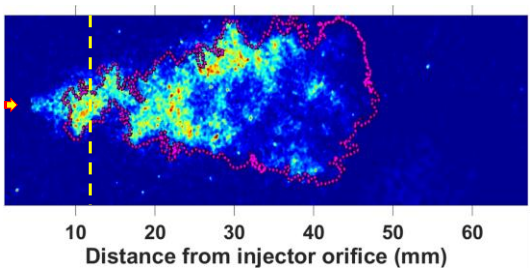

Figure 78: Simultaneous PLIF imaging for a 0.5/0.9/0.5 ms injection sequence. Image is acquired at ~1480 µs ASOI

The spatial presence of soot can be understood from Fig. 79 which has raw schlieren images for similar ASMI times for the three dwell time variation cases at 800 K ambient and 1200 bar injection pressure. For the 0.5/0.3/0.5 ms case in Fig. 79, soot formation appears to have already begun at 1 ms ASMI, whereas for the 0.5/0.6/0.5 ms it is still in its initial stages. For the 0.5/0.9/0.5 ms case soot formation is even more delay as indicated by the very dim luminosity at this timing. The duration of formation of the soot is also an indication of net

soot production. For the low dwell time case, the soot luminosity lasts for ~2 ms where as for the intermediate dwell time it lasts for ~1.2 ms and for the low dwell time case it lasts for ~0.9 ms from the high-speed movies (not shown here). Thus, as the dwell time increases the high temperature soot is reduced. As can be seen in the simultaneous PLIF imaging of Fig. 76 for the 0.5/0.3/0.5 ms case, the injection of main occurs in a rich formaldehyde environment; this will promote richer ignition of the main and thus cause higher soot, which is evident from Fig. 79.

Additionally, for the intermediate dwell time case of 0.5/0.6/0.5 ms from PLIF imaging of Fig. 77 it can be seen that the formaldehyde presence is still rich but not as much as in the 0.5/0.3/0.5 ms case of Fig. 76. Thus, relatively lower soot production can be expected as evident from 0.5/0.6/0.5 ms case from Fig. 79. From the high dwell time case (0.5/0.9/0.5 ms) of Fig. 79, it can be observed that the formaldehyde has decreased in intensity and the high temperature combustion products, denoted from schlieren boundary, started travelling downstream.

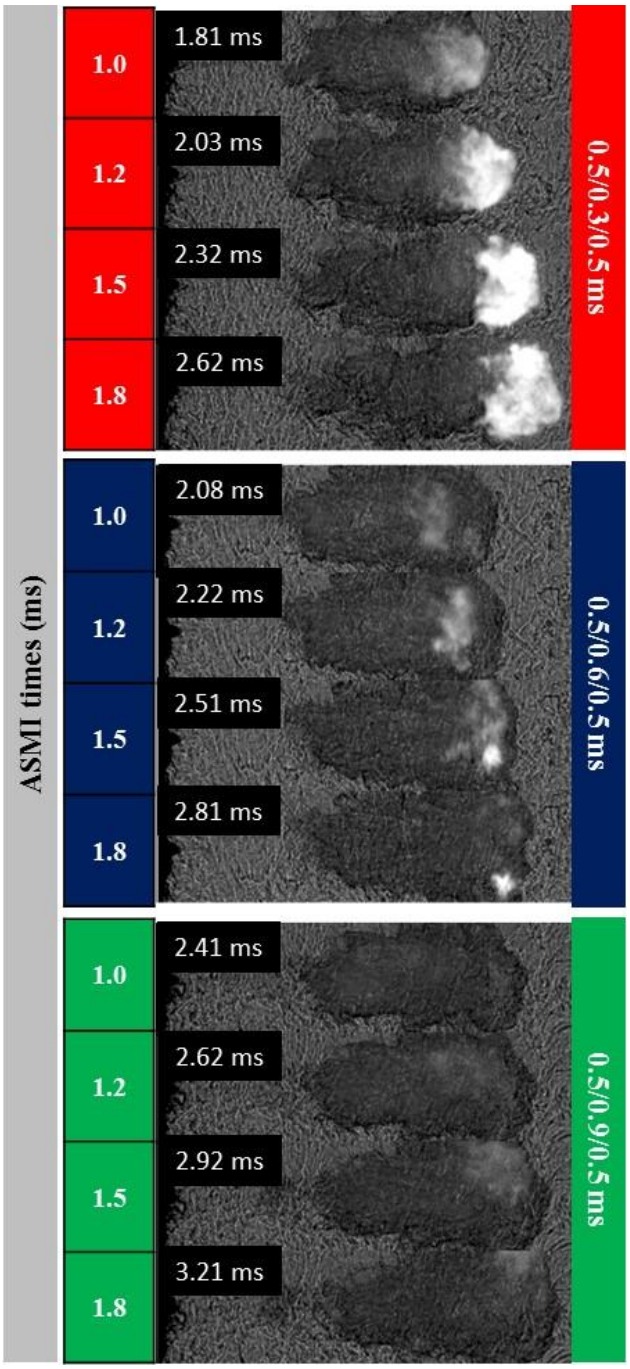

Figure 79: Soot luminosity images for three injection sequences: 0.5/0.3/0.5 ms, 0.5/0.6/0.5 ms and 0.5/0.9/0.5 ms; for a set of fixed after start of main injection (ASMI) times at 1800 K ambient and 1200 bar injection pressure

Thus, the production of soot (originating from a rich ignition of main spray) due to reaction from low temperature intermediates, giving low soot for the high dwell time case of 0.5/0.9/0.5 ms as evident from Fig. 79. This dependence of soot production on dwell time is in agreement with the observations made by Cung et. al. [Cung et al. 2015] where an increase in the dwell time resulted in a lower amount (qualitatively) of soot formation based on luminosity imaging. However, opposite agreement was obtained in laser extinction measurements by Bruneaux et al. [Bruneaux and Maligne 2009] based on soot optical thickness (*KL*) measurements. But since the measurement from Bruneaux et al. were done for a distance up to 6 mm from the nozzle only, the downstream soot formation information was not revealed. The temporal and spatial presence of soot formation is dependent upon the dwell time, the higher the dwell time the later the formation of soot, since soot is mainly formed by the main injection at 800 K ambient condition. The dwell time thus influences the level of soot formation, which is impacted by the relative richness of the (main) ignition mixture. Higher presence of reactive pilot species will accelerate its rich ignition leading to more soot production.

3.15.5 Low temperature ignition enhancement

Efforts were also made to study if the ignition of the injected mass is effected by (a) using a split injection strategy, (b) varying the split injection strategy, and (c) varying the injection pressure at low temperature conditions such as 750 K where ignition delays are usually very high (also shown previously). Fig. 80, shows the heat release profiles of the different tests averaged over 3 test repeats.

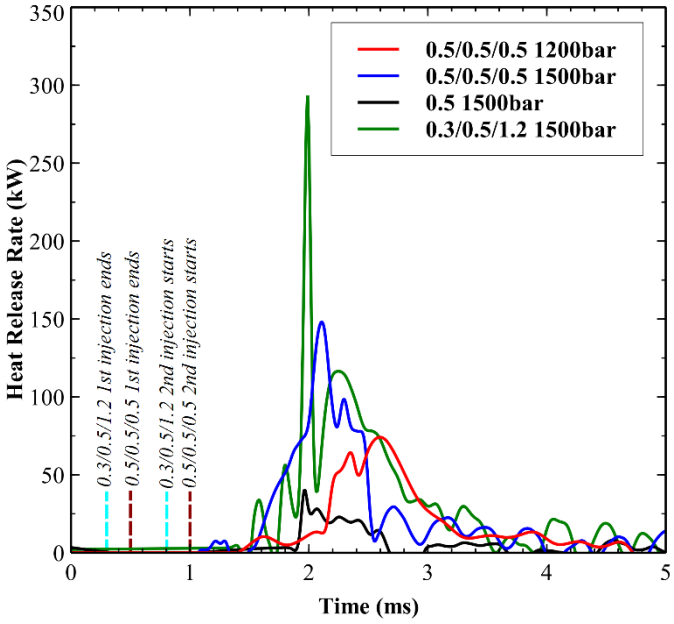

Figure 80: Heat release profiles for limited variations in injection sequence and injection pressure at 750 K ambient temperature

The red and blue curves in the plot represent the same injection strategy of (0.5/0.5/0.5 ms) but different injection pressures of 1200 bar and 1500 bar. The HRR plots for these conditions are already present in the previous sections, but are presented here for comparison with other test data.

The black and blue lines in Fig. 80 show the benefit of split injections for an early ignition of the injected fuel mass. The black line denotes a single injection of 0.5 ms with a 1500 bar injection pressure into a 750 K ambient. It is noticed that, the ignition delay for such an injection is ~2 ms whereas the ignition delay of a multiple injected fuel of 0.5/0.5/0.5 ms strategy at the same injection pressure is ~1.4 ms. In actuality, it can be said that it is the main injection that ignites in the split injection case [Skeen et al. 2015b]. The pilot injection warms the ambient and creates a good mix of reactive environment for the main to benefit from and ignite. Also, from Fig. 80, it can be noticed that a change in the injection strategy from 0.5/0.5/0.5 ms to 0.3/0.5/1.2 ms injection does not help in an early ignition of the injected mass. Although, a higher premixed peak is seen in the 0.3/0.5/1.2 ms case, since now the net vaporized mass at the time of ignition is higher than the 0.5/0.5/0.5 ms case

owing to net longer injection duration for 0.3/0.5/1.2 ms case at the same injection pressure.

3.16 Concluding remarks

A close-coupled split injection strategy has been explored in the controlled environment of a constant volume combustion chamber under diesel engine-like conditions with a focus on ambient conditions representative of the low temperature combustion regime (900 K, 800 K and 750 K at 22.8 Kg/m^3 with 15% O_2 in ambient). Simultaneous imaging of formaldehyde signal from PLIF imaging, vapor/flame boundaries from schlieren imaging and high temperature soot imaging from natural luminosity have been used to gain deep insights in the combustion process of various split injection schemes. The conclusions can be summarized as:

- Simultaneous PLIF-Schlieren imaging provides a unique way to look into ignition, vapor/flame propagation and soot production processes simultaneously.
- Heat release rate (HRR) of main injection for 900 K and 800 K ambient cases occurs in diffusion or mixing controlled phase only whereas pilot HRRs show both premix and mixing controlled behavior.
- Schlieren softening event signifying bulk first stage ignition of fuel-air mixture at similar equivalence ratio was seen in an obvious manner in 900 K and 800 K pilot ignition cases and mildly in 750 K case. High level of formaldehyde signal was observed during schlieren softening.
- At 900 K ambient case, main injection enters a zone of no formaldehyde signal but with receding schlieren boundaries from pilot combustion which signify high-temperature products; whereas at 800 K and 750 K main injection happens in low-temperature species ambient signified by formaldehyde signal.
- At both 900 K and 800 K ambients, the ignition delay time of the main is reduced by a factor of two over the pilot ignition time. Due to earlier and close-to-upstream (fuel-rich) ignition of the 900 K main injection, higher PAH signal from

PLIF and soot production from luminosity was observed in the 900 K main injection than the 800 K main injection.

- Dwell time variations were performed at the 800 K ambient condition. Early (fuel-rich) ignition of the injected main spray is a result from the local reactive ambient signified by formaldehyde presence. These conditions can be controlled by increasing the dwell time between successive injections such that main injection happens in a lesser reactive pilot field. Increasing the dwell time showed qualitative trends of lower soot production.
- Studies in the lower end of the LTC regime (750 K) showed an evidence of significant advancement of ignition (by ~ 0.8 ms) when the injection pressure was increased from 1200 bar to 1500 bar. A 9% net improved combustion efficiency was observed with usage of higher injection pressure at 750 K.
- The use of split injections in itself is beneficial in causing early ignition when compared to a single injection at 750 K ambient case where diesel spray usually have long ignition delay. Changing the mass proportions in pilot and main was not seen to alter ignition of main in the LTC condition of 750 K.

CHAPTER 13

IGNITION, LIFT-OFF MECHANISMS AND SOOT PRODUCTION[5]

From a single injection diesel spray combustion standpoint, one of the key areas of diesel spray combustion research is that of emissions formation, especially soot formation. The complex soot formation process in diesel spray combustion is a strong factor of the thermal and species ambient conditions.[Pei, Hawkes, et al. 2015] On further investigation for possible causes for soot formation, it was found that soot formation is linked to the ignition and lift-off characteristics.[Skeen et al. 2016, Idicheria and Pickett 2005, Musculus et al. 2002, Siebers and Higgins 2001] Also, it was observed that ignition and lift-off formation are in-turn inter-related in diesel spays.[Pickett et al. 2005] Thus an understanding of the ignition and lift-off processes of spray-flames is important to later understand the closely linked emissions aspect.

3.17 History of ignition and lift-off studies for single injection

CFD has been instrumental in revealing the basic mechanisms by which the interdependencies of ignition, lift-off and soot formation exists. Many of the previous works have investigated this aspect with various types of CFD model formulation methodologies.[Hessel et al. 2014, Mueller et al. 2003, Pei, Hawkes, et al. 2015, Abraham 2015]

The existence of lift-off height (or distance or length) has been a matter of investigation from the era of gas jet diffusion flames. Many theories have been put-forth to explain this phenomenon since it one of the dominant factors effecting emissions. The theories conceived for the traditional single injections are put-forth further. The premixedness theory [Vanquickenborne and Van Tiggelen 1966] suggested that flame exhibits a stabilization location due to axial velocity (U_s) along the stoichiometric mass fraction contour (where the fuel and air are premixed) being equal to the local turbulent flame speed. The

[5] The material contained in this chapter has been submitted to *International Journal of Engine Research*
Ahmed Abdul Moiz, Cung, Khanh, and Seong-Young Lee. 2016. Ignition, Lift-off and Soot Formation in Double Injection Spray-Flames. Under review at *International Journal of Engine Research*

large-scale mixing model (or vortex-flame stabilization concept) [Broadwell et al. 1985] hypothesizes that the flame stabilization happens due to the re-entrainement of the hot gases towards upstream of the stabilization location resulting from convection by large-scale turbulent structures; this causes ignition of the non-combusting structures of the ensuing jet. Another well-known theory is that of the partially-premixed flame propagation where the flame stabilization is assumed as a propagation (and stabilization) phenomenon of triple flames. [Müller et al. 1994, Chen et al. 2000, Buckmaster 2002]. A triple flame is a conglomeration of a lean and a rich premixed flame sections, meeting with a diffusion flame at a "triple point". A diffusion flamelet extinction theory [Peters and Williams 1983] was put forth explaining that turbulent flame can be assumed as a collection of laminar flamelets and lift-off happens as the local stoichiometric scalar dissipation rate in the region upstream of the lift-off is higher than the quenching scalar dissipation rate for a laminar diffusion flamelet; thus no ignition happens there. All of the above mentioned theories have experimental evidences, although the range of experimental conditions investigated for validation might be narrow. These gas jet stabilization theories can be used to explain a diesel spray flame stabilization phenomenon. Results from Siebers and Higgins[Siebers and Higgins 2001] support the premixedness theory where the temperature dependence of the lift-off height by their empirical model comes very close to that of the premixedness model. Although, the model of Siebers and Higgins does not explain the dependence of lift-off on orifice diameter and chamber density, it captures the linear relation of lift-off and injection velocity based on the mechanism of flame propagation. The flamelet extinction theory can be used to explain the lift-off location on a few aspects - increase in ambient temperature causes increase in the quenching limit of the (laminar) diffusion flamelet leading to stabilization of flame closer to nozzle where higher scalar dissipation rate prevails; increase in ambient density causes increase in jet spread leading to decrease in stoichiometric scalar dissipation rate and increase in reaction rate which together cause shorter lift-off; increased injection velocity would increase the lift-off since scalar dissipation rate upstream would increase and lift -off has to move downstream to match the quenching limit. Picket et al.[Pickett et al. 2005] concluded that auto-ignition might be the dominant mechanism to cause lift-off in diesel sprays since a similar Arrhenius-type expression associated with the

ignition delay was also arrived at for the residence time of the fuel from the nozzle orifice to the lift-off location. Moreover, the existence of cool-flame upstream of the lift-off gives an indication that the first-stage ignition reactions occurring in the cool-flame develop into second stage ignition reactions at the lift-off location and cause flame stabilization; although enhancement of flame propagation due to this cool-flame is not yet ruled-out. Pickett et al.[Pickett, Kook, Persson, et al. 2009] also offered a mechanism of turbulent mixing with the high-temperature combustion product at jet edges by laser-igniting the zone upstream of lift-off. Ameen et al. [Ameen and Abraham 2014] used RANS and LES modeling approaches to understand the ignition and lift-off. Their results show that fuel gets ignited at multiple points around the jets in the fuel-air mixing layers which lies in the boundary zones towards the edges of the jet. In these zone the mixture fraction is rich and ignition happens when the strain rates are within the ignition limits. The ignition kernels generated in this fashion grow in time and finally merge to form a continuous flame front. This points towards an auto-ignition mechanism. The authors also explained the generation of lift-off as the minimum axial distance from the orifice until which the local scalar dissipation rate is not favorable of ignition. Such a linkage between scalar dissipation (mixing field) and an auto-ignition event can be found in prior works *[Ameen and Abraham 2014, Bajaj et al. 2013, Campbell et al. 2009, Felsch et al. 2009] for a* non-premixed combustion environment. Thus, further understanding of the ignition process and transient flame development can be obtained by utilizing the reactive species presence and surrounding scalar dissipation rate field, and has been performed as part of this thesis. Ameen et al. [Ameen and Abraham 2014] also observed re-ignition kernels near the lift-off zone in the LES models and not in the RANS simulations. This points towards an auto-ignition stabilized flame front. Kokjohn et al.[Kokjohn and Reitz 2011] explored the possibility of a combined occurrence of two stabilization mechanisms viz. auto-ignition and premixed flame stabilization. By using both Chemkin based well-mixed model to support auto-ignition together with a G-equation model to support premix flame propagation, the authors observed very similar results in terms of ignition, lift-off and soot formation, with and without the use of the flame propagation model. However, by using flame propagation model simultaneously, features of edge or triple-flame structure were observed at the lift-off location. The purely kinetics

based combustion model was not able to capture these features. Thus, lift-off can be explained by a variety of reasons which constitute many theories. Considering some of the dominant theories and applying it to the subsequent flame of a split injection flame would shed light on the reasons for its unique ignition and stabilization. Such work has been done as part of this thesis as discussed in the results and discussions section. Some of the relevant literature is discussed in the next section.

3.18 Background

3.18.1 Ignition and lift-off mechanism differences

From a split injection diesel spray combustion standpoint, there has not been much emphasis on performing detailed experimental and CFD studies in understanding the ignition and lift-off mechanism of the subsequent injections. In the past, some conclusions on ignition of main spray were revealed by Felsch et. al[Felsch et al. 2009] as part of establishing a flamelet modeling approach to model split injections. The study revealed that higher scalar dissipation rates prevalent during the main injection enhances the local mixing and fuel conversion leading to a quicker *flame propagation* controlled main ignition. These scalar dissipation rates are lower than the quenching scalar dissipation rates, and thus allow the survival of the main flame. Similar levels of scalar dissipation rates as present in the main ignition surroundings would not allow the pilot to ignite. This is because, the pilot ignition occurs by *auto-ignition* and auto-ignition does not occur at such high scalar dissipation rates. A similar result was concluded recently by Gong et al.[Gong et al. 2015] using a Eulerian stochastic fields model coupled with RANS turbulence modeling. Their study was part of studies related to laser ignition supported flame stabilization event in diesel sprays. . Lim et al. [Lim et al. 2010] used a flamelet modeling technique similar to Hasse and Peters [Hasse and Peters 2005] but only applying flamelet equations applied near the stoichiometric region. They concluded that that the main injection ignition delay is independent of the ambient temperature like the pilot injection. This is because the main ignition occurs by the propagation of radicals and heat which is effected by the local scalar dissipation rate and not the ambient temperature. This is yet another literature concluding the main flame is flame propagation mechanized.

It is also necessary to check if this different mode of ignition and stabilization of main event exists for different test conditions, how it is impacted by varying ambients, whether or not it is a unique main flame phenomenon and is lift-off a quasi-steady event (like pilot flame) or an unsteady event changing rapidly as time progresses. This would provide causal links to the soot formation processes which are largely not understood for split injection strategies.

To investigate the ignition and lift-off physics in the subsequent injections, some of the prior works prior works [Ameen and Abraham 2014, Bajaj et al. 2013, Campbell et al. 2009, Felsch et al. 2009] highlighting a linkage between scalar dissipation and ignition event was considered. The investigative tools used in those works were re-applied for the subsequent (main) injection in the thesis. Also work by Gordon et al. [Gordon et al. 2007a, b] which takes support from the DNS studies of Echeki and Chen *[Echekki and Chen 2003]* was considered as an investigative aid. Experimental evidence of the importance of HO_2 species in characterizing ignition in low temperature oxidation of hydrocarbons was provided by Blocquet et al. [Blocquet et al. 2013]. The work of Gordon et al. [Gordon et al. 2007a, b] highlights the HO_2 radical depletion followed by the OH species increase as a thermal runaway event signifying an auto-ignition process and a simultaneous rise of the radical HO_2 along with OH species as signifying a premixed flame propagation type ignition.

3.19 Results

3.19.1 Effect of ambient temperature on combustion characteristics

In Fig. 81, the experimental and numerical AHRRs for the 0.5/0.5/0.5-ms schedule at 800 K and 900 K ambient temperatures are presented. Each experimental profile represents the average of repeated runs obtained while performing single shot PLIF and simultaneous Schlieren tests. The apparent heat release from experiment is calculated using the Equation 8. The CFD heat release plotted here is not the chemical heat release but the apparent heat release calculated using a pressure derivation as done for experiments. The AHRR obtained in this way for CFD is slightly lower in magnitude than the chemical heat release. However, the shape of a pressure-derived AHRR and the chemical heat release rate are similar.

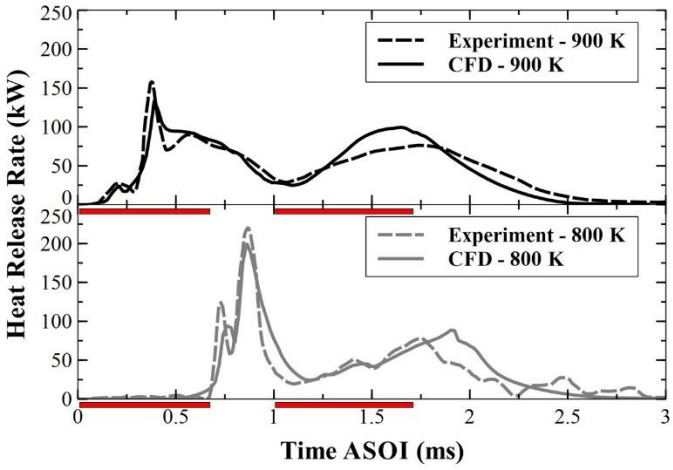

Figure 81: Apparent heat release rate profiles for the different ambient temperature cases for the 0.5/0.5/0.5-ms injection sequence at 1200 bar injection pressure. The time axes are highlighted for the duration of individual injections

In Fig. 81, rectangular highlighting box near the time axes gives an idea of the actual visualized injection duration. As expected, the AHRRs in Fig. 81 show that higher ambient temperatures lead to earlier ignition of the pilot and main sprays. For both of these cases, heat release due to ignition and combustion of the main injection can be clearly differentiated from that associated with the pilot. It can also be seen that, for both 900 K and 800 K ambients, the pilot flames shows a combination of premixed combustion phase and a mixing-controlled combustion phase characteristics; whereas the main flames show a mixing-controlled combustion phase only. In a premixed combustion phase, the conversion of the premixed fuel (fuel+oxidizer) into some production species takes place. The mixing controlled combustion phase has a positive slope of AHRR in the active main injection periods as observed in Fig. 81. This is a characteristic of the mixing controlled combustion phase. Thus, as also pointed out by Campbell et al.[Campbell et al. 2009] mixing controlled combustion can be termed as an injection rate controlled combustion. This also acts as a proof that the effective injection duration in the experiments was indeed longer than measured using ROI as explained in the ROI section. Of greater interest from Fig. 81, it is observed that first- and second-stage ignition of the pilot spray begins *before the end* of the pilot injection for the 900 K ambient condition. For the 800 K ambient condition, first-stage

ignition of the pilot begins *almost at the end* of the pilot injection with second-stage ignition occurring during the dwell. On comparison with the raw images from the high speed camera in Fig. 82, it can be observed that, 'schlieren softening' at ~0.29ms and ~0.70 ms for the 900 K and 800 K ambient cases respectively occurs at similar times as shown by the initial heat release rise in the corresponding plot in Fig. 81. Schlieren softening denotes a first stage ignition event, in which the temperature of the local gases rises to match that of the ambient such that there is no refractive index gradient in the line of sight. From the corresponding CFD temperature clips, it can be observed that schlieren softening effect is generated by temperature homogeneity. Additionally, since the mixture formation in terms of schlieren softening is simulated in reasonable agreement with the experiments, it can be said that the CFD simulations are well validated in terms of vaporized fuel-air mixture formation. At times of ~0.42 ms and ~0.83 ms for the 900 K and 800 K ambient cases respectively, as the combustion temperature rises, the schlieren softening is ceased due to the formation of low-medium temperature intermediates. The temperature increase can be gauged by the corresponding CFD clips which actually denote the premixed peak from the AHRR plot of Fig. 81.

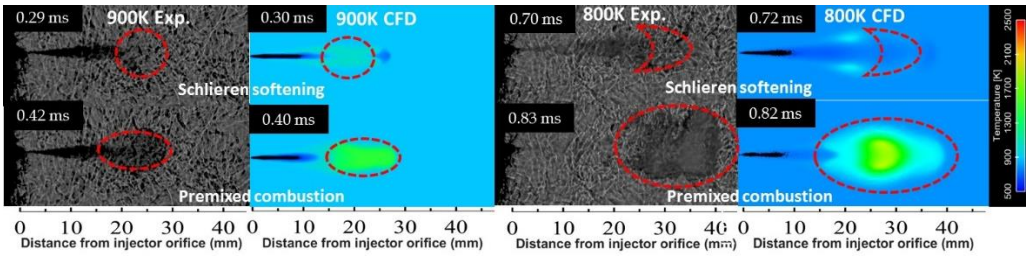

Figure 82: Raw schlieren images and temperature CFD clips for the 0.5/0.5/0.5-ms injection event at 900 K (left), 800 K (right). The dash lines indicate schlieren softening while the bold lines indicate a luminosity event. In the CFD images, the black color contour near the nozzle is indicative of liquid droplets of even the smallest size

The liquid length and lift-off predictions from CFD have been given in Fig. 83 and the ignition delay and lift-off lengths are tabulated in Table 9. Liquid lengths from the CFD are calculated based on 99% extent of the injected liquid fuel mass along the injector axial direction. The liquid length experimental measurement for the pilot and main injection for the 900 K and

800 K were measured as 9.3 mm and 10.2 mm respectively. It was found by Pickett et al[Pickett, Kook, et al. 2009a] in a low density, low temperature ambient that in a split injection event, the liquid from subsequent injections also travels farther than the first injection, but the final penetration distances are not significantly different. Thus the pilot and main liquid lengths can be estimated to be the same within reasonable accuracies. The liquid length profiles from the CFD shown in Fig. 83 lie close to the experimental values. Apart from that, it can be observed from CFD liquid length predictions that the initial rate of rise of liquid length is higher for the main injection than the pilot. This is perhaps due to the lower density ambient experienced by the leading edge of the main liquid injection, which makes it to travel faster than the pilot, in addition to the slipstream effect[Skeen et al. 2015b]. The ignition delay of the pilot injection was calculated from the pressure trace corresponding to the first increase of pressure by 0.24 bar. However for the main injection, ignition delay was calculated as the time delay after the start of main injection times where the AHRR increases by 20% from the value at the minimum near the main injection timing following Skeen et al.[Skeen et al. 2015b] The same definition of ignition delay was applied for analysis of the experimental and CFD generated data. Experimental measurements of the flame lift-off length commonly rely on chemiluminescence signal from the excited state hydroxyl radical (OH*). The experimental images usually show an initial sharp rise and a peak, which is followed by a levelling-off region for the OH* intensity. Thus, the experimental LOL is usually determined as the location of the signal intensity at 50% of levelling off value. However OH* is not included in the chemical mechanism considered in this work. Thus, the CFD-based lift-off lengths correspond to the most upstream position where the OH reaches 14% of its maximum ground state OH concentration in the quasi-steady combustion state[Pei, Hawkes, et al. 2015]. This is following the study performed by Pei et al.[Pei, Hawkes, et al. 2015] for combusting spray A simulations with OH* chemistry revealing that 50% of OH* peak value corresponds approximately to 14% of OH. No measurements were performed relating to lift off for split injection cases in the present work. Although, there were measurements performed for a single 6 ms injection at 900 K, which resulted in a measured lift-off of 19.3 mm; which can be considered as the lift-off for the pilot injection. The CFD lift-off of 21.7 mm for the pilot injection at 900 K ambient is in

reasonable agreement with the experimental value. No measurement for the lift-off of main injection has been made, although Skeen et al. [Skeen et al. 2015b] reported a lift-off of 13-15 mm for a similar injector with 1500 bar injection pressure at 900 K, 22.8 kg/m3 ambient. The quasi steady lift -off of ~15 mm for the CFD of the main flame at 900 K is in reasonable agreement, noting that the lift-off increases as the injection pressure decreases. There is no lift-off for the 800 K pilot injection, since the ignition (and flame stabilization) of the pilot happens almost to the end of the pilot injection. There is no measurement made for the lift-off of the main injection of 800 K, but data from ECN[Pickett et al. 2014b] shows a steady lift off of 27 mm for a single injection which is close to 27.3 mm average lift-off length observed from CFD. Moreover, schlieren images for a similar 800 K injection from Skeen et al.[Skeen et al. 2015b] have a reported value of ~25 mm for the main lift-off. With similar liquid and lift-off lengths from measurements from this work and from various other sources falling close to CFD values, it can be said that CFD predictions are within reasonable agreement. This is even more important since the main ignition and flame propagation characteristics are sensitive to the environment left behind by the pilot combustion.

Table 9: Pilot and main ignition delay (ID) and lift-off length (LOL) obtained from both experiment and CFD of a1200 bar injection for the 0.5/0.5/0.5-ms injection sequence

T_{amb}(K) /ρ_{amb}(Kg/m^3)	Pilot ID(ms) Exp./CFD	Pilot LOL(mm) Exp./CFD	Main ID(ms) Exp./CFD	Main LOL(mm) Exp./CFD
900/22.8	0.38±0.05/0.4	19.3±1.9/21.7	0.23±0.04/0.19	13.3/15
800/22.8	0.89±0.08/0.9	-	0.31±0.07/0.29	23.6/27.3

The axial distance between the corresponding liquid length and lift-off length from Fig. 83 give an indication of the spatial constraints for the ambient air-entrainment into the flame, indicating possible presence of richer/leaner mixtures in the flame region. For the pilot of the 900 K, there is a ~12 mm gap, whereas for the main of the 900 K this gap reduced to 6 mm. The gap, ~15 mm, is highest for the main of the 800 K case.

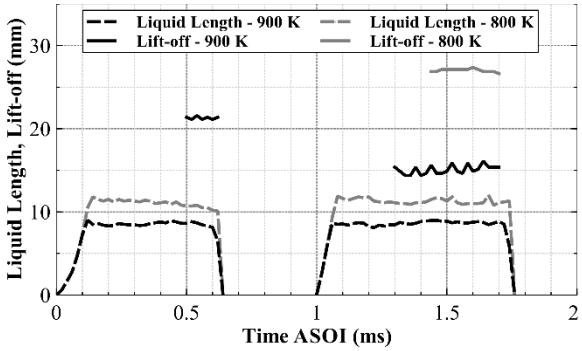

Figure 83: Liquid length and lift off prediction from CFD for the 900 K and 800 K cases

3.19.2 Simultaneous Schlieren-PLIF

Image sets acquired using a simultaneous schlieren/luminosity and 355-nm PLIF technique are presented in this section in Figures 84 and 85. The aim of these figures is to visualize the spatial presence of cool-flame species (using 355-nm PLIF signal) and the high temperature flame (using luminosity signal) for the entire combustion event. These figures are also used to validate the CFD model, since the spread of reactive radicals and high temperature presence for the ambient of the main injection is vital to investigate its ignition characteristics. In the figures of this section, a superimposed natural luminosity boundary (red contour line), if any, from the high speed camera confirms the PAH intensity signal from the ICCD. If the PLIF signal lies within the red contour boundary, it is most probably a PAH signal since PAH is a soot indicator and its presence downstream is linked to the bright (soot) luminosity. Inferences about the signals of formaldehyde and PAH (or soot) being temporally and spatially separated and also varying in their intensities were found in Refs.[O'Connor and Musculus 2013a, Lachaux and Musculus 2007, Bruneaux 2008].

Fig. 84 shows the set of images for the 900 K ambient injection case. The white text box in the right-bottom in each individual image contains the total intensity counts (x10^5) of the schlieren image which contained the luminosity signal from the combustion event.

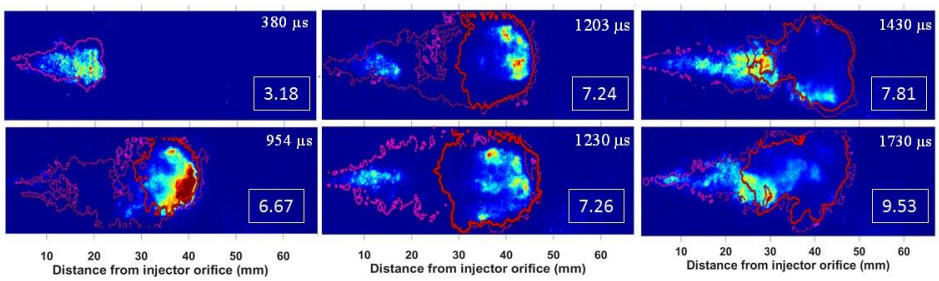

Figure 84: Simultaneous PLIF imaging of the 0.5/0.5/0.5-ms spray combustion event at 1200 bar for the 900 K ambient case; dotted pink contour line denote schlieren boundaries, red contour line denotes soot luminosity, background Red-Blue-Green image is a PLIF image for formaldehyde measurement. Red indicates high intensity and blue indicates low intensity in the RGB color scheme. The white text box in right bottom of each image is divided over 1E+05 and indicates the net luminous intensity

One observation that can be made in Fig. 84 is that the injection of main is occurring in an environment of high temperature gases which have receded upstream[Knox and Genzale 2015a] as evident from the schlieren boundaries from the image of 954 µs. The intensity count at the end of main injection times is 92% higher than the intensity count at the end of pilot injection signifying increased soot production for the main injection over the pilot.

Fig. 85 shows the 800 K ambient condition tests with the white boxes indicating the total intensity counts (x10^5).

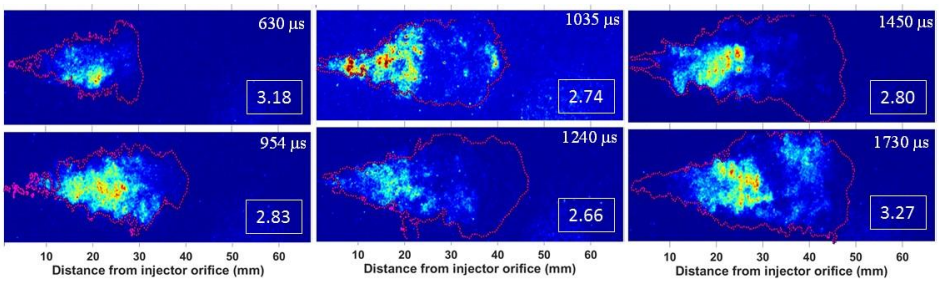

Figure 85: Simultaneous imaging of 0.5/0.5/0.5-ms spray combustion event at 1200 bar for 800 K ambient case. Red indicates high intensity and blue indicates low intensity in the RGB color scheme

A general observation from the Fig. 85 is that the injection of main happens in an environment of low temperature reactive species signified by formaldehyde from 355-nm PLIF as in 954 µs. The intensity count decreases in some images due to blocking of some light through the camera filter. However, between 630 µs and 954-µs, there was dim soot luminosity visualized from the high speed camera images with net intensity count increasing (not shown here).

It is known from studies in the past[Skeen et al. 2016, Idicheria and Pickett 2005] that soot formation is linked to the ignition and lift-off characteristics. This it can be said that, comparing between the soot luminosities of the pilot and main injections, earlier ignition and increased soot for the 900 K is due to its injection in a high temperature environment provided by the recessed pilot combustion products as shown in Fig. 84 at 754 µs. Also, earlier ignition and increased soot for the 800 K main injection is due to its injection into an environment of low temperature reactive intermediates as evident from the image at 954 µs in Fig. 85, where there is appearance of a high signal of formaldehyde (PLIF) near the nozzle. Here, the usage of term soot is in analogy to the luminosity signals since a 600-nm short pass filter was used. Although formaldehyde is not a reactive intermediate, its presence is an indicator that reactive species such as hydrogen peroxide and hydroperoxyl are present. Thus, not only the low temperature intermediates, recessing from the pilot spray play a key role in its earlier ignition as in the case of 800 K ambient injections, but also the recessed high temperature products of the pilot combustion increase the local temperature of the main spray to ignite quicker as in 900 K. The high temperature combustion products for the 900 K case can also have traces of ignition enhancing species which can accelerate ignition of main injection. The roles of low temperature reactive species and high temperature combustion products might be two different mechanisms which aid in the main ignition and lift-off, thus affecting the later soot formation. The mechanisms of ignition and lift-off affecting the soot formation is investigated in more detail in further sections using Figure 84 and 85 as part of validation. Evidence of the surrounding high ambient temperature together with the presence of reactive radicals aiding in shortening the ignition delay by about half was provided by Skeen et al.[Skeen et al. 2015b] They have performed closed homogenous reactor simulations which took inputs such as

local equivalence ratios from another one-dimensional jet model. They concluded that both the temperature and reactive radicals can have effect on reducing the main ignition delays in almost similar magnitudes. In the present work, 3D CFD RANS detailed chemistry simulations are used to investigate further. CFD validations are performed in the next section with the formaldehyde species presence from the 355-nm PLIF and approximate soot contours from the luminosity measurements from Figures 84 and 85.

3.19.3 IXT and simultaneous Schlieren-PLIF

The purpose of this section is to look into the spatial presence of formaldehyde and qualitative soot presence from the experiments and check if CFD has been able to capture these details. Fig. 86 shows the intensity IXT contours from experiments (Figures 86a and 86b) and soot and formaldehyde IXT contour overlapped with temperature iso-lines from CFD simulations (Figures 86c and 86d). Also shown in Fig. 86 are 900 K and 800 K schlieren/PLIF experimental images for the limited time-instants of tests performed.

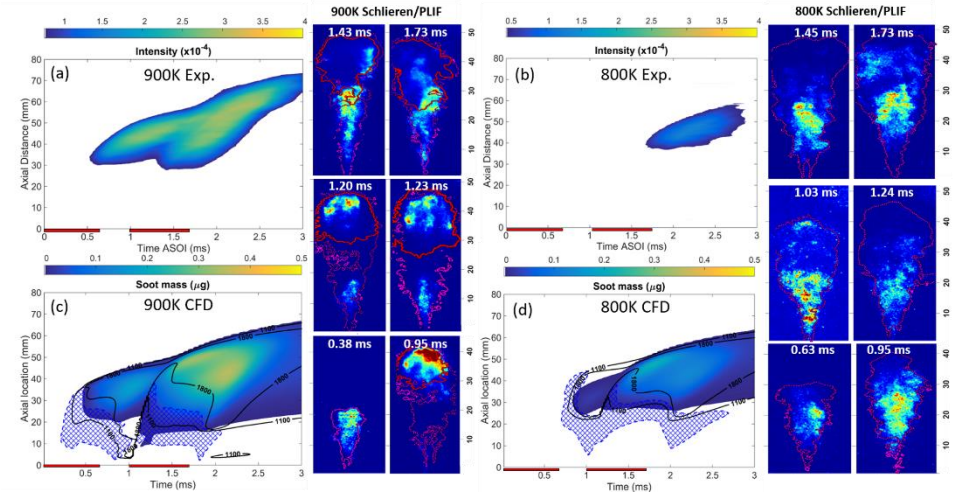

Figure 86: Intensity (top) and soot (bottom) IXT contour of 0.5/0.5/0.5-ms injection sequence for the 900 K ambient (left) and 800 K ambient (right) overlapped with 1% formaldehyde mass fraction bounded patch and cross-sectionally averaged temperature iso-lines across a spatial bound of mixture fraction of 0.1%

The false-color PLIF images provide a qualitative representation of the formaldehyde and PAH distribution at select times during the combustion event as observed using the PLIF

diagnostic. For each single-shot PLIF image, a corresponding high-speed schlieren/luminosity movie was acquired. Since they were 3 repeats for the PLIF shots (so 3 repeats for schlieren), only one of the schlieren movie was used to determine the vapor and soot boundaries to overlay on the false-color images. The presence of a superimposed natural luminosity boundary (red contour line) obtained via high speed imaging, confirms the PAH intensity signal from the PLIF images. Inferences about the signals of formaldehyde and PAH (or soot) being temporally and spatially separated and also varying in their intensities can also be found in Refs.[O'Connor and Musculus 2013a, Lachaux and Musculus 2007, Bruneaux 2008]. These figures are used to validate the spatial distribution of formaldehyde (cool-flame products) and soot predicted by the CFD model as presented in the adjacent IXT plot.

In Fig. 86c and 86d, cross-sectionally averaged temperature contours are overlaid in bold lines. The temperature iso-lines of 1100 K and 1800 K broadly indicate the cool flame region and the high temperature combustion region, respectively. While calculating the cross-sectionally averaged temperature, care is taken not to average the ambient temperatures by averaging the temperature field within a 0.1% mixture fraction bounded region. A 0.1% mixture fraction region would signify a reasonable presence of the fuel/air reaction mixture. Also, in Fig. 86c and 86d, soot mass is plotted in shading and formaldehyde presence is shown by the overlapped cross-hatched patch. The formaldehyde patch is bounded by 1% formaldehyde mass fraction (dashed) line, thus the hatch region signifies any formaldehyde mass fraction greater than 1%. From Fig. 86, it can be observed that the main flame soot is higher in magnitude than the pilot flame soot and also that the experiment and CFD plots have reasonable agreement in terms of (qualitative) soot presence. However, the validations cannot be performed with higher accuracy due to the definitions of soot from experiments and CFD not matching. This is more evident in the 800 K case. In the CFD plots of Fig. 86c and 86d, the placement of formaldehyde contours is comparable to the axial placement of formaldehyde from the adjacent PLIF images, further validating the CFD model. From Fig. 86, a validation relating to CH_2O-soot overlap can be observed for the 900 K case. From Fig. 86c, for the 900 K case, it can be observed that there are regions between axial locations ~20-30 mm from the nozzle orifice, where there is combined appearance of

formaldehyde and region of higher soot presence. This kind of combined appearance was also seen throughout the adjacent 900 K schlieren/PLIF images, where RGB coloring of formaldehyde and red boundary from soot luminosity overlapped between axial locations of ~20-30 mm. Thus, from Fig. 86, one can observe a reasonable agreement of CH_2O and soot (luminosity) species between experiment and CFD. The model also confirms that there is temporal and spatial separation with a marginal overlap between CH_2O and PAH for 900 K (conventional ECN Spray A condition) and 800 K cases.

In Fig. 86c, just before the start of main injection (~1 ms), in the upstream regions, there is a high temperature (1800 K) iso-line indicating combustion recession[Knox and Genzale 2015a] from the pilot flame for the 900 K CFD case, which was also observed in adjacent 900 K schlieren/PLIF experimental images at 0.95 ms. After the main injection ends there is an increase in temperature (actually ~1600 K, not shown) upstream, signifying a combustion recession event of the main. No such combustion recession event was observed for the 800 K either experimentally or from CFD. Instead, a high spatial presence of formaldehyde was seen at 0.95 ms in the adjacent experimental 800 K schlieren/PLIF images which is confirmed by CFD. The low temperature reactive species (800 K case) and high temperature combustion products (900 K case) aid the main ignition and lift-off. Evidence of the surrounding high ambient temperature together with the presence of reactive radicals aiding in shortening the ignition delay by about half was provided by Skeen et al.[Skeen et al. 2015b] They have performed closed homogenous reactor simulations which took inputs such as local equivalence ratios from another one-dimensional jet model. They concluded that both the temperature and reactive radicals can have effect on reducing the main ignition delays in almost similar magnitudes. With this well validated combustion model which predicts the formaldehyde (cool-flame) and soot contours reasonably, the next section deals with ignition and lift-off stabilization characteristics.

3.19.4 Main ignition and lift-Off characteristics

It was found by Gordon et al. [Gordon et al. 2007a, b] that the HO_2 radical depletion followed by the OH species increase is linked to the thermal runaway event signifying an auto-ignition process whereas a simultaneous rise of the radical HO_2 along with OH species signifies a

premixed flame propagation type ignition. Experimental evidence of the importance of HO_2 species in characterizing ignition in low temperature oxidation of hydrocarbons was provided by Blocquet et al.[Blocquet et al. 2013]. Additionally, from prior works[Ameen and Abraham 2014, Bajaj et al. 2013, Campbell et al. 2009, Felsch et al. 2009], scalar dissipation rate (χ) was found to be an important variable to investigate the connection between the mixing field and combustion characteristics in a non-premixed combustion environment. The buildup of the radical HO_2 might be delayed due to higher scalar dissipation rates (χ) present in the ambient flow field, which in turn extends the ignition time. Such a linkage between the scalar dissipation and an auto-ignition event can be found in the work of Bajaj et al.[Bajaj et al. 2013] and Campbell et al.[Campbell et al. 2009] Thus, further understanding of the ignition process and transient flame development can be obtained by utilizing the reactive species presence and surrounding scalar dissipation rate field. In this work, the scalar dissipation rate (χ) is calculated based on Equation 12 as

$$\chi \cong c_{\chi} \frac{\varepsilon}{k} Z''^2 \tag{12}$$

where ε is the turbulent dissipation, k is the turbulent kinetic energy, Z''^2 is the mixture fraction variance and c_{χ} is a time scale ratio assumed to be a constant with a value of 2.0.

The scalar dissipation rate is processed further and extracted over the stoichiometric mixture. This gives a stoichiometric scalar dissipation rate (χ_{st}) which is more physical to understand the ignition, combustion and its dependence on the surrounding turbulent field. An IXT plot is used to investigate further. Fig. 87a and 87c show trends of HO_2 and OH species formation and depletion for the 900 K and 800 K ambient cases. In Fig. 87b and 87d, the OH species (solid line), HO_2 radical presence (hatched region bounded by dashed line) and the stoichiometric scalar dissipation rate field (shaded region) are shown as an IXT plot.

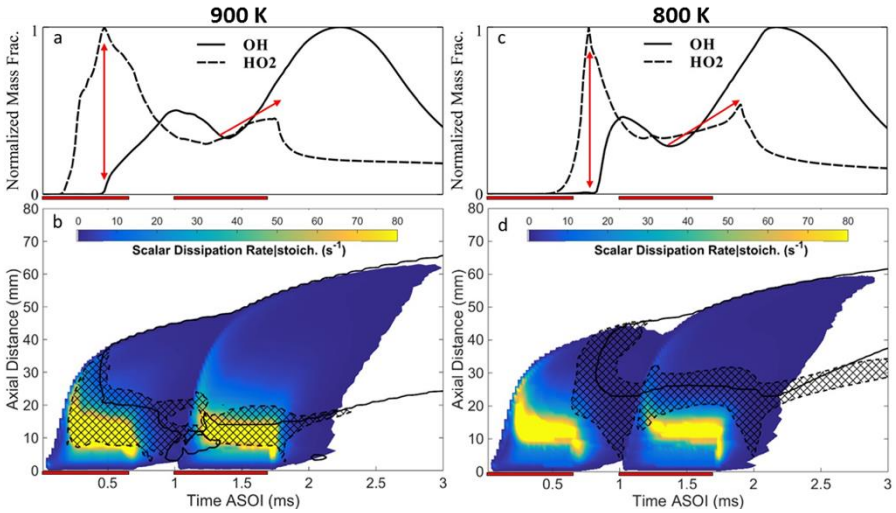

Figure 87: Cross-sectionally averaged scalar dissipation rate extracted along the iso-stoichiometric fuel mixture line

Left: 900 K; Right-800 K. Black cross-hatch patch is 1% HO_2 mass fraction bounded. Black bold curve is the 14% mass fraction of OH. Actual injection duration is highlighted near the time axis.

Fig. 87a for the 900 K ambient temperature and Fig. 87c for the 800 K ambient temperature show that the peak mass fraction of HO_2 formed from the first (pilot) injection, is nearly coincident in time with the onset of OH formation (formed in the high-temperature ignition). Following high-temperature ignition, both the HO_2 and OH mass fractions approach quasi-steady until reactions from the second (main) injection begin. The behavior observed here for the first injection is characteristic of a two-stage auto-ignition and flame-stabilization process.[Gordon et al. 2007a] Different from the first injection, during ignition of the second (main) injection, the HO_2 and OH mass fractions begin to increase almost simultaneously for both 900 K and 800 K ambient temperatures. Following previous studies which employed direct numerical simulations and probability density function approaches for modeling, this is indicative of premixed flame-propagation mechanized ignition and flame-stabilization process for the main. [Gordon et al. 2007a, b, Echekki and Chen 2003]

More details about ignition and lift-off characteristics can be obtained from Fig. 87b for the 900 K ambient temperature where it is seen that the ignition of the pilot injection (generation of OH species) takes place in a region where a low value of χ_{st} prevails around 0.5 ms. The high χ_{st} values present upstream in these time instants are not accommodative of an auto-ignition event. For an auto-ignition event to take place these high χ_{st} value should drop below a certain $\chi_{igntion.[Bajaj\ et\ al.\ 2013]}$ The OH species field signifying the lift-off, also gets stabilized in a region of a lower χ_{st} region. This is in accordance to the traditional view of a diesel flame at 900 K, in which the auto-ignition and flame lift-off mechanisms are by auto-ignition at 900 K.[Bajaj et al. 2013] However, it is found that, this behavior does not hold true for the conditions in which the main is ignited and stabilized. Shortly before and around 1 ms, at axial locations between 15-20 mm, it is observed that there is a depletion of HO_2 radical (caused by thinning of the HO_2 cross-hatch region) creating a hole in the cross-hatch patch. At the same time, downstream, there is a combustion recession event causing OH to form upstream near the injector. These are the conditions in which the main injection enters the chamber. Thus, it can also be said that the combustion recession species are not totally composed of complete combustion products like CO_2 and H_2O, but do have hot temperature intermediates like OH to effect the combustion chemistry of the oncoming main injection.

As the main injection enters the combustion chamber, the liquid jet is seen to by-pass the local flow field which also contains the OH species. There is by-passing of OH species field due to its presence seen in the upstream axial locations until ~1.3 ms. The by-passing causes the OH species, which is a high temperature reactive species, to create a thermal blanket upstream around the entering main injection. This thermal blanket causes a faster conversion of fuel, producing reactive species at a faster rate. It can be seen that at ~1.2 ms, the hole in the HO_2 field is filled due to this effect. These newly produced reactive species along with the species left behind by the pilot (e.g. OH) are believed to accelerate the main ignition chemistry. Additionally, it can be observed that production of OH species (between 15-20 mm) has started almost simultaneously with the replenishing event of the HO_2 species. This event is the ignition event of the main, which is a flame propagation triggered event since an ignition event mechanized by auto-ignition for the main injection cannot be generated in a higher χ_{st} field[Bajaj et al. 2013, Ameen and Abraham 2014] where the main

is seen to get ignited. Evidence of such an event not occurring in auto-ignition mode has also been given by Felsch et al.[Felsch et al. 2009] using flamelet RANS modeling and Gong et al.[Gong et al. 2015] using Eulerian stochastic field RANS model. It can be said that, in fact, the high scalar dissipation rates are the reason for faster ignition of main since they enhance the mixing in the local flow field which directly enhances the flame propagation based ignition event. Also, it can be seen that the flame stabilization of the main injection takes place in a higher χ_{st} field, indicating that the stabilization mechanism is also by flame propagation.

Interestingly, the IXT plot of Fig. 87d depict a stark difference from the 900 K case (cf. Fig. 87b). In Fig. 87d, for the 800 K case, *both the pilot and main* ignite in a lower χ_{st} field. For the 900 K case, only the pilot ignited in a lower χ_{st} field and not the main. It is known that the scalar dissipation rate at which ignition takes place (χ_{ign}) is reduced as the ambient temperature is lowered. Since this was a modeled χ, a cross check with a 1D flamelet code was done to make sure if the ignition events naturally shifted to a lower χ region when the ambient conditions reduce from 900 K to 800 K. A 1D flamelet code was ran by changing the ambient conditions from 900 K to 800 K and an ignition χ reduction of 1.85 was observed; which is close to ignition χ reduction of ~2 observed in the present work with the well-mixed reactor. As the main injection enters the chamber, it is seen that HO_2 presence is receded slightly towards downstream perhaps due to quenching of the reactive radicals due to the cooler vaporizing main spray. However, there is still some HO_2 present in the upstream location of the OH iso-line until ~1.3 ms (main ignition time) to enhance its ignition. This quenching must have been minimal in the 900 K case since the ambient consisted of much hotter species. The main ignition of 800 K case can be categorized as premixed in nature due to OH formation and HO_2 formation starting to increase simultaneously during ignition (cf. Fig. 87c). The buildup of pool of radicals in the pre-ignition zone before thermal runaway (ignition) event occurs is a less rigorous indicator but renders useful in recognizing the effect of these precursors in ignition processes.

Fig. 88 shows a snapshot in the quasi-steady lift-off instants for the pilot and main injections of 900 K (left) and 800 K (right) ambients. For the quasi-steady state of a flame

stabilization event, considering the axial spread of a species can also be approximated as time history of its concentration. From Fig. 88, it can be observed that there is high HO_2 build-up upstream to the formation of the OH species for the pilot injections of both the 900 K and 800 K ambient temperature cases (although 800 K pilot flame does not have a lift-off as per definition due to injection ending before flame stabilization). According to Gordon et al. [Gordon et al. 2007a, b] the build-up of HO_2 before being depleted into OH downstream, even in a spatial sense, signifies auto-ignition stabilization mechanism. For the main injections of both the 900 K and 800 K ambients, in their quasi-steady lift-off times, there is no appreciable build-up of HO_2 upstream of the OH formation, even if the lift-off of 800 K main is much higher than 900 K main flame. This characteristic of main flame signifies premix flame stabilization following Gordon et al. [Gordon et al. 2007a, b]

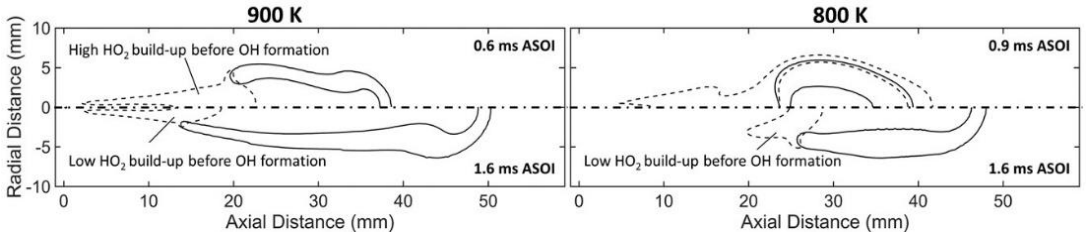

Figure 88: HO_2 and OH line contours for a quasi-steady time for the pilot (top-half: 0.6 ms ASOI) and main (bottom-half: 1.6 ms ASOI) indicating HO_2 radical build-up relation to auto-ignition and lift-off mechanism for the 900 K (left) and 800 K (right) ambients

To put more emphasis on the uniquely different main flame stabilization event inferred from prior research and which can also be proven in the present case, shown in Fig. 89 is the instantaneous heat release rate per unit volume of substance (J/s-m^3) that is originated from the fuel. Also the temperature contours are shown as the second half of the image. 900 K pilot, 900 K main and 800 K main are shown in Fig. 89. From the HRR and temperature contours, two different stabilization mechanisms can be suggested. There is a two-stage ignition with an auto-ignition induced flame front in the base of the 900 K pilot flame (signified by high temperature region) in Fig. 89a. An 800 K pilot flame was not considered since quasi-steady flame stabilization assumption does not apply due to stabilization of first injection taking place after the injection has stopped.

For the main injections of 900 K and 800 K cases, the flame (signified by high temperature region) inhibits the ignition in fuel-rich mixtures by precluding the surrounding oxygen from mixing into the base of jet. This is realized by considering the geometry of the flame base (shown by wavy curve at lift-off). The geometry of the flame base for the pilot flame is more flat. For the main flame base of 900 K (cf. Fig. 89b), the inhibiting of oxygen in the low temperature region, due to the geometry of the flame base and low lift-off itself, prevents the first-stage ignition in providing sufficient radicals to trigger the second ignition and forming an ignition flame front downstream of the spray. Similar features of the flame base can be seen for the 800 K main flame (cf. Fig. 89c). A significant heat release rate from low temperature premixed region upstream of the main flame suggests a flame propagation ignition process. The main flame bases of 900 K and 800 K cases actually have a similar structure to that of a triple flame[Lyons 2007] which is related to a premixed flame stabilization concept. The main ignition and stabilization happens at a higher ambient temperature for the main due to increased local temperature form the combustion of pilot. The problem of main flame simulation to be reduced to studying single injection at higher ambient temperatures (but similar densities). This kind of assumption however does not consider the reactive species left behind by the pilot combustion. Gong et al.[Gong et al. 2014] performed high-fidelity large eddy simulations on a similar ECN Spray A case as in this work and found that auto-ignition and flame propagation mechanisms also exist in a single injection flame and they compete with each other. The occurrence of these mechanisms is dependent upon the ambient temperatures in which they occur. They found that at high temperatures (~1000 K), the (single injection) flame base is stabilized by premixed flame propagation. Additionally, in a different study, Gong et al.[Gong et al. 2015] used a Eulerian stochastic fields model coupled with RANS turbulence modeling to simulate a laser ignition supported flame stabilization event in diesel sprays and concluded a premixed flame stabilization event for the laser ignited flame (which has similarity to split injection flames).

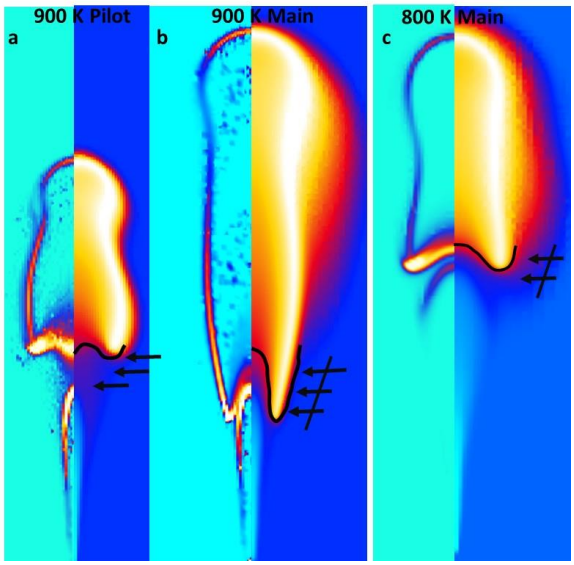

Figure 89: A half split CFD center clip of heat release rate in the left half and temperature in the right half for the pilot and main quasi-steady flame for the 900 K ambient case and main quasi-steady flame for the 800 K case

Since, HO_2 was the sole species considered in congruence with OH species to study the ignition and lift-off characteristics, it would be interesting to check the trends of other low and medium temperature species in defining the combustion regime. Fig. 90 (left) shows the trends of normalized quantities of low-medium temperature (LMT) species ($C_{12}H_{25}$, CH_2O, HO_2) and high temperature (HT) species (CO, OH) along with the heat release rate for 900 K ambient case. The trends of LMT species are similar for the pilot and main injection and so are the trends of HT species. Thus, the observation considering just HO_2 species as done in previous discussions is valid when other species are considered as well. The main ignition and lift-off is influence by the presence of all these species (both LMT and HT) in the ambient of the main injection (cf. Fig. 90 left). Also, shown in Fig. 90 (right) is the instantaneous heat release rate per unit volume of substance (J/s-m^3) that is originated from the fuel along with the temperature contours for the 900 K ambient case.

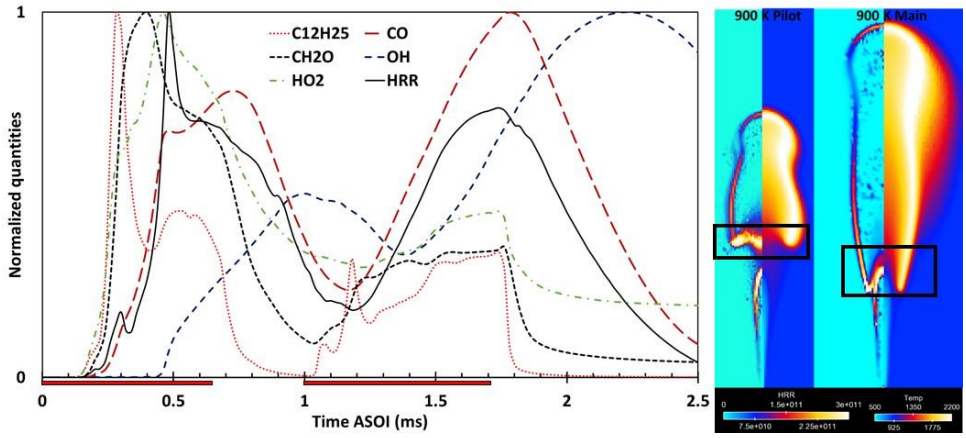

Figure 90: Left: Line profiles of normalized quantities of mass fraction of $C_{12}H_{25}$, CH_2O, HO_2, CO, OH and heat release rate for the 900 K ambient case. Actual injection duration is highlighted near the time axis. Right: A half split CFD center clip of heat release rate in the left half and temperature in the right half for the pilot and main quasi-steady flame for the 900 K ambient case.

The buildup of pool of radicals in the pre-ignition zone is a less rigorous indicator but renders useful in studying the effect of these precursors in ignition. Further analysis of ignition and lift-off mechanism is beyond the scope of present work, however the investigation shown here does provide useful insights into the main flame ignition and lift-off processes.

Majority of past theories support the claim of premixed flame propagation mechanized ignition and flame propagation for the main flame and it is also shown to be true by analyzing/interpreting the CFD results in various manners in the present work. Yet it can be argued that the ignition and flame stabilization are auto-ignition in nature for the main. Xu et al. [Xu et al. 2016] investigated the Damkohler number, and at a higher ambient temperature (1200 K) injection in the same ECN Spray A condition as the present work, they observed high Damkohler numbers associated near the ignition spots. From Xu et al.[Xu et al. 2016] these high Damkohler numbers further correspond to an auto-ignition tendency defined by chemically explosive modes which correspond to flammability of the fuel-air mixture. In a general sense, a higher Damkholer number corresponds to higher reaction rate role over convective transport rate to cause ignition event, which is an auto-ignition

concept. So on similar lines, for the main flames which are at higher ambient temperatures, their classification can be done as auto-ignition stabilized (which is contrast to Gong et al.[Gong et al. 2014] work mentioned previously). Pei et al. [Pei 2013] performed simulations with a transported probability density function model for similar spray A case as in the present work and at temperature 800 K, 900 K and 1000 K. They found the occurrence of re-ignition kernels in the lift-off region. Although they found that the flame stabilizes in a region where re-ignition spots occur, the ambient field velocity at lift-off was low at around 10 m/s. Pei et al.[Pei 2013] concluded that it may be possible that turbulent transport plays a role in the stabilization, as turbulent velocity fluctuations at lift-off location were found in the same order of magnitude as the flow field velocity. But re-ignition at the flame stabilization strongly indicates auto-ignition stabilization as the dominant mechanism. Apart from the discussion relating to ignition and flame stabilization, there is also a possibility that the main flame can be a temporarily steady event. A temporary main flame stabilization event ("main" here is the post-laser ignited flame) was actually observed in the work of Pickett et al.[Pickett, Kook, Persson, et al. 2009] (and numerically by Gong et al. [Gong et al. 2015]) in a study related to laser ignition supported flame stabilization event in diesel sprays. In their laser ignition study, the laser ignition generated flame in the region upstream of the lift-off (which was termed as main flame) sustained closer to the nozzle for almost 1 ms but rapidly traveled back to the original lift-off position. Thus, it can be said that in a split injection combustion case, while the post-combustion pilot resources are being exhausted, they promote ignition reactions in their vicinity. After they are exhausted the lift-off travels back. This aspect was also mentioned in the work by Skeen et al.[Skeen et al. 2015b] in work relating to split injection spray combustion. To support this behavior, the work of Pickett et al.[Pickett et al. 2005] can be used. Picket et al.[Pickett et al. 2005] introduced the concept of the residence time for a fuel droplet travelling from the nozzle orifice to the lift off location. This residence time for the main injection should be lower since the fuel droplets travel faster in lower densities created due to pilot combustion. Thus a low stabilization is imminent for the main injection. The low stabilization event is over after the ongoing main combustion exhausts the reactive radicals and ambient (cooler) entraining air substitutes the hot temperature from the pilot combustion. Another way to

look at this temporary event would be by applying the vortex stabilization theory by Broadwell et al.[Broadwell et al. 1985] As depicted in Fig. 91, as main flame enters the pilot flame, the expansion of the main flame (dilatation) within the traveling pilot flame causes a locally reversed flow at the point of intersection of main flame head with the pilot. This reverse flow coupled with the air entrainment from the ongoing main injection, can results in re-entrainment of reactive radicals and high temperature combustion products into the region upstream of the main flame base. This may support the flame at a region further upstream than would otherwise be possible. As the main flame head moves downstream, the reverse flow and entrainment field vortex also moves further downstream. Thus, it becomes weaker to support the pilot lifted flame at upstream locations and so the lift-off moves further downstream.

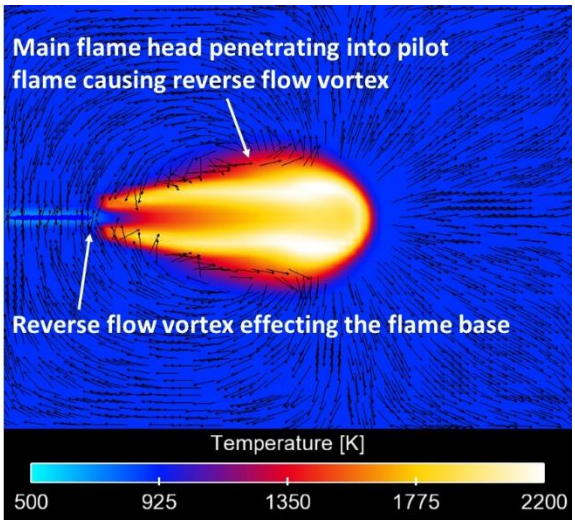

Figure 91: Velocity vectors overlaid on temperature contour for time instant of 1.6 ms ASOI for 900 K ambient case. Velocity higher than 10 m/s has not been shown

In the absence of experimental evidence for long second injection, this transient behavior of main flame cannot be proven at this stage. To summarize, the main ignition and lift-off were found to be mechanized by premixed flame propagation by performing similar investigation in the present work as in some literature. The idea that indicators of premixed flame propagation might appear is always a possibility. As discussed in the manuscript, however, it is difficult to conclude that premixed flame propagation dominates the flame stabilization process given the literature evidence collected against it and in support of auto-

ignition. To gain more perspective, this study can be extended to accommodate high-fidelity LES model approaches which resolve the sub-grid turbulence and make visualization of detailed features like re-ignition kernels a possibility for main flame.

Since the ignition and flame-lift off have an impact on the soot formation processes of the main (and possibly on the pilot due to mutual flame interactions), a brief analysis using mixture fraction (Z) and Temperature (T) plots is provided below to help understand the level of soot in relation to oxygen presence and turbulent kinetic energy (TKE) availability within the spray-flame.

3.20 CFD Analysis of pilot-main sooting characteristics

It is possible to correlate a Z-T plot, to actual location in a flame up to some degree of accuracy. An illustrative diagram has been provided in Fig. 35, with Z-T plot in the bottom and actual locations of the flame in the top. It can be seen that this plot has a delta-like (Δ) shape.

A quantity of normalized soot mass is plotted in the soot Z-T plot by normalizing the soot at any time instant with the peak soot value recorded in the entire combustion event. Fig. 92 provides such a soot Z-T plot for the 900 K case over six key time instants. The reader is advised to refer to Fig. 35 to correlate the locations of a Z-T plot with actual locations in a flame.

From the Z-T plot of Fig. 92, it can be observed that at 0.5 ms the pilot just started to form soot with most of the soot forming at higher than stoichiometric Z's between ~Z=0.05-0.1. Stoichiometric combustion of n-dodecane takes place at Z=0.04 at 15% ambient oxygen level. The next time instant of 0.6 ms is just before the end of injection of pilot, where combustion is steady. The soot Z-T plot has taken a V-like shape. There are bins developed in the bottom section which relates to a spatial location of far outer region of flame. This means that apart from soot formation taking place in central core of the flame, soot in the outer periphery of the exposed flame tends to form in leaner regions due to interaction (mixing) of soot with ambient oxygen. At around 1 ms, most of the soot is found in the near stoichiometric region (Z_{st}=0.04). At 1.3 ms, the main injection has entered and started its combustion phase. It is obvious to notice, that soot starts generating at higher Z's of Z=~0.18

unlike ~ Z= 0.1 for the pilot flame (at 0.5 ms). Thus, soot generation takes place in richer regions for the main injection and occurs faster in main injection than the pilot. It can also be observed at 1.3 ms that the bottom bins (lean region) show higher magnitudes of soot and are more dispersed unlike the time instant of 1 ms where soot was formed in the richer bins. The bottom bins correspond to the outer locations of the flame where the pilot reaction mixture resides. ~1.3 ms is the time instant when the mixture fraction of the main interacts with the soot cloud of the pilot. Around 1.3 ms the pilot soot field gets leaner due to increased mixing created by the oncoming main and the soot is moved to leaner regions (before getting oxidized in next time instant). This interaction effect of the main on the pilot thus results in higher oxygen availability, perhaps by breaking into the diffusion flame sheet of the pilot flame and entraining more oxygen from the ambient to mix with the pilot soot which was formed around stoichiometric-to-rich region before. A similar hypothesis was presented by O'Connor et al. through experimentation.[O'Connor and Musculus 2013b, O'Connor and Musculus 2014]

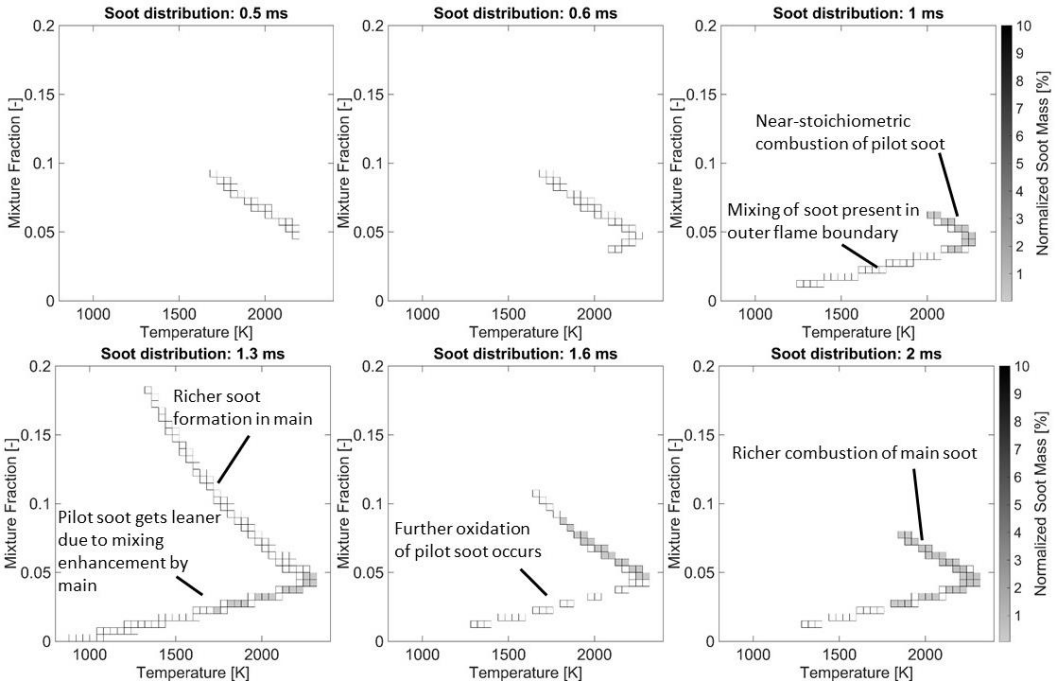

Figure 92: Mixture fraction-Temperature plot with soot mass fraction colored to explain ignition and flame characteristics of pilot and main

At 1.6 ms, soot is still being formed in richer regions as well as the leaner regions. The formation of soot in the leaner regions with lower magnitudes signifies soot oxidation due to the enhanced mixing induced in the pilot, since now the main injection is even more penetrated into the pilot regions. The formation of soot in the richer regions is due to the rich combustion of main due to low air entrained owing to low lift off (discussed as part of Fig. 93). At a time instant of 2 ms, which is 1 ms after the injection of main, the soot is still being formed at higher than stoichiometric Z's; whereas at 1 ms, which is 1 ms after start of pilot injection, soot was formed in relatively leaner regions. Fig. 93 shows a set of oxygen distribution Z-T plots in the top and turbulent kinetic energy (TKE) Z-T plots in the bottom to gauge the effect of turbulence on oxygen distribution which had impacted higher soot formation in main and reduced the soot production in pilot by main induced pilot soot oxidation. Volume percent of oxygen between 0 - 0.5% is considered for oxygen Z-T plot whereas a 0 - 0.5 of TKE fraction (fraction of TKE/TKE_{max} at any time instant in the computational domain) is plotted for the TKE Z-T plot.

It can be observed from Fig. 93 that at 0.6 ms, when the pilot injection is about to end and when there is a quasi-steady lift off developed, the region just upstream of the lift-off (left-side binned region: cf. Fig. 35) has indications of oxygen presence (from oxygen Z-T plot) and higher TKE present (from TKE Z-T plot). The dark TKE binned region to the left in 0.6-ms is the region upstream of the lifted flame where mixing between injection fuel and air takes place. It can be observed that the TKE and oxygen level in this region is higher at 0.6 ms than at 1.6 ms indicating a higher level of air entrainment at 0.6 ms. In other words, pilot flame has higher level of air entrainment than the main, perhaps due to its higher low lift off than the main flame. To notice in all the plots, is the level of TKE in the bins at the bottom region which constitute the far outer region of the flame and the bins in the upper-right side which indicate the high temperature flame region. At 1.6 ms, these bins show both higher magnitude and spread of TKE fraction than the ones in 0.6 ms. This is due to the effect of induced turbulence of the main injection on the pilot after start of main injection times. This results in a higher level of oxygen supply as evident from the bins in bottom region of the oxygen TKE plot in the corresponding time instants. As said before in the soot Z-T plot discussion, the interaction effect of the main on the pilot results in higher oxygen availability

(increased mixing), perhaps by breaking into the diffusion flame sheet of the pilot flame and entraining more oxygen from the ambient to oxidize the pilot soot.

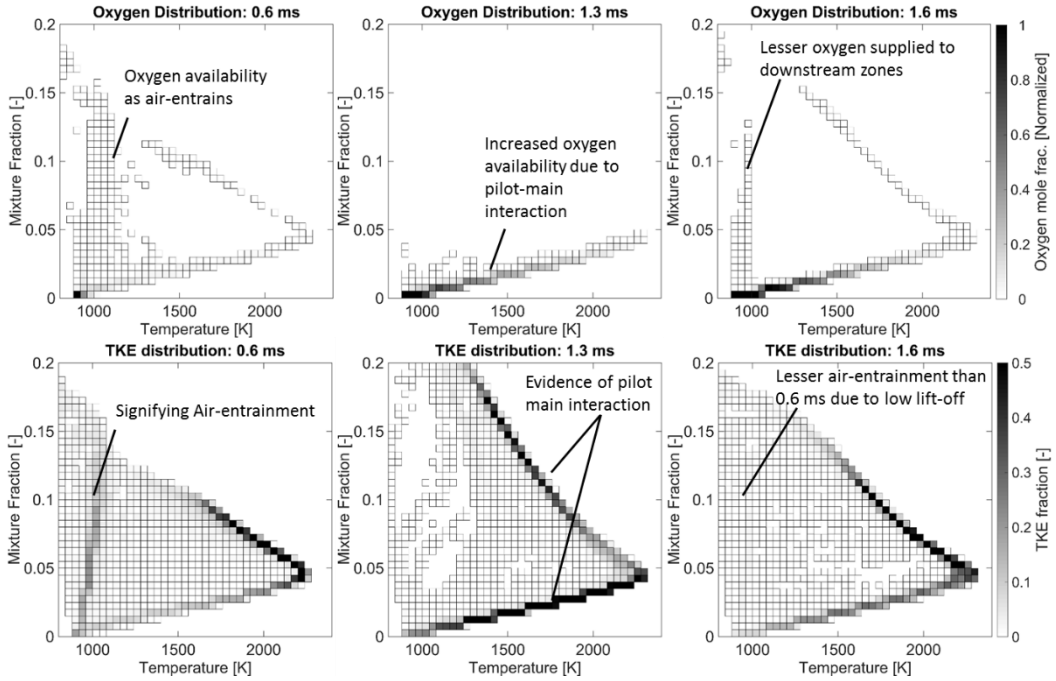

Figure 93: Z-T plot with oxygen and TKE fraction distribution

This effect is more evident at 1.3 ms in the TKE Z-T plot when the main starts interacting with the pilot soot cloud and where there is increased magnitude of TKE presence in the far-upper-right side and bottom side bins indicating the central region and the far outer region of the flame respectively. Lesser oxygen and TKE availability of the main flame (as in 1.6 ms) than the pilot flame (as in 0.6 ms) is observed due to the lower main flame lift-off than the pilot. Similar behavior of pilot-main soot formation and pilot soot oxidation are observed in the 800 K case too. However soot does not form in as rich regions as in the 900 K, but high temperature soot does burn in similar mixture fraction locations. Also, the peak soot mass recorded in the 800 K case, is almost 10 times lower than that recorded in the 900 K case.

Fig. 94 shows the Z-T soot mass fraction plot for the 800 K case. The Z-T plots shown below follows the same illustration as provided in Fig. 35. Similar behavior of soot formation and pilot soot oxidation are observed in the 800 K case too. However soot does not form in as

rich regions as in the 900 K, but high temperature soot does burn in similar mixture fraction locations. The normalize soot mass plotted here is normalized with the peak soot mass recorded in the 800 K case, which is almost 10 times lower than that recorded in the 900 K case. The reason for the low soot can be inferred form the oxygen and TKE Z-T plots in Fig. 95.

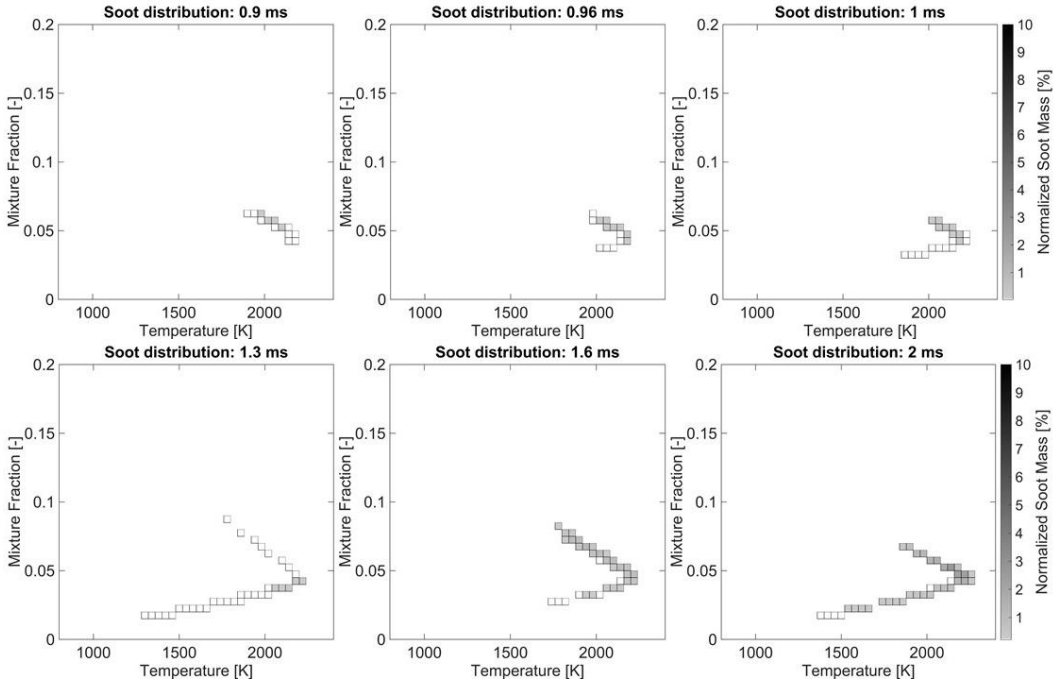

Figure 94: Mixture fraction-Temperature plot with soot mass fraction colored to explain ignition and flame characteristics of pilot and main

Fig. 95 shows the oxygen and TKE distribution for the 800 K case. Comparing with Fig. 93, there are stark differences in the oxygen and TKE distribution which is biased towards lower Z value in 800 K than 900 K case.

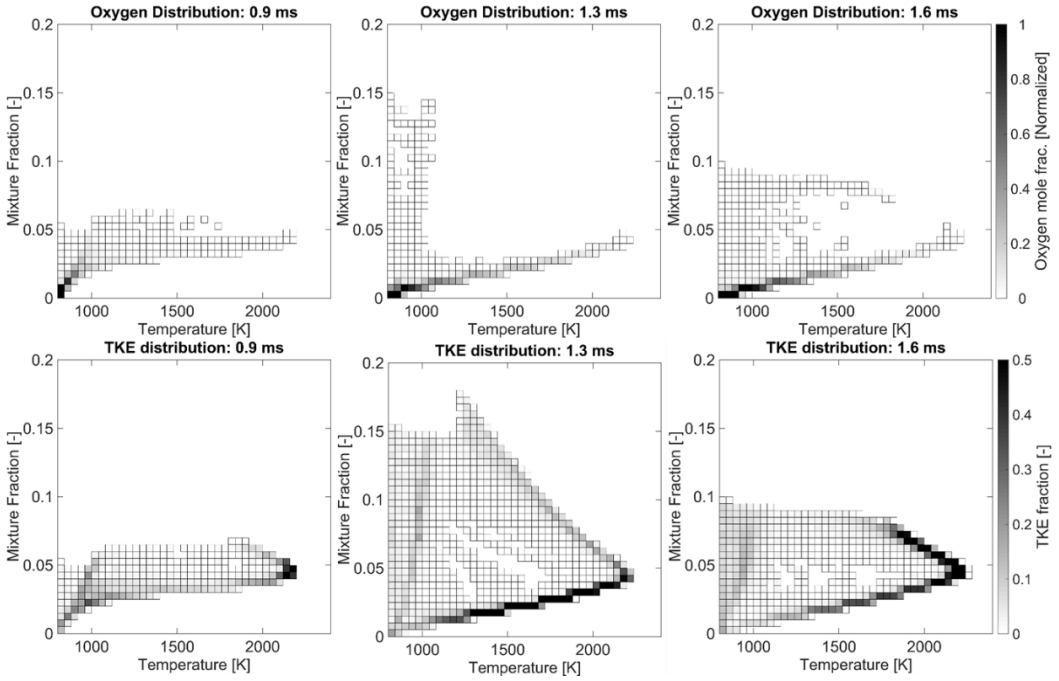

Figure 95: Mixture fraction-Temperature plot with oxygen volume fraction and TKE fraction colored to explain ignition and flame characteristics of pilot and main

Almost all the bins in the Z-T plot are filled with some level of oxygen and TKE. Generally comparing, 900 K case (Fig. 93) and 800 K (Fig. 95), it can be observed that higher chemical and fluidic activity occurs in the leaner regions for the 800 K than the 900 K case especially in the low temperature region indicated by the left-most bins. This is due to the higher lift-off for the main injection of the 800 K case than the 900 K case.

To summarize, using the Z-T plots, it was found that the main not only ignites richer and produces more soot quickly but also helps in oxidation of pilot soot by enhancing mixing. The higher soot content of the main was linked due to low air-entrainment by considering the low level of TKE and oxygen species entrained. The low entrainment has a causal link with the low lift-off, as has also been known experimentally [Siebers and Higgins 2001].
Effort is also made to study the soot production from individual injections. This is made possible in a simple way by having a scalar transport passive for each injections flow field. This scalar passive is effectively a 'tracer' species for each injections and mimics the mixture fraction space. By considering a suitable threshold for each injections tracer limit, a mixture

fraction-like space was prepared for each injections spatial spread. Then this space is chosen to visualize the soot present in the respective injections domain prepared previously. A multiplication of the binarized mixture fraction space so prepared with the soot spread, reveals the soot spaces for pilot, main and the common space of soot spread. This is used to generate an IXT plot. Integrations of soot for each injections are shown in the line plot in Fig. 96 along with the IXT contours. As seen in the Fig. 96, the experimental plot is shown to the left-most side with 900 K case in the top and 800 K case in the bottom. The 900 K case shows clear pilot and main soot islands where as the 800 K case shows a single island.

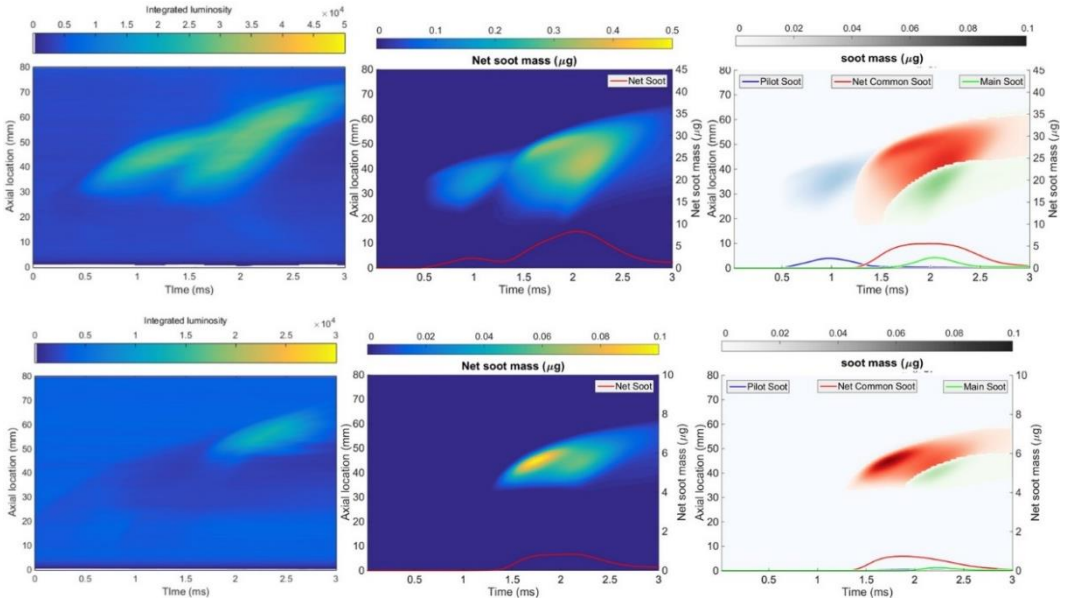

Figure 96: Soot decomposition using mixture fraction fields of respective injections. Line plots indicate net soot mass. Experimental conoturs (left -most top 900 K and bottom 800 K) are from natural luminosity (with schlieren) imaging, CFD soot contours (middle top 900 K and bottom 800 K) are from net soot plotting. Right-most top 900 K and bptthm 800 K plots are after applying a 'filter' of respective injection's mixture fraction fields; a commong soot area is the dominant one

Later in the CFD analysis, it is revealed to be predominantly a common soot production between pilot and main injections. To the center of the Fig. 96, there is net soot plotted from CFD which is later discretized in to pilot-common-main soot regions in the right-most

set of plots (900 K on top and 800 K on bottom). Although, this spatial technique of soot production is very general since it does not resolve the common region of soot production (which is a critical area of research), it is simple to implement and results in at least knowing the pilot-main only regions. It is seen that for the 900 K, there is almost equal amount of soot produced from individual injections. The common contribution from both the injections is the major portion of the soot spread. For the 800 K case, this is also true, except that the pilot and main only portions are not equal anymore, since not much soot is produced during the pilot combustion.

3.21 Concluding remarks

A split injection scheme with two 0.5-ms injections separated by a 0.5-ms dwell was adopted with n-Dodecane as fuel. Combustion experiments in a 15% O_2, 22.8 kg/m^3 ambient were performed at 900 K and 800 K ambient temperatures. Experimental investigation consisted of schlieren imaging to record the flame luminosity along with the flame boundaries and using the PLIF to measure the formaldehyde and PAH signal. It has been observed that the ambient of the main injection for the 900 K case consists of high temperature species from the combustion recessed pilot whereas for the 800 K case the ambient consists of reactive radicals from mild pilot combustion. Also shorter ignition delay and lift-off were also observed in both these ambient cases. The reactive species present in the local ambient prior to the main injection accelerate its ignition while high temperature in the main ambient accelerates fuel conversion. Integrated intensity plots (names IXT plots) provided a convenient way to gauge the qualitative soot trends in the cases tested.

To investigate the ignition and flame lift-off mechanisms, 3D CFD detailed chemistry RANS simulations were employed with a well-mixed combustion model and with reduced chemistry employed in every CFD cell. IXT plots revealed important temporal and spatial (along spray axis) information of the CFD output parameters of soot, temperature, scalar dissipation rate, OH, HO_2 and CH_2O specie fields. Many theories and interpretations from previous literature have been put to use to explain the flame stabilization mechanism as premixed flame controlled in the main flame.

- In one attempt, hydroperxyl (HO_2) and hydroxyl (OH) radicals are taken as an indicator species to understand the ignition and lift-off mechanisms. The main flame was observed to follow a premixed flame propagation mechanism since a near simultaneous formation of HO_2 and OH was seen during ignition and lift-off times.
- Ignition and flame stabilization of main flame occurs in a much higher scalar dissipation rate (χ_{st}) field (than pilot flame) for the 900 K case supporting premixed flame propagation mechanism. This ignition χ was found to be lower for the 800 K case due to its dependence on the ambient temperature fields
- A high heat release rate generating from the premixing zone for the main flame further supported the premixed flame propagation stabilized flame base. The non-flat and converging shape of the main flame base may be the reason to support this behavior. The pilot flame showed distinct two-stage auto-ignition stabilized flame base per heat release visualization.

That said, re-ignition kernels generating in the flame base of a higher ambient gas temperature single injection flame with similar lift-off length as of the main flame shows strong signs of auto-ignition stabilization mechanism as seen in prior works of Pickett et al.[Pickett, Kook, Persson, et al. 2009] and Pei et al.[Pei 2013] Besides the mechanism discussion, the unique flame stabilization event of the main flame closer to the nozzle orifice might as well be a temporary event. The main flame stabilization was observed to be temporary in a different but relatable work by Pickett et al.[Pickett, Kook, Persson, et al. 2009] and pointed out previously by Skeen et al.[Skeen et al. 2015b] for split injection spray combustion event. Supporting theories of main flame stabilization to be a temporary event were put-forth in this work based on residence time criteria arising from Picket et al. [Pickett et al. 2005] and a vortex stabilization theory of Broadwell et al.[Broadwell et al. 1985]

These ignition and stabilization mechanisms of second injection predominantly effect the net soot production processes. Numerical investigation of soot production was performed. Mixture fraction (Z) - temperature (T) plots were employed by discretizing the Z-T space of the spray-flame processes and correlating it with actual locations of the flame. Z-T plots were binned and filled with the average target quantities of interests viz., soot mass (normalized), oxygen fraction, turbulent kinetic energy (TKE) fraction.

- The low lift-off in main flame is responsible for its quicker and higher soot formation occurring in rich regions, due to low air entrainment leading to rich ignition of the combustible mixture.
- Z-T space analysis also revealed a mechanism of mixing enhancement of pilot soot promoted by the main flame. It was found that, during the mutual turbulent interaction of the constituting injections, the main flame causes soot oxidation of the pilot soot (at both the ambient temperature cases) by availing more oxygen to the pilot soot region.

CHAPTER 14

LARGE-EDDY SIMULATIONS[6]

3.22 Background

The present study is a follow-up of a series of studies as in Refs. [Cung et al. 2015, Moiz et al. 2015] in which extensive experimental and computational fluid dynamics (CFD) studies were performed to understand the ignition and sooting characteristics of split injections. As part of the experimental campaign, a PLIF technique is used along with application of schlieren imaging technique, combined with natural luminosity imaging in a nearly simultaneous fashion, to reveal the ignition and soot characteristics of the main injection. A Large Eddy Simulation (LES) based turbulence modelling approach was employed as explained later in chapter 3.2. The paper presents the experimental and numerical setups to begin with, followed by experimental results at 800 K and 900 K ambient cases. This is followed by CFD validation section of 900 K ambient case using LES model, after which a dwell time variation case of 0.65 ms is investigated for reduced net soot production. Performing a dwell time variation with a well-validated LES approach enables us to provide some insights into the soot production process with split injections. An ambient of 15% oxygen in the chamber was used. This is the post-burn composition of hydrocarbon mixture which signifies the usage of exhaust gas re-circulation (EGR) in a diesel engine. EGR usage causes a net molar reduction of oxygen level (from a natural ambient of 21% oxygen) in the combustion chamber. The other ambient conditions of 22.8 kg/m^3 ambient density and 800 K, 900 K of ambient temperatures are typical ambient conditions of a light-duty diesel engine at the time of fuel injection.

As part of experimental optical diagnostics, simultaneous acquisition of schlieren and PLIF imaging was performed as shown in Fig. 28. The pressure trace from the CV was also recorded. A single-hole solenoid injector (Injector# 375020) from the Engine Combustion Network (ECN) [Pickett et al. 2014b] community was used to create split injections using a

[6] "The material contained in this chapter was previously published in *Combustion & Flame*
Moiz, Ahmed Abdul, Muhsin M. Ameen, Seong-Young Lee, and Sibendu Som. 2016. "Study of soot production for double injections of n-dodecane in CI engine-like conditions." *Combustion and Flame* 173: 123-131.

MOSFET driver. The rate of injection (ROI) was experimentally determined using spray momentum flux measurements [Johnson et al. 2010]. As can be seen in Fig. 97, the rate of injection profile, shows a 0.3 ms injection of pilot spray, a 0.5 ms of dwell time and a 1.2 ms injection of main spray, giving it the nomenclature of 0.3/0.5/1.2 ms. The measured ROI profile has noise arising from experimental artifacts. To avoid this noise to bleed into the CFD simulations, a standardized rate of injection (ROI) profile from CMT-Motores Térmicos was used as the CFD input, as seen in Fig. 97.

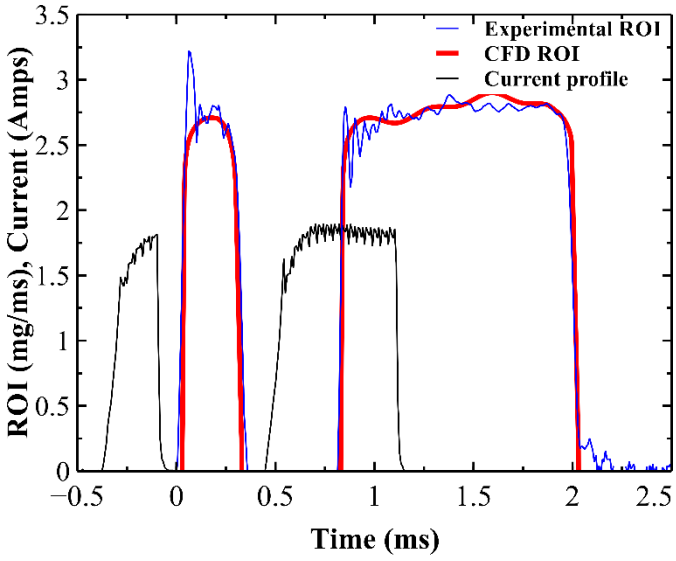

Figure 97: Rate of injection measured, used for CFD and the corresponding current profiles

In this work, LES was performed through a Lagrangian-parcel, Eulerian-fluid approach using the CFD software CONVERGE [Richards et al. 2012]. A base grid size of 1 mm is used along with local embedding of 62.5 µm in the form of a cylinder with diameter of 4 mm and height of 5 mm near the nozzle. Adaptive mesh refinement (AMR) is also used and gets activated whenever the sub-grid velocity gradient is higher than 0.1 m/s or the sub-grid temperature gradient exceeds 2.5 K. This setup leads to a 62.5 µm grid in the entire spray and flame region with grid-convergent results [Pei, Som, Pomraning, et al. 2015]. The dispersed phase is modeled using the traditional Lagrangian-parcel method. More details about the spray models employed in this study are discussed in detail in Refs. [Pei, Som, Kundu, et al. 2015,

Pei, Som, Pomraning, et al. 2015] and hence the governing equations are not discussed here for the sake of brevity.

A well-mixed turbulent combustion model is employed. The chemical kinetics are modeled using a 54-species, 269-reaction mechanisms for n-Dodecane [Yao et al. 2015]. The present work uses a Hiroyasu model [Hiroyasu and Kadota 1976] to simulate soot formation and Nagel Strickland-Constable (NSC) model [Nagle and Strickland-Constable 1962] to simulate soot oxidation which is explained in chapter 5.

The effect of the sub-grid fluctuations are incorporated using the well-validated one-equation dynamic structure sub-grid scale (SGS) model [Pomraning and Rutland 2002]. This computational setup has been employed in previous studies Refs. [Pei, Som, Kundu, et al. 2015, Pei, Som, Pomraning, et al. 2015] for LES of a single injection of n-Dodecane and it was shown that the model is able to predict ignition delay, lift-off length and soot contours accurately. A total cell count of 22 million was observed at 2 ms after start of injection (ASOI) time for the 0.3/0.5/1.2 ms case. Until 2 ms ASOI, the 0.3/0.5/1.2 ms case consumed ~48,000 core hours with ~20 days of wall-clock time. It is to be noted that, LES results in this study are based on a single realization and accurate *quantitative results* can only be obtained by performing multiple realizations. However, a single LES realization can provide valuable *qualitative description* of the flame development as noted in author's previous studies [Pei, Som, Kundu, et al. 2015, Pei, Som, Pomraning, et al. 2015, Xue et al. 2013].

3.23 Results and discussion

Table 10 shows the ignition delays from the experimental cases of 900 K and 800 K ambient gas temperatures and the 900 K CFD case for two dwell time variations.

Table 10: Ignition delay measurements from experiments and CFD

Experiment	**Pilot ignition delay**	**Main ignition delay**
900K: (0.3/0.5/1.2 ms)	0.27 $\pm$ 0.01 ms	0.16 $\pm$ 0.02 ms
800K: (0.3/0.5/1.2 ms)	0.58 $\pm$ 0.06 ms	0.21 $\pm$ 0.04 ms
CFD	**Pilot ignition delay**	**Main ignition delay**
900K: (0.3/0.5/1.2 ms)	0.26 ms	0.14 ms
900K: (0.3/0.65/1.2 ms)	0.26 ms	0.165 ms

The 900 K CFD case was extensively validated against the experiments which will be discussed later. The ignition delay of the first injection is calculated from the pressure trace corresponding to the first increase of pressure by 0.024 bar. However for the second injection, ignition delay was calculated after the start of main injection (ASMI) where the apparent heat release rate increases by 20% from the value at the minimum near the main injection timing following Skeen et al. [Skeen et al. 2015b] recommendation. More than two-fold increase in ignition delay is observed for the pilot injection going from 900 K to 800 K ambient. The ignition delay for the second injection is almost half of the pilot injection for the cases shown in Table 9.

As shown in Fig. 30 in the PLIF experimental setup section (chapter 6.4.3), the raw simultaneous imaging of PLIF and schlieren acquired in a nearly simultaneous fashion. The HS schlieren with natural luminosity image is acquired with a 600 nm short pass filter on the high-speed camera. The 600 nm short pass filter enabled the visualization of only the high temperature soot species along with other minor species which emit in the wavelengths lower than 600 nm. The images comprising formaldehyde PLIF in Fig. 30 are not from the same injection event since the ICCD camera can only capture a single shot. Separate injection and pre-burn event were needed to obtain each ICCD image to realize 3 repeats for the same test condition. The mean image of the 3 repeats is used for presenting results here. While one ICCD image was being taken, a high-speed (HS) schlieren movie was recorded for the whole injection-spray-combustion event. The HS schlieren image shown on the right has been extracted from one of the three repeats for the corresponding ICCD

PLIF shot. These are called simultaneous since at least one (out of the 3 repeats) ICCD image lies in the same injection cycle to one schlieren image. The liquid length section is shown covered by a shaded region in Fig. 30. The spray combustion event does not vary drastically from run to run, the repeatability being fairly good. The penetration of the downstream hot flame and upstream cool flame, and the overall shape of the PAH in jet head and CH_2O in the upstream near region looks very similar between the 3 repeats. This was seen in other test results too. Hence, only 3 repeats were performed in the experiment to maintain minimum statistics. Slight liquid scatter is observed in the PLIF shots near the nozzle during the liquid injection durations as can be seen within the masked zone, signifying liquid length extent in the PLIF images of Fig. 30. Although this very weak fluorescence signal was observed near the nozzle from liquid fluorescence, the downstream target measurement (after the masked zone) is not mixed with this signal, as seen in the Fig. 30 and so is unambiguous in deciding that downstream signal was a formaldehyde (PAH) signal and not a fuel liquid scatter.

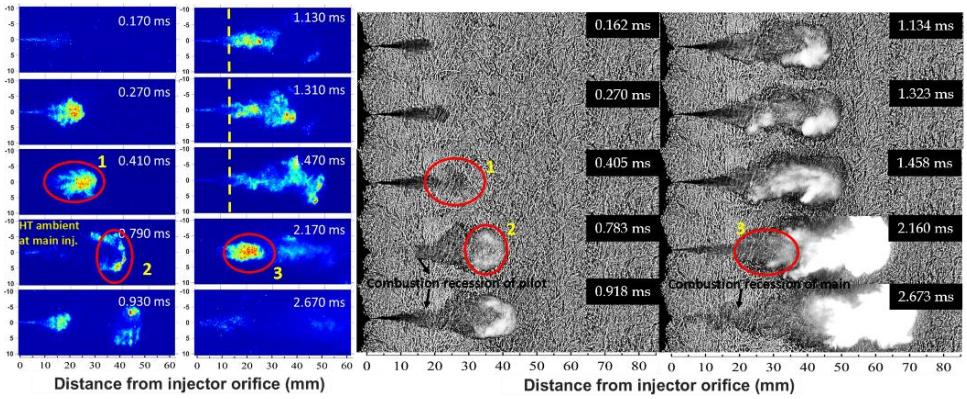

Figure 98: Simultaneous PLIF (left) and Schlieren (right) of the 0.3/0.5/1.2 ms injection at 900 K ambient. Dashed (yellow) line indicated the main lift-off length, circles (red) indicate marked events as described in figure discussion, arrows (black) show combustion recession event

Fig. 98 shows the schlieren-PLIF imaging for 900 K ambient case using 0.3/0.5/1.2 ms injection strategy. A dashed line in the top-right PLIF image sets indicate the quasi-steady lift-off. Points of interest have been marked in Fig. 98 with circles. Point 1 corresponds to

schlieren softening (right image set), which indicates large-scale organization of vaporized fuel mass, possibly with similar equivalence ratios and fluid temperatures, ready to undergo a first stage ignition.

This first stage ignition is visualized as a formaldehyde signal (left image set). Point 2 shows luminosity occurrence in the right image set which constitutes of soot matter as well as its precursor species (PAH) as seen from the left image set. This is one of the advantages of the PLIF technique for formaldehyde detection since the signal detection wavelength of PAH lies close to that of formaldehyde [Harrington and Smyth 1993], which enables visualization of both these species simultaneously. Usually, PAH is formed at a different spatial location than formaldehyde, which makes the PLIF technique useful to detect the formaldehyde presence and to differentiate it from the PAH signal, as in this case. From the time instants of ~0.79 ms and ~0.9 ms (from both HS and ICCD images), one can visualize the ambient conditions in which the main injection enters the combustion chamber, as further explained here. A combustion recession event [Knox and Genzale 2015b] of the pilot is happening with no evidence of reactive radicals (signified by formaldehyde presence) in the immediate ambient of the main injection. Combustion recession is an end of injection transient phenomena where shortly after the end of injection, under high-temperature ambient combustion conditions, the recently prevalent lifted flame seemingly propagates back towards the injector. This is due to the generation of auto-ignition spots upstream at end of injection times. Thus, combustion recessing is a series of high temperature ignition events, which occur upstream thus consuming the low-medium temperature reactive species (signified by formaldehyde). The presence of local high temperature due to combustion recession existing near the main liquid fuel injection leads to earlier ignition in a fuel-rich manner, leading to more PAH and soot formation downstream. Point 3 signifies the after end of injection times where combustion recession [Knox and Genzale 2015b] starts to occur for the main injection. As this happens, the left over upstream low and medium temperature main reactive species (with low axial velocities) experience an immediate increase in their production and are soon exhausted as temperature rises with high temperature chemical reactions occurring. Thus, a higher level of formaldehyde trace is seen upstream in the region marked as point 3 (left image set) which gets consumed in later time instants.

Fig. 99 shows simultaneous schlieren-PLIF imaging at 800 K ambient. Point 1 here shows the development of first-stage ignition kernels in the form of a cool flame signified by formaldehyde presence from the formaldehyde PLIF. These first stage ignition kernels travel downstream and later auto-ignite (as point 2) producing high temperature combustion species (CO, OH etc.).

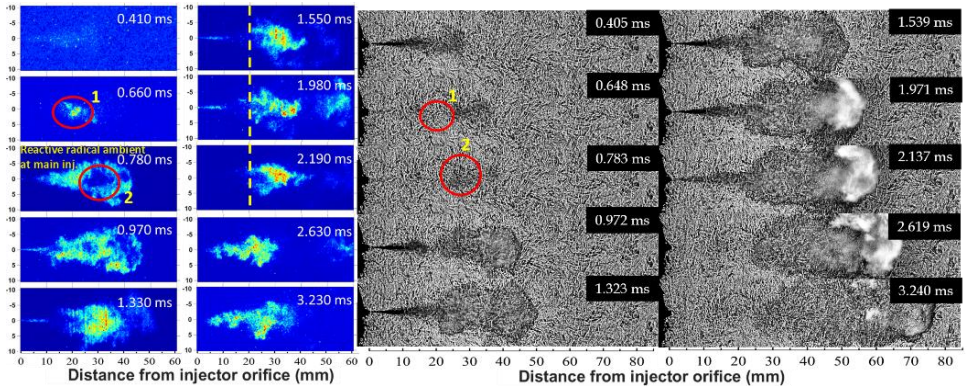

Figure 99: Simultaneous PLIF (left) schlieren (right) of the 0.3/0.5/1.2 ms injection at 800 K ambient. Dashed (yellow) line indicates main lift-off length, circles (red) indicate marked events as described in figure discussion

From the time instants of ~0.78 ms and ~0.97 ms (both from HS and ICCD), one can visualize the ambient in which the main injection enters the combustion chamber. A spatial presence of low temperature reactive radicals (signified by formaldehyde presence) lies in the immediate vicinity of the main injection, unlike the high temperature ambient for the main injection for the 900 K ambient case (cf. Fig. 98). Skeen et al. [Skeen et al. 2015b] performed closed homogenous reactor simulations which took inputs such as local equivalence ratios from a one-dimensional jet model to investigate the effect of high-temperature and reactive radicals on main ignition. They concluded that both the temperature and reactive radicals can have effects on reducing the main ignition delays in almost similar magnitudes. Thus the reduction in ignition delays of main by almost a factor of two over pilot are imminent (cf. Table 9). This promotes the PAH and soot formation due to the nature of fuel rich ignition. The dashed line in the top-right PLIF image set in Fig. 99 shows the lift-off location. It can be

observed that the quasi-steady lift-off location in the 800 K ambient case is further away from the nozzle (21 mm) when compared to the 900 K case (13 mm).

From Table 10, it is observed that the ignition delays for the 900 K case for both injections are lower than the 800 K case. The associated quasi-steady lift-off length behavior with the ignition delay trend as seen in both the cases is expected from previous well established studies [Pickett et al. 2005] that were primarily for single injection sprays, but can be extended to split injection sprays. It was also found for a single injection diesel spray that the total amount of air entrained upstream of the lift-off length increases due to an increase in lift-off length with decreasing ambient gas temperatures [Siebers and Higgins 2001]. Using empirical laws derived from multiple datasets, Siebers [Siebers and Higgins 2001] concluded that higher lift-off lengths cause higher air entrainment, which leads to a leaner central reaction zone at near-downstream locations of the lift-off length. Leaner conditions cause less soot formation (as seen in the 800 K case of Fig. 100). This theory will be put to use in the upcoming CFD discussion section.

Temporal and spatial flame luminosity was calculated by integrating flame luminosity at each axial location for each frame of a natural luminosity acquired image as in Fig. 100. This is named as an IXT (Intensity-aXial-Time) plot defined mathematically as in Eq. 12.

$$IXT(x,t) = \int_{-R}^{R} I(x,r,t)dr \tag{12}$$

where x is the intensity axial direction, r is the radial direction, and R is intensity boundary width. Aspects such as lift-off length, flame height, and some aspects of internal flame structure can be studied by the *IXT* contours. IXT plot has been employed in the previous study by the authors [Cung et al. 2015] to explore the flame luminosity profile of various split injection sequences. Also plotted in Fig. 100 are the apparent heat release rate (AHRR) profiles for the same cases.

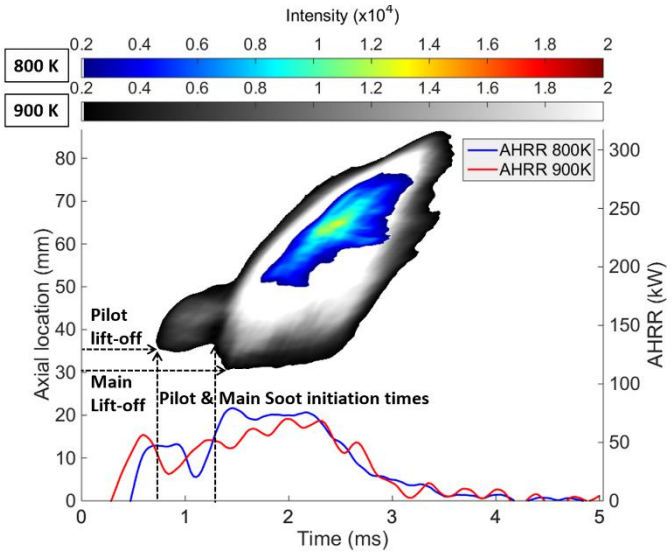

Figure 100: *IXT* plot, apparent heat release rate of the 0.3/0.5/1.2 ms injection at 900 K and 800 K cases

The CV pressure trace is used to determine the AHRR from the combustion event. The AHRR profiles are a mean of 3 tests for each condition. The relationship used in the AHRR calculated is provided by the Eq. 2.

$$\frac{dQ}{dt} = \frac{\gamma}{\gamma-1} P \frac{dV}{dt} + \frac{1}{\gamma-1} V \frac{dP}{dt} = \frac{1}{\gamma-1} V \frac{dP}{dt} \tag{13}$$

where P is chamber pressure, V is the combustion vessel volume (1.1L), and γ is specific heat ratio (1.35). The combustion efficiencies calculated for both the 900 K and 800 K injection cases come close to 92% although major qualitative differences in the soot production are observed in Fig. 100, where the 900 K case (shown in gray scale) has a higher level of soot production than the 800 K case (shown in RGB scale). Additionally, in the 800 K case, the pilot does not exhibit any soot luminosity, and becomes evident only during the end of main spray injection times. Also, the fact that the main injection stabilizes at a lesser lift-off length than the pilot injection is observed in Fig. 100 for the 900 K case.

3.23.1 CFD validation and simulation with varying dwell times

The effect of changing the dwell time was investigated using a well validated CFD simulation against the 900 K case of a 0.3/0.5/1.2 ms injection. The validation process consisted of considering both the non-reacting and reacting spray parameters which include vapor penetration (of both the injections), heat release and qualitative soot presence. Simulations for the reacting cases were performed until end of injection times.

Fig. 101 shows the non-reacting vapor penetration which was performed to validate the vaporizing spray before setting up a reacting case. LES calculations can predict the vapor penetration very well for both the injections.

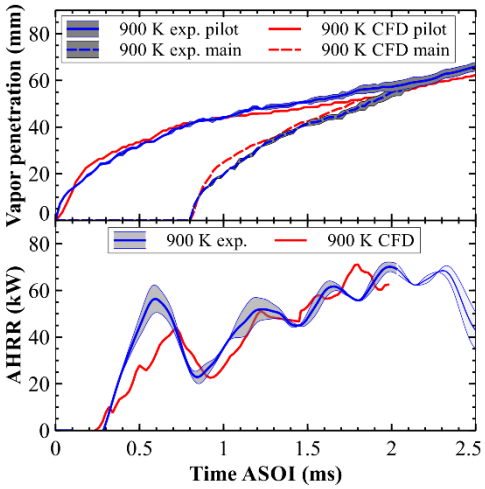

Figure 101: Non-reacting vapor penetration and (reacting) apparent heat release rate for the 900 K case

This is consistent with authors' previous findings for single injection simulations with LES [Xue et al. 2013]. It can be noted from experiments that the main injection travels faster than the pilot injection, since the slope of the second injection is higher than the first injection. This was termed as 'slip stream' effect [Skeen et al. 2015b], since the main injection is now traveling in a spray cooled field of higher density created by the pilot injection and hence slips through it quicker than it would in a lower density hot gas. The simulation captures this phenomenon very well. At the bottom of Fig. 101, the AHRR profiles

are shown. The CFD heat release plotted here is not the chemical heat release but the pressure-derived (apparent) heat release, as done in the experiments. The plots show overall good agreement between simulations and experiments.

Fig. 102 shows a comparison of line-of-sight integrated IXT plot for natural luminosity imaging with a similarly plotted soot plot from CFD.

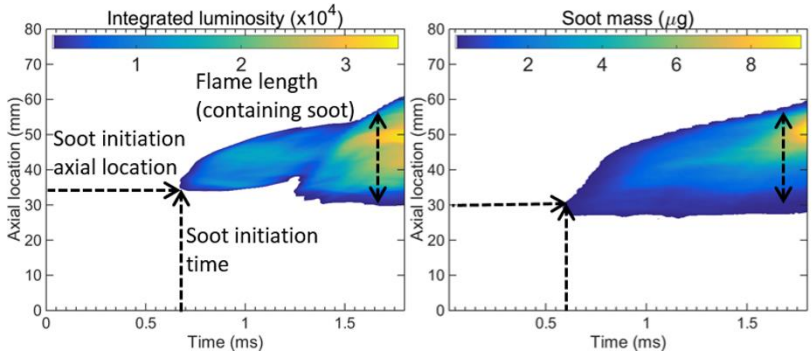

Figure 102: Integrated luminosity from experiment (left) and soot from CFD (right) for the 900 K case

For the CFD soot mass spread, the soot mass along the line-of-sight has been integrated and projected on a plane. This which was considered for transverse integration operations along the axial length for the various time steps leading to the plot in Fig. 102 (right). Luminosity visualization with a 600 nm short pass filter does not directly correlate to soot particle measurements as in a laser incandescence measurement, but is a good indication of high temperature or high concentration soot. Fig. 102 depicts that it is a good estimate for qualitative indication of soot presence. The start of soot production (along X-axis) and the flame lengths containing soot (along Y-axis) are very well matched between CFD and experiment.

Simulation of a split injection spray-combustion event has been a challenge within the spray-flame community and was an issue of interest in the ECN 4 workshop as well [Pickett et al. 2014a]. In view of this, involving high fidelity LES calculations with a detailed chemistry well-mixed combustion model is believed to be a good approach. Using this well validated CFD simulation, a variation in dwell time was performed. The dwell time was increased from 0.5

ms to 0.65 ms at 900 K ambient gas temperature, with the injection durations being the same. The ignition delay of the main injection in this case was 0.165 ms which is 0.025 ms longer than the 0.3/0.5/1.2 ms main injection (ignition delay: 0.14 ms). The lift-off lengths for the main injection for both dwell time variations were calculated from the 14% OH magnitude, at the farthest upstream position of its presence [Pei, Hawkes, et al. 2015] to account for similarity with experiments. These were calculated as 22.4 mm for the 0.3/0.5/1.2 ms case and 24.6 mm for the 0.3/0.65/1.2 ms case for their respective main injections. Although the simulation shows higher lift-off length, the simulation set-up correctly predicts the change in lift-off lengths with changing ambient conditions [Pei, Som, Pomraning, et al. 2015]. Hence, the conclusions derived from LES are expected to hold good in spite of the differences in predicted lift-off lengths.

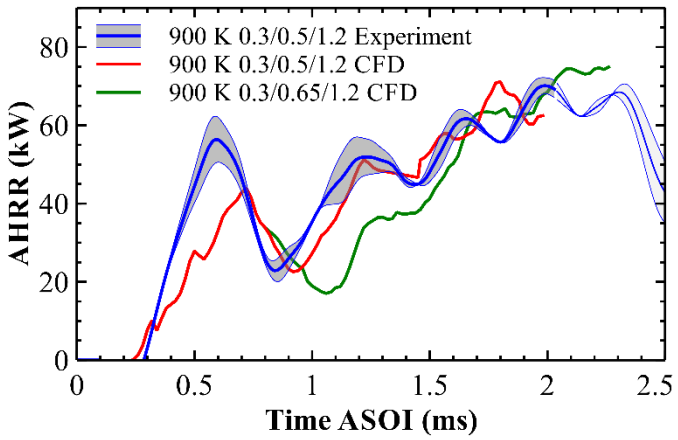

Figure 103: Heat release rate from the experiment and CFD for the 0.3/0.5/1.2 ms case along with CFD results for the 0.3/0.65/1.2 ms, 900 K case

Fig. 103 shows the heat release rate of the various 900 K cases investigated. It can be observed that as the dwell time is increased (by 0.15 ms) in the simulations, there is a delay in the start of heat release from the second injection. The difference in the behavior of heat release rate begins at 0.8 ms ASOI, until when both the dwell time cases have identical heat release. It is seen that the pilot injection still has the potential of releasing heat after 0.8 ms which was rather quenched by the oncoming main injection for the 0.3/0.5/1.2 ms case. Thus, as the dwell time is increased by 0.15 ms, the heat release rate during the dwell time

is seen to be marginally higher for the 0.3/0.65/1.2 ms case. At the same time the 0.3/0.65/1.2 ms case takes longer to achieve the eventual rise in heat release rate from the second injection which now occurs at ~1.1 ms ASOI, in contrast to ~0.9 ms ASOI for the 0.3/0.5/1.2 ms case. This change in behavior of heat release rate from the second injection due to the variation in dwell time, effects the spray-flame in general, and main soot formation characteristics in particular.

The upcoming analysis deals with investigating how changes in the dwell-time affects the soot formation on a *qualitative* sense. Multiple LES realizations are needed for *quantitative* comparisons with experiments. In previous work done by Pei. et al. [Pei, Som, Pomraning, et al. 2015], it was found that that ignition delay is fairly repeatable from realization to realization, whereas there can be up to 5 mm variation in lift-off length from one realization to the next for a single injection case at similar experimental conditions with n-Dodecane as fuel. However, this study is geared more towards getting a qualitative sense of soot dependence when the dwell time is changed. Hence, at many places qualitative terms like 'percentage change' are used rather than absolute measurable quantities.

Fig. 104 (top) shows a schematic for calculation of air entrainment rate. A cell flowrate-weighted radial mean value of the equivalence ratio enclosed in a region bounded by 0.1% mixture fraction surface was obtained at the lift-off location. An inverse of such equivalence ratio was estimated as an air entrainment quantity, following Siebers and Higgins [Siebers and Higgins 2001]. Azimov and Kim [Azimov and Kim 2011] have performed air-entrainment estimate following a different approach involving direct mass measurements of air and fuel entrainments from their LES calculations. They had very close air-entrainment estimates as Siebers and Higgins [Siebers and Higgins 2001], which is used in the present study.

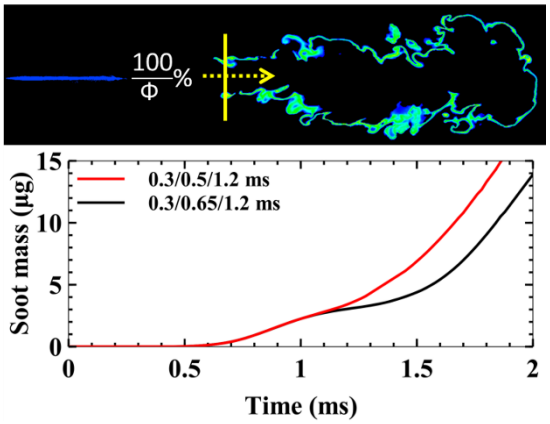

Figure 104: (top) Illustrative image of OH species with liquid injection to illustrate the calculation of air entrainment percentage as $\frac{100}{\Phi}$% at the lift-off location marked as solid yellow line. (bottom) Soot production trends for both the dwell time cases

For the quasi-steady main flame lift-off times for 0.3/0.5/1.2 ms case, an air-entrainment of 72.6% was obtained whereas the 0.3/0.65/1.2 case yielded 81.9% air-entrainment rate. The 12.8% increase in the air-entrainment of 0.3/0.65/1.2 ms case over 0.3/0.5/1.2 ms case is due to the lift-off length of the former main flame being 2.2 mm longer that of the latter. The increased air entrainment may also arise from a higher radial expansion of the wider main flame observed for 0.3/0.65/1.2 ms case (not shown here), which creates a stronger entrainment current near the lift-off base location. This is one of the theories supporting an air-entrainment concept by Rhim and Farrell [Rhim and Farrell 2000], who suggested that a significant part of the overall ambient gas is entrained from the downstream spray region. Thus, with more air entrainment, fuel leaning of the fuel-air mixture for the 0.3/0.65/1.2 ms case causes lower soot production as shown in Fig. 104 (bottom) where the solid lines show the soot mass. At end of the respective main injection times for the both the dwell time cases, the net soot production was calculated to be ~14.2% lesser for 0.3/0.65/1.2 ms case over 0.3/0.5/1.2 ms case. A similar trend of reduction in soot production rates with increasing dwell times was observed by Hasse with a turbulence-chemistry interaction combustion model [9]. Thus, it can be said that a higher level of air entrainment causes slightly leaner combustion of the main spray for the 0.3/0.65/1.2 ms injection case than the 0.3/0.5/1.2 ms injection case, resulting in lesser soot production. The mechanism for air-

entrainment for a split injection flame is expected to be a symbiotic relationship between the interaction levels of both the injections and the correspond lift-off lengths for the varying dwell time cases.

3.24 Concluding remarks

Analysis of soot production trends for split injections of n-Dodecane fuel in a controlled environment of constant volume combustion vessel was performed. Experiments done with 0.3/0.5/1.2 ms split injection scheme show the benefit of using a split injection to get higher combustion efficiency, while keeping soot in low-limits when the ambient gas temperature is reduced from 900 K to 800 K. A reduction in ignition delay of the main injection by almost a factor of two over pilot was observed for both the 900 K and 800 K ambient conditions. Ignition and stabilization of the main spray-flame closer to the liquid injection (fuel rich zone) was observed which results in its higher PAH and soot formation downstream. For 900 K condition, the reduction in main ignition delay is believed be due to the high temperature combustion recession event in which the main injection is injected. For the 800 K case, the reduced ignition delay is believed to be due to the local presence of pilot generated low temperature reactive species signified by the formaldehyde presence. Simulation of a 900 K ambient gas temperature 0.3/0.5/1.2 ms injection was performed using a LES framework and extensively validated to simulate important split injection related mechanisms of slip-stream effect in non-reacting environments along with reduced main ignition delays, lift-off lengths and the general soot spread in reacting ambients. A slight increase in dwell time from 0.5 ms to 0.65 ms revealed a 14.2% decrease in soot production. A 12.8% increase in air-entrainment for the 0.3/0.65/1.2 ms case was found to predominantly cause lower soot production. The increased air entrainment is due to an increased lift-off length along with stronger entrainment current generated near the lift-off base location from a higher radial expansion of the 0.3/0.65/1.2 ms main flame.

CHAPTER 15

CONCLUSIONS AND FUTURE WORK

Low temperature combustion is the path forward for efficient engines. Single injection diesel sprays have been well documented for majority of the novel combustion regimes. Although advanced injection strategies, like split injections, have yet to be understood. This study, focuses on understanding the ignition, flame stabilization and soot production characteristics of the main injection in various split injection schedules under various ambient conditions. A state-of-the-art constant volume combustion vessel allowing for optical access permitting the usage of high end laser diagnostics was utilized. Both non-reacting and reacting sprays were investigated. A range of experimental techniques like Mie scattering, schlieren, natural luminosity, OH* chemiluminescence and planar laser induced fluorescence were used, often simultaneously. Computation fluid dynamic simulations free from Lagrangian particle, grid selection and combustion model artifacts were setup. Low fidelity RANS and high fidelity LES were performed to assist the observations from experiments. Some of the conclusion which can be derived from the present work can be summarizes as follows.

- For non-reacting cases, main vapor penetration was accelerated with a shorter dwell time, as main injection provides higher momentum to the pilot injection compared to longer dwell cases in both experimental and numerical results.
- Flame luminosity imaging of main combustion enabled characterization of the ignition processes and flame structure for each case of dwell time. It is possible to conceptually categorize the shape of the main flame depending on when it is injected.
- As dwell time increases, ignition delay of main flame increases, but the trends of LOL and ignition location are not well defined. Dwell time effects were also investigated from a combustion efficiency point of view and the possibility of having a thermodynamic sweet-spot was evaluated.

- Unique phenomenon like the slip-stream effect (when the second injection penetrates faster) and combustion recession (a spray flame ignites upstream at end of injection) were observed and documented.
- The observed accelerated ignition and lower flame stabilization of the second (main) flame are in contrast to the behaviors of the first (pilot) flame in a double split injection schedule.
- The reactive species like hydroxyl radicals and peroxide species present in the ambient of the main injection predominantly cause earlier main ignition. The higher temperature field induced by their presence cause faster main fuel liquid-to-vapor conversion.
- Unlike auto-ignition dominated events of the pilot spray-flame, the possibility of flame propagation being the dominant ignition and flame stabilization mechanism for the second injection was argued. Integrated plots (called IXT plots) were used to analyze the flame structure behavior with respect to scalar dissipation rate to arrive at such conclusions.
- It is known that the soot production is very much effected from the ignition and flame stabilization events. Thus, they were studied simultaneously to refrain from inaccurate conjectures. Investigation in mixture fraction and temperature space of pilot-main spray combustion revealed that, the lower lift-off of main results in lower air-entrainment which causes richer ignition of main resulting in quicker and higher soot formation. The effect of main injection in enhancing the oxidation of pilot soot by inducing enhanced mixing was also revealed.

Since ignition and flame stabilization have ever been discussed due to lack of experimental evidence, an experimental settings can be devised in the future to understand the underlying mechanisms. One such attempt was done by Pickett et al. [Pickett, Kook, Persson, et al. 2009]. Since actual usage of injectors is with multiple nozzles, considerations of performing experiments with multiple nozzle split injections should be made. Understanding soot production has been done with a natural luminosity imaging technique with spectral filters to narrow down to visualize the dominant soot radiation wavelengths. Experimenting with quantitative soot measurement techniques like laser induced

incandescence can be planned. Split injections are also majorly used to counter soot-NOx trade-off. NOx measurement technique can be implemented in the constant volume combustion vessel with either optical or exhaust gas analysis methods to further delve into proper setting up of split injection schedules. During the course of experimentation, low temperature combustion was the major driving force, but it was observed that as the ambient temperature is set to lower values ($\leq$ 750 K), the repeatability of tests is significantly affected. This seems to be a common issue with pre-burn type combustion vessels and can be considered to be tackled in future work for accurate testing of LTC regimes and at the same time helping the modeling community to model the various phenomenon.

APPENDIX

3.25 Permissions for copyright

Chapter 9

Elsevier Science and Technology Journals LICENSE
TERMS AND CONDITIONS

Aug 28, 2016

This is a License Agreement between Ahmed Abdul Moiz ("You") and Elsevier Science and Technology Journals ("Elsevier Science and Technology Journals") provided by Copyright Clearance Center ("CCC"). The license consists of your order details, the terms and conditions provided by Elsevier Science and Technology Journals, and the payment terms and conditions.

All payments must be made in full to CCC. For payment instructions, please see information listed at the bottom of this form.

License Number	3893050821060
License date	Jun 07, 2016
Licensed content publisher	Elsevier Science and Technology Journals
Licensed content title	PROCEEDINGS OF THE COMBUSTION INSTITUTE
Licensed content date	Jan 1, 2000
Type of Use	Thesis/Dissertation
Requestor type	Author of requested content
Format	Print, Electronic
Portion	chapter/article
Title or numeric reference of the portion(s)	All of content
Title of the article or chapter the portion is from	Spray–combustion interaction mechanism of multiple-injection under diesel engine conditions
Editor of portion(s)	Volker Sick
Author of portion(s)	Khanh Cung
Volume of serial or monograph.	35
Issue, if republishing an article from a serial	3
Page range of the portion	vol. 35, Issue 3, Pgs-3061-3068
Publication date of portion	23 August 2014
Rights for	Main product
Duration of use	Life of current edition
Creation of copies for the disabled	no
With minor editing privileges	no
For distribution to	Worldwide
In the following language(s)	Original language of publication
With incidental promotional use	no
The lifetime unit quantity of new product	Up to 999
Made available in the following markets	Education
Specified additional information	I am the second author of this publication and need to use it as is in my PhD dissertation
The requesting person/organization is:	Ahmed Abdul Moiz
Order reference number	
Author/Editor	Ahmed Abdul Moiz
The standard identifier of New Work	http://digitalcommons.mtu.edu/
The proposed price	Free
Title of New Work	Low temperature double injection diesel spray combustion: Ignition, flame stabilization and soot formation characteristics in engine-like conditions
Publisher of New Work	Michigan Technological University
Expected publication date	Sep 2016
Estimated size (pages)	200
Total (may include CCC user fee)	0.00 USD

Chapter 10

Michigan Tech **Ahmed Abdul Moiz <amoiz@mtu.edu>**

RE: Permission for using paper in PhD thesis / 2015-01-0374

Nikole Aston <nikole.aston@sae.org> Wed, Oct 12, 2016 at 10:23 AM
To: Ahmed Abdul Moiz <amoiz@mtu.edu>
Cc: Mandy May <Mandy.May@sae.org>

Dear Ahmed,

Please be advised, reproduction use of SAE Paper: 2015-01-0374, is hereby granted, and subject to the following terms and conditions:

-Permission is granted for non-exclusive English language rights, and for the specific use as indicated in your email;

-Permission is required for new requests, or for further use of the material;

-The SAE material must be clearly identified and include the following statement "Reprinted with Permission from SAE International";

-This permission does not cover any third-party copyrighted work which may appear in the material requested;

-Licensor's use of this material, in whole or in part, is entirely its responsibility, and SAE International does not warrant or is not responsible for any use of the material.

Thank you.

Best,

Nikole Aston

IP Compliance Specialist

Michigan Tech

Ahmed Abdul Moiz <amoiz@mtu.edu>

Copyright permission

Combustion Office <office@combustioninstitute.org>

Fri, Oct 14, 2016 at 1:02 PM

To: Ahmed Abdul Moiz <amoiz@mtu.edu>

Hello Ahmed,

Thank you for reaching out to us. We do not hold a copyright on the papers that were presented at the 9th USNCM, so as long as it was not published elsewhere, you are free to use it. I hope that I answered your question, please let me know if you need anything moving forward, otherwise good luck with your thesis.

Best,

David

David Sharbaugh

Administrative Assistant

The Combustion Institute

Office@combustioninstitute.org

CombustionInstitute.org

Chapter 14

ELSEVIER LICENSE
TERMS AND CONDITIONS

Nov 04, 2016

This Agreement between Ahmed Abdul Moiz ("You") and Elsevier ("Elsevier") consists of your license details and the terms and conditions provided by Elsevier and Copyright Clearance Center.

License Number	3981980190419
License date	Nov 04, 2016
Licensed Content Publisher	Elsevier
Licensed Content Publication	Combustion and Flame
Licensed Content Title	Study of soot production for double injections of n-dodecane in CI engine-like conditions
Licensed Content Author	Ahmed Abdul Moiz,Muhsin M Ameen,Seong-Young Lee,Sibendu Som
Licensed Content Date	November 2016
Licensed Content Volume Number	173
Licensed Content Issue Number	n/a
Licensed Content Pages	9
Start Page	123
End Page	131
Type of Use	reuse in a thesis/dissertation
Portion	full article
Format	both print and electronic
Are you the author of this Elsevier article?	Yes
Will you be translating?	No
Order reference number	
Title of your thesis/dissertation	Ignition, lift-off and soot formation in multiple injection low temperature combustion diesel engine systems
Expected completion date	Sep 2016
Estimated size (number of pages)	200
Elsevier VAT number	GB 494 6272 12
Requestor Location	Ahmed Abdul Moiz 2110 Woodmar Apt D HOUGHTON, MI 49931 United States Attn: Ahmed Abdul Moiz
Total	0.00 USD

Figure 1

ELSEVIER LICENSE
TERMS AND CONDITIONS

Aug 28, 2016

This Agreement between Ahmed Abdul Moiz ("You") and Elsevier ("Elsevier") consists of your license details and the terms and conditions provided by Elsevier and Copyright Clearance Center.

License Number	3865051263137
License date	May 09, 2016
Licensed Content Publisher	Elsevier
Licensed Content Publication	Applied Energy
Licensed Content Title	Effects of ultra-high injection pressure and micro-hole nozzle on flame structure and soot formation of impinging diesel spray
Licensed Content Author	Xiangang Wang,Zuohua Huang,Wu Zhang,Olawole Abiola Kuti,Keiya Nishida
Licensed Content Date	May 2011
Licensed Content Volume Number	88
Licensed Content Issue Number	5
Start Page	1620
End Page	1628
Type of Use	reuse in a thesis/dissertation
Intended publisher of new work	other
Portion	figures/tables/illustrations
Number of figures/tables/illustrations	1
Format	both print and electronic
Are you the author of this Elsevier article?	No
Will you be translating?	No
Order reference number	
Original figure numbers	Fig 3
Title of your thesis/dissertation	Ignition, lift-off and soot formation in multiple injection low temperature combustion diesel engine systems
Expected completion date	Sep 2016
Estimated size (number of pages)	200
Elsevier VAT number	GB 494 6272 12
Requestor Location	Ahmed Abdul Moiz 2110 Woodmar Apt D HOUGHTON, MI 49931 United States Attn: Ahmed Abdul Moiz
Billing Type	Invoice
Billing Address	Ahmed Abdul Moiz 2110 Woodmar Apt D HOUGHTON, MI 49931 United States Attn: Ahmed Abdul Moiz
Total	0.00 USD
Total	0.00 USD

Figures 2, 8 and 9

Michigan Tech

Ahmed Abdul Moiz <amoiz@mtu.edu>

SAE International - Using Figures and manuscript content from SAE publication

4 messages

copyright <copyright@sae.org> Thu, Jun 2, 2016 at 2:50 PM

To: "amoiz@mtu.edu" <amoiz@mtu.edu>

Dear Ahmed,

Reproduction use of

Figure 17 from Siebers, D., "Scaling Liquid-Phase Fuel Penetration in Diesel Sprays Based on Mixing-Limited Vaporization," SAE Technical Paper 1999-01-0528, 1999, doi:10.4271/1999-01-0528;

FIgure 11 from Bobba, M., Musculus, M., and Neel, W., "Effect of Post Injections on In-Cylinder and Exhaust Soot for Low-Temperature Combustion in a Heavy-Duty Diesel Engine," SAE Int. J. Engines 3(1):496-516, 2010, doi:10.4271/2010-01-0612;

FIgure 13 from Desantes, J., Arrègle, J., López, J., and García, A., "A Comprehensive Study of Diesel Combustion and Emissions with Post-injection," SAE Technical Paper 2007-01-0915, 2007, doi:10.4271/2007-01-0915,

is hereby granted subject to the following terms and conditions:

·Permission is granted for non-exclusive English language rights, and for the specific use as indicated in your email;

·Permission is required for new requests, or for further use of the material;

-The SAE material must be clearly identified and include the following statement “SAE Int. 2014-01-2676 Reprinted with Permission from SAE International”;

·We also request that you include a complete reference to the SAE document in the reference section for each figure used;

-The permission does not cover any third-party copyrighted work which may appear in the material requested;

·Licensor's use of this material, in whole or in part, is entirely its responsibility, and SAE International does not warrant or is not responsible for any use of the material.

**Permission is confirmed upon receipt of the copyright release fee(s). Submission of payment constitutes Licensor's acceptance of the terms and conditions of this permission. If paying by check, please make payable to SAE International, and enclose a copy of this letter with your payment.

To expedite the process, you may contact me to pay by credit card, securely. If payment is not received within 30 days after receipt of this email, this copyright release will be terminated.

Please mail payment to:

SAE International

ATTN: Customer Service 1990/1207

400 Commonwealth Drive

Warrendale, PA 15096-0001

Best regards,

Nikole Aston

Copyright Administrator

SAE INTERNATIONAL

400 Commonwealth Drive

Warrendale, PA 15096 USA

o +1.724.772.4095

e nikole.aston@sae.org

Figures 4,5 and 16

Michigan Tech

Ahmed Abdul Moiz <amoiz@mtu.edu>

RE: Permission to use Figures in PhD thesis / SAE Figures Request

Nikole Aston <nikole.aston@sae.org> Wed, Oct 12, 2016 at 10:31 AM
To: Ahmed Abdul Moiz <amoiz@mtu.edu>
Cc: Mandy May <Mandy.May@sae.org>

Dear Ahmed,

Please be advised, reproduction use of Figure 19 of SAE Paper 970873; Figure 2 of SAE Paper 2005-01-1091; and Figure 2 of SAE Paper 960034, is hereby granted, and subject to the following terms and conditions:

-Permission is granted for non-exclusive English language rights, and for the specific use as indicated in your email;

-Permission is required for new requests, or for further use of the SAE material;

-The SAE material must be clearly identified and include the following statement "Reprinted with Permission from SAE International";

-We also request that you include within the reference section of your work, a complete reference to each SAE document for corresponding figures used;

-This permission does not cover any third-party copyrighted work which may appear in the material requested;

-Licensor's use of this material, in whole or in part, is entirely its responsibility, and SAE International does not warrant or is not responsible for any use of the material.

Thank you.

Best,

Nikole Aston

IP Compliance Specialist

Figure 6

ELSEVIER LICENSE
TERMS AND CONDITIONS

Aug 28, 2016

This Agreement between Ahmed Abdul Moiz ("You") and Elsevier ("Elsevier") consists of your license details and the terms and conditions provided by Elsevier and Copyright Clearance Center.

License Number	3883781125388
License date	Jun 07, 2016
Licensed Content Publisher	Elsevier
Licensed Content Publication	Progress in Energy and Combustion Science
Licensed Content Title	Conceptual models for partially premixed low-temperature diesel combustion
Licensed Content Author	Mark P.B. Musculus,Paul C. Miles,Lyle M. Pickett
Licensed Content Date	April–June 2013
Licensed Content Volume Number	39
Licensed Content Issue Number	2-3
Licensed Content Pages	38
Start Page	246
End Page	283
Type of Use	reuse in a thesis/dissertation
Portion	figures/tables/illustrations
Number of figures/tables/illustrations	1
Format	both print and electronic
Are you the author of this Elsevier article?	No
Will you be translating?	No
Order reference number	
Original figure numbers	Figure 30
Title of your thesis/dissertation	Ignition, lift-off and soot formation in multiple injection low temperature combustion diesel engine systems
Expected completion date	Sep 2016
Estimated size (number of pages)	200
Elsevier VAT number	GB 494 6272 12
Requestor Location	Ahmed Abdul Moiz 2110 Woodmar Apt D HOUGHTON, MI 49931 United States Attn: Ahmed Abdul Moiz
Total	0.00 USD

Figure 7

ELSEVIER LICENSE
TERMS AND CONDITIONS

Aug 28, 2016

This Agreement between Ahmed Abdul Moiz ("You") and Elsevier ("Elsevier") consists of your license details and the terms and conditions provided by Elsevier and Copyright Clearance Center.

License Number	3865060794665
License date	May 09, 2016
Licensed Content Publisher	Elsevier
Licensed Content Publication	Applied Energy
Licensed Content Title	Response of different injector typologies to dwell time variations and a hydraulic analysis of closely-coupled and continuous rate shaping injection schedules
Licensed Content Author	A. Ferrari,A. Mittica
Licensed Content Date	1 May 2016
Licensed Content Volume Number	169
Licensed Content Issue Number	n/a
Start Page	899
End Page	911
Type of Use	reuse in a thesis/dissertation
Intended publisher of new work	other
Portion	figures/tables/illustrations
Number of figures/tables/illustrations	1
Format	both print and electronic
Are you the author of this Elsevier article?	No
Will you be translating?	No
Order reference number	
Original figure numbers	Figure 26
Title of your thesis/dissertation	Ignition, lift-off and soot formation in multiple injection low temperature combustion diesel engine systems
Expected completion date	Sep 2016
Estimated size (number of pages)	200
Elsevier VAT number	GB 494 6272 12
Requestor Location	Ahmed Abdul Moiz 2110 Woodmar Apt D HOUGHTON, MI 49931 United States Attn: Ahmed Abdul Moiz
Billing Type	Invoice
Billing Address	Ahmed Abdul Moiz 2110 Woodmar Apt D HOUGHTON, MI 49931 United States Attn: Ahmed Abdul Moiz
Total	0.00 USD
Total	0.00 USD

Figure 10

ELSEVIER LICENSE
TERMS AND CONDITIONS

Aug 28, 2016

This Agreement between Ahmed Abdul Moiz ("You") and Elsevier ("Elsevier") consists of your license details and the terms and conditions provided by Elsevier and Copyright Clearance Center.

License Number	3865051113373
License date	May 09, 2016
Licensed Content Publisher	Elsevier
Licensed Content Publication	Renewable and Sustainable Energy Reviews
Licensed Content Title	Fuel injection strategies for performance improvement and emissions reduction in compression ignition engines—A review
Licensed Content Author	Balaji Mohan,Wenming Yang,Siaw kiang Chou
Licensed Content Date	December 2013
Licensed Content Volume Number	28
Licensed Content Issue Number	n/a
Start Page	664
End Page	676
Type of Use	reuse in a thesis/dissertation
Portion	figures/tables/illustrations
Number of figures/tables/illustrations	2
Format	both print and electronic
Are you the author of this Elsevier article?	No
Will you be translating?	No
Order reference number	
Original figure numbers	Figure 3 and 8
Title of your thesis/dissertation	Ignition, lift-off and soot formation in multiple injection low temperature combustion diesel engine systems
Expected completion date	Sep 2016
Estimated size (number of pages)	200
Elsevier VAT number	GB 494 6272 12
Requestor Location	Ahmed Abdul Moiz 2110 Woodmar Apt D HOUGHTON, MI 49931 United States Attn: Ahmed Abdul Moiz
Billing Type	Invoice
Billing Address	Ahmed Abdul Moiz 2110 Woodmar Apt D HOUGHTON, MI 49931 United States Attn: Ahmed Abdul Moiz
Total	0.00 USD
Total	0.00 USD

Figure 14

Michigan Tech

Ahmed Abdul Moiz <amoiz@mtu.edu>

Usage of figures in dissertation

3 messages

Ahmed Abdul Moiz <amoiz@mtu.edu> Sun, Jul 31, 2016 at 6:26 PM

To: "Som, Sibendu" <ssom@anl.gov>

Hi Sibendu,

I was wondering if i can use the below figures in my dissertation, These figures are from your 24th ILASS publication titled - "Comparison of RANS and LES turbulence models against constant volume diesel experiments." Author listing is - S. Som, P. Senecal, E. Pomraning.

I am using these figures to support the usage of the 42 species Chalmers mechanism in one of my simulation work.

Thanks a lot in advance.

--

Regards,

Ahmed Abdul Moiz

(906)-370-5894

ME-EM graduate student

Michigan Technological University

Som, Sibendu <ssom@anl.gov> Sun, Jul 31, 2016 at 10:17 PM

To: Ahmed Abdul Moiz <amoiz@mtu.edu>

Figure 15

Michigan Tech **Ahmed Abdul Moiz <amoiz@mtu.edu>**

Usage of figures in dissertation

3 messages

Ahmed Abdul Moiz <amoiz@mtu.edu> Sun, Jul 31, 2016 at 6:36 PM

To: tlu@engr.uconn.edu

Hi Dr. Lu,

I am PhD student from Michigan Tech University. I was introduced to the 54 species Yao mechanism during my previous work at ANL and i happen to use it in my PhD simulation work as well.

I was wondering if i can use the below figures in my dissertation, This figure set (Fig. 9) are from your publication from the 9th U.S. National Combustion Meeting titled - "A Hybrid Mechanism for n-Dodecane Combustion with Optimized Low-Temperature Chemistry." Author listing is - T. Yao, Y. Pei, B.-J. Zhong, S. Som

I am using these figures to support the usage of your 54 species mechanism in some of my simulation works which are now part of the PhD dissertation.

Thanks a lot in advance.

--

Regards,

Ahmed Abdul Moiz

(906)-370-5894

ME-EM graduate student

Michigan Technological University

Lu, Tianfeng <tianfeng.lu@uconn.edu> Sun, Jul 31, 2016 at 8:08 PM

To: Ahmed Abdul Moiz <amoiz@mtu.edu>

Dear Ahmed,

Yes, please feel free to use these figures. You can cite the US meeting paper as we don't have a journal publication yet.

Best,

Tianfeng

Tianfeng Lu

Associated Professor

Department of Mechanical Engineering

University of Connecticut

191 Auditorium Road Unit-3139

Storrs, CT 06269-3139

Phone: (860) 486-3942(O)

Fax: (860) 486-5088

Figure 105

Michigan Tech **Ahmed Abdul Moiz <amoiz@mtu.edu>**

Permission to use SAE figures in PhD thesis

Nikole Aston <nikole.aston@sae.org> Fri, Nov 4, 2016 at 10:15 AM

To: Ahmed Abdul Moiz <amoiz@mtu.edu>

Dear Ahmed,

Thank you for your request.

Please be advised, reproduction use of Figure 9 of SAE 2015-01-0799, is hereby granted, and subject to the following terms and conditions:

-Permission is granted for non-exclusive English language rights, and for the specific use as indicated in your email;
-Permission is required for new requests, or for further use of the material;
-The SAE material must be clearly identified and include the following statement "Reprinted with Permission from SAE International";
-We also request that you include a complete reference to the SAE document in the reference section for each figure used;
-This permission does not cover any third-party copyrighted work which may appear in the material requested;
-Licensor's use of this material, in whole or in part, is entirely its responsibility, and SAE International does not warrant or is not responsible for any use of the material.

Best,

Nikole Aston

IP Compliance Specialist

SAE INTERNATIONAL

3.26 Supplementary figures

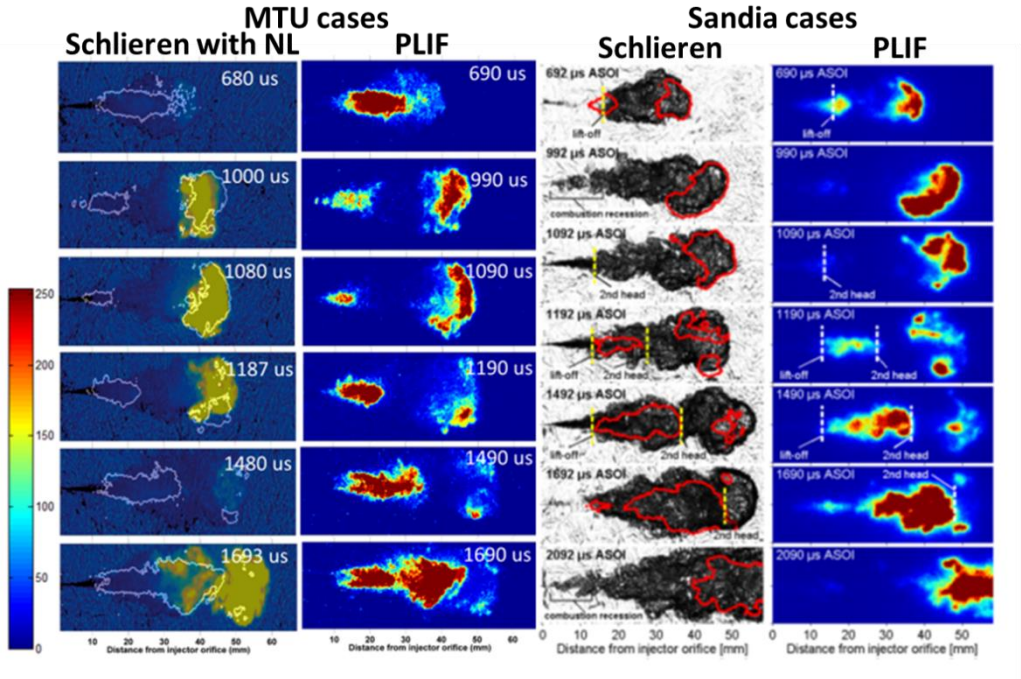

Figure 105: Comparison of MTU tests and Sandia tests with Schlieren and PLIF imaging. The Sandia image set is from Ref. [Skeen et al. 2015b]

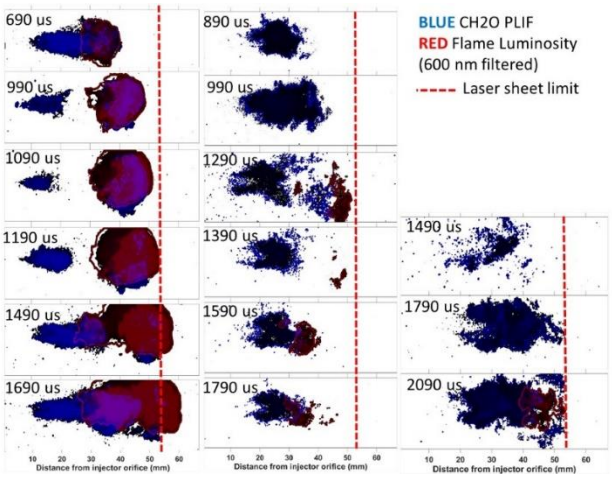

Figure 106: Simultaneous PLIF-NL results for 900 K (left), 800 K (middle) and 750 K (right) ambients

Observations for 900 K case:

- Formaldehyde is seen very early, with subsequent ignition and flame formation happening at the spray tip
- Formaldehyde gets consumed as flame matures
- Faster formaldehyde consumption takes place for the second spray as it shoots into the high temperature environment of the first flame

Observations for 800 K case:

- Formaldehyde is seen at later times
- Mature flame is observed at higher temporal and spatial points
- Formaldehyde remains unconsumed for higher periods of time, meaning low combustion efficiency

Observations for 750 K case:

- Formaldehyde is seen at very late durations with a very weak signal.
- Spray is more or less a low reactive vapor-radical mixture for longer duration
- Ignition of first and second injection occurs more or less as a single event
- Formaldehyde upstream is unconsumed even after flame has extinguished, meaning very low combustion efficiency

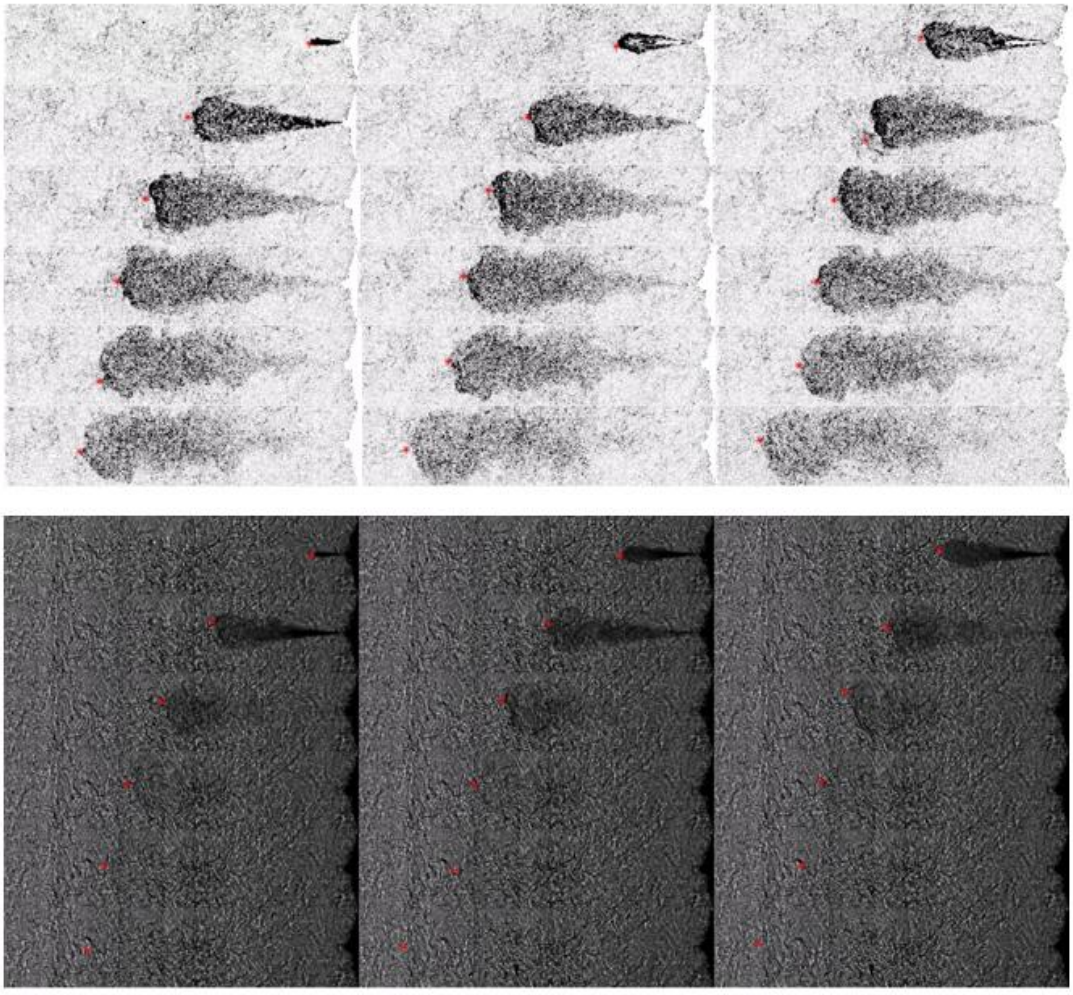

Figure 107: Top - Sample MATLAB processed images of non-reacting (vapor) penetration case with the plume tip penetration marked a red dot. Bottom - Raw images with the red dot in display

Image processing steps:

- Performing bg_img = $20*(I_n - I_{n-1}) + 20*(I_{n-1} - I_n)$ to get a background image
- Performing img = $20*(I_n - I_{n-1}) + 20*(I_{n-1} - I_n)$ on every other image with a spray
- Sub_im = (img - bg_img)
- Final image = Imcomplement(sub_Img)

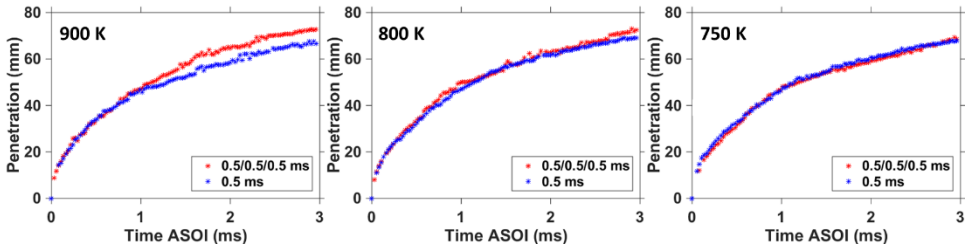

Figure 108: Non reacting (vapor) penetration profiles of 900 K , 800 K and 750 K cases for the 0.5/0.5/0.5 ms injection strategy at 1500 bar injection of n-Dodecane

- For the 900 K case, single short injection is slower than the split injection. Since the second injection moves past the vapor of the first injection through the cooled ambient gases created due to vaporization of the first injection (Second injection has higher liquid content since it experiences cooler regions,there is a 'slip stream' effect and thus it moves faster and stronger).
- For the 800 K case, single short injection moves at the same pace as split injection. It may be attributed due to the lower vaporization of the first injection, causing a lower level of 'slip stream effect'. However we see at at higher ASOI times of ~2.8 ms the second injection vapor begins to have faster penetration. The intensity gradients of the first and second injection are visibly similar, meaning they are of similar densities with the first injection being slightly lighter in intensity due to higher vaporized content. The second injection travels in the cooler regions created by the first.
- For the 750 K case, the penetration profiles are similar and second injection might take even longer to pass the first injection. The same reasoning can be applied as in the 800 K case.

BIBLIOGRAPHY

"Fossil, US OIl Production and Imports." Accessed 04/27/2016. http://energy.gov/science-innovation/energy-sources/fossil.

"Our Nation's Air." Accessed 04/27/2016. https://www3.epa.gov/airtrends/2011/report/fullreport.pdf.

"Virtual Injection Rate Generator." Accessed 2/15/2016. http://www.cmt.upv.es/ECN03.aspx#model.

Abdelghaffar, WA, K Karimi, and MR Heikal. 2007. Fuel spray penetration in high pressure diesel engines. SAE Technical Paper.

Abraham, J, FV Bracco, and RD Reitz. 1985. "Comparisons of computed and measured premixed charge engine combustion." *Combustion and flame* 60 (3):309-322.

Abraham, John. 2015. "Critical observations on the modeling of nonreacting and reacting diesel sprays." *Proceedings of the Institution of Mechanical Engineers, Part D: Journal of Automobile Engineering*:0954407014565407.

Afzal, H, C Arcoumanis, M Gavaises, and N Kampanis. 1999. "Internal flow in diesel injector nozzles: modelling and experiments." *IMechE Paper S* 492:25-44.

Aleiferis, PG, J Serras-Pereira, A Augoye, TJ Davies, RF Cracknell, and D Richardson. 2010. "Effect of fuel temperature on in-nozzle cavitation and spray formation of liquid hydrocarbons and alcohols from a real-size optical injector for direct-injection spark-ignition engines." *International Journal of Heat and Mass Transfer* 53 (21):4588-4606.

Allen, Jeff, Graham Hargrave, and Yong Khoo. 2003. In-nozzle and spray diagnostic techniques for real sized pressure swirl and plain orifice gasoline direct injectors. SAE Technical Paper.

Ameen, Muhsin M, and John Abraham. 2014. RANS and LES study of lift-off physics in reacting diesel jets. SAE Technical Paper.

Amini, Behnaz, and Hasan Khaleghi. 2011. "A comparative study of variant turbulence modeling in the physical behaviors of diesel spray combustion." *Thermal Science* 15 (4):1081-1093.

Amsden, Anthony A, PJ O'rourke, and TD Butler. 1989. KIVA-II: A computer program for chemically reactive flows with sprays. Los Alamos National Lab., NM (USA).

Arrègle, Jean, José V Pastor, J Javier López, and Antonio García. 2008. "Insights on postinjection-associated soot emissions in direct injection diesel engines." *Combustion and Flame* 154 (3):448-461.

Azimov, UB, and KS Kim. 2011. "Large-eddy simulation of air entrainment during diesel spray combustion with multi-dimensional CFD." *International Journal of Automotive Technology* 12 (6):795-812.

Badami, Marco, F Mallamo, F Millo, and EE Rossi. 2003. "Experimental investigation on the effect of multiple injection strategies on emissions, noise and brake specific fuel consumption of an automotive direct injection common-rail diesel engine." *International journal of engine research* 4 (4):299-314.

Bae, Choongsik, and Jinsuk Kang. 2006. "The structure of a break-up zone in the transient diesel spray of a valve-covered orifice nozzle." *International Journal of Engine Research* 7 (4):319-334.

Bajaj, Chetan, Muhsin Ameen, and John Abraham. 2013. "Evaluation of an unsteady flamelet progress variable model for autoignition and flame lift-off in diesel jets." *Combustion Science and Technology* 185 (3):454-472.

Bakenhus, Marco, and Rolf D Reitz. 1999. Two-color combustion visualization of single and split injections in a single-cylinder heavy-duty DI diesel engine using an endoscope-based imaging system. SAE Technical Paper.

Balles, EN, and JB Heywood. 1989. "Spray and flame structure in diesel combustion." *Journal of Engineering for Gas Turbines and Power* 111 (3):451-457.

Baniasad, Mohammad Saeid. 1994. "Analysis of fuel injection rate in diesel injection systems." Imperial College London (University of London).

Baratta, Mirko, Andrea Emilio Catania, and Alessandro Ferrari. 2008. "Hydraulic circuit design rules to remove the dependence of the injected fuel amount on dwell time in multijet CR systems." *Journal of Fluids Engineering* 130 (12):121104.

Beatrice, C, P Belardini, C Bertoli, MG Lisbona, and GM Rossi Sebastiano. 2002. "Diesel combustion control in common rail engines by new injection strategies." *International Journal of Engine Research* 3 (1):23-36.

Bhattacharjee, Subhasish, and Daniel C Haworth. 2013. "Simulations of transient n-heptane and n-dodecane spray flames under engine-relevant conditions using a transported PDF method." *Combustion and Flame* 160 (10):2083-2102.

Blocquet, Marion, Coralie Schoemaecker, Damien Amedro, Olivier Herbinet, Frédérique Battin-Leclerc, and Christa Fittschen. 2013. "Quantification of OH and HO2 radicals during the low-temperature oxidation of hydrocarbons by Fluorescence Assay by Gas Expansion technique." *Proceedings of the National Academy of Sciences* 110 (50):20014-20017.

Bobba, Mohan, Mark Musculus, and Wiley Neel. 2010. "Effect of post injections on in-cylinder and exhaust soot for low-temperature combustion in a heavy-duty diesel engine." *SAE International Journal of Engines* 3 (1):496-516.

Bolla, Michele, Nicolò Frapolli, Yuri M Wright, and Konstantinos Boulouchos. 2014. "An Extended CMC Model for the Simulation of Diesel Engines with Multiple Injections." International Multidimensional Engine Modeling Users' Group Meeting.

Borz, Meghan J, Yoontak Kim, and Jacqueline O'Connor. 2016. The Effects of Injection Timing and Duration on Jet Penetration and Mixing in Multiple-Injection Schedules. SAE Technical Paper.

Bosch, Wilhelm. 1966. The fuel rate indicator: a new measuring instrument for display of the characteristics of individual injection. SAE Technical Paper.

Brands, Thorsten, Thomas Huelser, Peter Hottenbach, Hans-Jürgen Koss, and Gerd Grunefeld. 2013. "Optical Investigation of Combusting Split-Injection Diesel Sprays Under Quiescent Conditions." *SAE International Journal of Engines* 6 (3):1626-1641.

Bravo, L, M Kurman, C Kweon, S Wijeyakulasuriya, and PK Senecal. 2014. Lagrangian Modeling of Evaporating Sprays at Diesel Engine Conditions: Effects of Multi-Hole Injector Nozzles With JP-8 Surrogates. DTIC Document.

Broadwell, James E, Werner JA Dahm, and M Godfrey Mungal. 1985. "Blowout of turbulent diffusion flames." Symposium (International) on Combustion.

Bruneaux, G. 2008. "Combustion structure of free and wall-impinging diesel jets by simultaneous laser-induced fluorescence of formaldehyde, poly-aromatic hydrocarbons, and hydroxides." *International Journal of Engine Research* 9 (3):249-265.

Bruneaux, Gilles, and David Maligne. 2009. "Study of the mixing and combustion processes of consecutive short double diesel injections." *SAE international journal of engines* 2 (1):1151-1169.

Buckmaster, J. 2002. "Edge-flames." *Progress in Energy and Combustion Science* 28 (5):435-475.

Campbell, JW, AD Gosman, and G Hardy. 2009. "Analysis of premix flame and lift-off in diesel spray combustion using multi-dimensional CFD." *SAE International Journal of Engines* 1 (1):571-590.

Catania, Andrea E, Alessandro Ferrari, Michele Manno, and Ezio Spessa. 2008. "Experimental investigation of dynamics effects on multiple-injection common rail system performance." *Journal of Engineering for Gas Turbines and Power* 130 (3):032806.

Catania, Andrea E, Alessandro Ferrari, and Ezio Spessa. 2009. "Numerical-experimental study and solutions to reduce the dwell-time threshold for fusion-free consecutive injections in a multijet solenoid-type CR system." *Journal of Engineering for Gas Turbines and Power* 131 (2):022804.

Chang, CT, and PV Farrell. 1997. A study on the effects of fuel viscosity and nozzle geometry on high injection pressure diesel spray characteristics. SAE Technical Paper.

Chen, M, M Herrmann, and N Peters. 2000. "Flamelet modeling of lifted turbulent methane/air and propane/air jet diffusion flames." *Proceedings of the Combustion Institute* 28 (1):167-174.

Chen, S Kevin. 2000. Simultaneous reduction of NOx and particulate emissions by using multiple injections in a small diesel engine. SAE Technical Paper.

Chen, S Kevin, and Arthur H Lefebvre. 1994. "Spray cone angles of effervescent atomizers." *Atomization and Sprays* 4 (3).

Colin, O, A Benkenida, and C Angelberger. 2003. "3D modeling of mixing, ignition and combustion phenomena in highly stratified gasoline engines." *Oil & gas science and technology* 58 (1):47-62.

Cung, Khanh D. 2015. "Spray and combustion characteristics of dimethyl ether under various ambient conditions: An experimental and modeling study." PhD, Mechanical Engineering-Engineering Mechanics, Michigan Technological University.

Cung, Khanh, Abdul Moiz, Jaclyn Johnson, Seong-Young Lee, Chol-Bum Kweon, and Alessandro Montanaro. 2015. "Spray–combustion interaction mechanism of multiple-injection under diesel engine conditions." *Proceedings of the Combustion Institute* 35 (3):3061-3068.

d'Ambrosio, S, and A Ferrari. 2015. "Potential of multiple injection strategies implementing the after shot and optimized with the design of experiments procedure to improve diesel engine emissions and performance." *Applied Energy* 155:933-946.

D'Errico, G, T Lucchini, F Contino, Mehdi Jangi, and X-S Bai. 2014. "Comparison of well-mixed and multiple representative interactive flamelet approaches for diesel spray combustion modelling." *Combustion Theory and Modelling* 18 (1):65-88.

Dec, John E. 1997. A conceptual model of di diesel combustion based on laser-sheet imaging*. SAE technical paper.

Desantes, JM, JV Pastor, JM García-Oliver, and JG Ramírez-Hernández. "Studies of DI Diesel Engine Cold Start Combustion in an Optical Engine."

Desantes, JM, R Payri, FJ Salvador, and J De la Morena. 2010. "Influence of cavitation phenomenon on primary break-up and spray behavior at stationary conditions." *Fuel* 89 (10):3033-3041.

Desantes, José M, Jean Arrègle, J Javier López, and Antonio García. 2007. A comprehensive study of diesel combustion and emissions with post-injection. SAE Technical Paper.

Doran, Eric M, Heinz Pitsch, and David J Cook. 2012. Multi-dimensional flamelet modeling of multiple injection diesel engines. SAE Technical Paper.

Echekki, Tarek, and Jacqueline H Chen. 2003. "Direct numerical simulation of autoignition in non-homogeneous hydrogen-air mixtures." *Combustion and Flame* 134 (3):169-191.

Ehleskog, Rickard, Raúl L Ochoterena, and Sven Andersson. 2007. Effects of multiple injections on engine-out emission levels including particulate mass from an HSDI diesel engine. SAE Technical Paper.

Farrar-Khan, JR, GE Andrews, and PT Williams. 1992. "Influence of nozzle sac volume on diesel spray droplet sizes." *Proceedings of the Institution of Mechanical Engineers, Part A: Journal of Power and Energy* 206 (4):239-248.

Felsch, C., M. Gauding, C. Hasse, S. Vogel, and N. Peters. 2009. "An extended flamelet model for multiple injections in DI Diesel engines." *Proceedings of the Combustion Institute* 32 (2):2775-2783. doi: 10.1016/j.proci.2008.05.053.

Ferrari, A, and A Mittica. 2016. "Response of different injector typologies to dwell time variations and a hydraulic analysis of closely-coupled and continuous rate shaping injection schedules." *Applied Energy* 169:899-911.

Ferrari, Alessandro, and Antonio Mittica. 2012. "FEM modeling of the piezoelectric driving system in the design of direct-acting diesel injectors." *Applied Energy* 99:471-483.

Ge, Hai-Wen, Michael Norconk, Seong-Young Lee, Jeffrey Naber, Steve Wooldridge, and James Yi. 2014. "PIV measurement and numerical simulation of fan-driven flow in a constant volume combustion vessel." *Applied Thermal Engineering* 64 (1):19-31.

Golovitchev, Valeri I, N Nordin, R Jarnicki, and J Chomiak. 2000. 3-D diesel spray simulations using a new detailed chemistry turbulent combustion model. SAE Technical Paper.

Gong, Cheng, Mehdi Jangi, and Xue-Song Bai. 2014. "Large eddy simulation of n-Dodecane spray combustion in a high pressure combustion vessel." *Applied Energy* 136:373-381.

Gong, Cheng, Mehdi Jangi, and Xue-Song Bai. 2015. "Diesel flame lift-off stabilization in the presence of laser-ignition: a numerical study." *Combustion Theory and Modelling* 19 (6):696-713.

Gonzalez D, Ma, Zhi W Lian, and RD Reitz. 1992. "Modeling diesel engine spray vaporization and combustion." *SAE transactions* 101 (3):1064-1076.

Gordon, Robert L, Assaad R Masri, Stephen B Pope, and Graham M Goldin. 2007a. "A numerical study of auto-ignition in turbulent lifted flames issuing into a vitiated co-flow." *Combustion Theory and Modelling* 11 (3):351-376.

Gordon, Robert L, Assaad R Masri, Stephen B Pope, and Graham M Goldin. 2007b. "Transport budgets in turbulent lifted flames of methane autoigniting in a vitiated co-flow." *Combustion and Flame* 151 (3):495-511.

Halstead, MP, LJ Kirsch, and CP Quinn. 1977. "The autoignition of hydrocarbon fuels at high temperatures and pressures—fitting of a mathematical model." *Combustion and flame* 30:45-60.

Han, Zhiyu, and Rolf D Reitz. 1995. "Turbulence modeling of internal combustion engines using RNG κ-ε models." *Combustion science and technology* 106 (4-6):267-295.

Han, Zhiyu, Ali Uludogan, Gregory J Hampson, and Rolf D Reitz. 1996. "Mechanism of soot and NOx emission reduction using multiple-injection in a diesel engine." *SAE transactions* 105:837-852.

Hardy, William L, and Rolf D Reitz. 2006. An experimental investigation of partially premixed combustion strategies using multiple injections in a heavy-duty diesel engine. SAE Technical Paper.

Harrington, Joel E, and Kermit C Smyth. 1993. "Laser-induced fluorescence measurements of formaldehyde in a methane/air diffusion flame." *Chemical Physics Letters* 202 (3-4):196-202.

Hasse, C, and N Peters. 2005. "A two mixture fraction flamelet model applied to split injections in a DI diesel engine." *Proceedings of the Combustion Institute* 30 (2):2755-2762.

Hasse, Christian Wolfgang. 2004. *A two-dimensional flamelet model for multiple injections in diesel engines*: Cuvillier Verlag.

Haworth, DC. 2010. "Progress in probability density function methods for turbulent reacting flows." *Progress in Energy and Combustion Science* 36 (2):168-259.

Hessel, Randy, Rolf D. Reitz, Mark Musculus, Jacqueline O'Connor, and Daniel Flowers. 2014. "A CFD Study of Post Injection Influences on Soot Formation and Oxidation under Diesel-Like Operating Conditions." *SAE International Journal of Engines* 7 (2):694-713. doi: 10.4271/2014-01-1256.

Heywood, John B. 1988. *Internal combustion engine fundamentals*. Vol. 930: Mcgraw-hill New York.

Higgins, Brian, Dennis L Siebers, and Allen Aradi. 2000. Diesel-spray ignition and premixed-burn behavior. SAE Technical Paper.

Hiroyasu, H, and To Kadota. 1976. Models for combustion and formation of nitric oxide and soot in direct injection diesel engines. SAE Technical Paper.

Hiroyasu, Hiro, and Masataka Arai. 1990. Structures of fuel sprays in diesel engines. SAE Technical Paper.

Hiroyasu, Hiro, Haiyan Miao, Tomo Hiroyasu, Mitunori Miki, Jiro Kamiura, and Shinya Watanabe. 2003a. "Optimization of Diesel Engine Emissions and Fuel Efficiency Using Genetic Algorithms and Phenomenological Model with EGR, Injection Timing and Multiple Injections." 5th Stuttgart Symposium, Stuttgart (Germany).

Hiroyasu, Hiro, Haiyan Miao, Tomo Hiroyasu, Mitunori Miki, Jiro Kamiura, and Sinya Watanabe. 2003b. "Genetic algorithms optimization of diesel engine emissions

and fuel efficiency with air swirl, EGR, injection timing and multiple injections." *SAE SP*:155-166.

Hotta, Yoshihiro, Minaji Inayoshi, Kiyomi Nakakita, Kiyoshi Fujiwara, and Ichiro Sakata. 2005. "Achieving lower exhaust emissions and better performance in an HSDI diesel engine with multiple injection." *SAE paper* (2005-01):0928.

Idicheria, Cherian A, and Lyle M Pickett. 2005. Soot formation in diesel combustion under high-EGR conditions. Sandia National Laboratories.

Jafarmadar, S, and A Zehni. 2009. "Multi-dimensional modeling of the effects of split injection scheme on combustion and emissions of direct-injection diesel engines at full load state." *Iranian Journal of Engineering* 22 (4).

Johnson, Jaclyn, Hai-Wen Ge, Jeffrey Naber, Seong-Young Lee, Eric Kurtz, and Nan Robarge. 2013. "Investigation of key mechanisms for liquid length fluctuations in transient vaporizing diesel sprays." *SAE International Journal of Engines* 6 (2013-01-1594):1202-1212.

Johnson, Samuel E, Jaclyn E Nesbitt, and Jeffrey D Naber. 2010. "Mass and momentum flux measurements with a high pressure common rail diesel fuel injector." ASME 2010 Internal Combustion Engine Division Fall Technical Conference.

Juli, J. 2002. "Planar Laser-Induced Fluorescence fuel concentration measurements in isothermal Diesel sprays." *Optics Express* 10 (7):309-323.

Kalghatgi, GT, Leif Hildingsson, Andrew Harrison, and Bengt Johansson. 2010. "Low-NOx, Low-Smoke Operation of a Diesel Engine Using 'Premixed Enough'Compression Ignition—Effects of Fuel Autoignition Quality, Volatility and Aromatic Content." THIESEL 2010 Conference on Thermo-and Fluid Dynamic Processes in Diesel Engines, Valencia, Spain, September.

Karimi, Kourosh. 2007. "Characterisation of multiple-injection diesel sprays at elevated pressures and temperatures." Citeseer.

Kastner, O, F Atzler, C Juvenelle, R Rotondi, and A Weigand. 2009. "Directly actuated piezo injector for advanced injection strategies towards cleaner diesel engines." 7th Int symposium towards cleaner diesel engine TDCE2009.

Kim, Myung Yoon, Seung Hyun Yoon, Ki Hyoung Park, and Chang Sik Lee. 2007. "Effect of multiple injection strategies on the emission characteristics of dimethyl ether (DME)-fueled compression ignition engine." *Energy & Fuels* 21 (5):2673-2681.

Klimenko, Alex Y, and Robert William Bilger. 1999. "Conditional moment closure for turbulent combustion." *Progress in energy and combustion science* 25 (6):595-687.

Knox, B. W., and C. L. Genzale. 2015a. "Reduced-order numerical model for transient reacting diesel sprays with detailed kinetics." *International Journal of Engine Research* 17 (3):261-279. doi: 10.1177/1468087415570765.

Knox, Benjamin W, and Caroline L Genzale. 2015b. "Reduced-order numerical model for transient reacting diesel sprays with detailed kinetics." *International Journal of Engine Research*:1468087415570765.

Kodavasal, Janardhan, George A Lavoie, Dennis N Assanis, and Jason B Martz. 2015. "Reaction-space analysis of homogeneous charge compression ignition combustion with varying levels of fuel stratification under positive and negative

valve overlap conditions." *International Journal of Engine Research*:1468087415613208.
Kojima, Jun, Yuji Ikeda, and Tsuyoshi Nakajima. 2000. "Spatially resolved measurement of OH*, CH*, and C 2* chemiluminescence in the reaction zone of laminar methane/air premixed flames." *Proceedings of the Combustion institute* 28 (2):1757-1764.
Kokjohn, Sage L, and Rolf D Reitz. 2011. "Investigation of the roles of flame propagation, turbulent mixing, and volumetric heat release in conventional and low temperature diesel combustion." *Journal of Engineering for Gas Turbines and Power* 133 (10):102805.
Kong, Song-Charng, Zhiyu Han, and Rolf D Reitz. 1995. The development and application of a diesel ignition and combustion model for multidimensional engine simulation. SAE Technical Paper.
Kundu, Prithwish, Yuanjiang Pei, Mingjie Wang, Raju Mandhapati, and Sibendu Som. 2014. "Evaluation of turbulence-chemistry interaction under diesel engine conditions with multi-flamelet RIF model." *Atomization and Sprays* 24 (9).
Lachaux, Thierry, and Mark PB Musculus. 2007. "In-cylinder unburned hydrocarbon visualization during low-temperature compression-ignition engine combustion using formaldehyde PLIF." *Proceedings of the Combustion Institute* 31 (2):2921-2929.
Ladommatos, N, S Abdelhalim, and H Zhao. 2000. "The effects of exhaust gas recirculation on diesel combustion and emissions." *International Journal of Engine Research* 1 (1):107-126.
Lafossas, F-A, Michel Castagne, Jean-Pierre Dumas, and Stephane Henriot. 2002. Development and validation of a knock model in spark ignition engines using a CFD code. SAE Technical Paper.
Lim, Jaeman, Sangyul Lee, and Kyoungdoug Min. 2010. "Combustion Modeling of Split Injection in HSDI Diesel Engines." *Combustion Science and Technology* 183 (2):180-201.
Liu, Alex B, Daniel Mather, and Rolf D Reitz. 1993. Modeling the effects of drop drag and breakup on fuel sprays. DTIC Document.
Lyons, Kevin M. 2007. "Toward an understanding of the stabilization mechanisms of lifted turbulent jet flames: experiments." *Progress in Energy and Combustion Science* 33 (2):211-231.
Magi, Venkatraman Iyer, John Abraham, Vinicio. 2001. "The k-ε model and computed spreading rates in round and plane jets." *Numerical Heat Transfer: Part A: Applications* 40 (4):317-334.
Mahr, Bernd. 2004. "Future and potential of diesel injection systems." In *Thermo-and Fluid Dynamic Processes in Diesel Engines 2*, 3-17. Springer.
Manente, Vittorio, Bengt Johansson, and W Cannella. 2011. "Gasoline partially premixed combustion, the future of internal combustion engines?" *International Journal of Engine Research* 12 (3):194-208.
Manente, Vittorio, Bengt Johansson, Per Tunestal, and William Cannella. 2010. "Effects of different type of gasoline fuels on heavy duty partially premixed combustion." *SAE International Journal of Engines* 2 (2):71-88.

Meijer, Maarten, Bart Somers, Jaclyn Johnson, Jeffrey Naber, Seong-Young Lee, Louis Marie Malbec, Gilles Bruneaux, Lyle M Pickett, Michele Bardi, and Raul Payri. 2012. "Engine combustion network (ECN): characterization and comparison of boundary conditions for different combustion vessels." *Atomization and Sprays* 22 (9).

Melton, Lynn A. 1983. "Spectrally separated fluorescence emissions for diesel fuel droplets and vapor." *Applied Optics* 22 (14):2224-2226.

Mie, Gustav. 1908. "Beiträge zur Optik trüber Medien, speziell kolloidaler Metallösungen." *Annalen der physik* 330 (3):377-445.

Mohan, Balaji, Wenming Yang, and Siaw kiang Chou. 2013. "Fuel injection strategies for performance improvement and emissions reduction in compression ignition engines—A review." *Renewable and Sustainable Energy Reviews* 28:664-676.

Moiz, Ahmed Abdul, Sibendu Som, Luis Bravo, and Seong-Young Lee. 2015. Experimental and Numerical Studies on Combustion Model Selection for Split Injection Spray Combustion. SAE Technical Paper.

Mojtabi, Mehdi. 2011. "Optical analysis of multi-stream GDI sprays under various engine operating conditions." © Mehdi Mojtabi.

Molina, Santiago, José Maria Desantes, Antonio Garcia, and José M Pastor. 2010. A numerical investigation on combustion characteristics with the use of post injection in DI diesel engines. SAE Technical Paper.

Mueller, Charles J, LM Pickett, DL Siebers, WJ Pitz, CK Westbrook, and GC Martin. 2003. "Effects of oxygenates on soot processes in DI diesel engines: experiments and numerical simulations." *SAE SP*:129-148.

Müller, CM, H Breitbach, and N Peters. 1994. "Partially premixed turbulent flame propagation in jet flames." Symposium (International) on Combustion.

Musculus, Mark P, John E Dec, and Dale R Tree. 2002. Effects of fuel parameters and diffusion flame lift-off on soot formation in a heavy-duty DI diesel engine. SAE Technical Paper.

Musculus, Mark PB, Paul C Miles, and Lyle M Pickett. 2013. "Conceptual models for partially premixed low-temperature diesel combustion." *Progress in Energy and Combustion Science* 39 (2):246-283.

Musculus, Mark PB, and Lyle M Pickett. 2005. "Diagnostic considerations for optical laser-extinction measurements of soot in high-pressure transient combustion environments." *Combustion and Flame* 141 (4):371-391.

Naber, Jeffrey D, and Dennis L Siebers. 1996. Effects of gas density and vaporization on penetration and dispersion of diesel sprays. Sandia National Laboratory.

Nagle, J, and RF Strickland-Constable. 1962. "Oxidation of Carbon between 1000-2000 C." Proceedings of the fifth carbon conference.

Neely, Gary D, Shizuo Sasaki, Yiqun Huang, Jeffrey A Leet, and Daniel W Stewart. 2005. New diesel emission control strategy to meet US Tier 2 emissions regulations. SAE Technical Paper.

Nehmer, Daniel A, and Rolf D Reitz. 1994. Measurement of the effect of injection rate and split injections on diesel engine soot and NOx emissions. SAE Technical Paper.

Nesbitt, Jaclyn E, Samuel E Johnson, Lyle M Pickett, Dennis L Siebers, Seong-Young Lee, and Jeffrey D Naber. 2011. "Minor species production from lean premixed

combustion and their impact on autoignition of diesel surrogates." *Energy & Fuels* 25 (3):926-936.
Nesbitt, Jaclyn E, Seong-Young Lee, Jeffrey D Naber, and Rajat Arora. 2010. "An optical study of spark ignition and flame kernel development near the lean limit at elevated pressure." ASME 2010 Internal Combustion Engine Division Fall Technical Conference.
Nishimura, Terukazu, Keiichi Satoh, Susumu Takahashi, and Katsuhiko Yokota. 1998. Effects of fuel injection rate on combustion and emission in a DI diesel engine. SAE Technical Paper.
Nordin, N. 1998. "Numerical Simulations of Non-Steady Spray Combustion Using a Detailed Chemistry Approach." *Licentiate of Engineering thesis, Department of Thermo and Fluid Dynamics, Chalmers University of Technology, Goteborg, Sweden*.
O'Connor, Jacqueline, and Mark Musculus. 2013a. "Effects of exhaust gas recirculation and load on soot in a heavy-duty optical diesel engine with close-coupled post injections for high-efficiency combustion phasing." *International Journal of Engine Research*:1468087413488767.
O'Connor, Jacqueline, and Mark Musculus. 2013b. "Post Injections for Soot Reduction in Diesel Engines: A Review of Current Understanding." *SAE International Journal of Engines* 6 (1):400-421. doi: 10.4271/2013-01-0917.
O'Connor, Jacqueline, and Mark Musculus. 2013a. "Optical Investigation of the Reduction of Unburned Hydrocarbons Using Close-Coupled Post Injections at LTC Conditions in a Heavy-Duty Diesel Engine." *SAE International Journal of Engines* 6 (1):379-399.
O'Connor, Jacqueline, and Mark Musculus. 2013b. "Post injections for soot reduction in diesel engines: A review of current understanding." *SAE Int. J. Engines* 6 (1):400-421.
O'Connor, Jacqueline, and MPB Musculus. 2014. "In-cylinder mechanisms of soot reduction by close-coupled post-injections as revealed by imaging of soot luminosity and planar laser-induced soot incandescence in a heavy-duty diesel engine." *SAE Int. J. Engines* 7 (2):2014-01.
Oijen, JA van, and LPH De Goey. 2000. "Modelling of premixed laminar flames using flamelet-generated manifolds." *Combustion Science and Technology* 161 (1):113-137.
Patterson, MA, S-C Kong, GJ Hampson, and Rolf D Reitz. 1994. Modeling the effects of fuel injection characteristics on diesel engine soot and NOx emissions. SAE Technical Paper.
Pei, Y. 2013. "Transported PDF modelling of spray combustion at practical diesel engine conditions." Ph. D. thesis, The University of New South Wales, Sydney, Australia.
Pei, Yuanjiang, Evatt R Hawkes, and Sanghoon Kook. 2013a. "A comprehensive study of effects of mixing and chemical kinetic models on predictions of n-heptane jet ignitions with the PDF method." *Flow, turbulence and combustion* 91 (2):249-280.
Pei, Yuanjiang, Evatt R Hawkes, and Sanghoon Kook. 2013b. "Transported probability density function modelling of the vapour phase of an n-heptane jet at diesel engine conditions." *Proceedings of the Combustion Institute* 34 (2):3039-3047.

Pei, Yuanjiang, Evatt R Hawkes, Sanghoon Kook, Graham M Goldin, and Tianfeng Lu. 2015. "Modelling n-dodecane spray and combustion with the transported probability density function method." *Combustion and Flame* 162 (5):2006-2019.

Pei, Yuanjiang, Ruiqin Shan, Sibendu Som, Tianfeng Lu, Douglas Longman, and Michael J Davis. 2014. Global Sensitivity Analysis of a Diesel Engine Simulation with Multi-Target Functions. SAE Technical Paper.

Pei, Yuanjiang, Sibendu Som, Prithwish Kundu, and Graham M Goldin. 2015. Large eddy simulation of a reacting spray flame under diesel engine conditions. SAE Technical Paper.

Pei, Yuanjiang, Sibendu Som, Eric Pomraning, Peter K Senecal, Scott A Skeen, Julien Manin, and Lyle M Pickett. 2015. "Large eddy simulation of a reacting spray flame with multiple realizations under compression ignition engine conditions." *Combustion and Flame* 162 (12):4442-4455.

Peters, Norbert. 1984. "Laminar diffusion flamelet models in non-premixed turbulent combustion." *Progress in energy and combustion science* 10 (3):319-339.

Peters, Norbert. 2000. *Turbulent combustion*: Cambridge university press.

Peters, Norbert, and Forman A Williams. 1983. "Liftoff characteristics of turbulent jet diffusion flames." *AIAA journal* 21 (3):423-429.

Pickett, L, G Bruneaux, and R Payri. 2014a. "ECN4 Proceedings." *Kyoto University, Kyoto Japan, 5-6 Sept 2015, http://www.sandia.gov/ecn/workshop/ECN4/ECN4.php*.

Pickett, L, G Bruneaux, and R Payri. 2014b. "Engine combustion network." *Sandia National Laboratories, Livermore, CA, http://www. ca. sandia. gov/ecn*.

Pickett, Lyle M, Sanghoon Kook, Helena Persson, and Öivind Andersson. 2009. "Diesel fuel jet lift-off stabilization in the presence of laser-induced plasma ignition." *Proceedings of the Combustion Institute* 32 (2):2793-2800.

Pickett, Lyle M, Sanghoon Kook, and Timothy C Williams. 2009a. "Transient liquid penetration of early-injection diesel sprays." *SAE International Journal of Engines* 2 (1):785-804.

Pickett, Lyle M, Sanghoon Kook, and Timothy C Williams. 2009b. "Visualization of diesel spray penetration, cool-flame, ignition, high-temperature combustion, and soot formation using high-speed imaging." *SAE International Journal of Engines* 2 (1):439-459.

Pickett, Lyle M, and Dennis L Siebers. 2004. "Soot in diesel fuel jets: effects of ambient temperature, ambient density, and injection pressure." *Combustion and Flame* 138 (1):114-135.

Pickett, Lyle M, Dennis L Siebers, and Cherian A Idicheria. 2005. "Relationship between ignition processes and the lift-off length of diesel fuel jets." *SAE transactions* 114 (3):1714-1731.

Pierce, Charles D, and Parviz Moin. 2004. "Progress-variable approach for large-eddy simulation of non-premixed turbulent combustion." *Journal of Fluid Mechanics* 504:73-97.

Pitsch, H, H Barths, and N Peters. 1996. Three-dimensional modeling of NOx and soot formation in DI-diesel engines using detailed chemistry based on the interactive flamelet approach. SAE Technical Paper.

Pitsch, H, and H Steiner. 2000. "Large-eddy simulation of a turbulent piloted methane/air diffusion flame (Sandia flame D)." *Physics of Fluids (1994-present)* 12 (10):2541-2554.

Pitsch, Heinz, M Chen, and Norbert Peters. 1998. "Unsteady flamelet modeling of turbulent hydrogen-air diffusion flames." Symposium (international) on combustion.

Pomraning, Eric, and Christopher J Rutland. 2002. "Dynamic one-equation nonviscosity large-eddy simulation model." *AIAA journal* 40 (4):689-701.

Pope, Stephen B. 1985. "PDF methods for turbulent reactive flows." *Progress in Energy and Combustion Science* 11 (2):119-192.

Pope, Stephen B. 2001. Turbulent flows. IOP Publishing.

Pope, Stephen B. 2004. "Gibbs function continuation for the stable computation of chemical equilibrium." *Combustion and flame* 139 (3):222-226.

Post, Scott L, and John Abraham. 2002. "Modeling the outcome of drop–drop collisions in Diesel sprays." *International Journal of Multiphase Flow* 28 (6):997-1019.

Reitz, Rolf D, and R Diwakar. 1987. Structure of high-pressure fuel sprays. Fluid Mechanics Dept., GM Research Labs., Warren, MI.

Rhim, Dong-Ryul, and Patrick V Farrell. 2000. Characteristics of air flow surrounding non-evaporating transient diesel sprays. SAE Technical Paper.

Richards, KJ, PK Senecal, and E Pomraning. 2012. CONVERGE 2.1.0 Theory Manual. In *Convergent Science, Inc., Middleton, WI*.

Rutland, CJ, N Ayoub, Z Han, G Hampson, S-C Kong, D Mather, D Montgomery, M Musculus, M Patterson, and D Pierpont. 1995. Diesel engine model development and experiments. SAE Technical Paper.

Schmidt, David P, and CJ Rutland. 2000. "A new droplet collision algorithm." *Journal of Computational Physics* 164 (1):62-80.

Schugger, Christian, and Ulrich Renz. 2003. "Experimental investigation of the primary breakup zone of high pressure diesel sprays from multi-orifice nozzles." 9 th International conference on liquid atomization and spray system, ICLASS.

Senecal, PK, E Pomraning, KJ Richards, and S Som. 2014. "Grid-Convergent Spray Models for Internal Combustion Engine Computational Fluid Dynamics Simulations." *Journal of Energy Resources Technology* 136 (1):012204.

Shayler, PJ, TD Brooks, GJ Pugh, and R Gambrill. 2005. The influence of pilot and split-main injection parameters on diesel emissions and fuel consumption. SAE Technical Paper.

Shimizu, Masanori, Masataka Arai, and Hiroyuki Hiroyasu. 1984. "Measurements of breakup length in high speed jet." *Bulletin of JSME* 27 (230):1709-1715.

Shrivastava, Rahul, R Hessel, and Rolf D Reitz. 2002. CFD optimization of DI diesel engine performance and emissions using variable intake valve actuation with boost pressure, EGR and multiple injections. SAE Technical Paper.

Siebers, Dennis L. 1998. Liquid-phase fuel penetration in diesel sprays. SAE technical paper.

Siebers, Dennis L. 1999. Scaling liquid-phase fuel penetration in diesel sprays based on mixing-limited vaporization. SAE technical paper.

Siebers, Dennis L, and Brian Higgins. 2001. Flame lift-off on direct-injection diesel sprays under quiescent conditions. SAE Technical Paper.

Singh, Satbir, Rolf D Reitz, and Mark PB Musculus. 2006. "Comparison of the characteristic time (CTC), representative interactive flamelet (RIF), and direct integration with detailed chemistry combustion models against optical diagnostic data for multi-mode combustion in a heavy-duty DI diesel engine." *SAE paper* (2006-01):055.

Skeen, Scott A, Julien Manin, and Lyle M Pickett. 2015a. "Simultaneous formaldehyde PLIF and high-speed schlieren imaging for ignition visualization in high-pressure spray flames." *Proceedings of the Combustion Institute* 35 (3):3167-3174.

Skeen, Scott A, Julien Manin, Lyle M Pickett, Emre Cenker, Gilles Bruneaux, Katsufumi Kondo, Tets Aizawa, Fredrik Westlye, Kristine Dalen, and Anders Ivarsson. 2016. "A Progress Review on Soot Experiments and Modeling in the Engine Combustion Network (ECN)." *SAE International Journal of Engines* 9 (2016-01-0734).

Skeen, Scott, Julien Manin, and Lyle M Pickett. 2015b. "Visualization of Ignition Processes in High-Pressure Sprays with Multiple Injections of n-Dodecane." *SAE International Journal of Engines* 8 (2):696-715.

Som, S, PK Senecal, and E Pomraning. 2012. "Comparison of RANS and LES turbulence models against constant volume diesel experiments." ILASS Americas, 24th Annual Conf. Liquid Atomization and Spray Systems, San Antonio, Texas.

Som, Sibendu, Douglas Longman, Shashi Aithal, Raymond Bair, Marta García, Shaoping Quan, KJ Richards, PK Senecal, Tushar Shethaji, and Marcus Weber. 2013. A numerical investigation on scalability and grid convergence of internal combustion engine simulations. SAE Technical Paper.

Tanov, Slavey, Robert Collin, Bengt Johansson, and Martin Tuner. 2014. "Combustion stratification with partially premixed combustion, PPC, using NVO and split injection in a LD-diesel engine." *SAE international journal of engines* 7 (4):1911-1919.

Tap, FA, and Denis Veynante. 2005. "Simulation of flame lift-off on a diesel jet using a generalized flame surface density modeling approach." *Proceedings of the Combustion Institute* 30 (1):919-926.

Thurnheer, T, D Edenhauser, P Soltic, D Schreiber, P Kirchen, and A Sankowski. 2011. "Experimental investigation on different injection strategies in a heavy-duty diesel engine: emissions and loss analysis." *Energy Conversion and Management* 52 (1):457-467.

Thygesen, Rene. 2012. *Development of a Partially Premixed Combustion Model for a Diesel Engine Using Multiple Injection Strategies*: Logos Verlag Berlin GmbH.

Tonini, S, M Gavaises, A Theodorakakos, and GE Cossali. 2010. "Numerical investigation of a multiple injection strategy on the development of high-pressure diesel sprays." *Proceedings of the Institution of Mechanical Engineers, Part D: Journal of Automobile Engineering* 224 (1):125-141.

Tow, TC, DA Pierpont, and Rolf D Reitz. 1994. Reducing particulate and NOx emissions by using multiple injections in a heavy duty DI diesel engine. SAE Technical Paper.

Vanquickenborne, L, and A Van Tiggelen. 1966. "The stabilization mechanism of lifted diffusion flames." *Combustion and Flame* 10 (1):59-69.

Vishwanathan, Gokul, and Rolf D Reitz. 2010. "Development of a practical soot modeling approach and its application to low-temperature diesel combustion." *Combustion Science and Technology* 182 (8):1050-1082.

Wang, Hu, Rolf Deneys Reitz, Mingfa Yao, Binbin Yang, Qi Jiao, and Lu Qiu. 2013. "Development of an n-heptane-n-butanol-PAH mechanism and its application for combustion and soot prediction." *Combustion and Flame* 160 (3):504-519.

Wang, Xiangang, Zuohua Huang, Wu Zhang, Olawole Abiola Kuti, and Keiya Nishida. 2011. "Effects of ultra-high injection pressure and micro-hole nozzle on flame structure and soot formation of impinging diesel spray." *Applied Energy* 88 (5):1620-1628.

Wang, Ziman, Miroslaw L. Wyszynski, Hongming Xu, Nik Rosli Abdullah, and Jakub Piaszyk. 2015. "Fuel injection and combustion study by the combination of mass flow rate and heat release rate with single and multiple injection strategies." *Fuel Processing Technology* 132:118-132. doi: 10.1016/j.fuproc.2014.11.024.

Xu, C, M Ameen, S Som, and T Lu. 2016. "Chemical explosive mode analysis for reacting spray flames under diesel engine conditions." Spring Technical Meeting of the Eastern States Section of the Combustion Institute.

Xue, Qingluan, Sibendu Som, Peter K Senecal, and E Pomraning. 2013. "Large eddy simulation of fuel-spray under non-reacting IC engine conditions." *Atomization and Sprays* 23 (10).

Yakhot, VSASTBCG, SA Orszag, S Thangam, TB Gatski, and CG Speziale. 1992. "Development of turbulence models for shear flows by a double expansion technique." *Physics of Fluids A: Fluid Dynamics (1989-1993)* 4 (7):1510-1520.

Yao, T, Y Pei, B.-J Zhong, S Som, and T Lu. 2015. "A hybrid mechanism for n-dodecane combustion with optimized low-temperature chemistry." 9th U. S. National Combustion Meeting, Cincinnati, Ohio, May 17-20, 2015.

Zeng, Wei, Min Xu, Ming Zhang, Yuyin Zhang, and David J Cleary. 2012. "Macroscopic characteristics for direct-injection multi-hole sprays using dimensionless analysis." *Experimental Thermal and Fluid Science* 40:81-92.

Zhang, Anqi, Alessandro Montanaro, Luigi Allocca, Jeffrey Naber, and Seong-Young Lee. 2014. "Measurement of Diesel Spray Formation and Combustion upon Different Nozzle Geometry using Hybrid Imaging Technique." *SAE International Journal of Engines* 7 (2014-01-1410):1034-1043.

Zhang, Fan, Rixin Yu, and Xue-Song Bai. 2015. "Effect of split fuel injection on heat release and pollutant emissions in partially premixed combustion of PRF70/air/EGR mixtures." *Applied Energy* 149:283-296.

Zhao, Hua. 2009. *Advanced Direct Injection Combustion Engine Technologies and Development: Diesel Engines*. Vol. 2: Elsevier.

Zhu, Jingyu, Olawole Abiola Kuti, and Keiya Nishida. 2013. "An investigation of the effects of fuel injection pressure, ambient gas density and nozzle hole diameter on surrounding gas flow of a single diesel spray by the laser-induced fluorescence–particle image velocimetry technique." *International Journal of Engine Research* 14 (6):630-645.